Characterization of Human Brain Functional Reorganization with Aging and Pathological Diseases

By

Jie Song

A dissertation submitted in partial fulfillment of the requirements for the degree of

Doctor of Philosophy

(Biomedical Engineering)

at the

UNIVERSITY OF WISCONSIN-MADISON

2014

Date of final oral examination: 7/14/2014

The dissertation is approved by the following members of the Final Oral Committee:

Vivek Prabhakaran, Assistant Professor, Radiology & Medical Physics

M. Elizabeth Meyerand, Professor, Biomedical Engineering & Medical Physics

Justin C. Williams, Associate Professor, Biomedical Engineering & Neurosurgery

Rasmus M. Birn, Assistant Professor, Psychiatry & Medical Physics

Mitchell E. Tyler, Senior Lecturer, Biomedical Engineering & Rehabilitation

Dana L. Tudorascu, Assistant Professor, Medicine and Biostatistics, University of Pittsburgh

Acknowledgements

The first draft of Acknowledgement was written in 2012 before I even have a thesis draft. I knew that down the road of starting a new life on the other side of the Pacific Ocean I would meet great people who I would never want to forget and would want to say Thank You out loud. Indeed, there are so many people who provided me tremendous support on the journey of successfully completing my PhD study and to whom I could not express more gratitude and appreciation.

I offer my deep thanks and appreciation to my advisor Dr. Vivek Prabhakaran. I am grateful to him for providing me the perfect advising distance that allowed me to explore new ideas and to learn from my own mistakes without getting far off track. I thank him for building up my confidence in my work and in myself with his patience and wisdom.

Many thanks to the members of my committee: Drs. Beth Meyerand, Justin Williams, Rasmus Birn, Dana Tudorascu and Mitch Tyler. They are incredibly supportive to the extent beyond my expectation. Thank you, Beth, for always recognizing every small piece of achievement and encouraging me to make it bigger with 100% support. Thank you for your generosity and for advising me with a few words but a lot of actions and a doer attitude.

I would like to express special gratitude to Dr. Wally Block for his wisdom and guidance I have received whenever I popped up in his office with a question or any confusion. Special thanks to my previous advisor Dr. Michelle Johnson at Marquette University. Dr. Johnson provided me assistantship and the freedom to pursue what I want to do. And a big thank you goes to Dr. Frederick J. Frigo at Marquette University who supported me transferring to UW-Madison.

I would like to thank all members and good friends in Prabhakaran Lab and Meyerand Lab. Without their support and friendship, I could not have gone this far. Especially, Dr. Veena Nair, always generous and accessible, provided me tremendous help and support, for which I own her a debt of gratitude. Dr. Cheng Guan Koay, a marvelous researcher and scientist, has always been extremely supportive, encouraging and fun to work with.

I want to thank Suhong Yu, Yinghua Tao, Haiyan Xu, Huimin Wu, Deb Horng, Larry Hernandez, Ricardo Pizarro, Megan Heenan, Karthik Rao, Yiyan Peng for being a wonderful company. Special thanks to Promita Hazra, Sanket Jain and Sihui Yang. I would not be as contented as I am now without you being there. Warmest thanks to the Skora family. Thank you for having me on Thanksgiving, Christmas and family parties. I enjoyed every piece of it. Thank you again, Teresa, for your generosity and kindness.

I would like to thank my parents for their unconditional love, support and encouragement. I sincerely thank them for working extremely hard to provide me, my sister Xing and brother Kai the best education and teaching us to be a better human being. To my sister and brother, thank you for always rooting for me without judgment. The most fun I have had is to grow up with you two. Special thanks to my aunts and uncles. I could not have done this without your vision and absolute confidence in me.

I am truly blessed to have met greater mentors, amazing friends and to be able to fully explore my potentials.

Table of Contents

ABSTRACT

The human brain is a complex structure consisting of spatially distributed but functionally related regions. It undergoes both morphological and functional modifications across the human lifespan. To gain an understanding of age-related functional reorganization of the human brain, we used MRI to quantitatively measure how brain regions are functionally connected and examined the complex pattern of interactions between brain regions using network analyses. In Chapter I, brain functional connectivity (FC) was evaluated using resting-state fMRI (rs-fMRI) in two groups of subjects classified by age. A statistical approach was applied to examine the reliability of FC across subjects and across multiple scan sessions. Results suggest that FC can be stably measured using rs-fMRI, and aging is associated with a decline in reliable connections suggesting the existence of age-related underlying changes in brain organization. In Chapter II, a network model was developed using graph theory in order to examine the complex patterns of FC and further investigated the effect of aging on brain network reorganization at whole brain-wide level and the local regional level. Two important networks--the default mode network (DMN), which includes bran regions that are most active when the brain is at wakeful rest, and the sensorimotor network involved in primary information processing, were shown to have distinct patterns of reorganization with aging. In Chapter III, this network model was applied to a group of epilepsy patients and age-matched healthy control subjects to examine the epileptic brain reorganizational changes. These epilepsy patients showed abnormal increases in the number of between-network connections that are weakly connected, leading to less differentiated brain functional divisions and significantly reduced efficiency for local information transmission. Collectively, the work presented in this thesis applies mathematical approaches to examine human brain reorganizational changes due to normal aging and pathological diseases. It provides a better understanding of how normal healthy aging modulates the brain network to produce a compensation mechanism in order to maintain the cognitive and sensorimotor behavioral performance with aging. This work is also intended to provide a baseline for examining network impairments and disease development in patient population such as epilepsy.

Chapter I

Introduction

The human brain is a complex structure built on multiple scales of time and space, in which billions of neurons are precisely organized into circuits, columns, functional areas as well as higher-order networks. The brain's complexity is also recognized by its dynamic changes, known as brain plasticity, across the human lifespan. Understanding the mechanism underlying brain reorganizational changes across many populations has been a major goal of translational and basic neuroscience for many decades (Jagust W 2009). Besides many other factors, aging is a natural process that reshapes the brain organization functionally and structurally. Aging has been reported to be a main risk factor for neurologic and neurodegenerative diseases, including stroke (Di Carlo 2009), Alzheimer's disease (AD), Parkinson's disease (PD), amyotrophic lateral sclerosis (ALS) and fontotemporal dementia (Risacher and Saykin 2013). Understanding the age-related brain network reorganization is of particular importance as it provides a baseline for examining network level impairments and disease development in different populations.

The Aging Brain

A central feature of normal aging is a general slowing in a variety of perceptual and cognitive operations (Salthouse 1996). Previous postmortem studies have investigated the effects of aging on the anatomy and physiology of the brain and described forms of age-related neural decline, such as reduced brain size, cerebral atrophy, loss of myelin, region-specific loss of neuronal bodies and synaptic loss (Raz, Rodrigue, and Haacke 2007). The advent of magnetic resonance imaging (MRI) provided an opportunity to observe age-related differences in brain structure and function *in vivo*. MRI methods enable longitudinal follow-up to gauge brain reorganizational changes. Determining brain changes in normal and successful aging can be addressed with the help of MRI, with which transition from normal aging to its pathological expressions such as neurodegenerative disease can be further understood.

In a previous longitudinal study, 92 nondemented older adults underwent MRI scans acquired at baseline, 2-year and 4-year follow-up (Resnick et al. 2003). The results reported evidence of substantial longitudinal declines in both gray and white matter brain volumes with aging. Moreover, these findings

also revealed that differential longitudinal declines in local brain volumes, with frontal and parietal lobes showing greater tissue loss compared with temporal and occipital regions. In another study conducted on 72 healthy adults, (Raz et al. 2005) measured a number of regional brain volumes and reported a significant longitudinal decline across a 5-year period with shrinkage magnitude varying across regions. The prefrontal region showed increased shrinkage with age. The prefrontal cortex is known as a late-developing region of the neocortex and is principally involved in higher executive functions such as cognitive function. All these cortical regions are linked to important brain functional networks such as the control/execution network, the default mode network and the motor control networks, which form the basis of brain functional reorganization with aging.

Brain Networks

Networks are everywhere—at macro level, there are social networks, internet networks, telecommunication networks, railroad networks, airline networks, power-line networks; at micro level, there are gene networks and neural networks. Similar to a road map describing the connections of regions in a space, a network characterizes interactions in a complex system. If we want to understand the complexity of a system, we must first understand its basic interaction patterns. In order to do so, we can build a network model that helps to reduce the complexity and provides an abstraction of the system.

Graph theory

Network analysis originated from the mathematical field of graph theory (Diestel 2000). Graph theory almost certainly began when, in 1735, Leonhard Euler solved a popular puzzle about bridges. There were seven bridges over the river Pregel and connecting four different land masses in the East Prussian city of Königsberg (now Kaliningrad) (Figure 1)(Alexanderson 2006). The problem was, "Does there exist any single path that crosses all seven bridges exactly once each and returns to the origin?" The answer is no as there is no such path now called an Euler tour (Diestel 2000). This solution is considered to be the first theorem of graph theory which studies similar problems by using graph representations—a set of nodes

(*n*) and links or connections (*l*) which connect the nodes (Figure 2). This mathematic object later leads to a wide application in many systems simplified by networks, since the nodes are not limited to represent land masses and the links limited to represent bridges. For instance, a typical social network study conducted by sociologists may involve the circulation of questionnaires, asking respondents to detail their interactions with others. Graph theory then can be applied here to reconstruct a network based on the responses in which nodes represent individuals and links represent the interactions between them. Utilizing graph theory based network analysis, researchers are able to investigate a variety of topics such as identifying critical nodes that substantially affect network connectivity, determining how efficient information flows in different portions of the network, examining how a cluster of nodes group together while other do not, or quantifying the hierarchical structures of a system. Most importantly, these questions can be investigated at large scale of the entire network, or at the level of sub-network and even at the individual nodal level, which provides an elegant way of examining a complex system from macroscopic to microscopic level.

The functional brain networks

For the complex brain system, billions of neurons are constantly sending and receiving signals from each other. This type of interactions is not a simple combination of each individual neuron's synapsing, and the complexity of the interactions makes the brain system adaptive to ever changing environment. A network model of the brain can help better understanding these complex interactions thoroughly from the level of whole brain system to individual brain regions of interest (ROI). Moreover, human brains demonstrate a large variability in size and surface shape (VanEssen and Drury 1997). With network modeling, these features become less important in the analysis of identifying similarities and differences in the brain network organization.

Modern brain mapping techniques—such as functional MRI, diffusion tensor imaging (DTI), electro- or magnetoencephalogram (EEG/MEG)—generate increasingly large datasets of the anatomical or functional connection patterns which form large and complex brain networks. In these brain networks,

nodes are generally defined as cortical and subcortical areas. Links or edges are defined based on the type of connections or connectivity (Rubinov and Sporns 2010). For structural connectivity, links are defined as axonal tracts. The anatomical network is constructed based on fiber bundles according to the regions they interconnect using diffusion MRI data (Hagmann et al. 2007). For functional connectivity, links are undirected statistical dependencies (i.e., cross-correlations) between regional temporal activities on the basis of functional MRI (fMRI) signals, or coherence in EEG/MEG signals. For effective connectivity, links are directed causal interactions or the influence one neuronal system exerts over another (Friston 1994). The effective network is then constructed based on a priori model for causal relationships. Each connectivity model has certain limitations and there is no general model existing that can be considered optimal for all kinds of data and experimental conditions. For instance, the structural network cannot resolve intracortical or intrinsic connections (Park and Friston 2013); the effective network requires an *a priori* model for directed causal connections and thus the validity of effective network depends on the validity of the connectivity model (Friston 1994). The functional network is often based on an a priori anatomical model, which can be constructed using high resolution images with high accuracy. It also assesses a pattern of correlated activity that may exist between anatomically unconnected regions. Therefore, for a system that is largely unknown, the functional connectivity approach is more useful and more exploratory in nature. In this thesis, we investigated age-related brain reorganization based on a functional network constructed from the functional connectivity analyses.

Resting-state fMRI (rs-fMRI) has become an important basis for functional network analysis, after the discovery of spatially organized temporal correlations of low-frequency spontaneous fluctuations (< 0.1 Hz) of blood-oxygen level dependence (BOLD) signals (Biswal et al. 1995). Rs-fMRI is commonly used for non-invasively investigating brain functions while the brain is at rest. It has enabled the measurements of functionally correlated brain activity known as resting-state functional connectivity (RSFC), or simply functional connectivity, throughout the brain in the absence of task-induced activity, leading to a comprehensive description of brain functional organization.

The effects of aging on functional connectivity have mainly been assessed using seed-based functional connectivity and independent component analysis (van de Ven et al. 2004, Biswal et al. 2010). Both methods have a limited capability of providing a complete view of the characteristics of connectivity among multiple brain regions. Advanced network analysis provides the ability to map out the complex patterns of interactions across multiple brain areas and to further examine the segregation of localized brain functional connections and the integration of brain regions that form a network (Friston 2002).

Age-related Brain Functional Reorganization

In brains of higher vertebrates, it is believed that the brain is functionally segregated into different brain regions and also functionally integrated globally during perception and behavior (Tononi, Sporns, and Edelman 1994, Friston 2002). The brain functional organization has drawn increasing attention in recent years with the prevalence of functional connectivity and network approach. Functional connectivity allows for an examination of functional reorganization at the level of pair-wise relationships between regions, while network approach examines brain reorganization at a higher network level via mapping out the patterns of interactions among multiple regions or sub-networks.

Brain functional connectivity analyses conducted by numerous previous studies have established that normal aging is accompanied by a general decline in simple sensorimotor function associated with decreased functional connectivity in the motor network (Wu et al. 2007), and reduction in the ability to inhibit default-mode activity associated with hyper functional connectivity in the default mode network (Grady et al. 2006). Another study using a machine learning method has revealed that the majority of the functional connections used by the classifier to distinguish subjects by age came from brain regions belonging to the sensorimotor and cingulo-opercular networks (Meier et al. 2012). However none of these studies examined the stability and reliability of these connections with aging.

In **Chapter II**, age-related brain functional reorganization is examined using a statistical approach applied on brain functional connectivity method. The test-retest reliability of brain functional connectivity is first examined across scan sessions and across subjects. Those significant and reliable brain functional

connections are then compared quantitatively between two age-groups, followed by a brain network analysis after linking each functional connection to a particular functional network.

Previous studies using graph theory in fMRI data have shown that aging is accompanied by a reduction in global and local network efficiency (Achard and Bullmore 2007), yet other studies have reported differences in modularity with aging (Meunier et al. 2009, Geerligs et al. 2014). In **Chapter III**, we extend these previous findings by examining age-related network reorganization within different functional networks as well as at regional level to identify critical brain areas where functional connectivity is significantly affected by aging effect. More specifically, network analysis based on graph theory is applied on two groups of normal healthy populations classified by age. Network properties including modularity (i.e., a measure of the community structure of a graph), global and local network efficiency (i.e., a measure of the level of global and local information processing, respectively), and functional connection strength (i.e., magnitude of temporal correlations between regions) are examined within each group and compared between groups. Multiple thresholds are applied to account for potential effect on group comparison due to thresholding of functional connectivity. A network disruption index, i.e., a measure of a radical reorganization of highly efficient "hub" regions, is used to determine age-related network reorganization and regional functional connectivity changes. This network model is further tested in different subjects and multiple scan sessions.

Structure of the thesis

To summarize, the main aim of this work is to build a network model for the human brain that represents a simplified interaction pattern in the complex brain system, in the same way as a roadmap represents the surrounding landscape. These interactions are examined as functional connectivity between brain regions. The network model is developed using graph theory. The thesis starts with examining the reliability of resting-state functional connectivity across different MRI scan sessions and across different subjects (**Chapter II**). A statistical approach, test-retest reliability, is used to examine the reliability of brain functional connectivity at the scale of individual functional connections between brain regions and at

whole brain-wide level of all connections. Brain functional connectivity is then compared between two groups of subjects classified by age, which shows rs-fMRI provides stable measurements for evaluating brain connectivity yet with an age-related decline in reliability. Then the complex pattern of functional interactions between brain regions is examined using graph-theory based network analysis based on rs-fMRI measurements (**Chapter III**). We found that brain organization is disrupted by aging with distinct patterns of alterations across different brain regions and different functional networks. Built on the findings we observed in normal healthy population, graph theory was further applied to epilepsy patients to provide insights of brain reorganizational changes due to abnormal disease interruption. The epilepsy patients, compared with age-matched healthy controls, showed abnormal increases in the number of functional connections between networks yet these connections were weakly connected leading to significantly reduced efficiency for information transfer among brain regions in the immediate neighborhood (**Chapter IV**). The last chapter (**Chapter V**) summarizes the main findings of the thesis, introduces preliminary work examining brain structural changes in stroke using DTI, and explores the potential of applying brain network modeling in clinical population to understand brain functional and structural reorganization under the presence of disease conditions.

References

Achard, S., and E. T. Bullmore. 2007. "Efficiency and cost of economical brain functional networks." *Plos Computational Biology* no. 3 (2):174-183. doi: ARTN e17
DOI 10.1371/journal.pcbi.0030017.

Alexanderson, G. L. 2006. "About the cover: Euler and Konigsberg's bridges: A historical view." *Bulletin of the American Mathematical Society* no. 43 (4):567-573. doi: Doi 10.1090/S0273-0979-06-01130-X.

Biswal, B. B., M. Mennes, X. N. Zuo, S. Gohel, C. Kelly, S. M. Smith, C. F. Beckmann, J. S. Adelstein, R. L. Buckner, S. Colcombe, A. M. Dogonowski, M. Ernst, D. Fair, M. Hampson, M. J. Hoptman, J. S. Hyde, V. J. Kiviniemi, R. Kotter, S. J. Li, C. P. Lin, M. J. Lowe, C. Mackay, D. J. Madden, K. H. Madsen, D. S. Margulies, H. S. Mayberg, K. McMahon, C. S. Monk, S. H. Mostofsky, B. J. Nagel, J. J. Pekar, S. J. Peltier, S. E. Petersen, V. Riedl, S. A. Rombouts, B. Rypma, B. L. Schlaggar, S. Schmidt, R. D. Seidler, G. J. Siegle, C. Sorg, G. J. Teng, J. Veijola, A. Villringer, M. Walter, L. Wang, X. C. Weng, S. Whitfield-Gabrieli, P. Williamson, C. Windischberger, Y. F. Zang, H. Y. Zhang, F. X. Castellanos, and M. P. Milham. 2010. "Toward discovery science of human brain function." *Proc Natl Acad Sci U S A* no. 107 (10):4734-9. doi: 10.1073/pnas.0911855107.

Biswal, B., F. Z. Yetkin, V. M. Haughton, and J. S. Hyde. 1995. "Functional Connectivity in the Motor Cortex of Resting Human Brain Using Echo-Planar Mri." *Magnetic Resonance in Medicine* no. 34 (4):537-541. doi: DOI 10.1002/mrm.1910340409.

Di Carlo, A. 2009. "Human and economic burden of stroke." *Age and Ageing* no. 38 (1):4-5. doi: DOI 10.1093/ageing/afn282.

Diestel, Reinhard. 2000. *Graph theory*. 2 ed: Springer.

Friston, K. J. 1994. "Functional and effective connectivity in neuroimaging: a synthesis." *Human Brain Mapping* no. 2 (1-2):56-78. doi: 10.1002/hbm.460020107.

Friston, K. J. 2002. "Beyond phrenology: What can neuroimaging tell us about distributed circuitry?" *Annual Review of Neuroscience* no. 25:221-250. doi: DOI 10.1146/annurev.neuro.25.112701.142846.

Geerligs, L., R. J. Renken, E. Saliasi, N. M. Maurits, and M. M. Lorist. 2014. "A Brain-Wide Study of Age-Related Changes in Functional Connectivity." *Cereb Cortex*. doi: 10.1093/cercor/bhu012.

Grady, C. L., M. V. Springer, D. Hongwanishkul, A. R. McIntosh, and G. Winocur. 2006. "Age-related changes in brain activity across the adult lifespan." *Journal of Cognitive Neuroscience* no. 18 (2):227-241.

Hagmann, P., M. Kurant, X. Gigandet, P. Thiran, V. J. Wedeen, R. Meuli, and J. P. Thiran. 2007. "Mapping Human Whole-Brain Structural Networks with Diffusion MRI." *Plos One* no. 2 (7). doi: ARTN e597
DOI 10.1371/journal.pone.0000597.

Jagust W, D'Esposito M. 2009. *Imaging the Aging Brain*: Oxford University Press.

Meier, T. B., A. S. Desphande, S. Vergun, V. A. Nair, J. Song, B. B. Biswal, M. E. Meyerand, R. M. Birn, and V. Prabhakaran. 2012. "Support vector machine classification and characterization of age-related reorganization of functional brain networks." *Neuroimage* no. 60 (1):601-13. doi: 10.1016/j.neuroimage.2011.12.052.

Meunier, D., S. Achard, A. Morcom, and E. T. Bullmore. 2009. "Age-related changes in modular organization of human brain functional networks." *Neuroimage* no. 44 (3):715-723. doi: DOI 10.1016/j.neuroimage.2008.09.062.

Park, H. J., and K. Friston. 2013. "Structural and functional brain networks: from connections to cognition." *Science* no. 342 (6158):1238411. doi: 10.1126/science.1238411.

Raz, N., U. Lindenberger, K. M. Rodrigue, K. M. Kennedy, D. Head, A. Williamson, C. Dahle, D. Gerstorf, and J. D. Acker. 2005. "Regional brain changes in aging healthy adults: General trends,

individual differences and modifiers." *Cerebral Cortex* no. 15 (11):1676-1689. doi: DOI 10.1093/cercor/bhi044.

Raz, N., K. M. Rodrigue, and E. M. Haacke. 2007. "Brain aging and its modifiers: insights from in vivo neuromorphometry and susceptibility weighted imaging." *Ann N Y Acad Sci* no. 1097:84-93. doi: 10.1196/annals.1379.018.

Resnick, S. M., D. L. Pham, M. A. Kraut, A. B. Zonderman, and C. Davatzikos. 2003. "Longitudinal magnetic resonance imaging studies of older adults: A shrinking brain." *Journal of Neuroscience* no. 23 (8):3295-3301.

Risacher, S. L., and A. J. Saykin. 2013. "Neuroimaging Biomarkers of Neurodegenerative Diseases and Dementia." *Seminars in Neurology* no. 33 (4):386-416. doi: DOI 10.1055/s-0033-1359312.

Rubinov, M., and O. Sporns. 2010. "Complex network measures of brain connectivity: Uses and interpretations." *Neuroimage* no. 52 (3):1059-1069. doi: DOI 10.1016/j.neuroimage.2009.10.003.

Salthouse, T. A. 1996. "The processing-speed theory of adult age differences in cognition." *Psychological Review* no. 103 (3):403-428. doi: Doi 10.1037/0033-295x.103.3.403.

Tononi, G., O. Sporns, and G. M. Edelman. 1994. "A Measure for Brain Complexity - Relating Functional Segregation and Integration in the Nervous-System." *Proceedings of the National Academy of Sciences of the United States of America* no. 91 (11):5033-5037. doi: DOI 10.1073/pnas.91.11.5033.

van de Ven, V. G., E. Formisano, D. Prvulovic, C. H. Roeder, and D. E. J. Linden. 2004. "Functional connectivity as revealed by spatial independent component analysis of fMRI measurements during rest." *Human Brain Mapping* no. 22 (3):165-178. doi: Doi 10.1002/Hbm.20022.

VanEssen, D. C., and H. A. Drury. 1997. "Structural and functional analyses of human cerebral cortex using a surface-based atlas." *Journal of Neuroscience* no. 17 (18):7079-7102.

Wu, T., Y. Zang, L. Wang, X. Long, M. Hallett, Y. Chen, K. Li, and P. Chan. 2007. "Aging influence on functional connectivity of the motor network in the resting state." *Neurosci Lett* no. 422 (3):164-8. doi: 10.1016/j.neulet.2007.06.011.

Figure 1: The geographic map of the Konigsberg Bridges. Adapted from (Alexanderson 2006). The four land masses are labeled as A, B, C and D. The seven bridges are labeled as a, b, c, d, e, f and g.

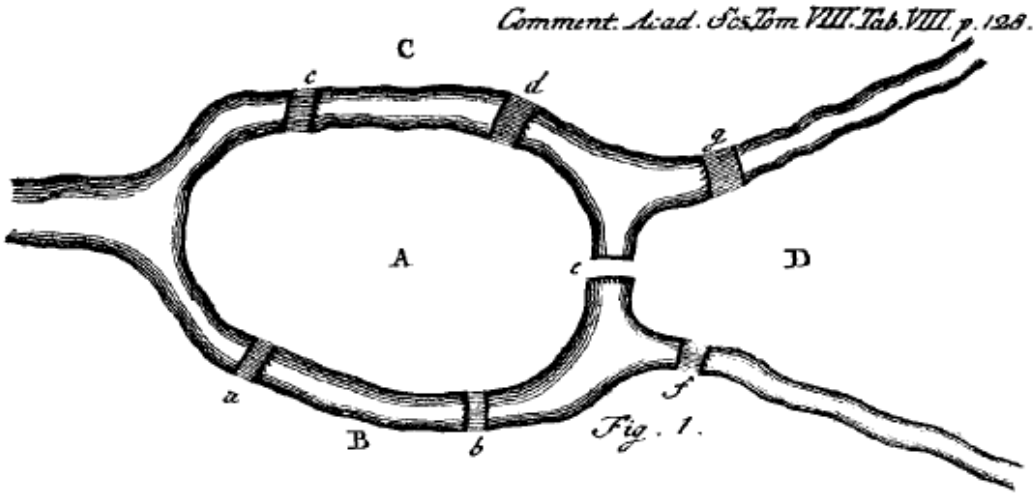

Figure 2: The graph representation of the Konigsberg Bridges—four land masses are represented by points and the seven bridges by lines which connect the points. Adapted from: http://physics.weber.edu/carroll/honors/konigsberg.htm

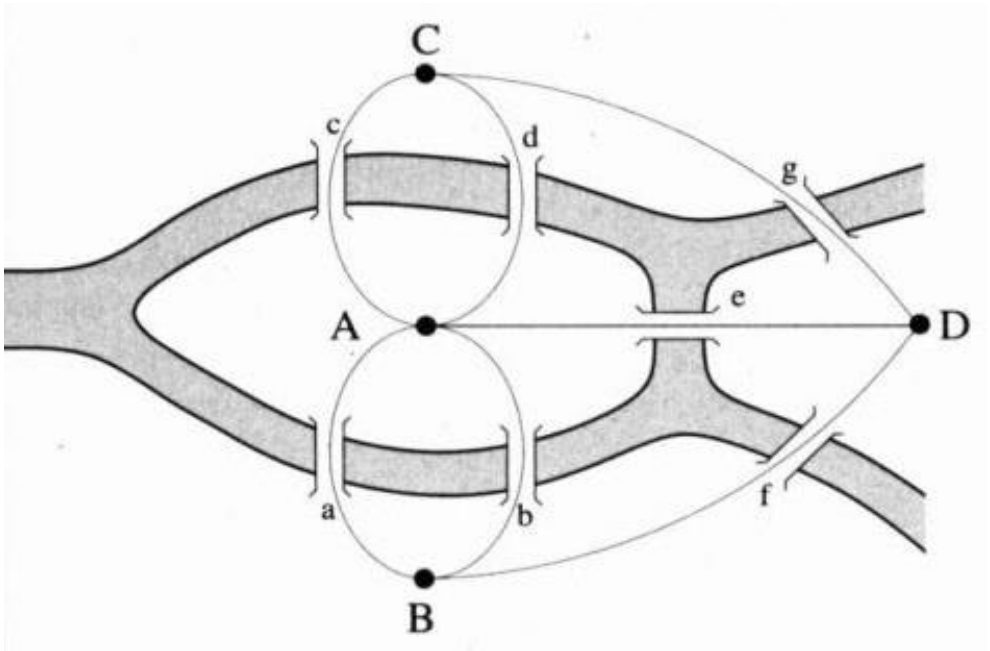

Chapter II

Age-related differences in test-retest reliability in resting-state brain functional connectivity

Jie Song, Alok S. Desphande, Timothy B. Meier, Dana L. Tudorascu, Svyatoslav Vergun, Veena A. Nair, Bharat B. Biswal, Mary E. Meyerand, Rasmus M. Birn, Pierre Bellec, Vivek Prabhakaran

Published in:

PLoS One. (2012) 7(12):e49847. doi: 10.1371/journal.pone.0049847.

Abstract

Resting-state functional MRI (rs-fMRI) has emerged as a powerful tool for investigating brain functional connectivity (FC). Research in recent years has focused on assessing the reliability of FC across younger subjects within and between scan-sessions. Test-retest reliability in resting-state functional connectivity (RSFC) has not yet been examined in older adults. In this study, we investigated age-related differences in reliability and stability of RSFC across scans. In addition, we examined how global signal regression (GSR) affects RSFC reliability and stability. Three separate resting-state scans from 29 younger adults (18-35 yrs) and 26 older adults (55-85 yrs) were obtained from the International Consortium for Brain Mapping (ICBM) dataset made publically available as part of the 1000 Functional Connectomes project www.nitrc.org/projects/fcon_1000. 92 regions of interest (ROIs) with 5 cubic mm radius, derived from the default, cingulo-opercular, fronto-parietal and sensorimotor networks, were previously defined based on a recent study. Mean time series were extracted from each of the 92 ROIs from each scan and three matrices of z-transformed correlation coefficients were created for each subject, which were then used for evaluation of multi-scan reliability and stability. The young group showed higher reliability of RSFC than the old group with GSR (p-value = 0.028) and without GSR (p-value < 0.001). Both groups showed a high degree of multi-scan stability of RSFC and no significant differences were found between groups. By comparing the test-retest reliability of RSFC with and without GSR across scans, we found significantly higher proportion of reliable connections in both groups without GSR, but decreased stability. Our results suggest that aging is associated with reduced reliability of RSFC which itself is highly stable within-subject across scans for both groups, and that GSR reduces the overall reliability but increases the stability in both age groups and could potentially alter group differences of RSFC.

Keywords: resting-state fMRI, functional connectivity, test-retest reliability, aging, global signal regression

Introduction

Since the discovery that the human brain at rest consists of spatially distributed but functionally connected regions in which coherent patterns of low-frequency fluctuations in the blood oxygen level-dependent (BOLD) signal are temporally correlated [1], resting-state functional MRI (rs-fMRI) has been used extensively for investigating brain functional connectivity (FC). Resting-state functional connectivity (RSFC) provides insight into the large scale structure of interactions between brain regions that support the integrated deviations of disease states from normally observed human health. These deviations may be a fundamental causative factor in both neuropathologic and neurodevelopmental conditions such as dementia [2-3], autism [4-6], schizophrenia [7-9], depression [10-11] and other conditions.

The reliability and stability of the RSFC method is critical to establish in normals as well as in normal development and normal aging so that deviations from these healthy states can be assigned to a particular disease state with certainty. Here, reliability is defined as the reproducibility of functional connections for a given subject across scan sessions, quantified with Intraclass Correlation coefficients (ICC). Reliability of RSFC has been evaluated in healthy young adults [12], and in healthy children as well as adolescents [13]. Stability is defined as the consistency of functional connections for a given subject across scans (within-subject) or in a given scan session across subjects (between-subject), quantified with Kendall's coefficient of concordance (W). Spatial consistency of RSFC has been demonstrated on young normal adults [14-16]. Although these results are encouraging, much more work needs to be done in order to explore normal age-related differences in RSFC. Previous studies on functional brain networks indicated that cost efficiency was reduced significantly in older normal people based on analyses of network efficiency [17], and that normal aging was associated with changes in modular organization of functional networks based on a graph theoretical analysis [18]. Furthermore, the modular organization of structural brain networks was similar between the young and middle age groups, but quite different from the old group based on an analysis of topological organization of structural brain networks in healthy individuals [19]. Another recent study found significant group-level variance in FC maps between young and old

groups [20]. However, to our knowledge, test-retest reliability and stability in RSFC has not yet been explicitly quantified in older adults. The main purpose of this study is to investigate test-retest reliability and stability of the RSFC parameters in both young and old groups.

In the present study, we divided all healthy subjects into two extreme groups by age. Study participants were selected from the ICBM dataset. The functional connectivity in the human brain consisting of 92 regions (Figure S1) was constructed by computing the correlation matrices across subjects and across each of the three scans. Similar to the method demonstrated in a recent study by Shehzad et al. [12] in which they assessed intersession (between-scan time-interval > 5 months), intrasession (between-scan time interval < 1 hour), and multi-scan (across all 3 scans) reliability and stability on 26 young adults, we measured multi-scan reliability and stability on both young and old adults based on region-of-interest (ROI) analyses. Our first goal was to compare test-retest reliability and stability of RSFC across scans between the young and old group.

Global signal, the spatial average of local signals from all cerebral voxels, has been suggested as a nuisance regressor for artifact reduction as it reflects coherent signal fluctuations across the brain [21]. While some studies indicate improved fMRI results after global signal regression [22], others suggest to avoid global scaling in fMRI analysis as it may decrease statistical power [23] and cause anti-correlations [24]. Our second goal in this study was to investigate how global signal regression (GSR) affects RSFC and the test-retest reliability and stability.

Results

Reliability of functional connectivity

To investigate the between-group differences of RSFC reliability, we calculated multi-scan ICCs for each correlation across all 3 scans for each group (Table 1). A reasonable criterion for interpreting ICC is that an ICC value of ≥ 0.75 is considered to be excellent/high reproducibility, ICC values in the range of 0.4 to 0.75 indicate fair to moderate reproducibility, and an ICC value of less than 0.4 indicates low to poor reproducibility [25]. In the present study, a threshold of an ICC value = 0.5 was used in order to confine

our age- and GSR-related analyses to functional connections that were reasonably reliable. Within each group, multi-scan ICC values for specific correlations were variable, ranging from effectively zero to moderate/high. Some multi-scan ICC measures are negative, theoretically, due to relatively lower between-subject variability compared with within-subject variability. However, the reasons for negative ICC values are still unclear [26] and our analysis was based on all positive ICCs.

Age-related differences in reliability of RSFC

Using Binomial proportion test, significant (i.e., correlation is significant at the group level for each of the 3 scans, p-value < 0.05 adjusted by FDR correction) and reliable (multi-scan ICC > 0.5) correlations was compared between the two groups (Figure 1; Table 2). We found that significantly higher proportion of reliable correlations from the young group than from the old group with GSR (p-value = 0.028; Figure S2) and without GSR (p-value < 0.001; Figure S3). The young group also showed significantly higher proportion of positive correlations as compared to the old group (p-value < 0.001) both with and without GSR (Table 3).

Significant versus non-significant correlations

Within each group, we tested the differences between significant and non-significant correlations using Wilcoxon rank-sum test, and we found that significant correlations were significantly more reliable than non-significant correlations ($p < 0.0001$ for both groups with GSR (Figure S4 a-b). The Wilcoxon rank-sum test was also used to test multi-scan ICCs without GSR and it showed that significant correlations were significantly more reliable than non-significant correlations only for the old group ($p < 0.0001$), and there was no significant difference between them in the young group ($p = 0.36$).

Positive versus negative correlations

Based on binomial proportion tests, we found significantly higher proportion of positive correlations than negative correlations in both groups with and without GSR ($p < 0.001$ for all comparisons) (Figure 2).

Negative correlations were found in both groups with GSR but none of them survived after FDR correction without GSR (Figure S4 c-d). The Wilcoxon rank-sum test suggested that multi-scan ICCs for positive correlations were significantly greater than for negative correlations ($p < 0.0001$ for all comparisons) in both groups with GSR.

Reliability and magnitude of functional connections

For each functional connection that was significant both with and without GSR, its magnitude (i.e., group-averaged multi-scan correlation coefficients) was Fisher z-transformed and plotted against the corresponding ICC value shown in Figure 3 and 4 for each group. Linear fitting revealed a trend of higher correlations leading to higher ICC measures (Figure 3-4, S5). Within each group, we carried out a Wilcoxon signed-rank test on the ICC values of these matched pairs of significant correlations. The results showed that ICC values were significantly greater without GSR (p-value < 0.0001). Within each group, a "left shift" of correlations was observed when GSR is applied (Figure 3b and Figure 4b), indicating reduced magnitude of correlations due to GSR.

Global signal regression factor in reliability of RSFC

Across all the connections between ROIs, using Binomial proportion test, we found significantly more reliable correlations without GSR than with GSR in both groups (p-value < 0.001, Figure 1, S2-3; Table 2), and significantly more positive correlations without GSR than with GSR (p-value < 0.001, Figure 2; Table 3). Within default and fronto-parietal network, we found significantly more reliable correlations with GSR than without GSR in both groups. However, it also showed significantly less reliable correlations between-network with GSR than without GSR in both groups (p-value < 0.001, Figure 5; Table 4). A direct comparison of ICC values with vs. without GSR was shown in Figure 6. ICC values for those reliable correlations (ICCs > 0.5) were reduced after GSR (i.e., regression lines were underneath the y=x line for ICCs > 0.5.)

Network analysis of significant and reliable correlations

Among 92 ROIs, 17 in the fronto-parietal network, 19 are in the default-mode network, 23 in the cingulo-opercular network and 33 in the sensorimotor network (Figure S1; Table S1). We found 1) highest number of significant and reliable correlations between regions in the sensorimotor network (Figure 5; Table 5), 2) least number of significant and reliable correlations between regions in the cingulo-opercular network in both groups with and without GSR (Figure 5; Table 5), 3) the old group had significantly less number of reliable correlations between-network than the young group with and without GSR (p-value < 0.001, Figure 5; Table 6), 4) the old group had significantly more reliable correlations within fronto-parietal and sensorimotor networks without GSR than the young group (p-value < 0.006, Figure 5; Table 6).

Group-level consistency across scans

We also assessed the consistency of group-averaged functional connectivity across scans. Group-level correlation matrices were obtained by averaging all z-transformed correlation coefficients across all subjects for each scan and each group. The reverse transformation was run on each resulting mean correlation coefficient, resulting in the creation of three 1 by 4186 matrices of correlation coefficients for each group. Group-averaged correlations for all three scans were then plotted against each other and the results exhibited high consistency between any two of them for both groups (Figure 7).

Stability of functional connectivity

To investigate the stability of RSFC, we measured the consistency of correlations within and between subjects using Kendall's W. More specifically, within each subject the rank order of correlations was evaluated across scans and within each scan session the rank order of correlations was evaluated across subjects. Within-subject across scans, Kendall's W measures were variable, ranging from moderate to high (Table 7). Between subjects within each scan, the measures were variable and much lower than the measures within-subject Kendall's W (Table 8).

Significant versus non-significant RSFC within subjects across scans

We compared the Kendall's W for significant and non-significant correlations within each subject across all three scans (Figure S6). The Wilcoxon rank-sum test demonstrated that significant correlations were significantly more stable than non-significant correlations for both groups with and without GSR (p-value < 0.0001 for all comparisons).

Positive versus negative RSFC within subjects across scans

The Wilcoxon rank-sum test demonstrated that positive correlations were significantly more stable than negative correlations for both groups with GSR (p-value < 0.0001 for all comparisons). No negative correlations were observed without GSR.

Age-related differences in stability of RSFC

Using Wilcoxon rank-sum test, we found no significant difference in stability of significant correlations between the two groups (p-value = 0.572 with GSR and p-value = 0.136 without GSR, Figure 8). Similarly, no significant differences in positive correlations were found between groups (p-value = 0.794 with GSR and p-value = 0.115 without GSR).

Global signal regression factor in stability of RSFC

The Wilcoxon rank-sum test suggested that Kendall's W within-subject across-scan for significant correlations with GSR was significantly greater than without GSR for both groups (p-value < 0.0001; Figure 8). For positive correlations, the old group showed significantly higher stability with GSR than without GSR (p-value = 0.024) but no significant differences in the young group (p-value = 0.768).

Stability between subjects within scan

We found the stability of RSFC for each scan was highly similar between subjects within scan (Figure 9) but much lower as compared to the stability of RSFC within subject across scans (Table 7-8). Higher stability of RSFC between subjects within scan was observed with GSR than without GSR (Figure 9, S7; Table 8).

Discussion

Growing evidence suggests that human brains undergo dynamic functional reorganizations during the lifespan. Resting-state functional connectivity provides insight into this large scale structural interaction between brain regions. The goal of the current study was to investigate age-related differences in reliability and stability of resting-state functional connectivity across scan sessions. We found that RSFC is more reliable for the young group and highly consistent for both groups, and that, consistent with previous studies [12, 24, 27, 28], regressing the global signal altered group differences of between-region functional connections.

Reliability

Highest reliability of RSFC in significant correlations

Multi-scan ICCs for statistically significant and positive significant correlations with GSR across subjects in each group exhibited higher degree of test-retest reliability compared with non-significant, and/or negative significant correlations. **Table S2** and **S3** display the significant and reliable functional connectivity measures which were observed to be part of the same functional networks, or corresponding with task-evoked activations. For example, we observed the most highly reliable (multi-scan ICC = 0.81) correlations between regions of left parietal and right precentral gyrus which were part of sensorimotor network in the old group without GSR. Correspondingly, correlations between regions of dorsal frontal cortex (dFC) and regions of inferior parietal lobe (IPL) as part of the fronto-parietal network were highly reliable (multi-scan ICC = 0.76) in the young group without GSR. Regions of the right thalamus and left

thalamus which were part of cingulo-opercular network were highly correlated (multi-scan ICC = 0.78) in the young group with GSR. Regions of right angular gyrus and left posterior cingulate cortex, part of default-mode network, exhibited highly reliable correlations (multi-scan ICC = 0.79) in the old group with GSR. These results are in agreement with task-evoked activations which have been demonstrated in previous studies [1, 15, 29-32].

Age-related differences in reliability of RSFC

Using the Binomial proportion test, we found significantly higher proportion of reliable correlations in the young group than in the old group across 92 ROIs. To further examine this difference in each correlation, we compared the RSFC within- and between-network and found that pronounced decreases in the proportion of reliable correlations between-network in the old group with and without GSR (p-value < 0.001, **Table 5-6**). However, the old group also showed pronounced increases in the proportion of reliable correlations within-network especially without GSR (p-value < 0.006, **Table 5-6**)

These findings suggest between-network connections may be more vulnerable to aging effects than within-network connections. This is consistent with our recent work using support vector machines which showed that between-network connections best differentiated older adults from younger adults based on their resting state functional connectivity [33]. Other studies have shown aging is associated with decreased functional connectivity in the DMN involving the superior and middle frontal gyrus, posterior cingulate cortices, and the superior parietal region [2, 20, 34-35]. Interestingly, we observed a significant increase in reliable connections in the DMN in the old group with GSR, whereas no significant differences were found in terms of the proportion of reliable correlations between the young and the old group without GSR. This further confirmed that group differences could be altered, or perhaps misinterpreted, after GSR [28].

GSR-related differences in reliability of RSFC

Binomial proportion test showed that the proportion of significant and reliable connections is significantly

decreased with GSR in both groups (**Figure 1**, **S2-3**; **Table 2**). Similarly, we observed significantly more positive correlations without GSR than with GSR in both group (**Figure 2**, **Table 3**). We also found that negative correlations were only present with GSR, exhibiting relatively low reliability (mean multi-scan ICCs < 0.3) and stability (multi-scan Kendall's *W* within subjects < 0.6 and between subjects within scan ≤ 0.06).These findings not only suggest higher reliability of RSFC without GSR than with GSR but also further confirms the observations in previous studies that GSR reduces the sensitivity for detecting true correlations [27] as well as negatively biases the correlations [24] and could fundamentally alter inter-regional correlations [28], especially when examining group differences.

Stability

Age-related differences in stability of RSFC

We examined all connections between ROIs across the pre-defined 92 seed regions using Wilcoxon rank-sum test. A high degree of multi-scan stability of RSFC within subjects was found in both groups and no significant difference between groups was observed (*p*-value = 0.572 with GSR and *p*-value = 0.136 without GSR). This suggests that functional connectivity observed from each subject is highly stable or consistent from scan to scan and this stability/consistency remains independent of aging effects. We also observed relatively lower Kendall's *W* scores across all correlations within each scan between subjects (**Table 8**), suggesting high individual variability exists in RSFC.

GSR-related differences in stability of RSFC

Although GSR significantly reduced the number of reliable connections in both groups (**Figure S2-3**; **Table 2-3**) especially those between-network connections (**Table 4**), it elevated the observed stability of RSFC both within-subject across scans (**Figure 8; Table 7**) and between subjects within scan (**Figure 9; Table 8**). These findings suggest GSR could potentially alter the pattern of RSFC in each observation from each subject and each scan and enhance the agreement/stability within subject from scan to scan or within scan from subject to subject. Furthermore, our results showed highly stable RSFC within each

individual across scan sessions (**Age-related differences in stability of RSFC**), suggesting highly consistent measurements of RSFC independent of aging factor. However, measures between subjects within each scan were relatively low, indicating the existence of individual variation. It may imply that variations of RSFC between individuals need further examination in order to discriminate from neuropathological changes.

Functional brain network with normal aging

Normal aging is associated with anatomical and functional changes as well as cognitive decline [34, 36]. However, the effect of aging on brain functional connectivity remains largely unknown. In the present study, we found fewer significant connections between ROIs from 92 pre-defined seed regions in the old group than in the young group. This is consistent with the observation made by Wu et al. [19], who investigated changes in small-world and modular organization of structural brain network with normal aging, demonstrating a notable decrease in the connector ratio and the intermodule connections in the old group.

Conversely, we observed concomitant age-related increases in reliable functional connections within sensorimotor and fronto-parietal networks. The old group showed significantly higher proportion of reliable connections than the young group without GSR within these two networks (**Figure 5; Table 5-6**). This could be potentially explained by a compensation mechanism that the decline of reliable functional connections between regions with aging, especially the long range connections between networks, is compensated by increased functional connections within networks.

In a recent study, Tomasi et al. [37] evaluated age-related effects on functional brain networks based on a sample of 913 healthy subjects using functional connectivity density mapping. In their study, global signal intensity was normalized across time points. They found that aging was associated with increases in long-range functional connectivity density in somatosensory and subcortical networks and pronounced decreases in the DMN and dorsal attention network. In our study, we also found that aging was associated with significant increases in proportion of functional connections in the sensorimotor network, whereas

no significant differences were found in DMN between the two age groups without GSR (**Figure 5; Table 5-6**). Interestingly, with GSR, there was increased proportion of reliable connections in DMN but no significant difference in the somatosensory network in the old group. This further draws attention to the issue of how global signal should be handled in data pre-processing in order to avoid the potential misinterpretation of group differences at functional network level. Research has shown an age-related reduction in occipital activity coupled with increased frontal activity, which is known as posterior-anterior shift in aging (PASA) [38], and age-related increases and correlations with parietal activity. In our study, occipital was not covered by the pre-defined seed regions, however, we observed increases in reliable connections in fronto-parietal network with aging without GSR (**Figure 5; Table 5-6**). The frontal-parietal network is engaged by a wide range of higher level cognitive tasks and is thought to be involved in active and adaptive task control [39]. This increase in reliable connections within frontal-parietal network might compensate the age-related decline in adaptive task control.

The cingulo-opercular network is engaged in a variety of tasks and thought to contribute to the flexible control of human goal-directed behavior and affect downstream sensorimotor processing through the stable task-set maintenance [39]. We observed the least number of reliable connections within cingulo-opercular network in both groups without age-related differences (**Table 5-6**), suggesting dynamic changes in functional connections within this network throughout adults' lifespan.

Additionally, GSR plays a significant role in the observed RSFC. We conclude that GSR reduces the overall reliability of RSFC (**Figure 1-2; Table 1-3**) but increases the stability in both age groups (**Figure 8-9; Table 7-8**), and that GSR affects the interpretation of group differences, especially, in each brain network presented in this study (**Figure 5; Table 4**).

Several alternatives to global signal regression have been proposed such as applying principal components analysis (PCA) to resting-state fMRI time-series in order to regress out the component most correlated with signal of interest [40-41]. Our future work will determine the test-retest reliability of connectivity measures using PCA.

Limitations

The age-related differences between young and old groups, presented in this study, were based on resting-state functional connectivity among 92 pre-defined seed regions. The axial slice acquisition of the fMRI data prevented the inclusion of the occipital and cerebellar networks in our analysis, as several subjects included in the ICBM dataset did not have coverage in these regions. The use of ROIs across the whole brain would have been ideal in that we would be able to assess the reliability of each correlation drawn from an even larger sample, however, the statistical tests presented in our study still showed significant age-related differences in RSFC.

Group differences in head movement have been shown by Van Dijk et al. [42] to significantly affect correlations between seed regions. Given our recent work [33], using the same ICBM dataset, showing that significantly more motion in the old group, it should be noted that the motion in older subjects was fairly constant from time to time point with no large spikes of motion present. Interestingly, after removal of motion-sensitive correlations, more than 70% of total correlations were preserved, suggesting that motion may account for some of the differences in connectivity observed in this study but the overall results should be robust based on Binomial proportion test and Wilcoxon rank-sum test.

In the present study, we examined how GSR affects RSFC primarily due to the ongoing debate on the use of GSR when studying RSFC. We found GSR reduces the overall reliability in young and old groups, reduces the magnitude of correlations and could potentially alter group differences. As shown in **Figure 3, 4 and S5,** a higher correlation leads to a higher reliability score. Therefore, the reduced reliability score (i.e., ICC value) for a functional connection, when global signal is removed, might be confounded by the reduced correlations due to GSR. But overall, GSR, as a factor of reducing correlation values, reduces ICC measures and thus the reliability of functional connections. Other factors such as the magnitude of noise and/or motion which affect correlation values could also potentially have an impact on ICC measures.

Materials and Methods

Participants

Resting-state fMRI data were obtained from 29 younger adults (18-35 years, mean age = 25.8 years; 13 males/16 females) and 26 older adults (55-85 years, mean age = 64.7 years; 11 males/15 females). All participants are right-handed.

fMRI data acquisition

Three resting-state scans from each subject were acquired using a 3.0 Tesla scanner. Each scan consisted of 128 gradient-echo EPI functional volumes (TR = 2.0 seconds; 64 × 64 matrix, 23 axial slices). For 19 out of the 29 younger adults, two scans were acquired with voxel size $4 \times 4 \times 5.5$ mm^3 and the third one was $4 \times 4 \times 4$ mm^3, while the other 10 subjects had all three scans with voxel size $4 \times 4 \times 4$ mm^3. 20 out of 26 older adults, two scans were acquired with voxel size $4 \times 4 \times 5.5$ mm^3 and the third one was $4 \times 4 \times 4$ mm^3, while the other 6 subjects had all three scans with voxel size $4 \times 4 \times 4$ mm^3. All individuals were asked to keep their eyes closed during the scan. As stated earlier, resting-state fMRI data presented in our study were obtained from the International Consortium for Brain Mapping (ICBM) dataset which were made publically available in the 1000 Functional Connectomes project www.nitrc.org/projects/fcon_1000. Each contributor's respective ethics committee approved submission of deidentified data. The institutional review boards of NYU Langone Medical Center and New Jersey Medical School approved the receipt and dissemination of the data.

fMRI data preprocessing

Data were preprocessed using scripts slightly adapted from fcon_1000 using a combination of AFNI (version AFNI_2009_12_31_1431, http://afni.nimh.nih.gov/afni) and FSL (version 4.1.4, www.fmrib.ox.ac.uk/fsl). Data were first deobliqued and reoriented to RPI orientation for use in FSL. AFNI was then used to perform the initial preprocessing steps of 1) slice time correction for interleaved

acquisition using Fourier-space time series phase-shifting, 2) motion correction to the average of the time series by aligning each volume to the mean image using Fourier interpolation, 3) skull stripping, and 4) selecting the eighth image for subsequent use in co-registration of BOLD images to the high resolution anatomic image. Further data preprocessing was carried out using FSL and comprised 5) spatial smoothing using a Gaussian kernel with FWHM = 6 mm, and 6) normalizing all volumes by a single scaling factor. Band-pass filtering (0.005-0.1 Hz) and detrending to remove linear and quadratic trends for each subject were then performed using AFNI. Masks of preprocessed data for each subject were generated using FSL. Functional data were then transformed into MNI152 (Montreal Neurological Institute 152-brain template; voxel size = $3 \times 3 \times 3$ mm^3) space using a three-step process: First, a 6 degree of freedom linear affine transformation was carried out using FLIRT [43-44] to align the functional data into structural space. The anatomical image was then aligned to the standard MNI152 space using a 12 degree of freedom linear affine transformation using FLIRT. The resulting transformation was then applied to each subject's functional dataset.

Nuisance signal regression

Signal associated with nuisance covariates consisting of global signal, white matter (WM), CSF and 6 motion parameters obtained during the motion correction step were removed from the resulting preprocessed fMRI time-course data. WM and CSF masks were created by segmentation of each subject's structural images and then applied to functional images to extract the WM and CSF signals. The global signal was calculated by averaging across all voxels in the brain. Following the regression of nuisance covariates, the residual signals were demeaned and re-sampled to the standard MNI-152 space (voxel size = $3 \times 3 \times 3$ mm^3).

One goal of the current study was to examine how global signal regression (GSR) affected the reliability and stability of RSFC; therefore we pre-processed the data in two parallel analyses, with and without global signal regression (GSR).

Resting-state functional connectivity

Regions of interest

92 spherical ROIs with radius 5mm (**Figure S1**; **Table S1**), derived from several meta-analyses of task-related fMRI studies previously defined by Dosenbach et al. [45], were selected in our study. Dosenbach et al. extracted time series from 160 seed regions covering several networks. Due to axial slice selection, not all subjects from ICBM datasets had EPI coverage of the occipital lobe and cerebellum, which resulted in 92 seed regions mainly consisting of default-mode, cingulo-opercular, fronto-parietal and sensorimotor networks. Some subjects had no signal in these areas and therefore were not included in our study.

Statistical methodology

Functional connectivity

Mean time series from each ROI were extracted, imported into MATLAB (R2010a, Mathworks), and correlated with that from every other ROI. Pearson correlation coefficients were calculated for each pair of regions for each subject and each scan. The resulting correlation coefficients were then *z*-transformed for calculations of multi-scan intraclass correlation coefficient (ICCs), or transformed into a distance measure in order to calculate Kendall's coefficient concordance (Kendall's *W*).

To determine the significance of each correlation, a one-sample *t*-test was run on the *z*-transformed correlation coefficients for both young and old group. Group-level significance of each correlation was defined by a two-sided *p*-value of 0.05, which was then adjusted for multiple comparisons using false discovery rate (FDR) correction (total 4186 correlations). More specifically, a significant correlation needs to be significant at the group level for each of the 3 scans with p-value < 0.05 adjusted by FDR correction. Within each group, positive correlations were determined by a right-tailed one-sample *t*-test with a *p*-value of 0.05 adjusted by FDR correction. Similarly, negative correlations were determined by a left-tailed one-sample *t*-test with a *p*-value of 0.05 adjusted by FDR correction.

Reliability of functional connectivity

We attempted to examine if significant connections observed in a first scan session would be reproducible within-subject in the following sessions and any changes between-subject would be due to subject difference. Intraclass correlation is defined as a ratio of the variance of interest over the sum of the variance of interest plus error [46], and has been frequently used to measure test-retest reliability in fMRI data [12-13], [47-48]. We calculated the third ICC values defined by Shrout and Fleiss [46] as follows:

$$ICC(3,1) = \frac{BMS - EMS}{BMS + (k-1)EMS} \quad (1)$$

,where *BMS* is between-subjects mean square, *EMS* is residual/error mean square, and *k* is the number of scans per subject, which is 3 in our case.

Theoretically, high ICC values suggest that compared to between-subject variability (i.e., BMS), within subject variability (i.e., EMS) across scans is relatively smaller, indicating high consistency or reliability of within-subject RSFC.

Given multi-scan ICC for each correlation, we examined the effect of the following factors on the multi-scan reliability of RSFC. 1) Statistically significance: significant correlations were compared with non-significant correlations. 2) Patterns: significantly positive correlations were compared with that of significantly negative correlations. 3) Age: significant and reliable correlations in the young group were compared with those in the old group; 4) GSR: significant correlations obtained with GSR were compared with those without GSR within each group.

Stability of functional connectivity

We used Kendall's coefficient concordance (Kendall's *W*) to estimate if overall connections were consistent across subjects and across scans. Kendall's *W* is a measure of agreement among raters based on

ranks rather than values, and has been used to assess the concordance of time courses within an individual using fMRI data [49-50]. We calculated Kendall's *W* as follows:

$$W = \frac{12(\sum_{i=1}^{n} R_i^2 - n\overline{R}^2)}{k^2(n^3 - n)} \quad (2)$$

where k is the number of scans or number of subjects , n is the number of correlations, R_i is the sum rank of the ith correlation across scans or subjects, $\overline{R}$ is the mean of R_i's. Kendall's *W* reflects the agreement in the rank order of correlations across subjects or across scans. In other words, it indicates how stable RSFC is within-subject across scans or within-scan across subjects. As with ICCs, we examined the effect of the following factors on the multi-scan stability of RSFC: statistically significance, patterns, age, and GSR.

Statistical tests

With Binomial proportion test, one can test the hypothesis of the equality of two binomial proportions. In our study, it was used to test the proportion of significant correlations versus non-significant, positive versus negative correlations between the young and the old group. Significant and non-significant correlations are treated as binomial measures (i.e., 1's and 0's respectively) and we tested the proportion of 1's in one group versus that in the other group (i.e., young vs. old).

Within each group, we tested the differences between significant and non-significant as well as between positive and negative correlations using Wilcoxon rank-sum test, which is a nonparametric test allowing to test measures of ICC or Kendall's *W* that are not normally distributed.

Acknowledgments

We would like to thank Yunzhi Lin and Alejandro Munoz-Del-Rio for statistical guidance. We would also like to thank 1000 Functional Connectome Project for providing open access to resting state fMRI datasets and data processing scripts.

References

1. Biswal B, Yetkin FZ, Haughton VM, Hyde JS (1995) Functional connectivity in the motor cortex of resting human brain using echo-planar MRI. Magn Reson Med 34: 537-541.

2. Andrews-Hanna JR, Snyder AZ, Vincent JL, et al. (2007) Disruption of large-scale brain systems in advanced aging. Neuron 56: 924-35.

3. Seeley WW, Crawford RK, Zhou J, et al. (2009) Neurodegenerative diseases target large-scale human brain networks. Neuron 62: 42-52.

4. Cherkassky VL, Kana RK, Keller TA, Just MA (2006) Functional connectivity in a baseline resting-state network in autism. Neuroreport 17: 1687-1690.

5. Kennedy DP, Courchesne E (2008). The intrinsic functional organization of the brain is altered in autism. NeuroImage 39: 1877-1885.

6. Di Martino A, Shehzad Z, Kelly AMC, Roy AK, Gee DG, et al. (2009) Autistic traits in neurotypical adults are related to cingulo-insular functional connectivity. Am J Psychiatry 166: 891-899.

7. Zhou Y, Liang M, Tian L, Wang K, Hao Y, et al. (2007) Functional disintegration in paranoid schizophrenia using resting-state fMRI. Schizophr Res 97: 194-205.

8. Bluhm RL, Miller J, Lanius RA, Osuch EA, Boksman K, et al. (2007) Spontaneous low-frequency fluctuations in the BOLD signal in schizophrenic patients: anomalies in the default network. Schizophr Bull 33: 1004-1012.

9. Jafri MJ, Pearlson GD, Stevens M, Calhoun VD (2008) A method for functional network connectivity among spatially independent resting-state components in schizophrenia. NeuroImage 39: 1666-1681.

10. Veer IM, Beckmann CF, van Tol MJ, Ferrarini L, Milles J, et al. (2010) Whole brain resting-state analysis reveals decreased functional connectivity in major depression. Front Syst Neurosci 4: 41.

11. Lui S, Wu Q, Qiu L, Yang X, Kuang W, et al. (2011) Resting-state functional connectivity in treatment-resistant depression. Am J Psychiatry 168: 642-648.

12. Shehzad Z, Kelly AMC, Reiss P, Gee DG, Gotimer K, et al. (2009) The resting brain: unconstrained yet reliable. Cerebral Cortex 19: 2209-2229.

13. Thomason ME, Dennis EL, Joshi AA, Joshi SH, Dinov ID, et al (2011) Resting-state fMRI can reliably map neural networks in children. NeuroImage 55: 165-175.

14. Van De Ven VG, Formisano E, Prvulovic D, Roeder CH, Linden DEJ (2004) Functional connectivity as revealed by spatial independent component analysis of fMRI measurements during rest. Human Brain Mapping 22: 165-178.

15. Damoiseaux J, Rombouts S, Barkhof F, Scheltens P, Stam C, et al. (2006) Consistent resting-state networks across healthy subjects. Proc Natl Acad Sci U S A 103: 13848-13853.

16. Chen S, Ross TJ, Zhan W, Myers CS, Chuang KS, et al. (2008) Group independent component analysis reveals consistent resting-state networks across multiple sessions. Brain Res 1239: 141-151.

17. Achard S, Bullmore E (2007) Efficiency and cost of economical brain functional networks. PLoS Comput Biol 3: 174-183.

18. Meunier D, Achard S, Morcom A, Bullmore E (2009) Age-related changes in modular organization of human brain functional networks. NeuroImage 44: 715-723.

19. Wu K, Taki Y, Sato K, Kinomura S, Goto R, et al. (2012) Age-related changes in topological organization of structural brain networks in healthy individuals. Human Brian Mapping 33: 552-68.

20. Biswal B (2010) Towards Discovery Science of Human Brain Function. Proceedings of the National Academy of Science 107: 4734-4739.

21. Hampson M, Peterson BS, Skudlarski P, Gatenby JC, Gore JC (2002) Detection of functional connectivity using temporal correlations in MR images. Human Brain Mapping 15: 247-262.

22. Birn RM, Diamond JB, Smith MA, Bandettini PA (2006) Separating respiratory-variation-related fluctuations from neuronal-activity-related fluctuations in fMRI. NeuroImage 31: 1536-1548.

23. Della-Maggiore V, Chau W, Peres-Neto PR, McIntosh AR (2002) An empirical comparison of SPM preprocessing parameters to the analysis of fMRI data. NeuroImage 17: 19-28.

24. Murphy K, Birn RM, Handwerker DA, Jones TB, Bandettini PA (2009) The impact of global signal regression on resting state correlations: Are anti-correlated networks introduced? NeuroImage 44: 893-905.

25. Sampat MP, Whitman GJ, Stephens TW, Broemeling LD, Heger NA, et al. (2006) The reliability of measuring physical characteristics of speculated masses on mammography. British Journal of Radiology 79: S134-140.

26. Muller R, Buttner P (1994) A critical discussion of intraclass correlation coefficients Stat Med 13: 2465-2476.

27. Weissenbacher A, Kasess C, Gerstl F, Lanzenberger R, Moser E, et al. (2009) Correlations and anticorrelations in resting-state functional connectivity MRI: A quantitative comparison of preprocessing strategies. NeuroImage 47: 1408-1416.

28. Saad ZS, Gotts SJ, Murphy K, Chen G, Jo HJ, et al. (2012) Trouble at rest: how correlation patterns and group differences distorted after global signal regression. Brain Connect 2: 25-32.

29. Greicius MD, Krasnow B, Reiss AL, Menon V (2003) Functional connectivity in the resting brain: A network analysis of the default mode hypothesis. Proc Natl Acad Sci U S A 100: 253-258.

30. Fox MD, Snyder AZ, Vincent JL, Corbetta M, Van Essen DC, et al. (2005) The human brain is intrinsically organized into dynamic, anticorrelated functional networks. Proc Natl Acad Sci U S A 102: 9673-9678.

31. Toro R, Fox PT, Paus T (2008) Functional coactivation map of the human brain. Cereb Cortex 18: 2553-2559.

32. Van Den Heuvel M, Mandal R, Hulshoff Pol H (2008) Normalized cut group clustering of resting-state fMRI data. PLoS ONE 3: e2001.

33. Meier TB, Desphande AS, Vergun S, Nair VA, Song J, et al. (2012) Support vector machine classification and characterization of age-related reorganization of functional brain networks. Neuroimage 60: 601-613.

34. Damoiseaux J, Beckmann C, Arigita E, Barkhof F, Scheltens Ph, et al. (2008) Reduced resting-state brain activity in the “default network” in normal aging. Cerebral Cortex 18: 1856-1864.

35. Koch W, Teipel S, Mueller S, Buerger K, Bokde A, et al. (2010) Effects of aging on default mode network activity in resting state fMRI: does the method of analysis matter? NeuroImage 51: 280-287.

36. Good C, Johnsrude I, Ashburner J, Henson R, Friston K, et al. (2001) A voxel-based morphometirc study of ageing in 465 normal adult human brains. NeuroImage 14: 685-700.

37. Tomasi D, Volkow N (2012) Aging and functional brain networks. Molecular Psychiatry 17: 471, 549-558.

38. Davis SW, Dennis NA, Daselaar SM, Fleck MS, Cabeza R (2009) Que PASA? The posterior-anterior shift in aging. Cerebral Cortex 18: 1201-1209.

39. Dosenbach NUF, Fair DA, Miezin FM, Cohen AL, Wenger KK, et al. (2007) Distinct brain networks for adaptive and stable task control in humans. PNAS 104: 11073-11078.

40. Chai XL, Castanon AN, Ongur D, Whitfield-Gabrieli S (2012) Anticorrelations in resting state networks without global signal regression. Neuroimage 59: 1420-1428.

41. Carbonell F, Bellec P, Shmuel A (2011) Global and system-specific resting-state fMRI fluctuations are uncorrelated: principle component analysis reveals anti-correlated networks. Brain Connect 1: 496-510.

42. Van Dijk KR, Sabuncu MR, Buckner RL (2012) The influence of head motion on intrinsic functional connectivity MRI. Neuroimage 59: 431-438.

43. Jenkinson M, Smith S (2001) A global optimisation method for robust affine registration of brain images. Med Image Anal 5: 143-156.

44. Jenkinson M, Bannister P, Brady M, Smith S (2002) Improved optimization for the robust and accurate linear registration and motion correction of brain images. Neuroimage 17: 825-841.

45. Dosenbach NUF, Nardos B, Cohen AL, Fair DA, Power JD, et al. (2010) Prediction of individual brain maturity using fMRI. Science 329: 1358-1361.

46. Shrout PE, Fleiss JL (1979) Intraclass correlations: uses in assessing rater reliability. Psychol Bull 86: 420-428.

47. Caceres A, Hall DL, Zelaya FO, Williams SCR, Mehta MA (2009) Measuring fMRI reliability with the intra-class correlation coefficient. NeuroImage 45: 758-768.

48. Meltzer JA, Postman-Caucheteux WA, McArdle JJ, Braun AR (2009) Strategies for longitudinal neuroimaging studies of overt language production. NeuroImage 47: 745-755.

49. Baumgartner R, Somorjai R, Summers R, Richter W (1999) Assessment of cluster homogeneity in fMRI data using Kendall's coefficient of concordance. Magnetic Resonance Imaging 17: 1525-1532.

50. Zang YF, Jiang TZ, Lu YL, He Y, Tian LX (2004) Regional homogeneity approach to fMRI analysis. NeuroImage 22: 394-400.

Figure Legends

Figure 1: Effects of aging and GSR on reliability of RSFC. Frequency plots of multi-scan ICCs for significant and reliable correlations (i.e., *p*-value < 0.05 adjusted by FDR correction, ICC > 0.5) showed pronounced decreases in significant and reliable (SigRe) correlations with aging and GSR. (Y—Young, O—Old, wGSR—with GSR, woGSR—without GSR)

Figure 2: Effects of aging and GSR on positive correlations. Frequency plots of multi-scan ICCs for significant positive correlations showed pronounced decreases in positive (Pos.) correlations with aging and GSR.

Figure 3: Reliability of RSFC *vs.* magnitude of functional connections in the young group. A left shift of data points indicates a reduction in the magnitude of functional connections when GSR is applied. The Wilcoxon signed-rank test shows reduced ICC values when GSR is applied (*p*-value < 0.0001). Each data point represents a correlation that is significant both with and without GSR. Linear regression fits were overlaid on the data.

Figure 4: Reliability of RSFC *vs.* magnitude of functional connections in the old group. A left shift of data points indicates a reduction in the magnitude of functional connections when GSR is applied. The Wilcoxon signed-rank test shows reduced ICC values when GSR is applied (*p*-value < 0.0001). Each data point represents a correlation that is significant both with and without GSR. Linear regression fits were overlaid on the data.

Figure 5: Effects of aging and GSR on brain functional networks. Pie chart illustrates the proportion of significant and reliable functional connections within each network. Binomial proportion tests showed aging was associated with significant decreases in reliable connections between-network but increases within sensorimotor and fronto-parietal networks. Each percentage number indicates the proportion of functional connections within corresponding networks.

Figure 6: Scatterplot of ICC for connections with *vs.* without GSR. GSR tends to reduce the reliability of connections (i.e., regression lines are under y = x when ICC > 0.3 for the young group and ICC > 0.15 for the old group). Each data point indicates a significant connection from each group. Black lines represent linear regression fits of the data and red lines represent y=x.

Figure 7: Scan 1 *vs.* scan 2 *vs.* scan 3. Group-averaged correlations from each scan session are plotted against each other. High consistency of RSFC from scan to scan is observed independent of aging and GSR factor. Overlaid blue lines represent linear regression fits of the data points and the *r*-values of the fit represent Pearson correlations of the data points.

Figure 8: Effects of aging and GSR on stability of RSFC within-subject across scans. Frequency plots of Kendall's *W* across scan sessions for significant correlations showed pronounced decreases in Sig. correlations with GSR. High stability of RSFC from scan to scan remains independent of aging effects.

Figure 9: Effects of aging and GSR on stability of RSFC between-subject within scan. GSR could potentially enhance the agreement/stability across scan sessions from subject to subject. Each black dot represents Kendall's *W* between subjects within each scan. Cross points represent Kendall's *W* values averaged across three scans.

Table Legends

Table 1: Multi-scan ICC measures.
Table 2: Effects of aging and GSR on significant and reliable correlations.
Table 3: Effects of aging and GSR on positive significant correlations.
Table 4: Effects of GSR on brain functional networks.
Table 5: Network analysis of significant and reliable correlations.
Table 6: Effects of aging on brain functional networks.
Table 7: Kendall's W within-subject across scans.
Table 8: Kendall's W between-subject within scan.

Supporting Information Legends

Figure S1: Shown are 92 regions of interest (ROIs) used in this study taken from Dosenbach et al. (2010). All 92 ROIs are displayed on a surface rendering of the brain (ICBM 152) visualized with the BrainNet Viewer (http: //www.nitrc.org/projects/bnv/). Red dots represent the ROIs from the default mode network, yellow for fronto-parietal, green for cingulo-opercular and blue for sensorimotor network.

Figure S2: Illustration of the significant and reliable functional connections with GSR in the young group (**a**) and in the old group (**b**). The young group showed significantly higher test-retest reliability in RSFC than the old group with GSR (Fisher's exact test: p-value = 0.032).

Figure S3: Illustration of the significant and reliable functional connections without GSR in the young group (**a**) and in the old group (**b**). The young group showed significantly higher test-retest reliability in RSFC than the old group without GSR (p-value < 0.001).

Figure S4: Box plots of multi-scan ICCs for significant and non-significant correlations with GSR (left), and without GSR (right) for young (a) versus old group (b), and for positive significant and negative significant correlations with GSR (left), and without GSR (right) for young (c) versus old group (d). Red lines represent the mean ICCs for those correlations.

Figure S5: Group-averaged multi-scan correlation coefficients plotted against their corresponding multi-scan ICCs with GSR (left) and without GSR (right) for the young group (a) and for the old group (b). Rug plots are shown on each axis representing the distribution of correlations and multi-scan ICCs. Blue dots are multi-scan ICCs and the red lines represent the linear fitting.

Figure S6: Stability within subjects across scans. Shown are box plots of Kendall's W for all, significant, non-significant, positive significant and negative significant correlations with GSR (left), and without GSR (right) for the young (a) versus the old group (b). Red lines represent the mean values of Kendall's W within subjects across scans.

Figure S7: Stability between-subject within scans. Shown are box plots of Kendall's W for all, significant, non-significant, positive significant and negative significant correlations with GSR (left), and without GSR (right) for the young (a) versus the old group (b). Red lines represent the mean values of Kendall's W between-subject within scans.

Table S1: Listed are 92 ROIs with their MNI coordinates and respective functional networks. 19 ROIs are from the default-mode network, 23 ROIs from the cingulo-opercular network, 17 ROIs from the fronto-parietal network and 33 ROIs from the sensorimotor network.

Table S2: Listed are significant and reliable correlations (i.e., *p*-value < 0.05 adjusted by FDR correction, ICC > 0.5) with GSR for young group (**a**) and old group (**b**) (only multi-scan ICCs > 0.6 are shown here due to the large number of correlations with ICC exceeding 0.5). Mean Rs are group-averaged correlation values from each scan.

Table S3: Listed are significant and reliable correlations (i.e., *p*-value < 0.05 adjusted by FDR correction, ICC > 0.5) without GSR for young group (**a**) and old group (**b**) (only multi-scan ICCs > 0.6 are shown here due to the large number of correlations with ICC exceeding 0.5). Mean Rs are group-averaged correlation values from each scan.

Table 1 Multi-scan ICC measures

Correlations	Young	Old
With GSR		
All	0.32 ± 0.14	0.27 ± 0.16
Significant	0.35 ± 0.15	0.32 ± 0.16
Non-significant	0.30 ± 0.14	0.26 ± 0.16
Positive significant	0.38 ± 0.14	0.34 ± 0.16
Negative significant	0.28 ± 0.13	0.24 ± 0.14
Without GSR		
All	0.39 ± 0.15	0.37 ± 0.14
Significant	0.39 ± 0.15	0.38 ± 0.14
Non-significant	0.39 ± 0.13	0.35 ± 0.14
Positive significant	0.39 ± 0.15	0.38 ± 0.14
Negative significant	N/A	N/A

Table 1 Listed are the mean and standard deviation of multi-scan ICCs given for all, significant, non-significant, positive significant or negative significant correlations for each group with and without GSR.

Table 2 Effects of aging and GSR on significant and reliable correlations

	Young	**Old**
With GSR		
All Significant	1477	1099
Significant and Reliable	246	153
Proportion of Sig. and Rel.	0.167	0.139
Without GSR		
All Significant	3478	3050
Significant and Reliable	842	618
Proportion of Sig. and Rel.	0.242	0.203

Table 2 Binomial proportion tests demonstrated that 1) the young group had statistically more significant and reliable correlations (i.e., FDR corrected p-value < 0.05, ICC value > 0.5) than the old group with GSR (p-value = 0.028) and without GSR (p-value < 0.001), and 2) higher proportion of significant and reliable correlations were found without GSR than with GSR in both groups (p-value < 0.001).

Table 3 Effects of aging and GSR on positive significant correlations

	Young	**Old**
Total number of correlations	4186	4186
With GSR		
Positive significant	1070	884
Proportion of Positive Correlations	*0.256*	*0.211*
Negative Significant	409	209
Proportion of Negative Correlations	*0.098*	*0.050*
Without GSR		
Positive significant	3648	3304
Proportion of Positive Correlations	*0.871*	*0.789*
Negative Significant	0	0

Table 3 Binomial proportion test demonstrated that 1) both groups had higher proportion of positive significant correlations than negative significant correlations (p-value < 0.001); 2) both groups had higher proportion of positive correlations without GSR than with GSR (p-value < 0.001).

Table 4 Effects of GSR on brain functional networks

Network	**Young**		**Old**	
	Binomial ProportionTest	***p*-value (CI=95%)**	**Binomial ProportionTest**	***p*-value (CI=95%)**
Default	wGSR > woGSR	0.001	wGSR > woGSR	< 0.001
Fronto-parietal	wGSR > woGSR	< 0.001	wGSR > woGSR	0.008
Sensorimotor	Not equal	0.915	wGSR < woGSR	0.001
Cingulo-opercular	Not equal	0.444	Not equal	0.909
Between-network	wGSR < woGSR	< 0.001	wGSR < woGSR	< 0.001

Table 4 Binomial proportion test showed the proportion of reliable functional connections was significantly affected by GSR both within- and between-network.

Table 5 Network analysis of significant and reliable correlations

Network	Young	Old
With GSR		
Total # of Sig. Re. Corr.	246	153
Default	33 (13.4%)	44 (28.8%)
Fronto-parietal	32 (13.0%)	20 (13.1%)
Sensorimotor	83 (33.7%)	42 (27.5%)
Cingulo-opercular	7 (2.8%)	6 (3.9%)
Between-network	91 (37.0%)	41 (26.8%)
Without GSR		
Total # of Sig. Re. Corr.	842	618
Default	49 (5.8%)	32 (5.2%)
Fronto-parietal	26 (3.1%)	38 (6.1%)
Sensorimotor	281 (33.4%)	247 (40.0%)
Cingulo-opercular	32 (3.8%)	23 (3.7%)
Between-network	454 (53.9%)	278 (45.0%)

Table 5 Binomial proportion test demonstrated that 1) the young group had significantly more between-network correlations than the old group with and without GSR (p-value < 0.015), and 2) both groups had significantly higher proportion of between-network correlations without GSR than with GSR (p-value < 0.001). Listed in parentheses are proportions of significant and reliable correlations observed in each network.

Table 6 Effects of aging on brain functional networks

Network	Binomial ProportionTest	*p*-value (CI=95%)
With GSR		
Default	Old > Young	< 0.001
Fronto-parietal	Not equal	0.985
Sensorimotor	Not equal	0.181
Cingulo-opercular	Not equal	0.570
Between-network	Old < Young	0.015
Without GSR		
Default	Not equal	0.594
Fronto-parietal	Old > Young	0.004
Sensorimotor	Old > Young	0.005
Cingulo-opercular	Not equal	0.938
Between-network	Old < Young	< 0.001

Table 6 Binomial proportion test showed the old group had significantly more reliable correlations within network than the young group and less reliable correlations between-network.

Table 7 Kendall's *W* within-subject across scans.

Functional Connections	Young	Old
With GSR		
All	0.67 ± 0.06	0.64 ± 0.06
Significant	0.77 ± 0.05	0.76 ± 0.04
Non-significant	0.56 ± 0.07	0.54 ± 0.06
Positive significant	0.66 ± 0.04	0.66 ± 0.04
Negative significant	0.52 ± 0.08	0.48 ± 0.07
Without GSR		
All	0.67 ± 0.06	0.63 ± 0.06
Significant	0.65 ± 0.06	0.63 ± 0.06
Non-significant	0.56 ± 0.08	0.50 ± 0.07
Positive significant	0.65 ± 0.06	0.63 ± 0.06
Negative significant	N/A	N/A

Table 7 Listed are the mean and standard deviation of Kendall's *W* within subject across scans for all, significant, non-significant, positive significant and negative significant correlations for both groups.

Table 8 Kendall's *W* between-subject within scan.

Functional Connections	**Young**				**Old**			
With GSR	**Scan 1**	**Scan 2**	**Scan 3**	**Mean**	**Scan 1**	**Scan 2**	**Scan 3**	**Mean**
All	0.30	0.30	0.32	0.31	0.32	0.29	0.30	0.30
Significant	0.50	0.49	0.52	0.50	0.51	0.48	0.49	0.49
Non-significant	0.10	0.10	0.12	0.11	0.13	0.12	0.11	0.12
Positive significant	0.23	0.23	0.23	0.23	0.26	0.24	0.24	0.25
Negative significant	0.06	0.06	0.06	0.06	0.05	0.03	0.03	0.04
Without GSR								
All	0.27	0.28	0.28	0.28	0.29	0.25	0.27	0.27
Significant	0.24	0.24	0.25	0.24	0.25	0.24	0.24	0.24
Non-significant	0.08	0.06	0.06	0.06	0.07	0.07	0.05	0.06
Positive significant	0.24	0.24	0.25	0.25	0.25	0.24	0.24	0.24
Negative significant	N/A	N/A	N/A	N/A	N/A	N/A	N/A	N/A

Table 8 Listed are the mean and standard deviation of Kendall's *W* between subjects within scan for all, significant, non-significant, positive significant and negative significant correlations.

Figure 1

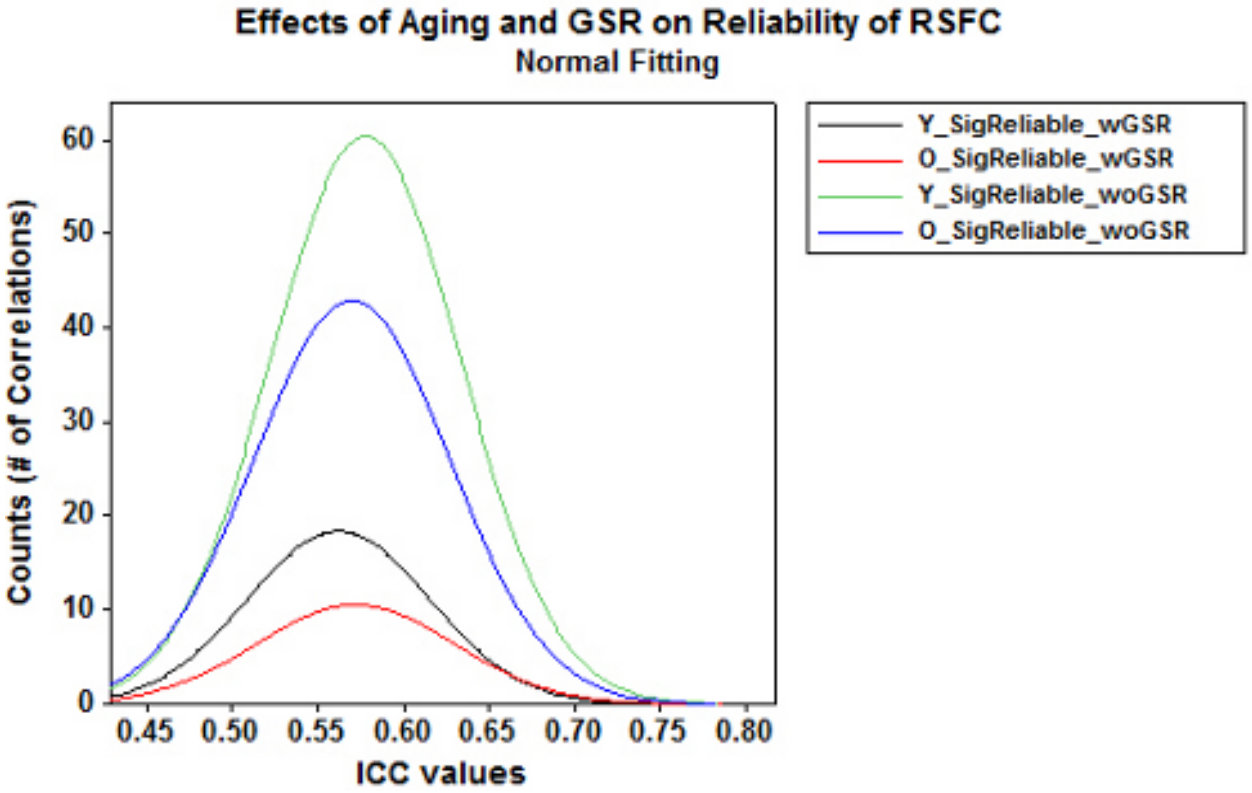
Effects of Aging and GSR on Reliability of RSFC
Normal Fitting
Y_SigReliable_wGSR
O_SigReliable_wGSR
Y_SigReliable_woGSR
O_SigReliable_woGSR
Counts (# of Correlations)
0
10
20
30
40
50
60
0.45
0.50
0.55
0.60
0.65
0.70
0.75
0.80
ICC values

Figure 2

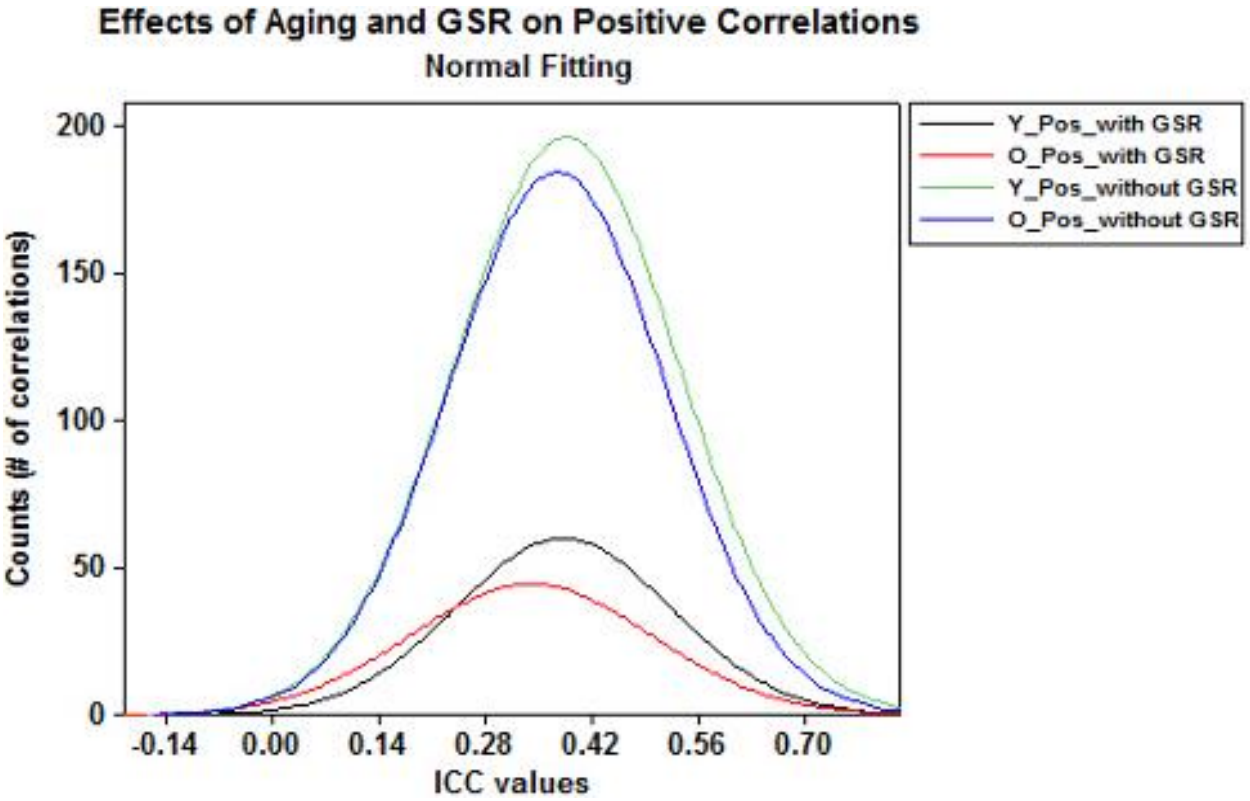
Effects of Aging and GSR on Positive Correlations
Normal Fitting
Y_Pos_with GSR
O_Pos_with GSR
Y_Pos_without GSR
O_Pos_without GSR
Counts (# of correlations)
200
150
100
50
0
-0.14
0.00
0.14
0.28
0.42
0.56
0.70
ICC values

Figure 3

a)

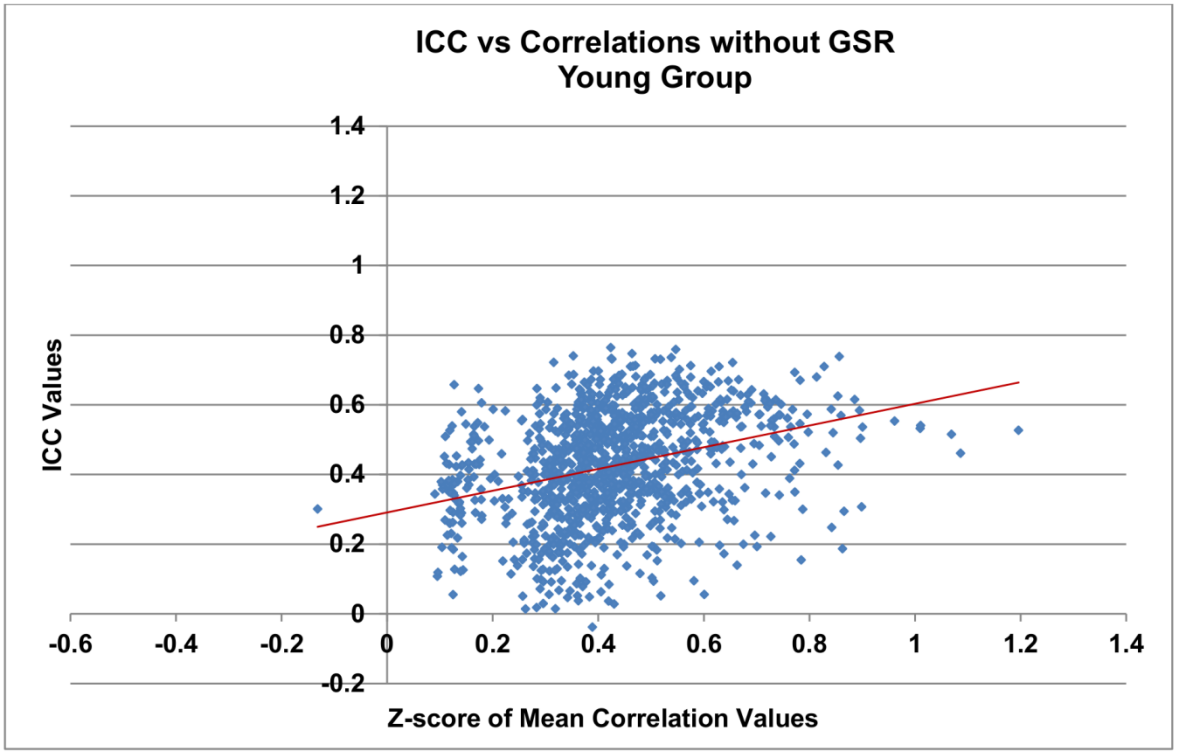
ICC vs Correlations without GSR
Young Group
ICC Values
Z-score of Mean Correlation Values
1.4
1.2
1
0.8
0.6
0.4
0.2
0
-0.2
-0.6
-0.4
-0.2
0
0.2
0.4
0.6
0.8
1
1.2
1.4

b)

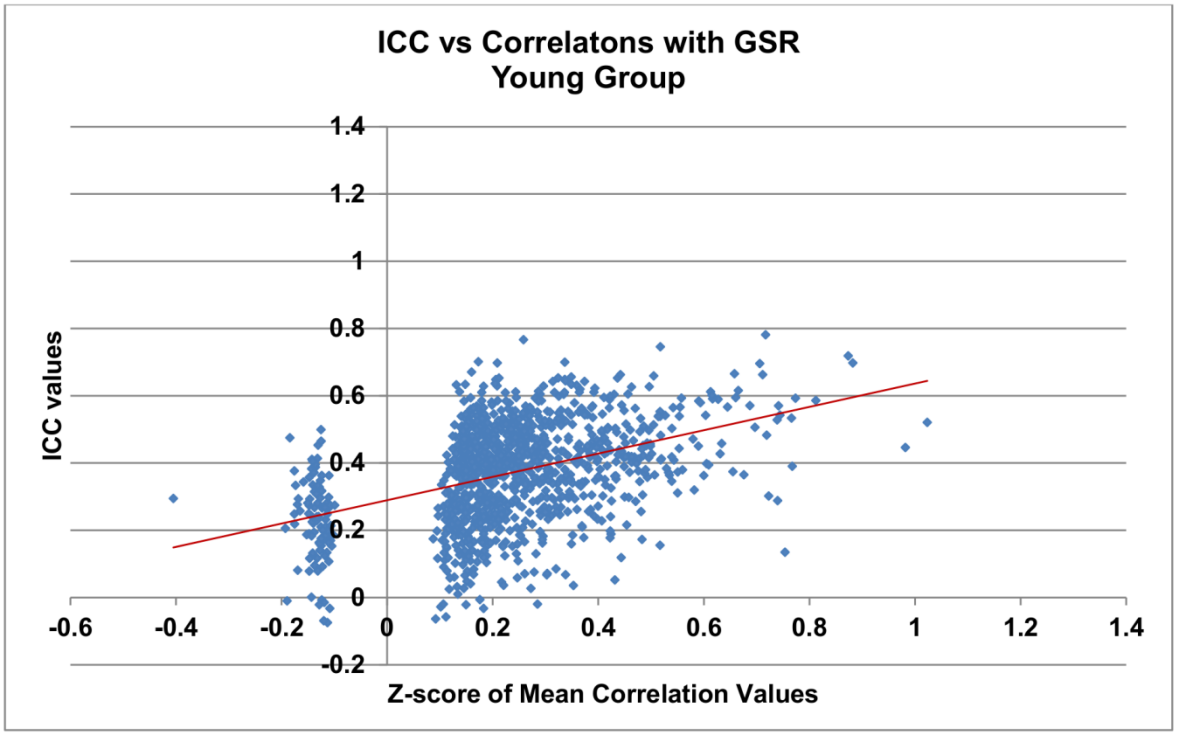
ICC vs Correlatons with GSR
Young Group
ICC values
Z-score of Mean Correlation Values
1.4
1.2
1
0.8
0.6
0.4
0.2
0
-0.2
-0.6
-0.4
-0.2
0
0.2
0.4
0.6
0.8
1
1.2
1.4

Figure 4

a)

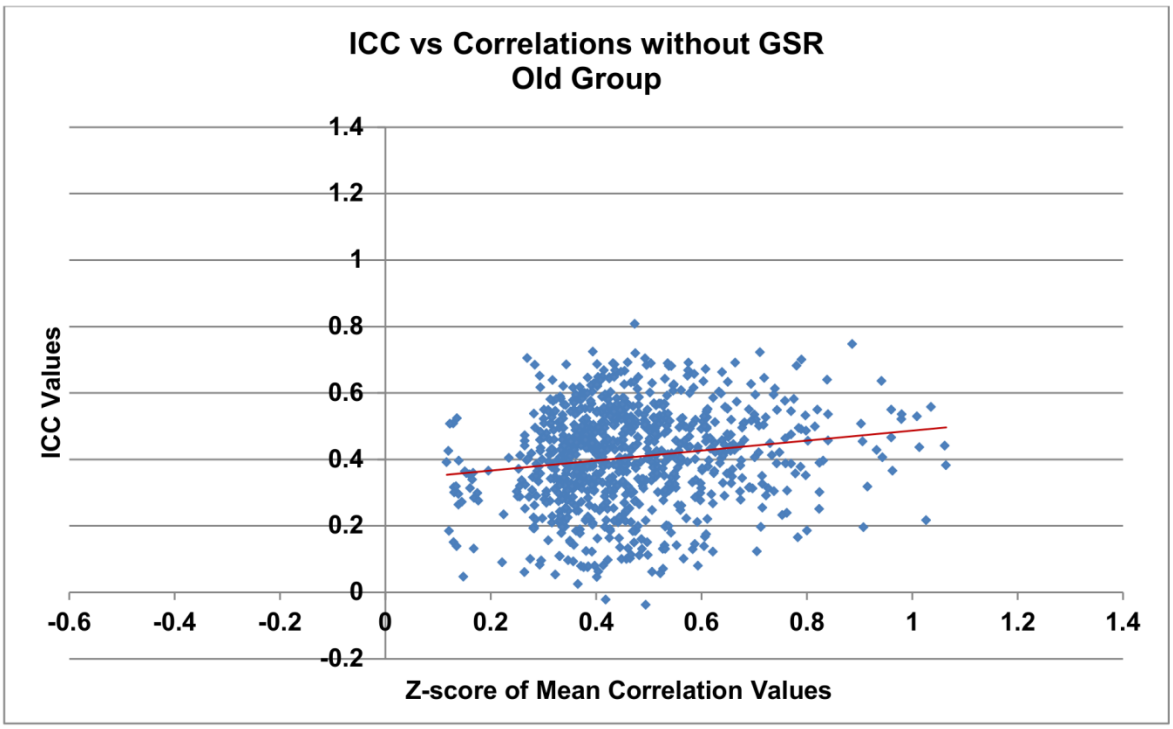
ICC vs Correlations without GSR
Old Group
ICC Values
1.4
1.2
1
0.8
0.6
0.4
0.2
0
-0.2
-0.6
-0.4
-0.2
0
0.2
0.4
0.6
0.8
1
1.2
1.4
Z-score of Mean Correlation Values

b)

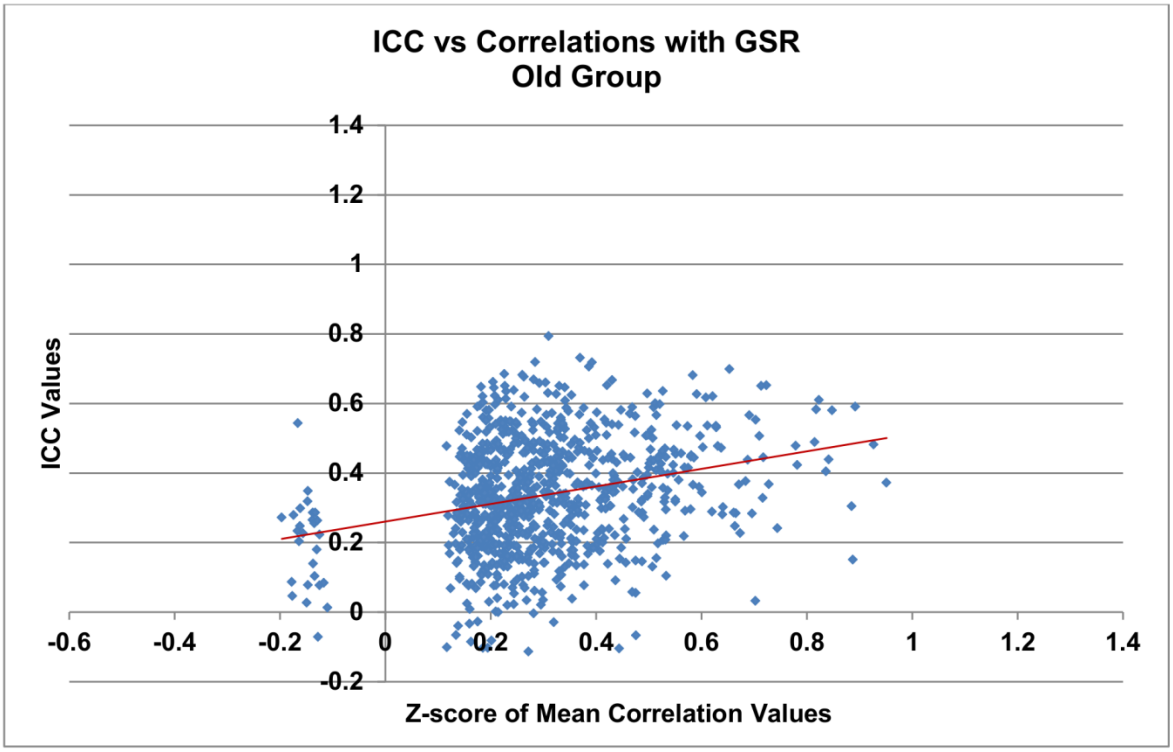
ICC vs Correlations with GSR
Old Group
ICC Values
1.4
1.2
1
0.8
0.6
0.4
0.2
0
-0.2
-0.6
-0.4
-0.2
0
0.2
0.4
0.6
0.8
1
1.2
1.4
Z-score of Mean Correlation Values

Figure 5

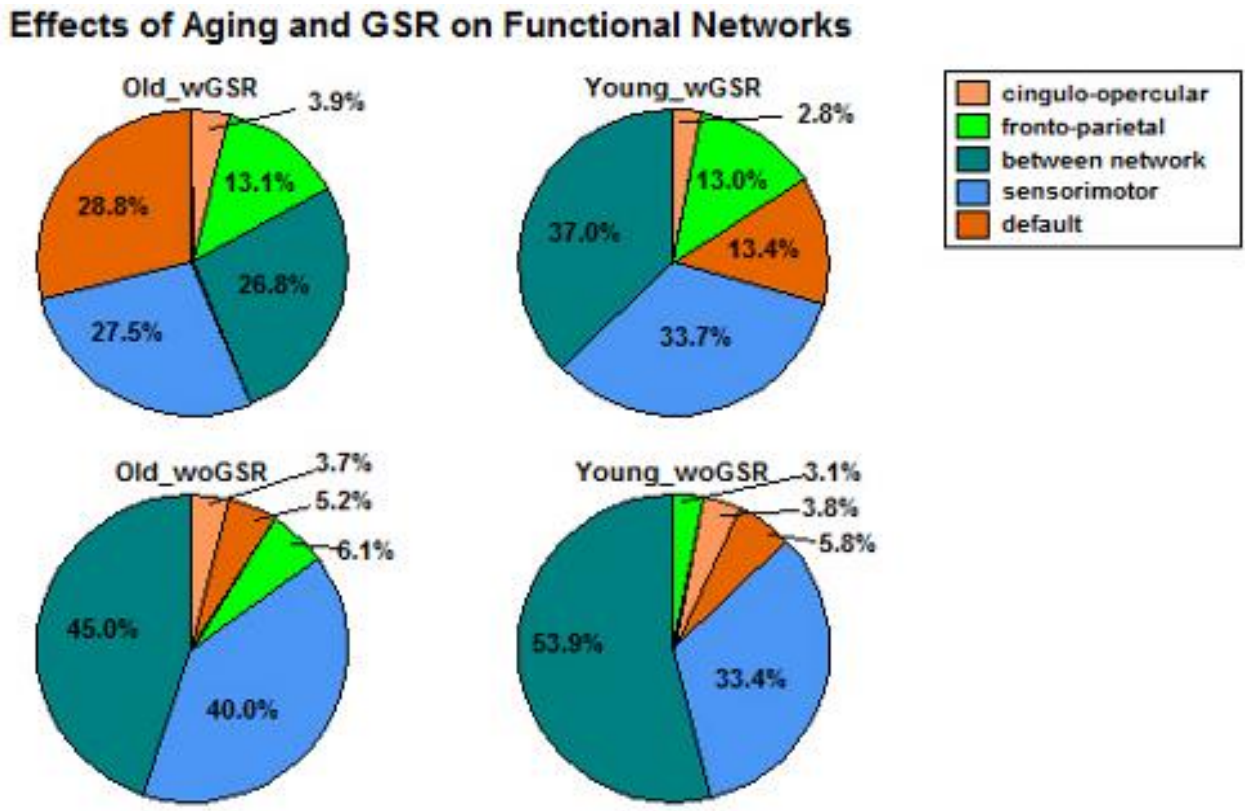
Effects of Aging and GSR on Functional Networks
Old_wGSR
3.9%
13.1%
28.8%
26.8%
27.5%
Young_wGSR
2.8%
13.0%
37.0%
13.4%
33.7%
cingulo-opercular
fronto-parietal
between network
sensorimotor
default
Old_woGSR
3.7%
5.2%
6.1%
45.0%
40.0%
Young_woGSR
3.1%
3.8%
5.8%
53.9%
33.4%

Figure 6

a)

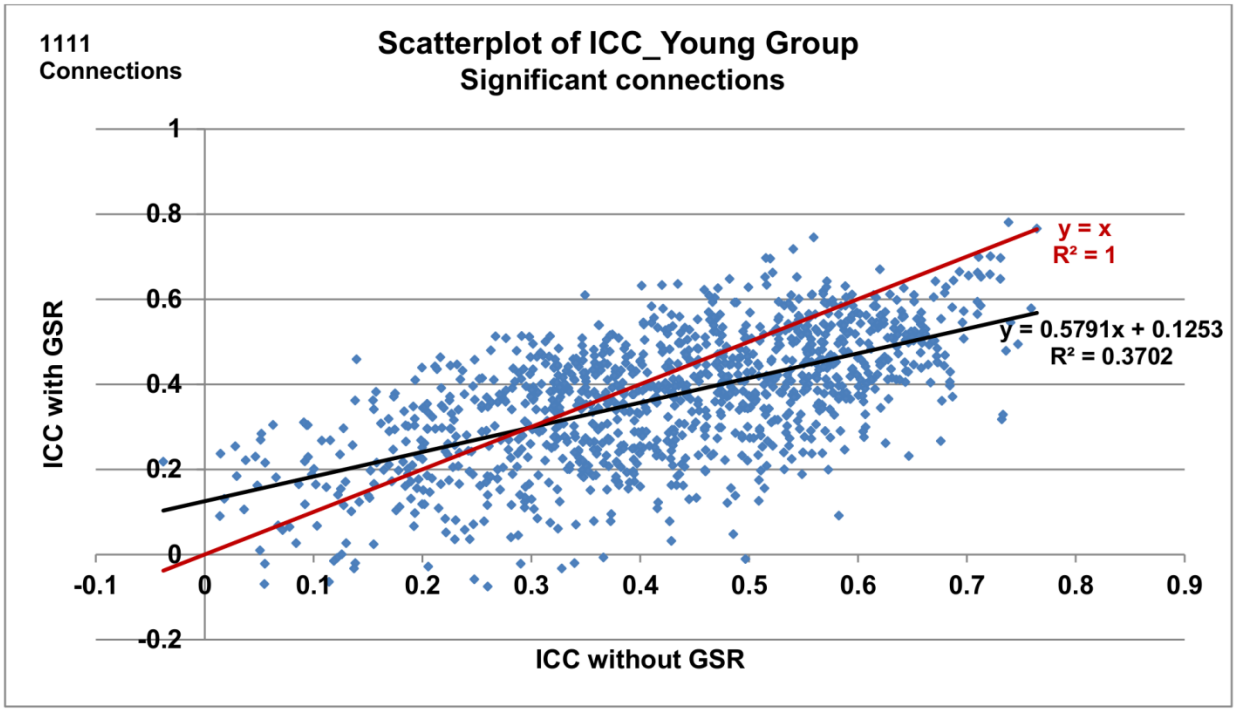
1111
Connections
Scatterplot of ICC_Young Group
Significant connections
y = x
R² = 1
y = 0.5791x + 0.1253
R² = 0.3702
ICC with GSR
ICC without GSR
1
0.8
0.6
0.4
0.2
0
-0.2
-0.1
0
0.1
0.2
0.3
0.4
0.5
0.6
0.7
0.8
0.9

b)

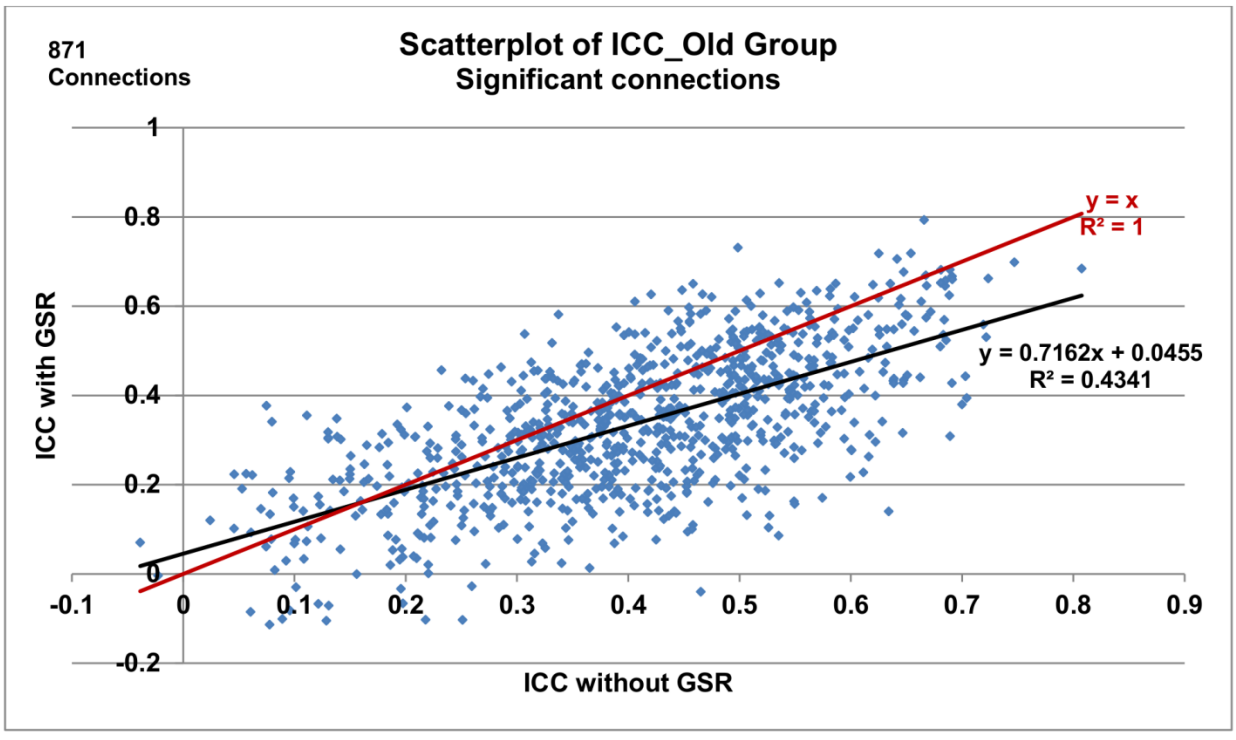
871
Connections
Scatterplot of ICC_Old Group
Significant connections
y = x
R² = 1
y = 0.7162x + 0.0455
R² = 0.4341
ICC with GSR
ICC without GSR
1
0.8
0.6
0.4
0.2
0
-0.2
-0.1
0
0.1
0.2
0.3
0.4
0.5
0.6
0.7
0.8
0.9

Figure 7

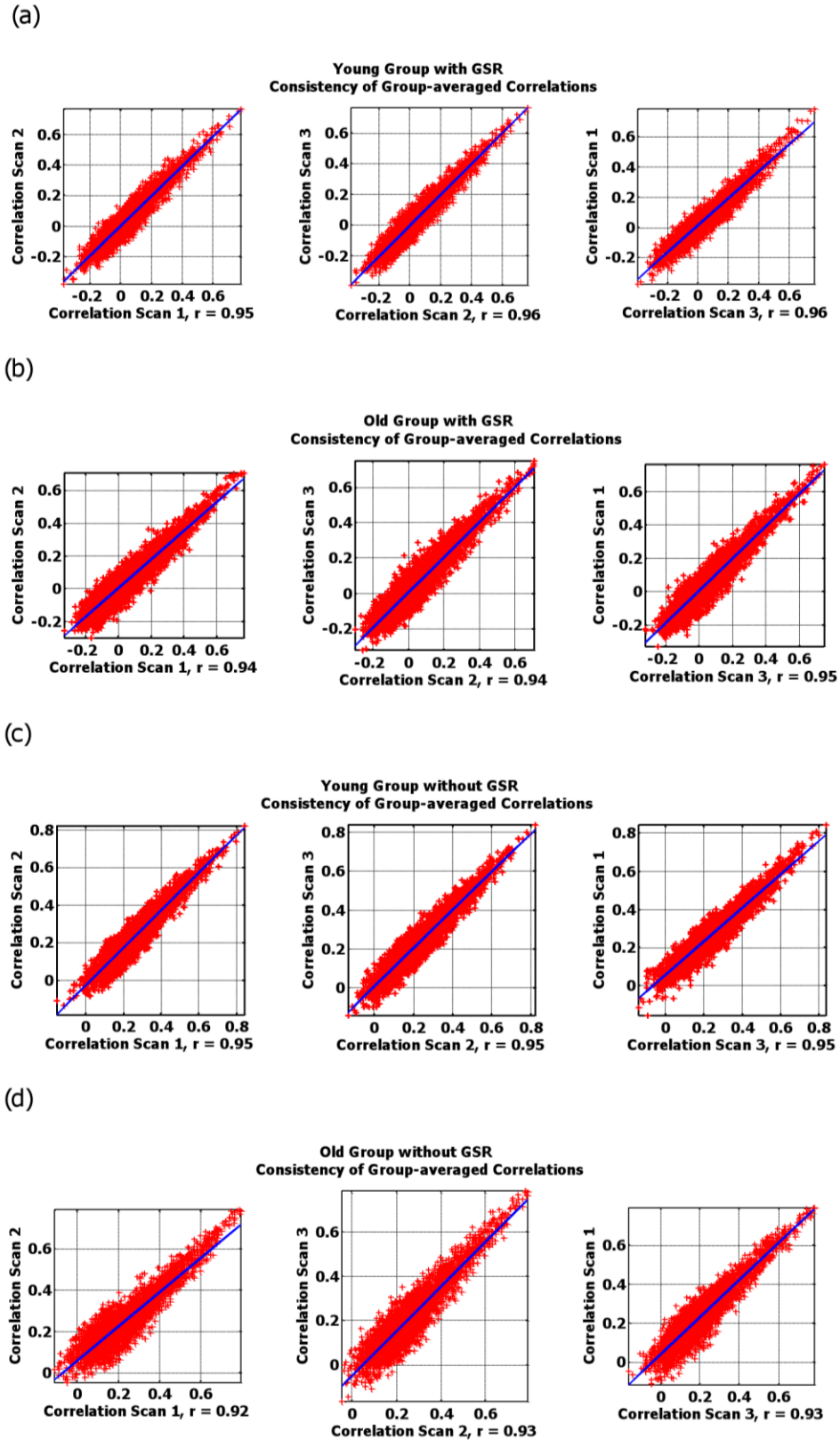
(a)
Young Group with GSR
Consistency of Group-averaged Correlations
Correlation Scan 2
Correlation Scan 1, r = 0.95
Correlation Scan 3
Correlation Scan 2, r = 0.96
Correlation Scan 1
Correlation Scan 3, r = 0.96
(b)
Old Group with GSR
Consistency of Group-averaged Correlations
Correlation Scan 2
Correlation Scan 1, r = 0.94
Correlation Scan 3
Correlation Scan 2, r = 0.94
Correlation Scan 1
Correlation Scan 3, r = 0.95
(c)
Young Group without GSR
Consistency of Group-averaged Correlations
Correlation Scan 2
Correlation Scan 1, r = 0.95
Correlation Scan 3
Correlation Scan 2, r = 0.95
Correlation Scan 1
Correlation Scan 3, r = 0.95
(d)
Old Group without GSR
Consistency of Group-averaged Correlations
Correlation Scan 2
Correlation Scan 1, r = 0.92
Correlation Scan 3
Correlation Scan 2, r = 0.93
Correlation Scan 1
Correlation Scan 3, r = 0.93

Figure 8

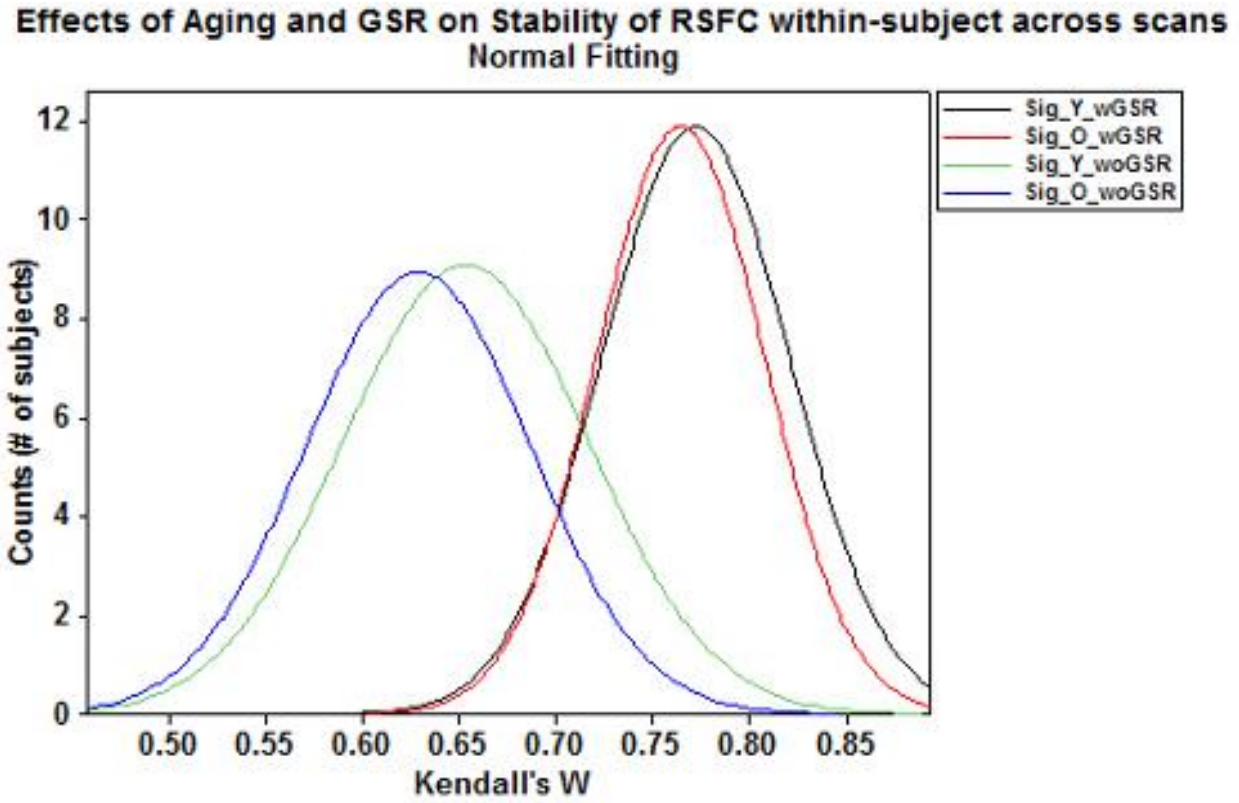
Effects of Aging and GSR on Stability of RSFC within-subject across scans
Normal Fitting
Sig_Y_wGSR
Sig_O_wGSR
Sig_Y_woGSR
Sig_O_woGSR
Counts (# of subjects)
0
2
4
6
8
10
12
0.50
0.55
0.60
0.65
0.70
0.75
0.80
0.85
Kendall's W

Figure 9

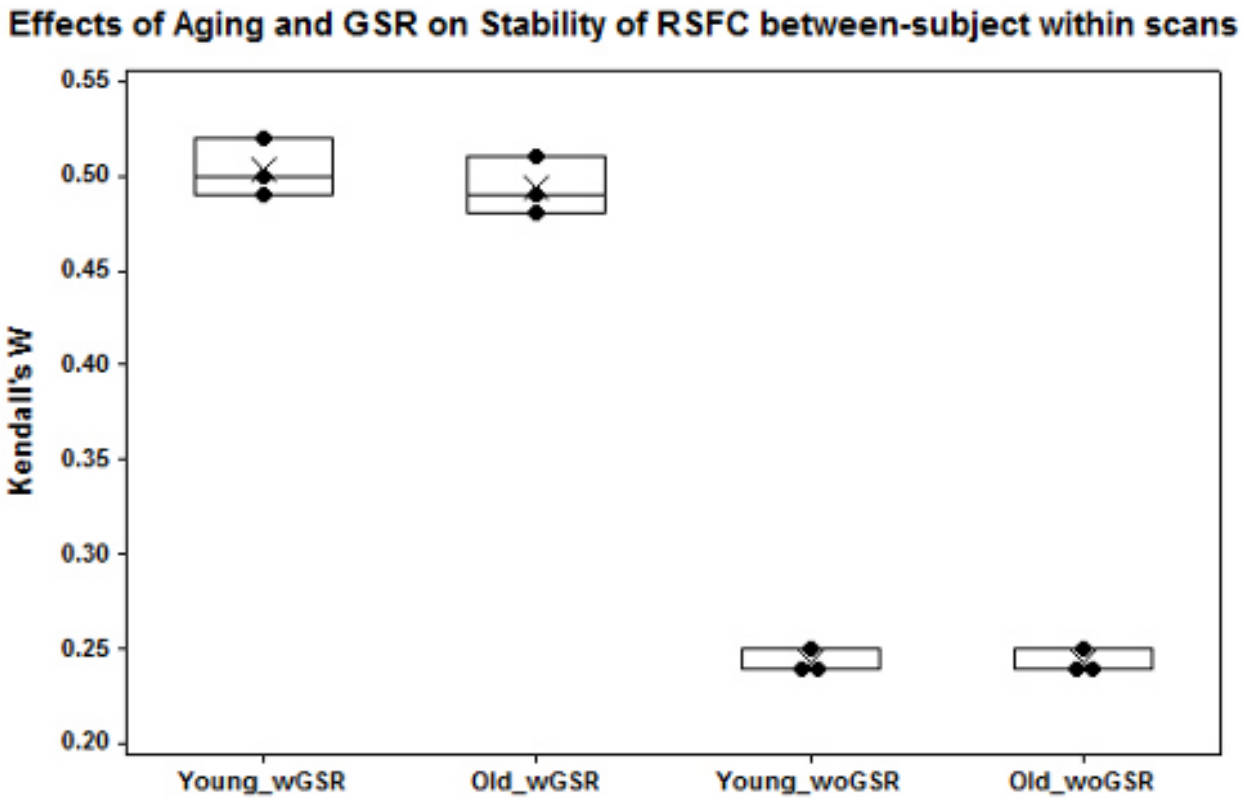
Effects of Aging and GSR on Stability of RSFC between-subject within scans
Kendall's W
0.55
0.50
0.45
0.40
0.35
0.30
0.25
0.20
Young_wGSR
Old_wGSR
Young_woGSR
Old_woGSR

Supplementary Materials

Figure S1 Shown are 92 regions of interest (ROIs) used in this study taken from Dosenbach et al. (2010).

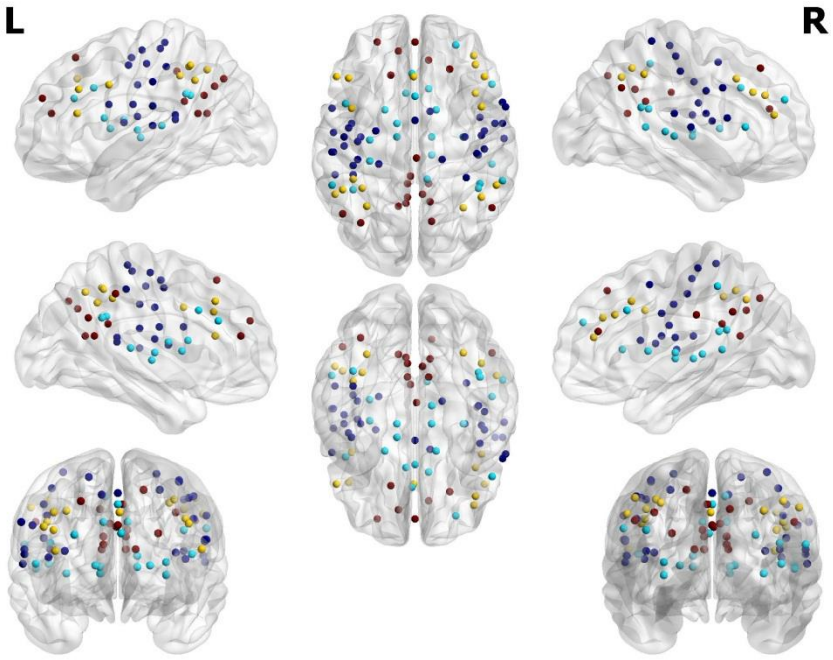

Figure S2 Illustration of the significant and reliable functional connections with GSR in the young group (**a**) and in the old group (**b**).

a)

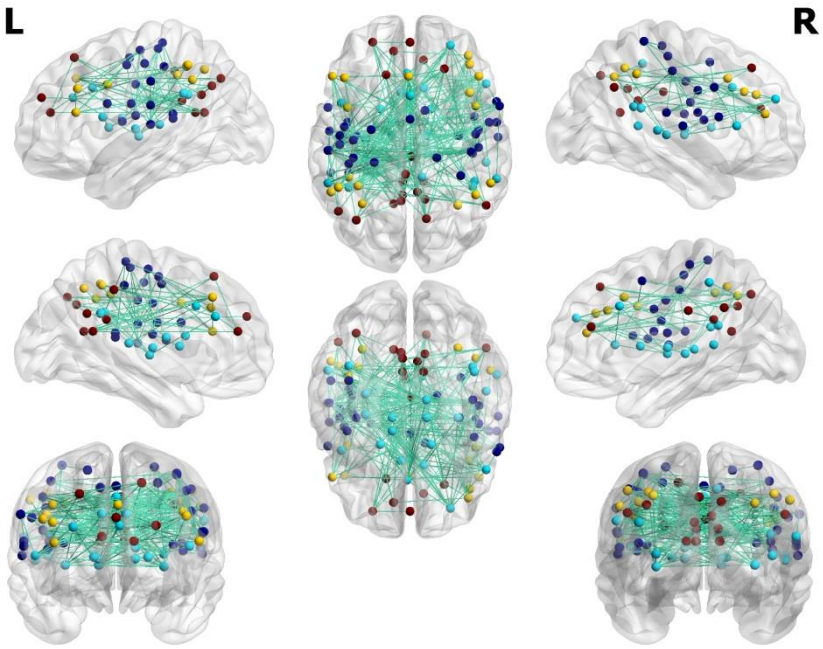

b)

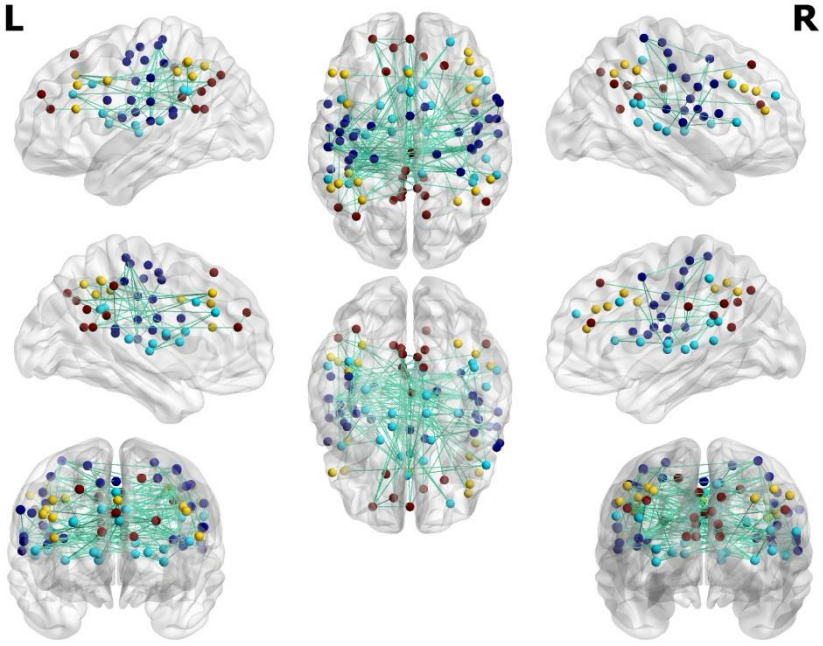

Figure S3 Illustration of the significant and reliable functional connections without GSR in the young group (**a**) and in the old group (**b**).

a)

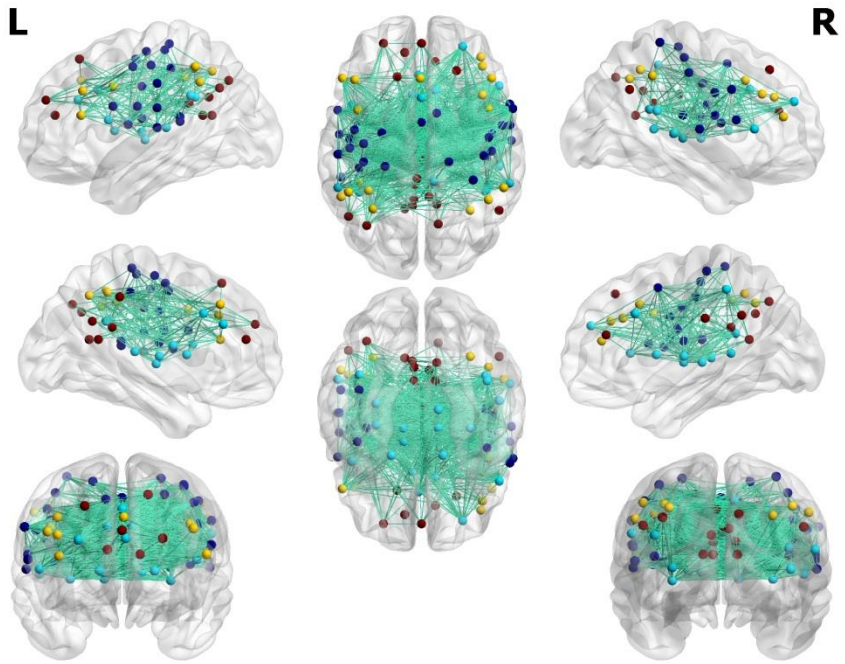

b)

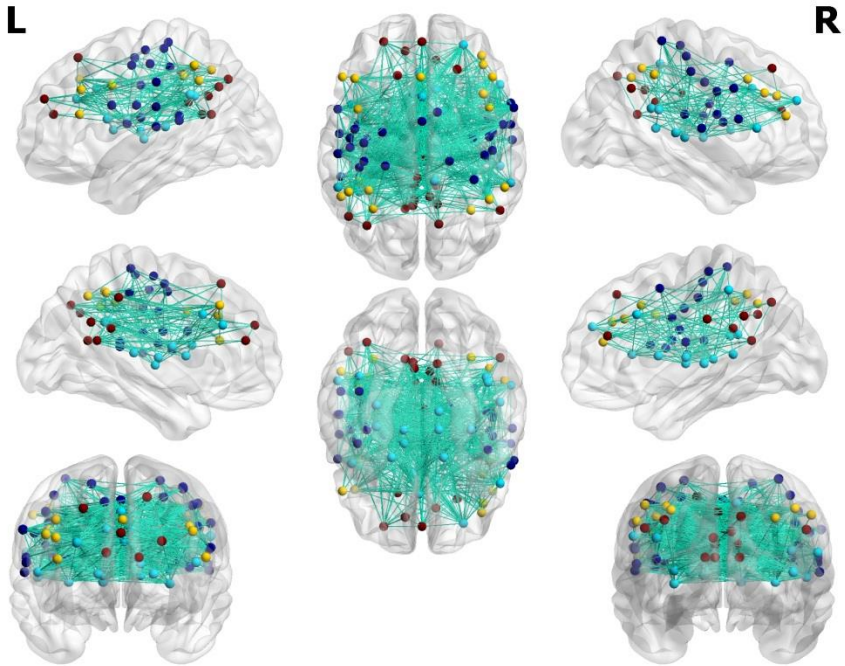

Figure S4 Box plots of multi-scan ICCs for significant, non-significant, positive and negative correlations for both groups.

a)

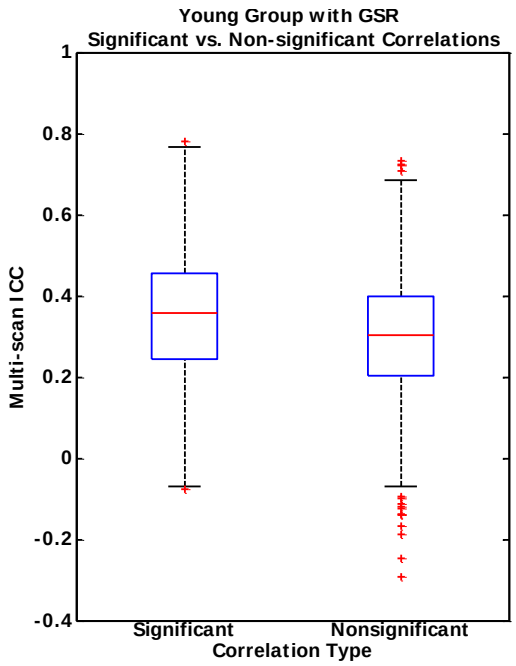

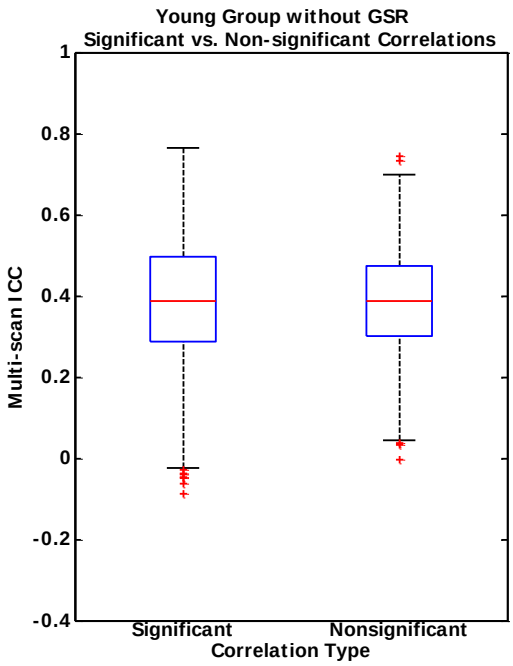

b)

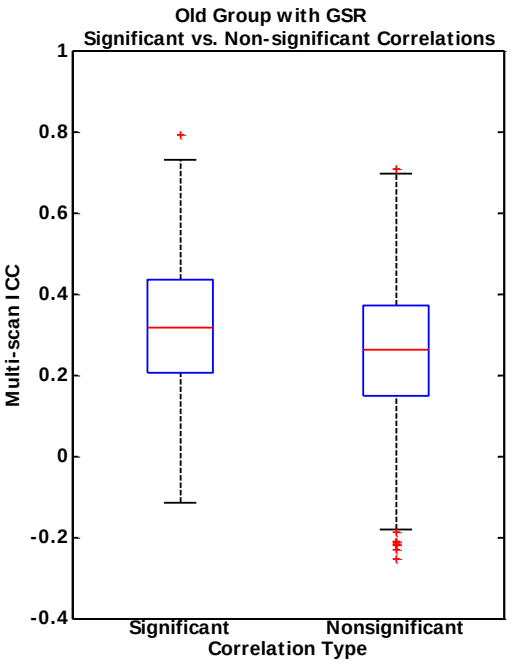

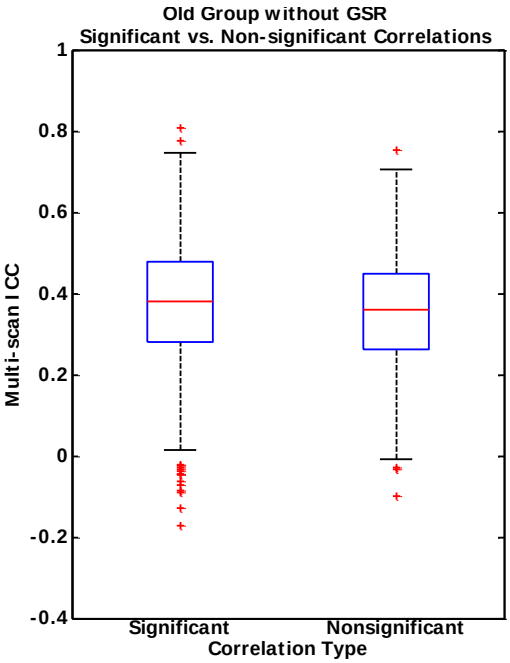

c)

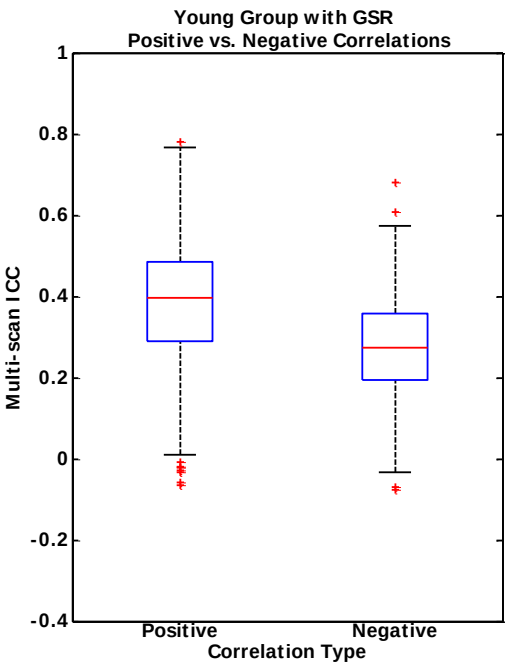
Young Group with GSR
Positive vs. Negative Correlations
Multi-scan ICC
1
0.8
0.6
0.4
0.2
0
-0.2
-0.4
Positive
Negative
Correlation Type

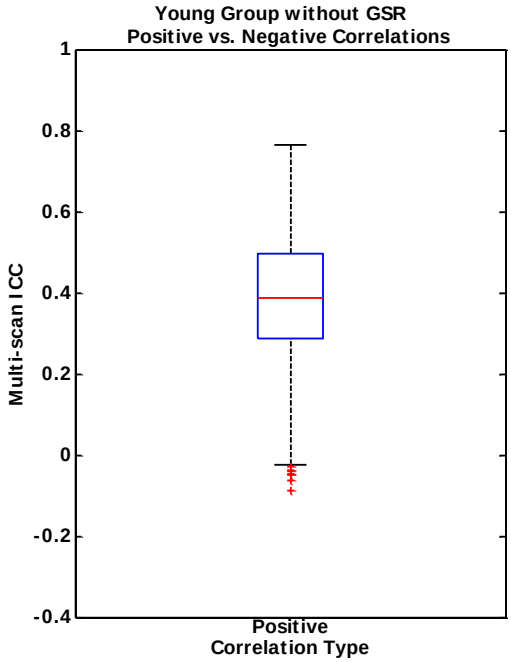
Young Group without GSR
Positive vs. Negative Correlations
Multi-scan ICC
1
0.8
0.6
0.4
0.2
0
-0.2
-0.4
Positive
Correlation Type

d)

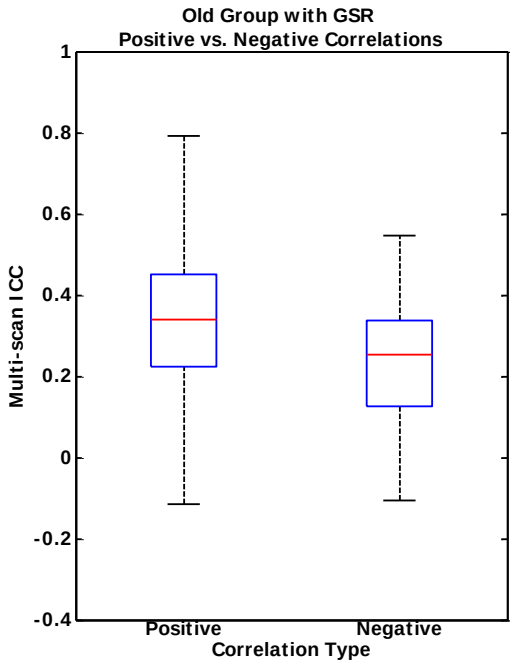
Old Group with GSR
Positive vs. Negative Correlations
Multi-scan ICC
1
0.8
0.6
0.4
0.2
0
-0.2
-0.4
Positive
Negative
Correlation Type

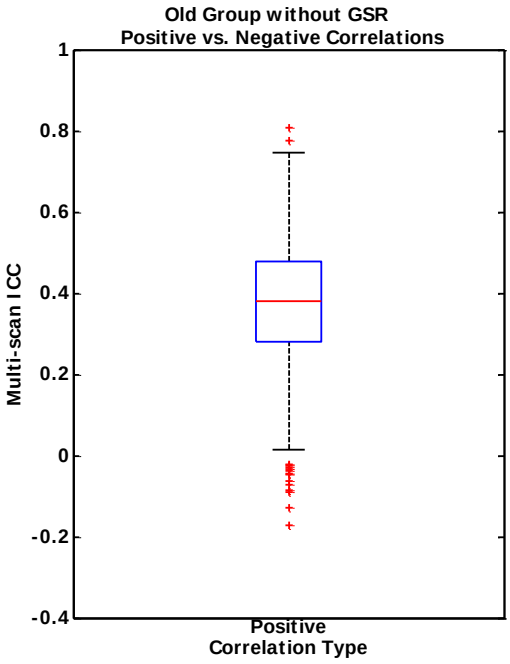
Old Group without GSR
Positive vs. Negative Correlations
Multi-scan ICC
1
0.8
0.6
0.4
0.2
0
-0.2
-0.4
Positive
Correlation Type

Figure S5 Group-averaged multi-scan correlation coefficients plotted against their corresponding multi-scan ICCs.

a)

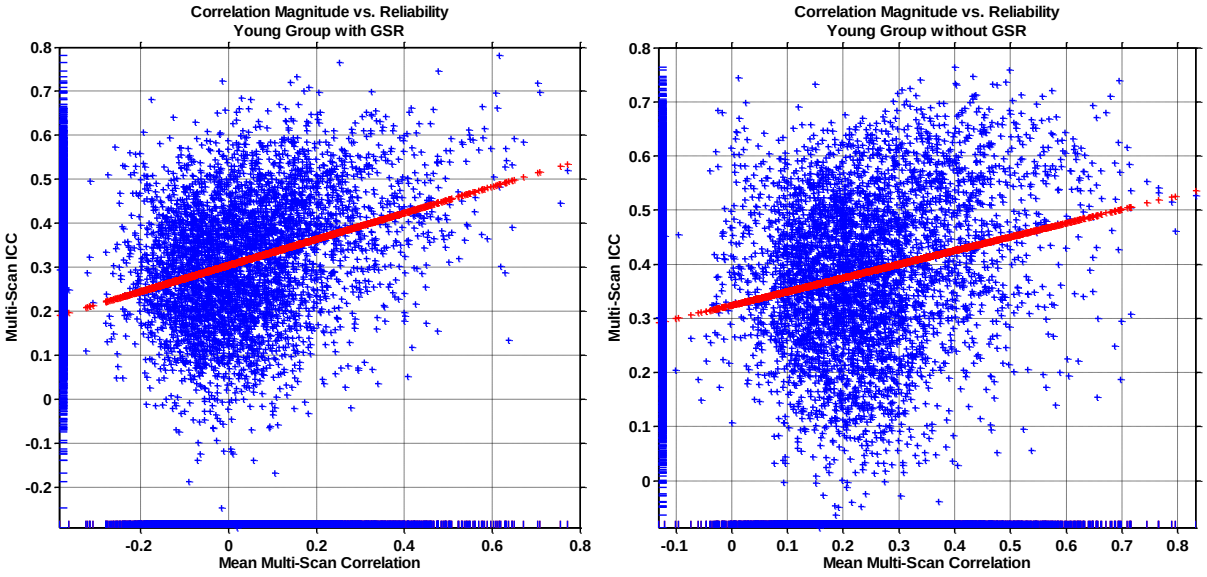

b)

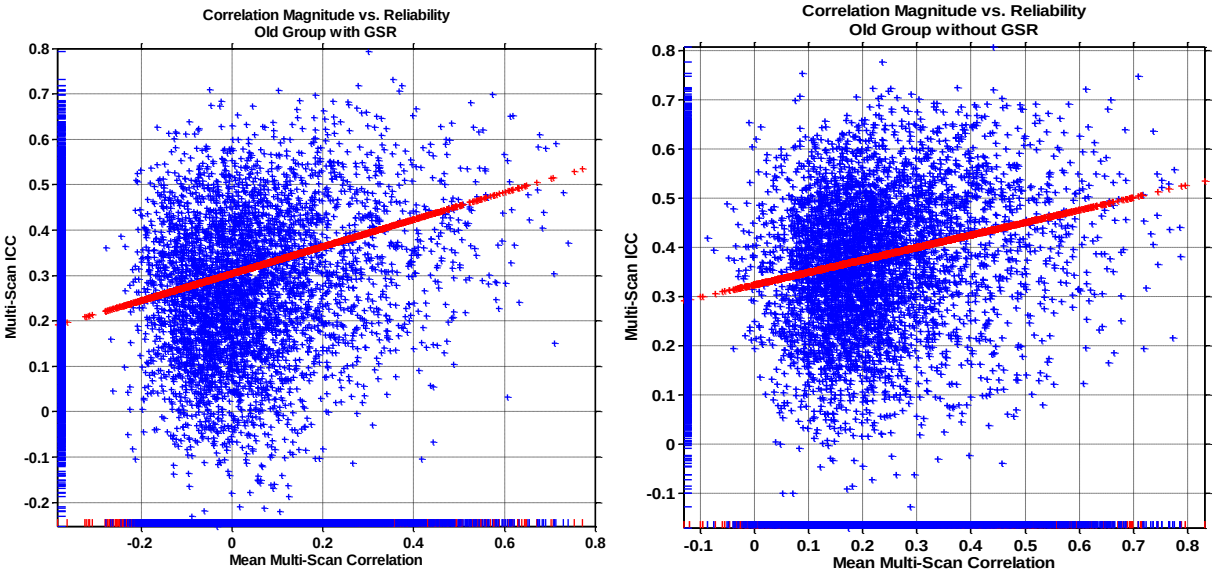

Figure S6 Stability within subjects across scans.

a)

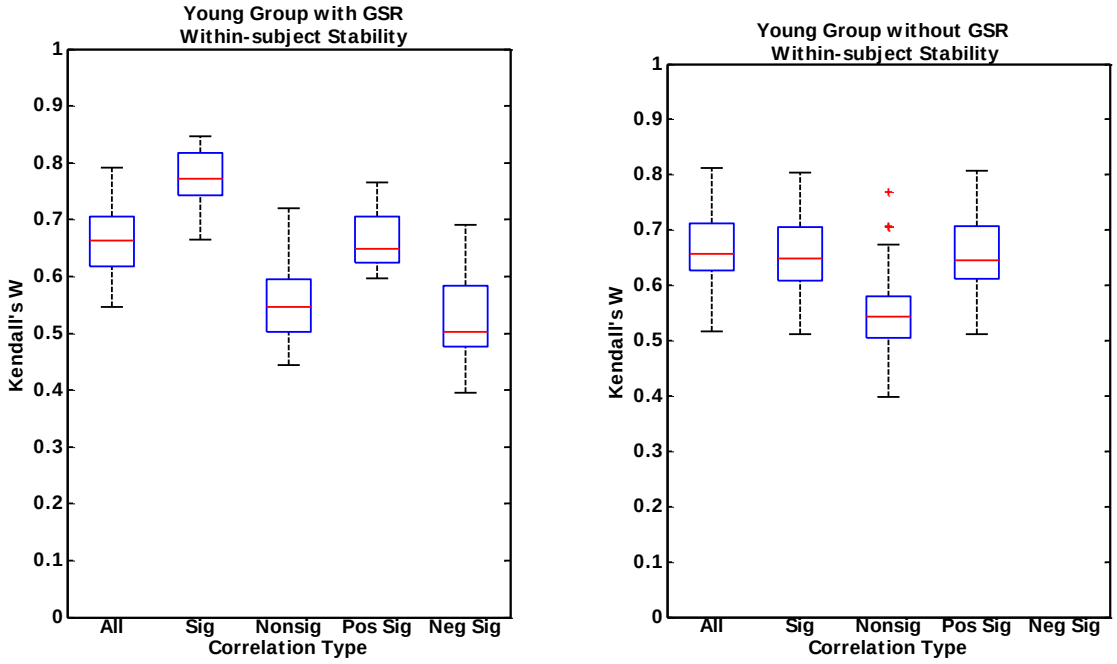

b)

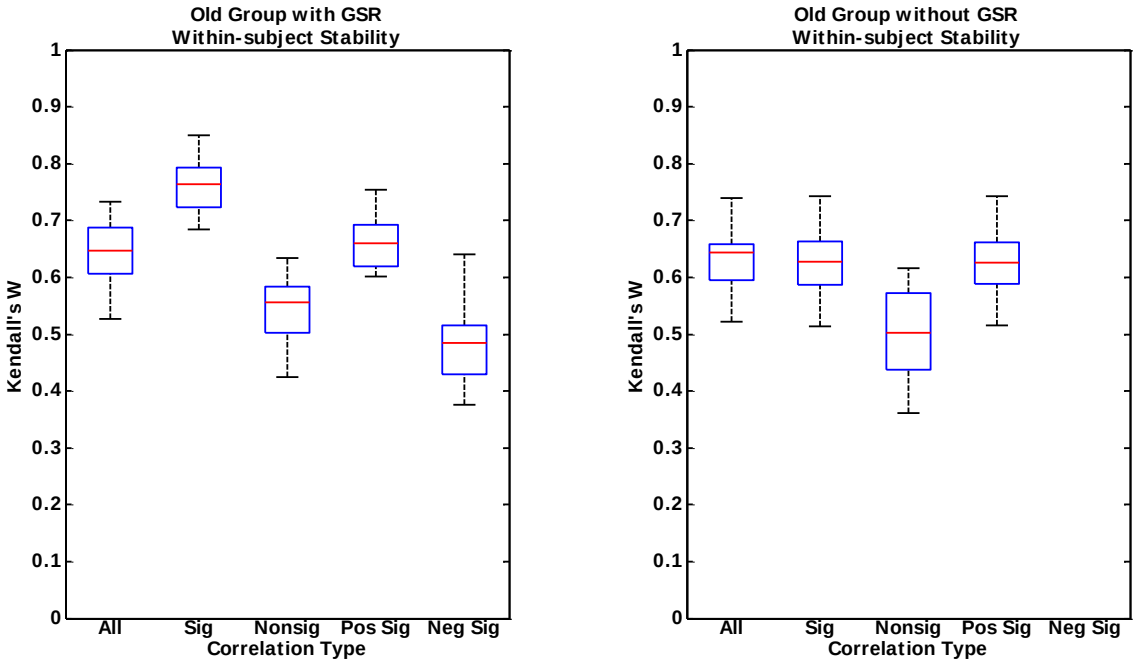

Figure S7 Stability between-subject within scans.

a)

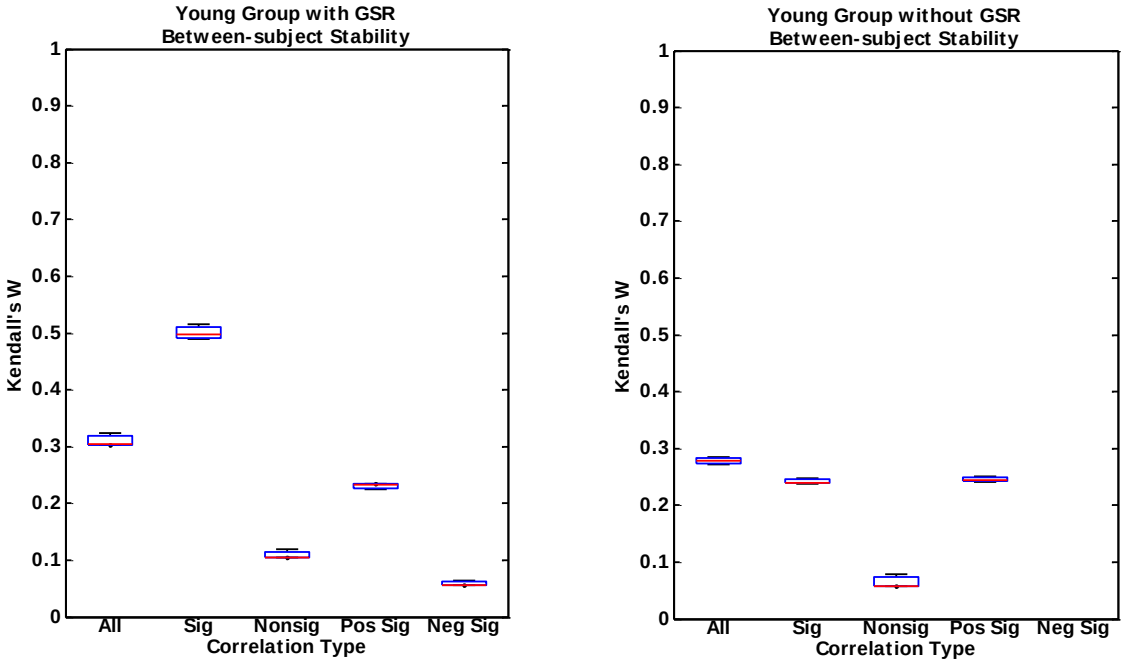

b)

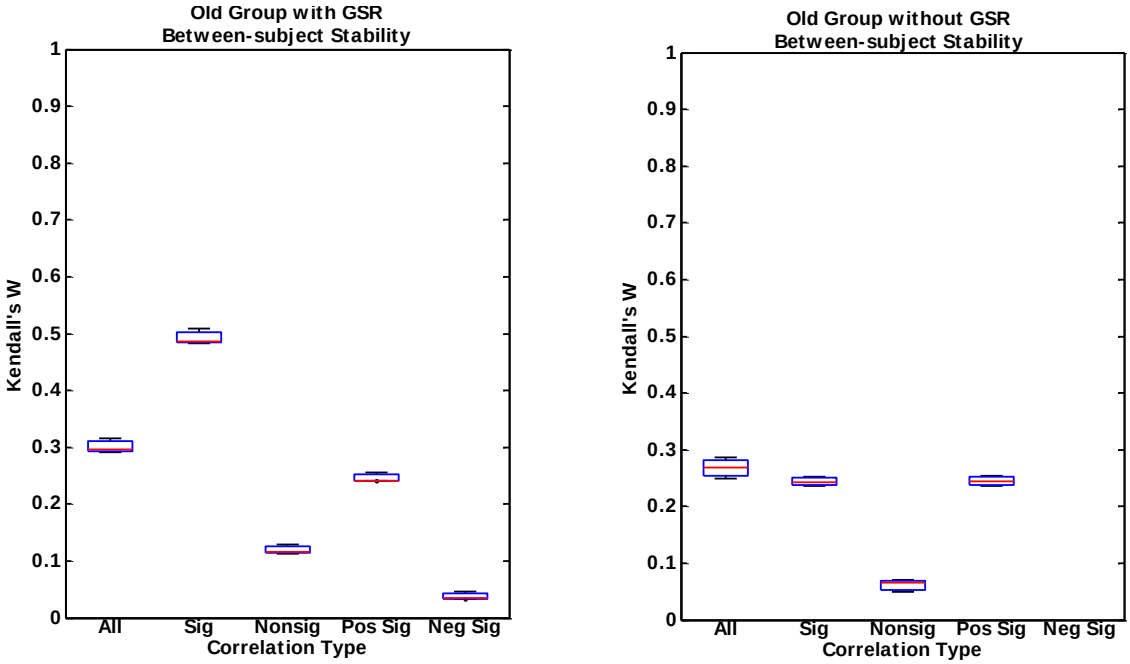

Table S1 Listed are 92 ROIs with their MNI coordinates and respective functional networks.

x	y	z	ROI lable	Network
0	51	32	M_mPFC	default
-25	51	27	L_aPFC_2	default
27	49	26	R_aPFC_2	cingulo-opercular
-11	45	17	L_vmPFC	default
39	42	16	R_vlPFC	fronto-parietal
9	39	20	R_ACC	default
40	36	29	R_dlPFC_1	fronto-parietal
23	33	47	R_sup_frontal	default
-2	30	27	M_ACC_1	cingulo-opercular
-16	29	54	L_sup_frontal	default
-1	28	40	M_ACC_2	fronto-parietal
46	28	31	R_dlPFC_2	fronto-parietal
-52	28	17	L_vPFC	fronto-parietal
-44	27	33	L_dlPFC	fronto-parietal
51	23	8	R_vFC_1	cingulo-opercular
9	20	34	R_dACC	cingulo-opercular
40	17	40	R_dFC_1	fronto-parietal
-6	17	34	L_basal_ganglia_1	cingulo-opercular
0	15	45	M_mFC	cingulo-opercular
58	11	14	R_frontal_1	sensorimotor
-46	10	14	L_vFC_1	cingulo-opercular
44	8	34	R_dFC_2	fronto-parietal
60	8	34	R_dFC_3	sensorimotor
-42	7	36	L_dFC	fronto-parietal
-55	7	23	L_vFC_2	sensorimotor
-20	6	7	L_basal_ganglia_2	cingulo-opercular
14	6	7	R_basal_ganglia_1	cingulo-opercular
10	5	51	R_pre_SMA	sensorimotor
43	1	12	R_vFC_2	sensorimotor
0	-1	52	M_SMA	sensorimotor
53	-3	32	R_frontal_2	sensorimotor
58	-3	17	R_precentral_gyrus_1	sensorimotor
-12	-3	13	L_thalamus_1	cingulo-opercular
-42	-3	11	L_mid_insula_1	sensorimotor
-44	-6	49	L_precentral_gyrus_1	sensorimotor
-26	-8	54	L_parietal_1	sensorimotor
46	-8	24	R_precentral_gyrus_2	sensorimotor
-54	-9	23	L_precentral_gyrus_2	sensorimotor
44	-11	38	R_precentral_gyrus_3	sensorimotor

-47	-12	36	L_parietal_2	sensorimotor
33	-12	16	R_mid_insula_1	sensorimotor
-36	-12	15	L_mid_insula_2	sensorimotor
-12	-12	6	L_thalamus_2	cingulo-opercular
11	-12	6	R_thalamus_1	cingulo-opercular
32	-12	2	R_mid_insula_2	cingulo-opercular
59	-13	8	R_temporal_1	sensorimotor
-30	-14	1	L_mid_insula_3	cingulo-opercular
-38	-15	59	L_parietal_3	sensorimotor
-47	-18	50	L_parietal_4	sensorimotor
46	-20	45	R_parietal_1	sensorimotor
-55	-22	38	L_parietal_5	sensorimotor
-54	-22	22	L_precentral_gyrus_3	sensorimotor
-54	-22	9	L_temporal_1	sensorimotor
41	-23	55	R_parietal_2	sensorimotor
42	-24	17	R_post_insula	sensorimotor
11	-24	2	R_basal_ganglia_2	cingulo-opercular
1	-26	31	M_post_cingulate	default
18	-27	62	R_parietal_3	sensorimotor
-38	-27	60	L_parietal_6	sensorimotor
-30	-28	9	L_post_insula	cingulo-opercular
-24	-30	64	L_parietal_7	sensorimotor
51	-30	5	R_temporal_2	cingulo-opercular
-41	-31	48	L_post_parietal_1	sensorimotor
-41	-37	16	L_temporal_2	sensorimotor
-53	-37	13	L_temporal_3	sensorimotor
-3	-38	45	L_precuneus_1	default
34	-39	65	R_sup_parietal	sensorimotor
8	-40	50	R_precuneus_1	cingulo-opercular
-41	-40	42	L_IPL_1	fronto-parietal
58	-41	20	R_parietal_4	cingulo-opercular
-5	-43	25	L_post_cingulate_1	default
9	-43	25	R_precuneus_2	default
43	-43	8	R_temporal_3	cingulo-opercular
54	-44	43	R_IPL_1	fronto-parietal
-55	-44	30	L_parietal_8	cingulo-opercular
-35	-46	48	L_post_parietal_2	fronto-parietal
42	-46	21	R_sup_temporal	cingulo-opercular
-48	-47	49	L_IPL_2	fronto-parietal
-41	-47	29	L_angular_gyrus_1	cingulo-opercular
-53	-50	39	L_IPL_3	fronto-parietal
5	-50	33	R_precuneus_3	default
44	-52	47	R_IPL_2	fronto-parietal

-5	-52	17	L_post_cingulate_2	default
10	-55	17	R_post_cingulate	default
-6	-56	29	L_precuneus_2	default
-32	-58	46	L_IPS_1	fronto-parietal
-11	-58	17	L_post_cingulate_3	default
32	-59	41	R_IPS	fronto-parietal
51	-59	34	R_angular_gyrus	default
-48	-63	35	L_angular_gyrus_2	default
11	-68	42	R_precuneus_4	default
-36	-69	40	L_IPS_2	default

Table S2 Listed are significant and reliable correlations (i.e., *p*-value < 0.05 adjusted by FDR correction, ICC > 0.5) with GSR for both groups.

a)

Young Group					
Correlation	**ICC**	**Mean R scan 1**	**Mean R scan 2**	**Mean R scan 3**	**Networks**
R_thalamus_1 - L_thalamus_2	0.78	0.63	0.61	0.61	cingulo-opercular - cingulo-opercular
R_IPL_2 - R_dFC_2	0.77	0.30	0.23	0.23	fronto-parietal - fronto-parietal
M_ACC_2 - M_ACC_1	0.75	0.52	0.48	0.43	fronto-parietal - cingulo-opercular
L_precuneus_2 - L_post_cingulate_2	0.72	0.71	0.72	0.69	default - default
L_precuneus_2 - L_IPL_3	0.70	0.16	0.18	0.17	default - fronto-parietal
L_mid_insula_2 - R_precentral_gyrus_2	0.70	0.33	0.29	0.35	sensorimotor - sensorimotor
L_post_cingulate_3 - L_post_cingulate_2	0.70	0.71	0.70	0.72	default - default
R_angular_gyrus - L_precuneus_1	0.70	0.25	0.19	0.18	default - default
L_post_cingulate_3 - L_precuneus_2	0.70	0.62	0.61	0.59	default - default
L_precuneus_2 - R_IPL_1	0.68	-0.17	-0.18	-0.17	default - fronto-parietal
L_IPL_2 - L_sup_frontal	0.67	0.15	0.16	0.16	fronto-parietal - default
L_precuneus_2 - L_post_cingulate_1	0.66	0.54	0.62	0.58	default - default
L_precentral_gyrus_3 - L_mid_insula_2	0.66	0.40	0.43	0.42	sensorimotor - sensorimotor
L_post_cingulate_1 - M_post_cingulate	0.66	0.60	0.61	0.62	default - default
R_precentral_gyrus_3 - L_precentral_gyrus_2	0.66	0.50	0.45	0.45	sensorimotor - sensorimotor
L_precentral_gyrus_3 - R_mid_insula_1	0.66	0.36	0.35	0.29	sensorimotor - sensorimotor
L_precentral_gyrus_3 - R_precentral_gyrus_2	0.65	0.29	0.32	0.33	sensorimotor - sensorimotor
L_angular_gyrus_2 - L_IPL_2	0.65	0.17	0.23	0.23	default - fronto-parietal

R_IPL_1 - R_dlPFC_1	0.65	0.39	0.39	0.45	fronto-parietal - fronto-parietal
L_parietal_5 - L_precentral_gyrus_2	0.65	0.27	0.34	0.37	sensorimotor - sensorimotor
R_IPL_1 - M_mFC	0.65	0.18	0.22	0.21	fronto-parietal - cingulo-opercular
L_IPL_3 - L_sup_frontal	0.64	0.31	0.34	0.33	fronto-parietal - default
R_angular_gyrus - L_IPL_3	0.64	0.32	0.38	0.37	default - fronto-parietal
L_parietal_4 - R_frontal_2	0.64	0.25	0.31	0.35	sensorimotor - sensorimotor
L_IPL_2 - L_parietal_8	0.64	0.17	0.22	0.22	fronto-parietal - cingulo-opercular
R_dFC_2 - L_basal_ganglia_1	0.63	0.14	0.16	0.15	fronto-parietal - cingulo-opercular
L_precuneus_1 - M_post_cingulate	0.63	0.32	0.33	0.36	default - default
L_parietal_8 - L_dFC	0.63	0.14	0.13	0.13	cingulo-opercular - fronto-parietal
R_IPL_1 - R_vlPFC	0.63	0.33	0.37	0.34	fronto-parietal - fronto-parietal
R_frontal_2 - R_dFC_2	0.63	0.18	0.21	0.22	sensorimotor - fronto-parietal
R_temporal_1 - R_precentral_gyrus_2	0.63	0.28	0.28	0.30	sensorimotor - sensorimotor
L_IPL_3 - L_aPFC_2	0.63	0.21	0.15	0.18	fronto-parietal - default
L_parietal_2 - R_precentral_gyrus_1	0.63	0.48	0.46	0.44	sensorimotor - sensorimotor
R_IPL_2 - R_dlPFC_2	0.63	0.45	0.44	0.41	fronto-parietal - fronto-parietal
L_IPL_2 - R_IPL_1	0.62	0.32	0.38	0.42	fronto-parietal - fronto-parietal
R_IPL_2 - R_dlPFC_1	0.62	0.32	0.34	0.38	fronto-parietal - fronto-parietal
R_precentral_gyrus_3 - R_frontal_2	0.61	0.60	0.56	0.58	sensorimotor - sensorimotor
L_aPFC_2 - M_mPFC	0.61	0.29	0.23	0.32	default - default
R_precuneus_3 - R_precuneus_2	0.61	0.56	0.57	0.52	default - default
L_IPL_3 - L_post_cingulate_1	0.61	0.12	0.15	0.14	fronto-parietal - default
L_post_cingulate_1 - L_vmPFC	0.61	0.20	0.22	0.29	default - default
L_IPS_2 - L_IPS_1	0.61	0.28	0.36	0.41	default - fronto-parietal
L_parietal_4 - R_precentral_gyrus_3	0.61	0.34	0.39	0.39	sensorimotor - sensorimotor

L_dlPFC - R_dlPFC_1	0.61	0.36	0.31	0.31	fronto-parietal - fronto-parietal
L_IPL_3 - R_sup_frontal	0.61	0.18	0.20	0.15	fronto-parietal - default
L_IPL_2 - L_dFC	0.61	0.32	0.36	0.24	fronto-parietal - fronto-parietal
M_SMA - R_dFC_3	0.61	0.23	0.24	0.19	sensorimotor - sensorimotor
R_angular_gyrus - R_dFC_3	0.61	-0.19	-0.19	-0.20	default - sensorimotor
L_IPL_3 - L_parietal_8	0.60	0.39	0.43	0.46	fronto-parietal - cingulo-opercular
L_parietal_7 - R_parietal_1	0.60	0.23	0.30	0.32	sensorimotor - sensorimotor
L_vFC_2 - L_vPFC	0.60	0.32	0.32	0.33	sensorimotor - fronto-parietal
R_IPL_2 - R_dFC_1	0.60	0.41	0.39	0.42	fronto-parietal - fronto-parietal
L_post_cingulate_2 - R_precuneus_3	0.60	0.55	0.56	0.54	default - default
L_post_cingulate_3 - L_post_cingulate_1	0.60	0.37	0.43	0.40	default - default
R_IPL_2 - R_vlPFC	0.60	0.31	0.34	0.30	fronto-parietal - fronto-parietal

b)

Old Group					
Correlation	**ICC**	**Mean R scan 1**	**Mean R scan 2**	**Mean R scan 3**	**Networks**
R_angular_gyrus - L_post_cingulate_3	0.79	0.35	0.24	0.31	default - default
R_angular_gyrus - R_sup_frontal	0.73	0.39	0.33	0.34	default - default
R_dFC_2 - R_dlPFC_1	0.72	0.27	0.26	0.30	fronto-parietal - fronto-parietal
R_angular_gyrus - R_post_cingulate	0.72	0.43	0.32	0.37	default - default
R_angular_gyrus - L_post_cingulate_2	0.71	0.41	0.33	0.36	default - default

L_parietal_4 - L_parietal_3	0.70	0.59	0.55	0.58	sensorimotor - sensorimotor
L_parietal_3 - R_precentral_gyrus_3	0.68	0.17	0.29	0.21	sensorimotor - sensorimotor
R_dFC_2 - M_ACC_2	0.68	0.27	0.21	0.28	fronto-parietal - fronto-parietal
L_IPS_1 - L_post_parietal_2	0.68	0.52	0.53	0.53	fronto-parietal - fronto-parietal
R_dlPFC_2 - R_aPFC_2	0.68	0.26	0.28	0.23	fronto-parietal - cingulo-opercular
R_dlPFC_1 - L_aPFC_2	0.67	0.24	0.35	0.24	fronto-parietal - default
R_dFC_2 - R_dlPFC_2	0.67	0.40	0.40	0.41	fronto-parietal - fronto-parietal
R_IPL_2 - L_post_parietal_2	0.66	0.17	0.22	0.22	fronto-parietal - fronto-parietal
L_parietal_8 - R_parietal_4	0.66	0.29	0.24	0.35	cingulo-opercular - cingulo-opercular
R_precentral_gyrus_3 - L_vFC_2	0.66	0.32	0.25	0.28	sensorimotor - sensorimotor
L_aPFC_2 - M_mPFC	0.65	0.41	0.39	0.39	default - default
L_precuneus_2 - R_post_cingulate	0.65	0.64	0.58	0.63	default - default
M_ACC_1 - R_dlPFC_1	0.65	0.30	0.32	0.33	cingulo-opercular - fronto-parietal
L_parietal_6 - L_parietal_4	0.65	0.62	0.62	0.59	sensorimotor - sensorimotor
L_angular_gyrus_2 - R_sup_frontal	0.65	0.23	0.21	0.22	default - default
L_precentral_gyrus_1 - L_vFC_2	0.65	0.13	0.19	0.21	sensorimotor - sensorimotor
L_angular_gyrus_2 - L_sup_frontal	0.65	0.39	0.29	0.31	default - default
R_precuneus_3 - R_sup_temporal	0.65	0.22	0.19	0.20	default - cingulo-opercular
R_post_cingulate - R_sup_frontal	0.64	0.29	0.21	0.22	default - default
L_post_cingulate_2 - R_precuneus_2	0.64	0.48	0.45	0.52	default - default
R_IPL_2 - L_IPL_1	0.63	0.23	0.21	0.23	fronto-parietal - fronto-parietal
M_ACC_2 - L_aPFC_2	0.63	0.32	0.32	0.26	fronto-parietal - default
R_dFC_1 - M_ACC_2	0.63	0.51	0.41	0.45	fronto-parietal - fronto-parietal
R_precuneus_3 -	0.63	0.36	0.30	0.28	default - default

R_sup_frontal					
L_post_cingulate_2 - R_precuneus_3	0.63	0.55	0.54	0.51	default - default
R_dFC_2 - R_dFC_1	0.62	0.32	0.33	0.37	fronto-parietal - fronto-parietal
L_sup_frontal - L_vmPFC	0.62	0.21	0.16	0.25	default - default
L_parietal_6 - L_precentral_gyrus_2	0.62	0.18	0.16	0.21	sensorimotor - sensorimotor
R_post_cingulate - R_precuneus_3	0.62	0.59	0.52	0.55	default - default
L_angular_gyrus_2 - L_post_cingulate_3	0.62	0.30	0.24	0.24	default - default
R_aPFC_2 - L_aPFC_2	0.62	0.55	0.56	0.52	cingulo-opercular - default
L_post_cingulate_3 - R_sup_frontal	0.61	0.28	0.22	0.18	default - default
L_precuneus_2 - L_post_cingulate_2	0.61	0.70	0.66	0.66	default - default
L_parietal_6 - L_parietal_2	0.61	0.23	0.18	0.22	sensorimotor - sensorimotor
L_IPS_2 - L_post_cingulate_2	0.61	0.36	0.33	0.30	default - default
L_precuneus_1 - L_parietal_5	0.60	0.16	0.14	0.25	default - sensorimotor
M_ACC_2 - M_ACC_1	0.60	0.49	0.47	0.45	fronto-parietal - cingulo-opercular
L_parietal_4 - L_precentral_gyrus_1	0.60	0.47	0.46	0.51	sensorimotor - sensorimotor
R_angular_gyrus - R_IPS	0.60	0.19	0.25	0.18	default - fronto-parietal

Table S3 Listed are significant and reliable correlations (i.e., *p*-value < 0.05 adjusted by FDR correction, ICC > 0.5) without GSR for both groups.

a)

Young Group					
Correlation	**ICC**	**Mean R scan 1**	**Mean R scan 2**	**Mean R scan 3**	**Networks**
R_IPL_2 - R_dFC_2	0.76	0.45	0.37	0.37	fronto-parietal - fronto-parietal
L_IPL_1 - L_parietal_5	0.76	0.55	0.46	0.49	fronto-parietal - sensorimotor

L_parietal_4 - R_precentral_gyrus_1	0.75	0.42	0.46	0.42	sensorimotor - sensorimotor
L_parietal_5 - R_precentral_gyrus_2	0.74	0.35	0.31	0.36	sensorimotor - sensorimotor
R_thalamus_1 - L_thalamus_2	0.74	0.71	0.69	0.68	cingulo-opercular - cingulo-opercular
L_parietal_4 - R_temporal_1	0.74	0.51	0.49	0.47	sensorimotor - sensorimotor
L_temporal_3 - L_parietal_4	0.73	0.39	0.37	0.45	sensorimotor - sensorimotor
R_parietal_3 - L_parietal_3	0.73	0.47	0.44	0.49	sensorimotor - sensorimotor
R_angular_gyrus - L_precuneus_1	0.73	0.43	0.37	0.40	default - default
L_parietal_5 - L_precentral_gyrus_2	0.73	0.45	0.46	0.52	sensorimotor - sensorimotor
R_angular_gyrus - R_sup_temporal	0.72	0.34	0.24	0.38	default - cingulo-opercular
L_precuneus_2 - L_IPL_3	0.72	0.31	0.28	0.32	default - fronto-parietal
R_precentral_gyrus_3 - L_precentral_gyrus_2	0.72	0.62	0.54	0.57	sensorimotor - sensorimotor
L_parietal_8 - L_temporal_1	0.72	0.35	0.29	0.25	cingulo-opercular - sensorimotor
L_precentral_gyrus_3 - R_precentral_gyrus_2	0.71	0.43	0.42	0.46	sensorimotor - sensorimotor
R_temporal_1 - R_precentral_gyrus_3	0.71	0.54	0.51	0.51	sensorimotor - sensorimotor
R_precuneus_3 - R_sup_temporal	0.71	0.35	0.27	0.37	default - cingulo-opercular
L_mid_insula_2 - R_precentral_gyrus_2	0.71	0.45	0.40	0.45	sensorimotor - sensorimotor
L_precentral_gyrus_3 - L_mid_insula_2	0.71	0.56	0.56	0.55	sensorimotor - sensorimotor
R_parietal_1 - R_precentral_gyrus_1	0.71	0.43	0.46	0.40	sensorimotor - sensorimotor
L_parietal_2 - R_precentral_gyrus_3	0.71	0.70	0.66	0.68	sensorimotor - sensorimotor
L_temporal_1 - L_parietal_4	0.70	0.45	0.43	0.42	sensorimotor - sensorimotor
L_precentral_gyrus_3 - R_mid_insula_1	0.70	0.54	0.50	0.47	sensorimotor - sensorimotor
R_temporal_2 - R_parietal_3	0.70	0.31	0.27	0.29	cingulo-opercular - sensorimotor
R_parietal_4 - L_parietal_4	0.70	0.28	0.34	0.32	cingulo-opercular -

					sensorimotor
R_sup_parietal - R_temporal_1	0.70	0.41	0.45	0.42	sensorimotor - sensorimotor
R_parietal_1 - L_mid_insula_2	0.70	0.40	0.33	0.39	sensorimotor - sensorimotor
L_IPL_1 - R_sup_parietal	0.70	0.37	0.38	0.39	fronto-parietal - sensorimotor
L_precentral_gyrus_3 - L_parietal_5	0.70	0.56	0.56	0.53	sensorimotor - sensorimotor
L_IPL_1 - L_parietal_3	0.70	0.33	0.29	0.31	fronto-parietal - sensorimotor
L_precuneus_2 - L_post_cingulate_1	0.69	0.63	0.66	0.65	default - default
R_sup_parietal - L_mid_insula_2	0.69	0.31	0.30	0.35	sensorimotor - sensorimotor
R_IPL_1 - L_vmPFC	0.69	0.12	0.15	0.10	fronto-parietal - default
L_IPL_1 - R_parietal_2	0.69	0.39	0.31	0.37	fronto-parietal - sensorimotor
L_post_parietal_1 - R_temporal_1	0.69	0.46	0.47	0.39	sensorimotor - sensorimotor
L_IPL_3 - L_sup_frontal	0.69	0.42	0.41	0.43	fronto-parietal - default
R_parietal_3 - L_parietal_4	0.69	0.46	0.42	0.50	sensorimotor - sensorimotor
R_parietal_1 - R_precentral_gyrus_2	0.69	0.35	0.33	0.34	sensorimotor - sensorimotor
R_post_cingulate - R_sup_temporal	0.68	0.35	0.31	0.33	default - cingulo-opercular
L_IPL_1 - R_parietal_1	0.68	0.43	0.38	0.43	fronto-parietal - sensorimotor
L_parietal_6 - R_parietal_3	0.68	0.49	0.45	0.55	sensorimotor - sensorimotor
R_parietal_2 - R_precentral_gyrus_2	0.68	0.29	0.28	0.33	sensorimotor - sensorimotor
L_post_cingulate_3 - R_precuneus_1	0.68	0.32	0.23	0.28	default - cingulo-opercular
R_temporal_1 - R_precentral_gyrus_2	0.68	0.46	0.42	0.44	sensorimotor - sensorimotor
L_temporal_3 - R_parietal_1	0.68	0.41	0.39	0.44	sensorimotor - sensorimotor
R_precentral_gyrus_3 - R_frontal_2	0.68	0.68	0.65	0.68	sensorimotor - sensorimotor
L_precentral_gyrus_3 - R_precentral_gyrus_1	0.68	0.48	0.56	0.51	sensorimotor - sensorimotor
L_IPL_1 - L_parietal_4	0.68	0.37	0.32	0.34	fronto-parietal -

					sensorimotor
R_temporal_3 - R_temporal_2	0.68	0.51	0.48	0.51	cingulo-opercular - cingulo-opercular
R_parietal_3 - R_parietal_1	0.68	0.43	0.45	0.49	sensorimotor - sensorimotor
R_sup_temporal - R_sup_frontal	0.68	0.22	0.16	0.23	cingulo-opercular - default
R_temporal_2 - L_parietal_4	0.68	0.43	0.40	0.39	cingulo-opercular - sensorimotor
L_temporal_2 - R_parietal_1	0.67	0.39	0.42	0.40	sensorimotor - sensorimotor
R_mid_insula_1 - R_precentral_gyrus_3	0.67	0.41	0.36	0.38	sensorimotor - sensorimotor
L_parietal_4 - L_mid_insula_2	0.67	0.37	0.35	0.39	sensorimotor - sensorimotor
L_post_parietal_1 - L_parietal_5	0.67	0.58	0.62	0.55	sensorimotor - sensorimotor
L_post_parietal_1 - R_precentral_gyrus_2	0.67	0.26	0.26	0.29	sensorimotor - sensorimotor
L_parietal_4 - R_frontal_2	0.67	0.42	0.44	0.50	sensorimotor - sensorimotor
L_temporal_3 - R_parietal_2	0.67	0.34	0.32	0.38	sensorimotor - sensorimotor
L_temporal_3 - L_temporal_2	0.67	0.65	0.65	0.66	sensorimotor - sensorimotor
R_IPL_2 - R_frontal_1	0.67	0.26	0.31	0.31	fronto-parietal - sensorimotor
L_post_cingulate_3 - R_temporal_2	0.67	0.26	0.22	0.22	default - cingulo-opercular
L_parietal_7 - R_parietal_1	0.67	0.45	0.49	0.52	sensorimotor - sensorimotor
L_post_parietal_1 - R_precentral_gyrus_1	0.67	0.34	0.41	0.32	sensorimotor - sensorimotor
L_parietal_5 - R_parietal_1	0.67	0.58	0.54	0.58	sensorimotor - sensorimotor
R_temporal_2 - L_parietal_7	0.67	0.33	0.32	0.34	cingulo-opercular - sensorimotor
R_sup_parietal - L_post_parietal_1	0.67	0.54	0.54	0.53	sensorimotor - sensorimotor
R_precentral_gyrus_3 - R_precentral_gyrus_1	0.67	0.59	0.55	0.53	sensorimotor - sensorimotor
L_parietal_3 - R_precentral_gyrus_1	0.66	0.34	0.39	0.34	sensorimotor - sensorimotor
L_precuneus_2 -	0.66	0.32	0.22	0.28	default - cingulo-opercular

R_sup_temporal					
R_parietal_1 - R_frontal_2	0.66	0.44	0.47	0.49	sensorimotor - sensorimotor
R_sup_temporal - L_parietal_4	0.66	0.18	0.20	0.16	cingulo-opercular - sensorimotor
L_parietal_5 - L_mid_insula_2	0.66	0.42	0.41	0.41	sensorimotor - sensorimotor
L_IPS_1 - L_precentral_gyrus_1	0.66	0.32	0.25	0.28	fronto-parietal - sensorimotor
R_parietal_1 - L_parietal_2	0.66	0.48	0.49	0.55	sensorimotor - sensorimotor
L_IPS_1 - L_parietal_3	0.66	0.25	0.22	0.22	fronto-parietal - sensorimotor
L_parietal_8 - M_mPFC	0.66	0.27	0.26	0.25	cingulo-opercular - default
R_parietal_4 - L_temporal_3	0.66	0.52	0.44	0.47	cingulo-opercular - sensorimotor
R_parietal_1 - R_temporal_1	0.66	0.53	0.51	0.49	sensorimotor - sensorimotor
R_parietal_3 - R_precentral_gyrus_1	0.66	0.30	0.34	0.37	sensorimotor - sensorimotor
L_parietal_5 - R_frontal_2	0.66	0.45	0.46	0.54	sensorimotor - sensorimotor
L_post_cingulate_3 - R_precuneus_2	0.66	0.46	0.46	0.42	default - default
L_parietal_5 - R_mid_insula_1	0.66	0.40	0.37	0.38	sensorimotor - sensorimotor
L_post_cingulate_2 - R_precuneus_2	0.66	0.55	0.54	0.54	default - default
L_post_cingulate_3 - L_post_parietal_2	0.66	0.11	0.12	0.15	default - fronto-parietal
R_IPL_1 - L_post_cingulate_1	0.66	0.17	0.14	0.12	fronto-parietal - default
L_post_cingulate_2 - L_IPL_3	0.66	0.27	0.24	0.24	default - fronto-parietal
L_precentral_gyrus_1 - R_frontal_2	0.66	0.34	0.37	0.41	sensorimotor - sensorimotor
L_parietal_3 - L_precentral_gyrus_2	0.66	0.33	0.37	0.38	sensorimotor - sensorimotor
L_parietal_7 - R_temporal_1	0.66	0.39	0.43	0.44	sensorimotor - sensorimotor
L_temporal_2 - R_parietal_3	0.66	0.31	0.32	0.32	sensorimotor - sensorimotor
L_parietal_6 - L_parietal_5	0.65	0.46	0.41	0.52	sensorimotor - sensorimotor
L_parietal_5 - L_dFC	0.65	0.20	0.23	0.24	sensorimotor - fronto-parietal

R_parietal_4 - L_parietal_6	0.65	0.31	0.28	0.28	cingulo-opercular - sensorimotor
L_parietal_5 - R_precentral_gyrus_1	0.65	0.41	0.48	0.46	sensorimotor - sensorimotor
L_parietal_4 - L_parietal_2	0.65	0.51	0.53	0.59	sensorimotor - sensorimotor
L_parietal_4 - R_precentral_gyrus_3	0.65	0.53	0.54	0.56	sensorimotor - sensorimotor
L_precuneus_1 - R_sup_frontal	0.65	0.44	0.39	0.37	default - default
L_temporal_2 - L_mid_insula_2	0.65	0.52	0.49	0.51	sensorimotor - sensorimotor
L_parietal_7 - R_post_insula	0.65	0.41	0.41	0.45	sensorimotor - sensorimotor
L_temporal_3 - L_parietal_3	0.65	0.33	0.28	0.38	sensorimotor - sensorimotor
L_IPL_1 - L_parietal_2	0.65	0.30	0.27	0.33	fronto-parietal - sensorimotor
R_sup_parietal - R_mid_insula_1	0.65	0.35	0.34	0.33	sensorimotor - sensorimotor
L_post_cingulate_3 - R_temporal_3	0.65	0.24	0.20	0.20	default - cingulo-opercular
L_parietal_2 - R_precentral_gyrus_2	0.65	0.48	0.40	0.42	sensorimotor - sensorimotor
R_parietal_1 - L_precentral_gyrus_2	0.65	0.46	0.43	0.47	sensorimotor - sensorimotor
R_precentral_gyrus_2 - L_precentral_gyrus_1	0.65	0.25	0.24	0.23	sensorimotor - sensorimotor
L_parietal_8 - L_temporal_2	0.65	0.30	0.28	0.20	cingulo-opercular - sensorimotor
L_parietal_4 - R_precentral_gyrus_2	0.65	0.30	0.29	0.34	sensorimotor - sensorimotor
L_parietal_5 - M_ACC_2	0.65	0.25	0.22	0.19	sensorimotor - fronto-parietal
L_precuneus_2 - R_IPL_2	0.65	0.17	0.18	0.14	default - fronto-parietal
L_post_cingulate_3 - L_post_parietal_1	0.65	0.19	0.15	0.17	default - sensorimotor
L_angular_gyrus_1 - M_mPFC	0.65	0.30	0.27	0.25	cingulo-opercular - default
L_parietal_7 - L_parietal_5	0.65	0.44	0.43	0.46	sensorimotor - sensorimotor
R_parietal_2 - M_ACC_2	0.65	0.24	0.18	0.12	sensorimotor - fronto-parietal
R_temporal_2 - L_thalamus_2	0.65	0.27	0.30	0.23	cingulo-opercular - cingulo-opercular

L_parietal_7 - L_mid_insula_2	0.65	0.36	0.33	0.35	sensorimotor - sensorimotor
R_parietal_3 - R_parietal_2	0.64	0.46	0.44	0.46	sensorimotor - sensorimotor
L_mid_insula_2 - R_precentral_gyrus_3	0.64	0.42	0.39	0.41	sensorimotor - sensorimotor
R_precentral_gyrus_3 - R_precentral_gyrus_2	0.64	0.51	0.44	0.43	sensorimotor - sensorimotor
L_precentral_gyrus_3 - R_parietal_1	0.64	0.46	0.45	0.45	sensorimotor - sensorimotor
R_parietal_3 - R_temporal_1	0.64	0.37	0.38	0.42	sensorimotor - sensorimotor
R_sup_parietal - R_parietal_2	0.64	0.61	0.60	0.59	sensorimotor - sensorimotor
L_parietal_7 - L_precentral_gyrus_1	0.64	0.39	0.39	0.42	sensorimotor - sensorimotor
L_parietal_2 - R_precentral_gyrus_1	0.64	0.60	0.56	0.56	sensorimotor - sensorimotor
R_temporal_2 - L_parietal_3	0.64	0.35	0.30	0.36	cingulo-opercular - sensorimotor
L_parietal_7 - R_precentral_gyrus_1	0.64	0.31	0.38	0.37	sensorimotor - sensorimotor
R_angular_gyrus - L_post_cingulate_3	0.64	0.48	0.41	0.45	default - default
R_sup_parietal - R_precentral_gyrus_2	0.64	0.24	0.27	0.33	sensorimotor - sensorimotor
R_angular_gyrus - R_post_cingulate	0.64	0.56	0.48	0.55	default - default
R_frontal_2 - L_dFC	0.64	0.25	0.24	0.25	sensorimotor - fronto-parietal
L_post_cingulate_3 - L_parietal_7	0.64	0.25	0.20	0.20	default - sensorimotor
L_temporal_3 - R_temporal_1	0.64	0.58	0.55	0.59	sensorimotor - sensorimotor
R_temporal_1 - L_dFC	0.64	0.25	0.22	0.16	sensorimotor - fronto-parietal
R_temporal_3 - L_parietal_4	0.64	0.23	0.28	0.24	cingulo-opercular - sensorimotor
L_basal_ganglia_2 - R_dFC_3	0.64	0.23	0.20	0.19	cingulo-opercular - sensorimotor
L_parietal_6 - R_temporal_1	0.64	0.44	0.42	0.43	sensorimotor - sensorimotor
R_precuneus_4 - R_angular_gyrus	0.64	0.22	0.27	0.26	default - default

R_parietal_3 - L_temporal_1	0.64	0.35	0.33	0.34	sensorimotor - sensorimotor
R_precuneus_1 - L_temporal_2	0.64	0.38	0.36	0.32	cingulo-opercular - sensorimotor
R_parietal_1 - R_mid_insula_1	0.64	0.39	0.33	0.38	sensorimotor - sensorimotor
R_parietal_3 - R_mid_insula_1	0.64	0.31	0.28	0.35	sensorimotor - sensorimotor
L_post_parietal_1 - L_parietal_7	0.64	0.48	0.49	0.48	sensorimotor - sensorimotor
L_post_cingulate_3 - L_post_cingulate_1	0.64	0.51	0.52	0.52	default - default
L_parietal_5 - R_temporal_1	0.64	0.51	0.52	0.47	sensorimotor - sensorimotor
L_post_parietal_1 - R_parietal_3	0.64	0.41	0.36	0.42	sensorimotor - sensorimotor
R_parietal_4 - L_temporal_2	0.63	0.44	0.42	0.40	cingulo-opercular - sensorimotor
L_post_cingulate_3 - R_basal_ganglia_2	0.63	0.26	0.26	0.26	default - cingulo-opercular
R_precuneus_3 - L_IPL_3	0.63	0.39	0.33	0.34	default - fronto-parietal
R_dFC_2 - L_vPFC	0.63	0.41	0.45	0.41	fronto-parietal - fronto-parietal
R_angular_gyrus - L_post_cingulate_2	0.63	0.55	0.52	0.53	default - default
R_sup_parietal - R_temporal_2	0.63	0.35	0.34	0.33	sensorimotor - cingulo-opercular
R_basal_ganglia_1 - R_dFC_3	0.63	0.27	0.26	0.20	cingulo-opercular - sensorimotor
R_IPL_2 - R_precuneus_3	0.63	0.31	0.30	0.28	fronto-parietal - default
R_sup_parietal - L_parietal_7	0.63	0.63	0.59	0.62	sensorimotor - sensorimotor
L_parietal_6 - R_precentral_gyrus_1	0.63	0.33	0.35	0.32	sensorimotor - sensorimotor
R_temporal_2 - L_parietal_5	0.63	0.38	0.34	0.38	cingulo-opercular - sensorimotor
L_temporal_1 - R_precentral_gyrus_2	0.63	0.39	0.35	0.37	sensorimotor - sensorimotor
R_IPL_1 - M_mPFC	0.63	0.21	0.18	0.17	fronto-parietal - default
R_parietal_1 - M_ACC_2	0.63	0.25	0.21	0.18	sensorimotor - fronto-parietal
R_parietal_2 - L_mid_insula_2	0.63	0.37	0.32	0.36	sensorimotor - sensorimotor
R_precuneus_3 -	0.63	0.61	0.61	0.56	default - default

R_precuneus_2					
L_IPL_3 - L_temporal_3	0.63	0.21	0.13	0.15	fronto-parietal - sensorimotor
R_temporal_3 - L_precentral_gyrus_1	0.63	0.28	0.30	0.28	cingulo-opercular - sensorimotor
R_sup_temporal - R_dFC_2	0.63	0.29	0.24	0.22	cingulo-opercular - fronto-parietal
L_IPL_1 - L_precentral_gyrus_2	0.63	0.27	0.22	0.27	fronto-parietal - sensorimotor
R_parietal_3 - R_post_insula	0.63	0.39	0.34	0.41	sensorimotor - sensorimotor
L_post_cingulate_3 - L_temporal_3	0.63	0.27	0.28	0.27	default - sensorimotor
R_mid_insula_1 - R_precentral_gyrus_2	0.63	0.40	0.42	0.44	sensorimotor - sensorimotor
L_post_cingulate_3 - R_sup_temporal	0.63	0.30	0.25	0.28	default - cingulo-opercular
L_post_parietal_1 - R_parietal_2	0.63	0.62	0.55	0.58	sensorimotor - sensorimotor
R_post_cingulate - R_precuneus_2	0.63	0.54	0.52	0.49	default - default
R_temporal_3 - R_sup_parietal	0.63	0.21	0.25	0.22	cingulo-opercular - sensorimotor
R_parietal_3 - L_precentral_gyrus_1	0.63	0.33	0.33	0.37	sensorimotor - sensorimotor
R_parietal_2 - L_precentral_gyrus_3	0.63	0.39	0.40	0.40	sensorimotor - sensorimotor
L_parietal_6 - L_parietal_3	0.63	0.67	0.69	0.72	sensorimotor - sensorimotor
L_post_cingulate_1 - L_temporal_1	0.62	0.26	0.23	0.24	default - sensorimotor
R_sup_parietal - L_precentral_gyrus_3	0.62	0.40	0.43	0.40	sensorimotor - sensorimotor
L_IPL_1 - R_mid_insula_1	0.62	0.21	0.19	0.19	fronto-parietal - sensorimotor
R_IPL_2 - L_IPL_3	0.62	0.41	0.47	0.51	fronto-parietal - fronto-parietal
L_angular_gyrus_2 - L_aPFC_2	0.62	0.35	0.25	0.36	default - default
L_temporal_2 - R_precentral_gyrus_2	0.62	0.36	0.34	0.36	sensorimotor - sensorimotor
L_parietal_4 - L_precentral_gyrus_2	0.62	0.47	0.44	0.49	sensorimotor - sensorimotor
R_parietal_4 - L_parietal_7	0.62	0.30	0.30	0.31	cingulo-opercular -

					sensorimotor
L_IPL_2 - L_post_parietal_1	0.62	0.25	0.19	0.19	fronto-parietal - sensorimotor
R_parietal_3 - R_precentral_gyrus_2	0.62	0.19	0.26	0.32	sensorimotor - sensorimotor
R_parietal_1 - L_dFC	0.62	0.24	0.18	0.18	sensorimotor - fronto-parietal
L_temporal_2 - L_post_parietal_1	0.62	0.37	0.41	0.32	sensorimotor - sensorimotor
R_sup_parietal - R_precentral_gyrus_1	0.62	0.34	0.41	0.36	sensorimotor - sensorimotor
L_IPL_1 - L_parietal_7	0.62	0.31	0.30	0.30	fronto-parietal - sensorimotor
R_precentral_gyrus_2 - R_frontal_2	0.62	0.55	0.51	0.51	sensorimotor - sensorimotor
L_IPL_1 - R_precentral_gyrus_2	0.62	0.20	0.14	0.22	fronto-parietal - sensorimotor
L_parietal_5 - L_parietal_3	0.62	0.47	0.41	0.51	sensorimotor - sensorimotor
L_angular_gyrus_2 - R_sup_temporal	0.62	0.23	0.12	0.25	default - cingulo-opercular
L_IPL_2 - L_sup_frontal	0.62	0.29	0.27	0.29	fronto-parietal - default
R_parietal_2 - R_temporal_1	0.62	0.48	0.45	0.44	sensorimotor - sensorimotor
L_parietal_8 - L_parietal_2	0.62	0.24	0.22	0.19	cingulo-opercular - sensorimotor
L_post_cingulate_3 - L_angular_gyrus_1	0.62	0.25	0.23	0.22	default - cingulo-opercular
R_angular_gyrus - R_IPL_1	0.62	0.26	0.31	0.31	default - fronto-parietal
R_parietal_1 - L_parietal_4	0.62	0.61	0.60	0.64	sensorimotor - sensorimotor
L_temporal_2 - R_precentral_gyrus_1	0.62	0.42	0.46	0.46	sensorimotor - sensorimotor
R_IPS - R_sup_temporal	0.62	0.25	0.17	0.22	fronto-parietal - cingulo-opercular
L_post_parietal_1 - R_frontal_2	0.62	0.33	0.37	0.37	sensorimotor - sensorimotor
L_vFC_2 - L_vPFC	0.62	0.46	0.44	0.46	sensorimotor - fronto-parietal
L_post_parietal_2 - L_parietal_5	0.62	0.49	0.45	0.46	fronto-parietal - sensorimotor
R_sup_temporal - L_parietal_7	0.62	0.18	0.20	0.14	cingulo-opercular - sensorimotor
R_temporal_3 - L_parietal_7	0.62	0.23	0.20	0.19	cingulo-opercular -

					sensorimotor
R_post_cingulate - L_parietal_7	0.62	0.27	0.20	0.21	default - sensorimotor
L_precentral_gyrus_2 - R_precentral_gyrus_2	0.62	0.58	0.54	0.56	sensorimotor - sensorimotor
R_sup_parietal - R_parietal_3	0.62	0.57	0.55	0.58	sensorimotor - sensorimotor
L_post_cingulate_2 - L_post_cingulate_1	0.62	0.72	0.69	0.71	default - default
R_parietal_4 - R_sup_parietal	0.62	0.25	0.31	0.33	cingulo-opercular - sensorimotor
L_IPL_1 - L_temporal_2	0.61	0.28	0.28	0.24	fronto-parietal - sensorimotor
L_parietal_2 - L_precentral_gyrus_2	0.61	0.66	0.60	0.63	sensorimotor - sensorimotor
L_IPL_1 - L_dFC	0.61	0.34	0.35	0.37	fronto-parietal - fronto-parietal
L_IPS_2 - L_IPS_1	0.61	0.45	0.50	0.56	default - fronto-parietal
R_post_cingulate - R_precuneus_1	0.61	0.35	0.24	0.31	default - cingulo-opercular
L_IPS_1 - R_mid_insula_1	0.61	0.13	0.12	0.18	fronto-parietal - sensorimotor
L_precentral_gyrus_1 - L_vPFC	0.61	0.34	0.27	0.30	sensorimotor - fronto-parietal
L_parietal_6 - R_precentral_gyrus_2	0.61	0.21	0.22	0.30	sensorimotor - sensorimotor
R_parietal_2 - M_mFC	0.61	0.31	0.23	0.21	sensorimotor - cingulo-opercular
R_ACC - M_mPFC	0.61	0.38	0.36	0.36	default - default
L_IPL_2 - L_IPL_1	0.61	0.45	0.45	0.43	fronto-parietal - fronto-parietal
L_post_cingulate_3 - R_post_insula	0.61	0.29	0.29	0.31	default - sensorimotor
L_temporal_2 - R_post_insula	0.61	0.61	0.61	0.63	sensorimotor - sensorimotor
L_parietal_8 - L_precentral_gyrus_1	0.61	0.27	0.25	0.27	cingulo-opercular - sensorimotor
L_thalamus_2 - R_mid_insula_1	0.61	0.30	0.31	0.25	cingulo-opercular - sensorimotor
L_parietal_1 - L_precentral_gyrus_1	0.61	0.40	0.35	0.43	sensorimotor - sensorimotor
L_IPL_2 - L_parietal_4	0.61	0.20	0.12	0.13	fronto-parietal - sensorimotor
L_angular_gyrus_1 - L_dlPFC	0.61	0.26	0.29	0.30	cingulo-opercular - fronto-

					parietal
L_temporal_2 - L_parietal_7	0.61	0.35	0.37	0.35	sensorimotor - sensorimotor
R_precuneus_2 - L_temporal_1	0.61	0.17	0.22	0.18	default - sensorimotor
R_parietal_4 - R_parietal_2	0.61	0.28	0.26	0.30	cingulo-opercular - sensorimotor
R_IPL_2 - L_post_cingulate_1	0.61	0.29	0.27	0.22	fronto-parietal - default
R_parietal_2 - L_precentral_gyrus_2	0.61	0.38	0.38	0.40	sensorimotor - sensorimotor
L_mid_insula_2 - R_mid_insula_1	0.61	0.62	0.59	0.58	sensorimotor - sensorimotor
L_IPL_1 - R_temporal_1	0.61	0.35	0.30	0.29	fronto-parietal - sensorimotor
L_post_parietal_2 - R_mid_insula_1	0.61	0.20	0.22	0.24	fronto-parietal - sensorimotor
R_sup_temporal - R_parietal_4	0.61	0.56	0.57	0.55	cingulo-opercular - cingulo-opercular
L_IPL_2 - L_post_parietal_2	0.61	0.51	0.51	0.47	fronto-parietal - fronto-parietal
L_temporal_3 - L_parietal_6	0.61	0.35	0.30	0.38	sensorimotor - sensorimotor
L_angular_gyrus_1 - L_sup_frontal	0.61	0.29	0.28	0.32	cingulo-opercular - default
L_parietal_8 - L_sup_frontal	0.61	0.21	0.22	0.28	cingulo-opercular - default
R_sup_parietal - R_post_insula	0.61	0.44	0.44	0.45	sensorimotor - sensorimotor
L_parietal_4 - R_mid_insula_1	0.61	0.34	0.38	0.38	sensorimotor - sensorimotor
L_parietal_3 - L_mid_insula_2	0.61	0.36	0.29	0.30	sensorimotor - sensorimotor
L_post_parietal_1 - R_mid_insula_1	0.61	0.34	0.35	0.29	sensorimotor - sensorimotor
R_temporal_2 - L_precentral_gyrus_1	0.61	0.44	0.38	0.42	cingulo-opercular - sensorimotor
R_parietal_2 - L_parietal_4	0.61	0.60	0.60	0.66	sensorimotor - sensorimotor
L_temporal_1 - L_thalamus_2	0.61	0.38	0.32	0.23	sensorimotor - cingulo-opercular
L_post_cingulate_2 - L_post_parietal_1	0.61	0.19	0.18	0.17	default - sensorimotor
R_precuneus_2 - R_parietal_4	0.61	0.23	0.25	0.19	default - cingulo-opercular
L_temporal_2 - R_temporal_1	0.61	0.60	0.58	0.61	sensorimotor - sensorimotor

L_parietal_8 - L_vmPFC	0.61	0.27	0.28	0.23	cingulo-opercular - default
L_angular_gyrus_1 - L_temporal_3	0.60	0.24	0.23	0.22	cingulo-opercular - sensorimotor
L_temporal_2 - L_parietal_4	0.60	0.37	0.38	0.39	sensorimotor - sensorimotor
L_parietal_7 - L_parietal_6	0.60	0.61	0.60	0.65	sensorimotor - sensorimotor
L_angular_gyrus_2 - R_IPL_2	0.60	0.32	0.34	0.34	default - fronto-parietal
L_angular_gyrus_2 - L_parietal_8	0.60	0.27	0.21	0.29	default - cingulo-opercular
R_mid_insula_1 - L_precentral_gyrus_2	0.60	0.46	0.45	0.45	sensorimotor - sensorimotor
R_precuneus_3 - L_parietal_8	0.60	0.20	0.15	0.17	default - cingulo-opercular
R_angular_gyrus - R_precuneus_2	0.60	0.44	0.48	0.43	default - default
L_parietal_7 - R_precentral_gyrus_2	0.60	0.22	0.27	0.31	sensorimotor - sensorimotor
L_temporal_3 - R_mid_insula_1	0.60	0.43	0.41	0.47	sensorimotor - sensorimotor
R_temporal_3 - L_vPFC	0.60	0.20	0.13	0.22	cingulo-opercular - fronto-parietal
L_parietal_5 - R_precentral_gyrus_3	0.60	0.52	0.56	0.58	sensorimotor - sensorimotor
L_precentral_gyrus_1 - R_precentral_gyrus_1	0.60	0.36	0.33	0.35	sensorimotor - sensorimotor
R_precuneus_3 - R_parietal_4	0.60	0.26	0.26	0.26	default - cingulo-opercular
L_temporal_2 - R_parietal_2	0.60	0.35	0.35	0.36	sensorimotor - sensorimotor
L_parietal_6 - L_parietal_4	0.60	0.64	0.59	0.67	sensorimotor - sensorimotor
L_IPS_2 - L_post_parietal_2	0.60	0.25	0.24	0.28	default - fronto-parietal
R_dFC_2 - R_ACC	0.60	0.29	0.22	0.20	fronto-parietal - default
R_parietal_2 - L_parietal_5	0.60	0.47	0.45	0.49	sensorimotor - sensorimotor
R_temporal_2 - R_parietal_1	0.60	0.41	0.35	0.40	cingulo-opercular - sensorimotor
L_post_parietal_2 - L_precentral_gyrus_1	0.60	0.36	0.36	0.42	fronto-parietal - sensorimotor
R_sup_parietal - L_temporal_3	0.60	0.34	0.35	0.36	sensorimotor - sensorimotor
R_mid_insula_2 - L_thalamus_2	0.60	0.42	0.41	0.38	cingulo-opercular - cingulo-opercular
R_parietal_3 - L_mid_insula_2	0.60	0.29	0.29	0.34	sensorimotor - sensorimotor

R_parietal_4 - R_dFC_1	0.60	0.25	0.25	0.21	cingulo-opercular - fronto-parietal
R_IPS - M_post_cingulate	0.60	0.30	0.30	0.23	fronto-parietal - default
R_parietal_3 - L_parietal_2	0.60	0.33	0.34	0.37	sensorimotor - sensorimotor
L_mid_insula_2 - R_basal_ganglia_1	0.60	0.28	0.21	0.15	sensorimotor - cingulo-opercular
L_IPL_1 - M_ACC_2	0.60	0.27	0.33	0.27	fronto-parietal - fronto-parietal
R_parietal_4 - L_precentral_gyrus_3	0.60	0.43	0.41	0.38	cingulo-opercular - sensorimotor
R_IPL_2 - R_dFC_3	0.60	0.22	0.18	0.22	fronto-parietal - sensorimotor
R_temporal_3 - R_precentral_gyrus_3	0.60	0.27	0.26	0.22	cingulo-opercular - sensorimotor
L_post_cingulate_3 - R_sup_parietal	0.60	0.19	0.13	0.19	default - sensorimotor
L_parietal_8 - R_temporal_1	0.60	0.34	0.29	0.24	cingulo-opercular - sensorimotor
L_IPL_3 - L_precuneus_1	0.60	0.39	0.40	0.38	fronto-parietal - default
L_parietal_8 - L_temporal_3	0.60	0.40	0.33	0.26	cingulo-opercular - sensorimotor

b)

Old Group					
Correlations	**ICC**	**Mean R scan 1**	**Mean R scan 2**	**Mean R scan 3**	**Networks**
L_parietal_3 - R_precentral_gyrus_3	0.81	0.40	0.51	0.41	sensorimotor - sensorimotor
L_precuneus_1 - L_temporal_3	0.78	0.21	0.30	0.20	default - sensorimotor
L_parietal_4 - L_parietal_3	0.75	0.72	0.71	0.70	sensorimotor - sensorimotor
R_IPL_2 - L_post_parietal_2	0.72	0.35	0.42	0.35	fronto-parietal - fronto-parietal
R_precuneus_3 - L_parietal_8	0.72	0.28	0.23	0.25	default - cingulo-opercular
L_precuneus_2 - L_parietal_8	0.72	0.21	0.20	0.24	default - cingulo-opercular
R_precentral_gyrus_2 - R_precentral_gyrus_1	0.72	0.66	0.61	0.57	sensorimotor - sensorimotor

R_temporal_1 - R_precentral_gyrus_2	0.72	0.49	0.42	0.42	sensorimotor - sensorimotor
L_precentral_gyrus_3 - L_precentral_gyrus_1	0.72	0.26	0.30	0.19	sensorimotor - sensorimotor
R_precuneus_3 - R_parietal_4	0.71	0.25	0.31	0.31	default - cingulo-opercular
L_mid_insula_2 - R_precentral_gyrus_3	0.71	0.27	0.25	0.19	sensorimotor - sensorimotor
R_parietal_1 - L_mid_insula_2	0.71	0.24	0.19	0.14	sensorimotor - sensorimotor
L_parietal_3 - R_precentral_gyrus_2	0.70	0.29	0.26	0.24	sensorimotor - sensorimotor
R_precentral_gyrus_1 - L_vFC_2	0.70	0.49	0.43	0.45	sensorimotor - sensorimotor
R_precuneus_1 - R_precentral_gyrus_2	0.70	0.26	0.22	0.21	cingulo-opercular - sensorimotor
L_precuneus_1 - R_dFC_3	0.70	0.30	0.34	0.27	default - sensorimotor
L_temporal_1 - R_temporal_1	0.70	0.68	0.64	0.66	sensorimotor - sensorimotor
L_precuneus_1 - R_frontal_2	0.69	0.32	0.36	0.33	default - sensorimotor
L_temporal_3 - L_parietal_4	0.69	0.32	0.39	0.29	sensorimotor - sensorimotor
L_parietal_8 - R_parietal_4	0.69	0.45	0.40	0.44	cingulo-opercular - cingulo-opercular
R_dFC_2 - R_dlPFC_2	0.69	0.52	0.55	0.49	fronto-parietal - fronto-parietal
L_temporal_2 - L_temporal_1	0.69	0.58	0.54	0.62	sensorimotor - sensorimotor
L_temporal_2 - R_temporal_1	0.69	0.51	0.46	0.50	sensorimotor - sensorimotor
R_dFC_2 - M_ACC_2	0.69	0.43	0.40	0.39	fronto-parietal - fronto-parietal
R_dFC_2 - R_dFC_1	0.69	0.46	0.49	0.45	fronto-parietal - fronto-parietal
L_parietal_4 - L_mid_insula_2	0.69	0.26	0.23	0.20	sensorimotor - sensorimotor
R_IPL_1 - M_ACC_2	0.69	0.42	0.42	0.31	fronto-parietal - fronto-parietal
R_precentral_gyrus_3 - L_vFC_2	0.69	0.45	0.39	0.39	sensorimotor - sensorimotor
R_precuneus_3 - R_sup_temporal	0.68	0.34	0.37	0.28	default - cingulo-opercular
R_precuneus_1 - R_mid_insula_1	0.68	0.23	0.23	0.18	cingulo-opercular - sensorimotor
L_parietal_6 -	0.68	0.28	0.27	0.28	sensorimotor -

R_precentral_gyrus_2					sensorimotor
R_precentral_gyrus_3 - R_precentral_gyrus_1	0.68	0.47	0.46	0.44	sensorimotor - sensorimotor
L_IPS_1 - L_post_parietal_2	0.68	0.65	0.68	0.64	fronto-parietal - fronto-parietal
L_aPFC_2 - M_mPFC	0.68	0.52	0.49	0.48	default - default
L_temporal_2 - L_parietal_4	0.68	0.30	0.25	0.21	sensorimotor - sensorimotor
R_frontal_2 - L_vFC_2	0.68	0.51	0.48	0.49	sensorimotor - sensorimotor
R_dlPFC_2 - L_aPFC_2	0.68	0.36	0.37	0.28	fronto-parietal - default
R_sup_frontal - R_dlPFC_1	0.68	0.30	0.30	0.25	default - fronto-parietal
R_temporal_2 - L_mid_insula_2	0.68	0.35	0.28	0.27	cingulo-opercular - sensorimotor
R_dlPFC_2 - R_ACC	0.68	0.23	0.31	0.22	fronto-parietal - default
R_precuneus_1 - L_temporal_1	0.67	0.36	0.43	0.34	cingulo-opercular - sensorimotor
L_temporal_1 - L_parietal_2	0.67	0.36	0.37	0.32	sensorimotor - sensorimotor
R_parietal_3 - L_parietal_4	0.67	0.57	0.55	0.51	sensorimotor - sensorimotor
R_parietal_2 - L_mid_insula_2	0.67	0.26	0.24	0.18	sensorimotor - sensorimotor
R_parietal_1 - R_vFC_2	0.67	0.24	0.26	0.19	sensorimotor - sensorimotor
R_basal_ganglia_2 - M_mPFC	0.67	0.21	0.15	0.16	cingulo-opercular - default
L_angular_gyrus_2 - L_sup_frontal	0.67	0.45	0.40	0.38	default - default
R_post_insula - L_temporal_1	0.67	0.52	0.52	0.51	sensorimotor - sensorimotor
R_dlPFC_1 - L_aPFC_2	0.67	0.37	0.45	0.35	fronto-parietal - default
R_angular_gyrus - L_post_cingulate_3	0.67	0.44	0.42	0.42	default - default
L_parietal_6 - L_parietal_2	0.66	0.44	0.42	0.40	sensorimotor - sensorimotor
L_parietal_4 - R_precentral_gyrus_3	0.66	0.54	0.61	0.55	sensorimotor - sensorimotor
R_IPS - R_dFC_2	0.66	0.32	0.35	0.25	fronto-parietal - fronto-parietal
R_parietal_1 - R_frontal_1	0.66	0.23	0.27	0.12	sensorimotor - sensorimotor
R_precuneus_1 - L_mid_insula_2	0.66	0.22	0.23	0.14	cingulo-opercular - sensorimotor

R_angular_gyrus - R_dlPFC_1	0.66	0.18	0.19	0.14	default - fronto-parietal
R_precentral_gyrus_3 - L_precentral_gyrus_2	0.66	0.54	0.52	0.52	sensorimotor - sensorimotor
L_temporal_3 - L_precentral_gyrus_1	0.66	0.26	0.37	0.19	sensorimotor - sensorimotor
R_dFC_2 - R_dlPFC_1	0.65	0.43	0.40	0.40	fronto-parietal - fronto-parietal
R_precuneus_4 - L_IPS_1	0.65	0.44	0.42	0.47	default - fronto-parietal
R_temporal_1 - L_precentral_gyrus_2	0.65	0.56	0.51	0.49	sensorimotor - sensorimotor
L_parietal_4 - R_precentral_gyrus_2	0.65	0.30	0.28	0.27	sensorimotor - sensorimotor
L_precuneus_1 - L_aPFC_2	0.65	0.19	0.24	0.18	default - default
R_precuneus_1 - R_temporal_1	0.65	0.39	0.40	0.30	cingulo-opercular - sensorimotor
L_parietal_5 - R_pre_SMA	0.65	0.29	0.32	0.28	sensorimotor - sensorimotor
L_parietal_4 - R_mid_insula_1	0.65	0.26	0.25	0.15	sensorimotor - sensorimotor
L_parietal_4 - R_precentral_gyrus_1	0.65	0.39	0.41	0.37	sensorimotor - sensorimotor
L_parietal_6 - L_temporal_1	0.65	0.41	0.40	0.41	sensorimotor - sensorimotor
L_parietal_3 - L_precentral_gyrus_2	0.65	0.37	0.36	0.33	sensorimotor - sensorimotor
R_parietal_3 - R_precentral_gyrus_2	0.65	0.22	0.23	0.22	sensorimotor - sensorimotor
L_mid_insula_2 - R_frontal_2	0.65	0.34	0.31	0.24	sensorimotor - sensorimotor
R_parietal_2 - R_mid_insula_1	0.65	0.28	0.26	0.19	sensorimotor - sensorimotor
R_temporal_1 - R_frontal_2	0.65	0.49	0.45	0.40	sensorimotor - sensorimotor
R_dlPFC_2 - R_aPFC_2	0.65	0.41	0.39	0.35	fronto-parietal - cingulo-opercular
R_parietal_2 - R_frontal_1	0.65	0.21	0.21	0.15	sensorimotor - sensorimotor
L_precuneus_1 - R_temporal_1	0.65	0.23	0.32	0.21	default - sensorimotor
L_precentral_gyrus_2 - L_mid_insula_1	0.65	0.41	0.43	0.39	sensorimotor - sensorimotor
L_temporal_3 - L_precentral_gyrus_2	0.65	0.43	0.38	0.40	sensorimotor - sensorimotor
L_precentral_gyrus_2 -	0.65	0.29	0.29	0.23	sensorimotor -

L_precentral_gyrus_1					sensorimotor
L_parietal_6 - R_precentral_gyrus_1	0.65	0.39	0.37	0.34	sensorimotor - sensorimotor
R_aPFC_2 - L_aPFC_2	0.64	0.63	0.62	0.60	cingulo-opercular - default
R_sup_parietal - L_precuneus_1	0.64	0.30	0.34	0.29	sensorimotor - default
L_parietal_8 - L_post_cingulate_1	0.64	0.25	0.20	0.12	cingulo-opercular - default
L_IPS_2 - L_vmPFC	0.64	0.32	0.28	0.32	default - default
L_precuneus_1 - L_precentral_gyrus_2	0.64	0.16	0.27	0.23	default - sensorimotor
L_precuneus_1 - L_parietal_5	0.64	0.38	0.40	0.42	default - sensorimotor
L_temporal_1 - R_precentral_gyrus_3	0.64	0.34	0.36	0.31	sensorimotor - sensorimotor
R_angular_gyrus - L_post_cingulate_2	0.64	0.49	0.49	0.49	default - default
R_sup_parietal - R_temporal_1	0.64	0.39	0.37	0.27	sensorimotor - sensorimotor
R_angular_gyrus - L_parietal_8	0.64	0.30	0.24	0.30	default - cingulo-opercular
M_mFC - L_sup_frontal	0.64	0.25	0.30	0.17	cingulo-opercular - default
L_parietal_6 - L_mid_insula_2	0.64	0.28	0.18	0.26	sensorimotor - sensorimotor
L_parietal_2 - R_precentral_gyrus_3	0.64	0.70	0.69	0.66	sensorimotor - sensorimotor
L_dFC - L_vPFC	0.64	0.40	0.43	0.33	fronto-parietal - fronto-parietal
R_IPL_1 - R_dlPFC_2	0.64	0.43	0.41	0.32	fronto-parietal - fronto-parietal
R_parietal_1 - R_precentral_gyrus_2	0.64	0.31	0.34	0.27	sensorimotor - sensorimotor
L_precuneus_1 - L_temporal_2	0.64	0.19	0.25	0.14	default - sensorimotor
L_post_cingulate_1 - L_mid_insula_3	0.64	0.19	0.23	0.20	default - cingulo-opercular
R_temporal_2 - L_precentral_gyrus_2	0.64	0.38	0.33	0.28	cingulo-opercular - sensorimotor
L_parietal_6 - L_parietal_4	0.64	0.74	0.75	0.71	sensorimotor - sensorimotor
L_mid_insula_2 - L_parietal_2	0.64	0.32	0.26	0.28	sensorimotor - sensorimotor
R_temporal_2 - R_precentral_gyrus_2	0.64	0.36	0.19	0.23	cingulo-opercular - sensorimotor
L_temporal_3 - R_temporal_1	0.63	0.60	0.49	0.53	sensorimotor -

					sensorimotor
R_IPL_2 - L_parietal_7	0.63	0.22	0.21	0.10	fronto-parietal - sensorimotor
R_precuneus_1 - L_temporal_3	0.63	0.32	0.40	0.28	cingulo-opercular - sensorimotor
L_temporal_3 - R_frontal_2	0.63	0.35	0.34	0.32	sensorimotor - sensorimotor
R_mid_insula_1 - R_precentral_gyrus_3	0.63	0.26	0.25	0.15	sensorimotor - sensorimotor
R_precentral_gyrus_1 - R_frontal_2	0.63	0.59	0.58	0.54	sensorimotor - sensorimotor
L_parietal_6 - R_precentral_gyrus_3	0.63	0.43	0.48	0.41	sensorimotor - sensorimotor
L_precentral_gyrus_2 - L_parietal_1	0.63	0.19	0.16	0.14	sensorimotor - sensorimotor
L_parietal_3 - R_temporal_1	0.63	0.41	0.39	0.37	sensorimotor - sensorimotor
R_precentral_gyrus_3 - R_precentral_gyrus_2	0.63	0.46	0.44	0.41	sensorimotor - sensorimotor
R_frontal_2 - R_vFC_1	0.63	0.24	0.25	0.16	sensorimotor - cingulo-opercular
L_parietal_2 - R_precentral_gyrus_1	0.63	0.48	0.50	0.42	sensorimotor - sensorimotor
L_precuneus_1 - L_temporal_1	0.63	0.22	0.32	0.23	default - sensorimotor
M_post_cingulate - R_post_insula	0.63	0.17	0.17	0.14	default - sensorimotor
L_post_cingulate_2 - L_angular_gyrus_1	0.63	0.12	0.19	0.18	default - cingulo-opercular
R_parietal_4 - R_vFC_1	0.63	0.37	0.42	0.34	cingulo-opercular - cingulo-opercular
L_mid_insula_1 - R_vFC_2	0.63	0.57	0.65	0.59	sensorimotor - sensorimotor
L_angular_gyrus_1 - L_post_cingulate_1	0.63	0.18	0.21	0.17	cingulo-opercular - default
R_dlPFC_1 - M_mPFC	0.63	0.26	0.34	0.27	fronto-parietal - default
R_angular_gyrus - R_post_cingulate	0.63	0.52	0.50	0.48	default - default
R_parietal_3 - R_precentral_gyrus_3	0.63	0.43	0.46	0.38	sensorimotor - sensorimotor
L_angular_gyrus_2 - L_post_cingulate_3	0.62	0.40	0.39	0.36	default - default
L_IPS_2 - R_IPL_1	0.62	0.17	0.23	0.15	default - fronto-parietal
L_post_cingulate_1 -	0.62	0.38	0.37	0.36	default - cingulo-opercular

R_thalamus_1					
R_mid_insula_1 - R_precentral_gyrus_1	0.62	0.53	0.50	0.47	sensorimotor - sensorimotor
L_temporal_3 - L_parietal_3	0.62	0.33	0.33	0.30	sensorimotor - sensorimotor
L_parietal_2 - R_vFC_2	0.62	0.20	0.26	0.19	sensorimotor - sensorimotor
R_parietal_1 - R_precentral_gyrus_1	0.62	0.38	0.40	0.33	sensorimotor - sensorimotor
R_precuneus_1 - R_ACC	0.62	0.14	0.20	0.13	cingulo-opercular - default
L_precentral_gyrus_1 - L_vFC_2	0.62	0.31	0.34	0.33	sensorimotor - sensorimotor
L_vFC_1 - R_vFC_1	0.62	0.40	0.36	0.39	cingulo-opercular - cingulo-opercular
L_parietal_7 - R_precentral_gyrus_2	0.62	0.23	0.24	0.23	sensorimotor - sensorimotor
L_precuneus_1 - L_precentral_gyrus_3	0.62	0.19	0.24	0.16	default - sensorimotor
R_basal_ganglia_2 - R_post_insula	0.62	0.25	0.18	0.15	cingulo-opercular - sensorimotor
L_parietal_4 - R_vFC_2	0.62	0.26	0.25	0.20	sensorimotor - sensorimotor
L_parietal_8 - M_post_cingulate	0.62	0.24	0.25	0.14	cingulo-opercular - default
L_parietal_3 - R_precentral_gyrus_1	0.62	0.38	0.35	0.33	sensorimotor - sensorimotor
L_parietal_2 - L_vPFC	0.62	0.23	0.29	0.28	sensorimotor - fronto-parietal
R_precentral_gyrus_3 - L_mid_insula_1	0.62	0.17	0.20	0.14	sensorimotor - sensorimotor
R_parietal_2 - R_precentral_gyrus_2	0.62	0.29	0.29	0.27	sensorimotor - sensorimotor
L_temporal_1 - R_frontal_2	0.62	0.39	0.40	0.34	sensorimotor - sensorimotor
R_temporal_2 - R_temporal_1	0.62	0.56	0.49	0.53	cingulo-opercular - sensorimotor
R_vlPFC - L_vmPFC	0.62	0.17	0.26	0.19	fronto-parietal - default
R_dlPFC_2 - R_sup_frontal	0.62	0.36	0.36	0.31	fronto-parietal - default
L_parietal_4 - L_vFC_2	0.61	0.31	0.31	0.30	sensorimotor - sensorimotor
R_sup_parietal - L_mid_insula_2	0.61	0.24	0.24	0.18	sensorimotor - sensorimotor
L_parietal_2 - L_precentral_gyrus_2	0.61	0.63	0.63	0.63	sensorimotor - sensorimotor

L_temporal_1 - R_mid_insula_1	0.61	0.47	0.43	0.43	sensorimotor - sensorimotor
L_temporal_3 - L_parietal_2	0.61	0.32	0.35	0.26	sensorimotor - sensorimotor
R_post_insula - R_mid_insula_1	0.61	0.50	0.55	0.48	sensorimotor - sensorimotor
L_parietal_6 - L_vFC_2	0.61	0.26	0.23	0.22	sensorimotor - sensorimotor
L_parietal_5 - L_precentral_gyrus_2	0.61	0.50	0.49	0.50	sensorimotor - sensorimotor
R_precentral_gyrus_3 - L_vPFC	0.61	0.22	0.23	0.25	sensorimotor - fronto-parietal
R_temporal_1 - L_vFC_2	0.61	0.43	0.32	0.32	sensorimotor - sensorimotor
L_temporal_2 - R_precentral_gyrus_3	0.61	0.26	0.23	0.20	sensorimotor - sensorimotor
R_precentral_gyrus_3 - R_vFC_2	0.60	0.21	0.27	0.19	sensorimotor - sensorimotor
L_parietal_6 - L_precentral_gyrus_2	0.60	0.37	0.36	0.39	sensorimotor - sensorimotor
L_precentral_gyrus_2 - L_vFC_2	0.60	0.54	0.57	0.57	sensorimotor - sensorimotor
R_precuneus_3 - R_temporal_2	0.60	0.17	0.29	0.16	default - cingulo-opercular
R_IPS - L_post_parietal_2	0.60	0.39	0.45	0.37	fronto-parietal - fronto-parietal
L_IPS_2 - R_dlPFC_1	0.60	0.17	0.21	0.13	default - fronto-parietal
L_temporal_3 - L_vFC_2	0.60	0.36	0.31	0.26	sensorimotor - sensorimotor
L_temporal_3 - R_precentral_gyrus_3	0.60	0.28	0.32	0.27	sensorimotor - sensorimotor
L_parietal_8 - M_mPFC	0.60	0.15	0.18	0.17	cingulo-opercular - default
L_temporal_3 - R_mid_insula_1	0.60	0.39	0.35	0.34	sensorimotor - sensorimotor
L_temporal_3 - R_parietal_2	0.60	0.28	0.36	0.32	sensorimotor - sensorimotor
L_IPL_3 - L_sup_frontal	0.60	0.27	0.25	0.31	fronto-parietal - default
L_mid_insula_2 - L_precentral_gyrus_2	0.60	0.49	0.45	0.45	sensorimotor - sensorimotor
L_temporal_3 - L_mid_insula_2	0.60	0.41	0.35	0.33	sensorimotor - sensorimotor
R_precuneus_4 - R_parietal_2	0.60	0.25	0.27	0.21	default - sensorimotor
L_temporal_2 - L_precentral_gyrus_1	0.60	0.21	0.24	0.14	sensorimotor - sensorimotor

M_post_cingulate - R_dFC_2	0.60	0.13	0.23	0.12	default - fronto-parietal
L_post_cingulate_1 - L_aPFC_2	0.60	0.23	0.21	0.14	default - default
R_parietal_1 - L_parietal_3	0.60	0.50	0.57	0.49	sensorimotor - sensorimotor
R_post_insula - R_parietal_1	0.60	0.34	0.33	0.23	sensorimotor - sensorimotor
L_angular_gyrus_2 - L_vmPFC	0.60	0.36	0.35	0.39	default - default
L_parietal_6 - R_parietal_1	0.60	0.57	0.59	0.53	sensorimotor - sensorimotor
L_post_parietal_1 - R_precentral_gyrus_2	0.60	0.23	0.22	0.17	sensorimotor - sensorimotor
R_parietal_3 - L_mid_insula_2	0.60	0.20	0.20	0.17	sensorimotor - sensorimotor
R_dlPFC_2 - M_mPFC	0.60	0.33	0.35	0.30	fronto-parietal - default
R_dFC_2 - L_vPFC	0.60	0.32	0.35	0.25	fronto-parietal - fronto-parietal
L_precentral_gyrus_3 - L_parietal_4	0.60	0.35	0.37	0.26	sensorimotor - sensorimotor

Chapter III

Age-related Reorganizational Changes in Modularity and Functional Connectivity of Human Brain Networks

Jie Song, Rasmus M. Birn, Mélanie Boly, Timothy B. Meier, Veena A. Nair, Mary E. Meyerand, Vivek Prabhakaran

At the time of submitting the dissertation, this work is under review by:

Brain Connectivity, 2014

Abstract

The human brain undergoes both morphological and functional modifications across the human lifespan. It is important to understand the aspects of brain reorganization that are critical in normal aging. To address this question, one approach is to investigate age-related topological changes of the brain. In this study, we developed a brain network model using graph theory methods applied to the resting-state functional MRI (fMRI) data acquired from two groups of normal healthy adults classified by age. We found that brain functional networks demonstrated modular organization in both groups with modularity decreased with aging, suggesting less distinct functional divisions across whole brain networks. Local efficiency was also decreased with aging but not global efficiency. Besides these brain-wide observations, we also observed consistent alterations of network properties at regional level in the elderly, particularly, in two major functional networks--the default mode and the sensorimotor network. Specifically, we found that measures of regional strength, local and global efficiency of functional connectivity were increased in the sensorimotor network while decreased in the default mode network with aging. These results indicate that global reorganization of brain functional networks may reflect overall topological changes with aging and that aging likely alters individual brain networks differently depending on the functional properties. Moreover, these findings highly correspond to the observation of decline in cognitive functions but maintenance of primary information processing in normal healthy aging, implying an underlying compensation mechanism evolving with aging to support higher level cognitive functioning.

Keywords: Resting-state functional connectivity, brain networks, aging, graph theory, modularity, efficiency, sensorimotor network, default mode network

Acronyms:

fMRI = functional MRI

RSFC = resting-state functional connectivity

DMN = default mode network

ACC = anterior cingulate cortex

AG = angular gyrus

PCG = precentral gyrus

Introduction

The topological aspects of human brain functional networks have drawn much attention in recent years. By modeling a large-scale brain network as a graph consisting of nodes (i.e., cortical and subcortical brain regions) and links (i.e., functional or anatomical connections among brain regions) (Rubinov and Sporns 2010), it is possible to construct a systematic, topological examination of brain functional or anatomical organization. This concept highlights the idea of understanding the complex brain system from information about how individual voxels or brain regions interact via functional or structural connections. Furthermore, rather than ascribing significant group differences or effects to particular voxels, as is historically done in functional neuroimaging, this concept also helps us to better understand how the brain network as a whole is organized in different populations.

Graph-theory based complex network analysis approach provides a powerful way of understanding the dynamic interactions of different brain regions and how these interactions produce complex behaviors. Graph metrics such as modularity, local efficiency, global efficiency and strength measures are often used to characterize brain network properties especially for group comparison. Modularity, in particular, is a ubiquitous property of complex, large-scale functional brain networks. Modules consist of densely intra-connected brain regions that are sparsely inter-connected with regions in other modules (Newman and Girvan 2004). Modular organization may represent stable subcomponents of the brain that facilitate the construction of a complex system from simple building blocks, and can be theoretically linked to network development (Alexander-Bloch et al. 2010), which has provided insights into abnormal brain development, neuropsychological conditions (Alexander-Bloch et al. 2014, Peng et al. 2014, Xu et al. 2013), and age-related neurodegenerative diseases (Gottlich et al. 2013, Kikuchi et al.

2013). Therefore, in the current study, we hypothesize that the brain functional modular structure can be affected by aging and that age-related changes in modularity can be revealed by graph theory analysis.

Previous studies on human brain aging have shown shrinkage of the adult brain as it ages, with a reported non-uniform pattern of changes in grey and white matter (Raz et al. 2005). These structural changes provide a fundamental basis for the hypothesized functional brain reorganization in relation to normal aging. Furthermore, previous graph theoretical analysis showed a substantial correspondence between structural connectivity and RSFC measured in the same subjects based on fMRI and diffusion spectrum imaging data (Hagmann et al. 2008). Here we test the hypothesis that the normal modular structure of functional brain networks might be altered with aging along with potential changes in functional connectivity measures such as local efficiency, global efficiency and strength. We further assessed these metrics at the local regional level for group comparison, which provides a finer-grained analysis of changes in network properties associated with aging.

Materials and Methods

Data acquisition

Participants were 26 younger adults (age 24.6 ± 3.3 years, 11 females) and 24 older adults (age 58.0 ± 6.1 years, 12 females) with no history of neurological or psychological disorders. Ten-minute resting-state fMRI scans were acquired from each subject as they rested with their eyes fixated on a cross projected to the center of a MR-safe screen. Imaging data was obtained on a 3.0 Tesla whole-body MRI scanner (DISCOVERY MR750, General Electric Medical Systems, Waukesha, WI, USA) with an 8-channel receive-only RF head coil array. This study was

approved by the University of Wisconsin-Madison Health Sciences Institutional Review Board. Written informed consent was provided by each participant.

T1-weighted structural images with 1 mm isotropic voxels were acquired axially with an MPRAGE sequence (TR = 8.132 ms, TE = 3.18 ms, TI = 450 ms, flip angle = 12º, field of view = 256 × 256 mm^2, matrix size = = 256 × 256, slice thickness = 1mm, number of slices = 156). BOLD EPI time series were collected in the sagittal plane with the following parameters: TR = 2.6 sec, TE = 22 ms, flip angle = 60º, field of view = 224 × 224 mm^2, matrix size = 64 × 64, slice thickness = 3.5mm, number of slices = 40 slices, 231 volumes.

Data processing

Resting-state fMRI data was processed in AFNI (Cox 1996) including the following initial preprocessing steps: 1) despiking to remove extreme outliers in the signal intensity time courses, 2) correcting for motion and slice-timing, 3) removing first three time points of the scan (total 231 time points). T1-weighted structural images were warped to standard MNI-space using a 12-parameter affine transformation. This transformation was combined with the T1-to-EPI alignment and used to map the functional EPI scans to MNI space with a resampling of 3mm resolution. The resulting structural images were later skull stripped and segmented into gray matter, white matter (WM) and cerebrospinal fluid (CSF) masks using FSL (Smith et al. 2004). The average signal time course from the WM and CSF masks and the 6 rigid body motion parameters were normalized and regressed out. The residuals from the functional data were spatially smoothed with a $4mm^2$ full width half maximum isotropic Gaussian kernel in AFNI and then temporally filtered with a band-pass from 0.01 to 0.1 Hz.

Head motion has been shown to significantly affect the RSFC measures (Van Dijk, Sabuncu, and Buckner 2012, Saad et al. 2009, Satterthwaite et al. 2012). Therefore, a secondary motion correction was performed to exclude certain time frames with motion above a more stringent threshold. A score of motion measurement corresponding to each time frame of fMRI scan was calculated as the square root of the sum of squares of the derivatives (SSD) of the six time courses of the motion parameters (Jones et al. 2010, Meier et al. 2012, Birn et al. 2013). In this study, any time frame associated with a score of SSD greater than 0.2 mm was censored and later excluded using the –censor option provided in the AFNI program, 3dDeconvolve. This option essentially performed zero-filling to maintain the same sampling rate and the same length of time series for each subject. To further eliminate group differences in motion contaminating functional connectivity assessments, we matched subjects from the two age groups with their average motion SSD across all these time points. This process resulted in two sub-groups with 16 subjects in each sub-group. Several younger subjects with small average motion SSD and several older subjects with relatively greater average motion SSD had to be removed in order to match the average motion for the two sub-groups. The younger sub-group had average motion SSD of 0.055 ± 0.018 mm, and the older sub-group had average motion SSD of 0.058 ± 0.019 mm. There was no significant group difference in terms of the average motion SSD (two-sample t-test, p-values = 0.39). The younger sub-group (ages 24.6 ± 3.5 years, 5 females) and older sub-group (ages 56.5 ± 5.3 years, 8 females) showed significant age differences (two-sample t-test, p-value < 0.00001), but no significant differences in gender (the Chi-square test, p-value = 0.47). Our findings presented here were based on data from these two sub-groups.

Resting-state functional connectivity (RSFC)

The RSFC was computed from 187 different brain regions defined within the sensorimotor, cingulo-opercular task control, fronto-parietal task control, dorsal/ventral attention, default mode, salience and subcortical/cerebellar networks (Power et al. 2011). In each of these brain regions, signals resulting from the processed functional data were extracted and averaged over a spherical region of interest (ROI) with a radius of 4mm. Pearson correlation coefficient (r_{ij}) was calculated for the *i*th and *j*th ROI. This generated a 187 × 187 adjacency matrix, M, for each subject, which served as the RSFC matrix for each subject within each group.

Thresholding brain networks

Thresholding a RSFC matrix is critical for obtaining a sparse adjacency matrix in that it should be optimal and contain not too little functional connections for detecting group differences but not too many functional connections that it may dilute group differences. The most commonly used approach for thresholding is to globally threshold the RSFC matrix at a fixed threshold, ρ, for any r_{ij} between -1 to 1. If $r_{ij} \geq \rho$, the corresponding element of the adjacency matrix, M_{ij}, is kept for the actual value of rij for a weighted adjacency matrix or is set to be 1 for a binary adjacency matrix. If $r_{ij} < \rho$, then M_{ij} is set to be 1 for both weighted and binary matrices. Note: except for strength, measures of modularity, local and global efficiency were computed using the binary adjacency matrix. One potential problem with this global thresholding method is that once thresholded, the sparse matrices are not fully connected from node to node (Alexander-Bloch et al. 2010). This disconnectedness of the resulting graphs may ultimately change the properties of the original global and local functional connectivity, which may bias the comparisons of graph-theoretic metrics between different groups of subjects. In this study, we anticipated that this might be a factor affecting our observations in age-related differences in

RSFC, and used a minimum spanning tree (MST) method in order to preserve fully connected brain graphs(Alexander-Bloch et al. 2010, Achard et al. 2012). In this present study, each MST per subject is a spanning tree of a weighted sub-graph that is fully connected with all nodes having maximum total weight of all links. Although the MST sparsely represents a "skeleton structure" of the brain graph, it does not form clusters or loops at regional level that keeps it from a biologically meaningful sparse representation (Alexander-Bloch et al. 2010). To obtain a sparse, fully connected and biologically meaningful graph, we added extra links to the MST from the remaining adjacency matrix. To do so, for each final sparse adjacency matrix, we added top 2% - 40% of the remaining links to the MST, respectively, to include the highest proportion of remaining functional connectivity. This ensured that each final graph per subject had equal number of links, and thus observations on age-related group differences were independent of number of functional connections. Several values of threshold were tested in order to examine the effect of different proportional thresholding on aging-related group differences. Thresholds from 2% to 40% were chosen based on the reasons that 1) the network measures are relatively constant over this range (Alexander-Bloch et al. 2010); 2) graphs become more random above a threshold level of 50% (Humphries, Gurney, and Prescott 2006). Current findings are based on thresholds from 2% to 8% at 2% intervals; results obtained from thresholds of 10% to 40% at 10% intervals can be found in the Supplementary Materials, appendix.

Measures of graph metrics

Graphs metrics including modularity, local and global efficiency and strength, were estimated using the Brain Connectivity Toolbox (Rubinov and Sporns 2010) with adaptation made for nodal or regional level calculation. Previous studies have reported age related changes in

connectivity and network measures on a global or brain-wide level (Geerligs et al. 2014, Alexander-Bloch et al. 2010, Meunier, Achard, et al. 2009) . In the current study, network measures were estimated at global and regional level, thus allowing an examination of age-related changes in functional connectivity at a brain-wide level and at regional level for a finer-grained analysis. Global level graph metrics were estimated by averaging each measure across all nodal regions and across all subjects in each group; regional level measures, except for modularity, were estimated for each node averaging across all subjects within each group. Statistical group comparison was conducted for each graph metric at each threshold using the Wilcoxon rank sum test.

Modularity is a global measure of how well a network can be decomposed into a set of sparsely interconnected but densely intra-connected modules (Newman 2004) and can be a valuable tool in identifying the functional blocks within the brain network. The optimal modular structure for a given network is typically estimated with optimization algorithms rather than computed exactly (Danon et al. 2005, Rubinov and Sporns 2010). In this study, network modularity was estimated via a 2-step approach to achieve an optimal module division, similar to the one applied in other studies (Rubinov and Sporns 2011, Geerligs et al. 2014). Modularity was first estimated using the algorithm by Newman-Girvan algorithm (Newman 2006a, b). Each module is extracted as a group of non-overlapping nodes by maximizing the number of within-module links and minimizing the number of between-module links among those nodes. As the optimal community structure and maximized modularity may vary from run to run due to heuristics in the algorithm (Rubinov and Sporns 2010), this step was repeated 500 times. In the second step, all previously detected community structures were refined using a fine-tuning algorithm (Rubinov and Sporns 2010, Sun et al. 2009) with maximum 500 times' iteration. Once an optimal modular structure of

the network has been identified, it is possible to assign topological roles to each node based on its density of intra- and inter-modular connections (Guimera et al. 2005). Therefore, intra-modular connectivity of each node was measured by the normalized intra-modular degree, that is, the within-module degree z-score (Rubinov and Sporns 2010). The within-module degree z-score is large for a node that has a large number of intra-modular connections relative to other nodes in the same module. We used the measure of within-module degree z-score to identify those "hub" nodes with high intra-modular connectivity and examined the age-related changes in these functionally important regions.

Local efficiency is a measure of information transfer in the immediate neighborhood of each node, indicating to what extent connections are being segregated into sub-networks (Achard et al. 2012), while global efficiency is a measure of information propagating in the whole network, indicating to what extent connections are being integrated into a whole brain-wide network (Rubinov and Sporns 2010). These two measures are both based on a pre-estimation of the minimum path length. For the local efficiency, the minimum path length is estimated as the shortest path length from node *i* to its nearest neighbor node *j* in the sub-graph they both belong to. For the global efficiency, the minimum path length is estimated as the shortest path length from node *i* to all other nodes *j* in the whole graph.

The strength of functional connectivity of each node is measured as the mean value of weights (i.e., cross-correlation coefficients) of all functional connections linking to the node. It provides an estimation of the functional importance of each node.

Measures of alteration of graph metrics

Age-related topological changes are different across brain locations and networks. These patterns of changes cannot be truly reflected with a solely brain-wide examination. However, it might be visualized by plotting, for a given graph metric, the mean value at each node in the younger group versus the difference between the older and younger groups at each node. This approach was originally reported and used for detecting functional network changes in comatose patients, and the gradient of a straight line fitted to the data was referred as a hub disruption index, κ (Achard et al. 2012). In this present study, the hub disruption index for a given graph metric, e.g., strength, was constructed by subtracting the younger group mean nodal strength from the mean strength of the corresponding node in the older group and plotting this group mean difference against the younger group mean. This transformation improves visualization of the age-related differences in profile of regional network properties.

Results

Altered modularity with aging

The functional networks representing patterns of cross-correlations between fMRI BOLD signals are illustrated using their adjacency matrices (Figure 1). Rows and columns in these matrices denote the 187 nodes, while elements of each matrix denote links or the cross-correlations between the corresponding nodes. Major functional networks from the younger (top panel) and older (bottom panel) groups are represented along the main diagonal of adjacency matrices. From the top left to the bottom right along the main diagonal in Figure 1, the square blocks represent the functional network of the sensorimotor, cingulo-opercular task control, fronto-parietal task control, dorsal/ventral attention, default mode, salience and subcortical/cerebellar networks.

At the global level, we observed that the mean modularity was reduced in the older group compared with the younger group over a range of different connection densities (Figure 2a). The older group showed higher variance of modularity across subjects compared with the younger group. Besides age-related differences in modularity between groups, both groups had mean values of modularity greater than 0.3 which were indicative of non-random community structure (Newman and Girvan 2004). This further suggested the presence of modular structure of functional brain networks across the adult life span. For both groups, modularity declined monotonically as a function of increasing connection density (Figure 2a).

At nodal level, a negative hub disruption index was observed for the measure of within-module degree *z* score consistently across different connection densities (Figure 3). Nodes that had dense intra-modular connections in the younger group (i.e., left ACC and left AG) were sparsely connected to other nodes within the same module in the older group, whereas nodes that had fewer intra-modular connections in the younger group (i.e., right PCG) were densely connected to other nodes within the same module in the older group.

Altered efficiency of functional connectivity with aging

At the whole-brain level, global efficiency was not significantly different between the two groups (Figure 2b) with hub disruption indices close to zero (Figure 4), while local efficiency was significantly reduced in the older group over a range of different connection densities (Figure 2c). The older group also showed higher variance of local efficiency compared with the younger group. Besides age-related differences in efficiency measures between the two groups, we observed that efficiency increased monotonically as a function of increasing connection density (Figures 2b, 2c) for both groups.

At nodal level, we observed markedly different patterns of age-related changes in network efficiency depending on the functional properties of individual brain regions. Both global and local efficiency was decreased in the DMN but increased in the sensorimotor network (Figures 4, 5, S3, S4). Our results also showed a negative hub disruption index for the measure of local efficiency (Figure 5), suggesting a potential age-induced exchange of a hub region with a nonhub region or vice versa.

Altered functional connectivity strength with aging

At the global level, the older group showed higher functional connectivity strength but not significantly different from the younger groups (Figures 2d, 6). At the global level, the hub disruption index of strength was 0.03, 0.11, 0.16 and 0.19 for thresholds of connection density at 2%, 4%, 6%, and 8% respectively (Figure 7). Small positive values of the hub disruption indices correspond to the slightly higher functional connectivity strength observed in Figures 2d and 6. At the regional level, we observed prominent group differences in the DMN and the sensorimotor network (Figure 7). Within the DMN, we found decreased within-network strength (Figure 8a) and a negative hub disruption index (Figure 9) with aging. In contrast, we found increased strength within the sensorimotor network (Figures 8b and 10a) and an overall increase in functional connectivity strength between the sensorimotor network and all other networks (Figure 8b), particularly, between the sensorimotor and attention networks (Figure 10b).

Age-related reorganizational changes in functional brain networks

Brain reorganization with aging undergoes dynamic changes across different functional brain networks. We further conducted a secondary analysis to quantify the changes in each brain

network using strength and degree (Figures S1, S2). Degree is a binary measure of functional connectivity and is estimated as the number of functional connections which survived thresholding. These two measures provide complementary aspects of network organization. Proportional tests were used to compare the proportions of strength and degree of each network to the total strength and degree in whole-brain networks, respectively. FDR correction was applied for multiple comparisons (Benjamini and Hochberg 1995).

We again observed distinct patterns of age-related reorganization in the DMN and the sensorimotor network (Figures S1, S2; Table 1). Within the DMN (i.e., elements within the square block of the RSFC matrices representing the DMN), both the strength (adjusted p-value = 0.024; Figure S1a) and degree (adjusted p-value = 0.0005; Figure S2a) significantly decreased with aging. In contrast, within the sensorimotor network, both the strength (adjusted p-value = 0.024; Figure S1a) and degree (adjusted p-value = 0.005; Figure S2a) significantly increased with aging. Between networks (i.e., the off-diagonal elements of the RSFC matrices), no significant age-related changes were observed in functional strength of between-network connections. However, the number of functional connections between the sensorimotor and all other networks significantly increased with aging (adjusted p-value < 0.00001; Figure S2 b-c). We also observed significantly increased between-network connections in the subcortical network (adjusted p-value = 0.005) in the older group (Figure S2 b-c). The older group showed significantly decreased proportion of between-network connections in both the frontal-parietal and salience networks (adjusted p-value < 0.01; Figure S2 b-c).

Table 1 Age-related network reorganization in the sensorimotor and DMN

Network Measures	**Within-network**		**Between-network**	
	DMN	***Sensorimotor***	***DMN***	***Sensorimotor***

Strength	↓	↑	→	→
Degree	↓	↑	→	↑

Arrows indicate directional changes of network measures with aging.

Discussion

In the present study, we used the correlations derived from the resting-state fMRI BOLD signals to develop a network model of the brain in two representative groups of healthy individuals. Graph-theory based network analysis was applied to examine age-related brain network reorganization. We found that similar to other studies (Meunier, Achard, et al. 2009, Bassett et al. 2010, Meunier, Lambiotte, et al. 2009, Geerligs et al. 2014), the functional brain networks of both groups exhibited modular organization (Figure 1). Graph theoretical work has shown that human brain consists of modular structures (Meunier, Lambiotte, et al. 2009, Bassett et al. 2010) which are altered in different clinical conditions such as Schizophrenia (Alexander-Bloch et al. 2010), Alzheimer's Disease (AD) (Brier et al. 2014) and in normal aging (Meunier, Achard, et al. 2009, Geerligs et al. 2014). This present study was partly motivated by recent work exploring brain network topology in comatose patients (Achard et al. 2012) based on graph metrics estimated from each individual brain region in the network. We adopted similar approach to conduct a finer-grained analysis of changes in brain functional reorganization associated with aging along with a systematic brain-wide network analysis. These findings are summarized in Table 2.

Table 2 Age-related network reorganization

Network Measures	**Effect of aging**
Modularity	↓
Local efficiency	↓
Global efficiency	→
Strength	→

Arrows indicate directional changes of network measures with aging.

Thresholding effect on brain network analysis

Several levels of threshold were tested in order to examine the effect of different proportional network thresholding on aging-related group differences. One way to control the thresholding effect is by evaluating the modularity measure. We observed both groups showing minimal values of modularity greater than 0.3 by the threshold level of 8% with total 187 brain regions, which were indicative of non-random community structure (Newman and Girvan 2004). In addition, modularity and local efficiency were significantly different between the two groups at threshold level of 2% to 4%. Therefore in this present study, with 187 brain regions and the minimum spanning tree method, a threshold level of top 2% to 4% of connections with highest functional strength provided a clear picture of network differences between the young and old groups.

Modularity decreases with healthy aging

The modular organization of human brain has been discussed in previous and recent studies (Szentagothai 1975, Eccles 1981, Gomez-Robles, Hopkins, and Sherwood 2014). Several studies have reported that the modular organization could be affected under neuropsychological conditions and disorders including depression (Peng et al. 2014), Schizophrenia (Alexander-Bloch et al. 2014), epilepsy (Xu et al. 2013) and age-related neurodegenerative diseases such as Parkinson's disease (Gottlich et al. 2013) and Alzheimer's disease (Kikuchi et al. 2013). One study also observed age-related alterations in the modular organization using cortical thickness analysis (Chen et al. 2011). Therefore, in our study we hypothesized that the brain functional

modular structure can be affected by aging. We further observed reduced modularity in the older group (Figure 2a). This age-related decline in modularity indicates less differentiated functional modular structure associated with aging. This alteration could be due to two main factors—an increase in inter-modular connections or decrease in intra-modular connections or a mix of the two factors. To further test this, we used the measure of hub disruption index to quantify the within-module functional connectivity at regional level. We found a consistent regional alteration of modularity in the older group over a range of different thresholds (Figure 3). Brain regions, such as left ACC and left AG as part of the DMN, which had dense within-module connections in the younger brain networks, had fewer within-module connections in the older group, whereas regions, such as right PCG, part of the sensorimotor network, which were sparsely connected to other regions within a module in the younger group, were densely connected in the older group. This regional alteration can be explained as the exchange of high-degree hub regions to low-degree non-hub regions or vice versa due to the effect of aging. This alteration of the order of importance of specific cortical regions within the same module indicates that although the whole-brain network could be equally well decomposed into a set of modules in both groups especially at higher thresholds (i.e., modularity was not significantly different between the two groups at threshold > 6%), functional identity of individual brain regions comprising specific modules might have markedly changed due to the effect of aging. Interestingly, although we observed an overall reduction of within-module functional connections in the older group, the total strength of functional connectivity seems increased in the older group (Figure 6) although not reaching statistical significance. To further explore this, we constructed a group-level whole-brain network by averaging each individual network across all subjects within each group and then calculated the strength and the number of within-network

connections and between-network connections. Results presented here are based on threshold level of top 2%. We found that the older group had fewer connections within-network but more connections between-network compared with the younger group (Table 3). This suggests a whole-brain level increased functional connectivity between networks and might be related to the over-activations in the elderly caused by less efficient use of neural resources (Geerligs et al. 2014, Morcom, Li, and Rugg 2007, Rypma, Eldreth, and Rebbechi 2007). A detailed group comparison of strength and degree for each individual network can be found in the Supplementary Materials (Figures S1, S2).

Table 3 Group-comparisons of strength and degree from whole-brain network analysis

	Strength		**Total**	**Degree**		**Total**
	Within-network	***Between-network***		***Within-network***	***Between-network***	
Young	234.34	118.07	352.41	1822	1781	3603
Older	211.58↓	146.32↑	357.90↑	1642↓	2186↑	3828↑

Arrows indicate directional changes of network measures with aging.

Reduced local efficiency but stable global efficiency with aging

Local efficiency was decreased in the older group (Figure 2c), while global efficiency was not affected by aging (Figure 2b). Local efficiency is a measure of local information processing. As discussed above, the whole brain-wide reduction of within-module connections in the elderly might lead to an over-recruitment of brain regions in order to process the seemingly overwhelming incoming information, which leads to less efficiency (Rypma, Eldreth, and Rebbechi 2007, Morcom, Li, and Rugg 2007). However, global efficiency is statistically stable between the two groups. This might be due to the equivalent amount of shortest path length for long-distance information processing in both groups (aided by the counterbalance of less within-

network connections but more between-network connections in the older group). This observation has some bearing on the neural bases for the pervasive age-related slowing effects on cognitive performance based on the processing-speed theory (Salthouse 1996). This theory suggests that cognitive performance is degraded when processing is slow because relevant operations cannot be successfully executed in limited time. This might be reflected by age-related reduction in local efficiency, which constrains the efficiency or effectiveness of specific processes of local information transfer. However, some relevant limitations may be partially overcome by experience as one view of expertise is that it serves to circumvent processing constraints or limitations (Salthouse 1991), which can be associated with the stable measurement of global efficiency observed in both age-groups. At regional level, local efficiency tends to decrease with a negative hub disruption index (Figure 5) which is consistent with the brain-wide decreased local efficiency. Global efficiency examined at regional level doesn't show significant group differences (Figure 4). However, both regional measures demonstrate distinct patterns of alteration in two important functional networks—the DMN and the sensorimotor network, which highlights the importance of examining brain reorganization at regional level as brain regions making up the different functional modules undergo different changes that may not be observed at the brain-wide level. Measures of local efficiency and global efficiency are decreased in the DMN but increased in the sensorimotor network (Figures 4-5, S3-S4).

The DMN is a nonhuman-specific intrinsic functional network, active all over the life from birth until aging where it is progressively modified, sensitive to different pathologies including AD, multiple sclerosis and mild cognitive impairment (MCI) and is known for its role in supporting high level cognitive functions (Mevel et al. 2010, Gili et al. 2011). The reduced efficiency in both local and global information processing in the DMN in relation to aging directly reflects a

decreased functional connectivity as observed in previous studies (Hafkemeijer, van der Grond, and Rombouts 2012, Damoiseaux et al. 2008) and in our study (Figure 8a). The decrease in functional connectivity leading to a decreased local and global efficiency may lead to the commonly observed age-related cognitive decline in patients with MCI and in the early stages of AD, two clinical conditions in which DMN shows decreased functional connectivity(Greicius et al. 2004, Sorg et al. 2007). The sensorimotor network, associated with primary information processing, showed increased local and global efficiency. This finding is consistent with the hypothesis that cognitive systems must compensate in aging for the general decline in sensorimotor abilities (Li and Lindenberger 2002, Seidler et al. 2010) as well as decreased functional connectivity and efficiency in DMN.

Altered functional connectivity in the default mode and the sensorimotor networks

The measure of strength of functional connectivity is highly consistent with all observations we have discussed. This is not surprising as we also found that the regional strength of functional connectivity was significantly decreased in the DMN and increased in the sensorimotor network (Table 1; Figures 7, 8). With the same number of functional connections, although brain-wide strength of RSFC seems to be higher in the older group (Figure 6), it is not significantly different between groups (Figure 2d). At the regional level, strength of functional connectivity showed similar pattern of changes in the DMN and sensorimotor networks as observed in the measures of local and global efficiency (Figure 7). The negative hub disruption index observed in the DMN indicates an exchange of hub to non-hub regions (Figure 9). This regional reorganization reveals a shift of functional importance of individual regions with aging and within the same functional module, which may not be easily observed in a brain-wide network analysis. We

observed that left ACC, left AG and right precuneus as part of the DMN switched from a hub region to a non-hub region with aging. These regions are associated with cognitive function (Pardo et al. 2007, Seghier 2013) and have shown decreased functional connectivity in AD patients (Hafkemeijer, van der Grond, and Rombouts 2012).

One previous study used test-retest reliability approach to examine age-related differences in RSFC and demonstrated increased reliable functional connections within the sensorimotor network in the older group (Song et al. 2012). Here, we observed an overall increase in functional connectivity across all regions belonging to the sensorimotor network (Figure 10a). Given that another previous study also observed an increase in functional connectivity between the sensorimotor and task-control networks (Meier et al. 2012), we further examined the connections between sensorimotor and all other networks in this study. We found a positive hub disruption index indicating increased connections between the sensorimotor network and other networks in the older group, particularly, between the sensorimotor and attention networks. This was further confirmed by the observation of increased number of connections and strength between these two networks (Table S1). This finding suggests that the attention network and the sensorimotor network have become less differentiated in normal aging, contributing to the reduced modularity, possibly due to the greater functional inter-dependence of these networks in the elderly.

This study does have limitations. The number of subjects is not large, with 16 subjects in each group. It is possible that the lack of significance for group comparison in brain-wide network analysis may be due to inadequate statistical power. However, we were able to uncover group differences at regional level. As we mentioned in the beginning, adult brain has shown shrinkage as it ages. The structural changes may have an impact on the results of functional connectivity

and network analysis. For future studies, examination of the regional network measures combined with local gray matter volume and subject's performance on cognitive tests may provide better understanding of age-related brain functional reorganization.

Conclusion

In the current study we have shown that human brain undergoes functional reorganization with aging at a whole brain-wide level and a regional level. The brain-wide network analysis showed reduced modularity and local efficiency in the older group possibly related to decreased intra-modular connections. We also conducted regional level network analysis for a finer-grained examination of age-related brain reorganization. We have shown that individual brain regions underwent distinct patterns of reorganization in terms of their functional properties. Brain regions in the DMN showed reduced local and global efficiency as well as regional functional connectivity, indicating a decline in high level cognitive functioning with aging, while an increase in these measures were observed in the sensorimotor network in the older group possibly indicating an underlying compensation mechanism for declined sensorimotor and cognitive abilities. Regional alteration also revealed a switch of functional importance of individual brain regions from a hub region to a non-hub region or vice versa. Our results suggest that brain-wide topological properties, such as modularity, are able to provide insights of brain network reorganization, but with a finer-grained analysis at regional level, more specific details of how individual brain regions with different functional properties evolve with aging are able to provide a better understanding of the aging brain.

Acknowledgements: The authors thank all subjects for their participation.

Disclosure statement: Portions of this work were previously presented in poster form at the 20th Annual Meeting of the Organization for Human Brain Mapping Annual Meeting. This work was supported by NIH grants RC1MH090912-01, K23NS086852, T32GM008692, UL1TR000427, and T32EB011434, by a Coulter Translational Research Award, an American Heart Association Postdoctoral Fellow Research Award, UW Milwaukee-Madison Intercampus Grants, and by Grants from the Shapiro Foundation and Foundation of ASNR award.

References

Achard, S., C. Delon-Martin, P. E. Vertes, F. Renard, M. Schenck, F. Schneider, C. Heinrich, S. Kremer, and E. T. Bullmore. 2012. "Hubs of brain functional networks are radically reorganized in comatose patients." *Proc Natl Acad Sci U S A* no. 109 (50):20608-13. doi: 10.1073/pnas.1208933109.

Alexander-Bloch, A. F., N. Gogtay, D. Meunier, R. Birn, L. Clasen, F. Lalonde, R. Lenroot, J. Giedd, and E. T. Bullmore. 2010. "Disrupted modularity and local connectivity of brain functional networks in childhood-onset schizophrenia." *Front Syst Neurosci* no. 4:147. doi: 10.3389/fnsys.2010.00147.

Alexander-Bloch, A. F., P. T. Reiss, J. Rapoport, H. McAdams, J. N. Giedd, E. T. Bullmore, and N. Gogtay. 2014. "Abnormal Cortical Growth in Schizophrenia Targets Normative Modules of Synchronized Development." *Biol Psychiatry*. doi: 10.1016/j.biopsych.2014.02.010.

Bassett, D. S., D. L. Greenfield, A. Meyer-Lindenberg, D. R. Weinberger, S. W. Moore, and E. T. Bullmore. 2010. "Efficient physical embedding of topologically complex information processing networks in brains and computer circuits." *PLoS Comput Biol* no. 6 (4):e1000748. doi: 10.1371/journal.pcbi.1000748.

Benjamini, Y., and Y. Hochberg. 1995. "Controlling the False Discovery Rate - a Practical and Powerful Approach to Multiple Testing." *Journal of the Royal Statistical Society Series B-Methodological* no. 57 (1):289-300.

Birn, R. M., E. K. Molloy, R. Patriat, T. Parker, T. B. Meier, G. R. Kirk, V. A. Nair, M. E. Meyerand, and V. Prabhakaran. 2013. "The effect of scan length on the reliability of resting-state fMRI connectivity estimates." *Neuroimage* no. 83:550-558. doi: DOI 10.1016/j.neuroimage.2013.05.099.

Brier, M. R., J. B. Thomas, A. M. Fagan, J. Hassenstab, D. M. Holtzman, T. L. Benzinger, J. C. Morris, and B. M. Ances. 2014. "Functional connectivity and graph theory in preclinical Alzheimer's disease." *Neurobiol Aging* no. 35 (4):757-68. doi: 10.1016/j.neurobiolaging.2013.10.081.

Chen, Z. J., Y. He, P. Rosa-Neto, G. L. Gong, and A. C. Evans. 2011. "Age-related alterations in the modular organization of structural cortical network by using cortical thickness from MRI." *Neuroimage* no. 56 (1):235-245. doi: DOI 10.1016/j.neuroimage.2011.01.010.

Cox, R. W. 1996. "AFNI: software for analysis and visualization of functional magnetic resonance neuroimages." *Comput Biomed Res* no. 29 (3):162-73.

Damoiseaux, J. S., C. F. Beckmann, E. J. Arigita, F. Barkhof, P. Scheltens, C. J. Stam, S. M. Smith, and S. A. Rombouts. 2008. "Reduced resting-state brain activity in the "default network" in normal aging." *Cereb Cortex* no. 18 (8):1856-64. doi: 10.1093/cercor/bhm207.

Danon, L., A. Diaz-Guilera, J. Duch, and A. Arenas. 2005. "Comparing community structure identification." *Journal of Statistical Mechanics-Theory and Experiment*. doi: Artn P09008

Doi 10.1088/1742-5468/2005/09/P09008.

Eccles, J. C. 1981. "The Modular Operation of the Cerebral Neocortex Considered as the Material Basis of Mental Events." *Neuroscience* no. 6 (10):1839-1855. doi: Doi 10.1016/0306-4522(81)90027-0.

Geerligs, L., R. J. Renken, E. Saliasi, N. M. Maurits, and M. M. Lorist. 2014. "A Brain-Wide Study of Age-Related Changes in Functional Connectivity." *Cereb Cortex*. doi: 10.1093/cercor/bhu012.

Gili, T., M. Cercignani, L. Serra, R. Perri, F. Giove, B. Maraviglia, C. Caltagirone, and M. Bozzali. 2011. "Regional brain atrophy and functional disconnection across Alzheimer's disease evolution." *J Neurol Neurosurg Psychiatry* no. 82 (1):58-66. doi: 10.1136/jnnp.2009.199935.

Gomez-Robles, A., W. D. Hopkins, and C. C. Sherwood. 2014. "Modular structure facilitates mosaic evolution of the brain in chimpanzees and humans." *Nat Commun* no. 5:4469. doi: 10.1038/ncomms5469.

Gottlich, M., T. F. Munte, M. Heldmann, M. Kasten, J. Hagenah, and U. M. Kramer. 2013. "Altered Resting State Brain Networks in Parkinson's Disease." *Plos One* no. 8 (10). doi: ARTN e77336

DOI 10.1371/journal.pone.0077336.

Greicius, M. D., G. Srivastava, A. L. Reiss, and V. Menon. 2004. "Default-mode network activity distinguishes Alzheimer's disease from healthy aging: Evidence from functional MRI." *Proceedings of the National Academy of Sciences of the United States of America* no. 101 (13):4637-4642. doi: DOI 10.1073/pnas.0308627101.

Guimera, R., S. Mossa, A. Turtschi, and L. A. N. Amaral. 2005. "The worldwide air transportation network: Anomalous centrality, community structure, and cities' global roles." *Proceedings of the National Academy of Sciences of the United States of America* no. 102 (22):7794-7799. doi: DOI 10.1073/pnas.0407994102.

Hafkemeijer, A., J. van der Grond, and S. A. Rombouts. 2012. "Imaging the default mode network in aging and dementia." *Biochim Biophys Acta* no. 1822 (3):431-41. doi: 10.1016/j.bbadis.2011.07.008.

Hagmann, P., L. Cammoun, X. Gigandet, R. Meuli, C. J. Honey, V. J. Wedeen, and O. Sporns. 2008. "Mapping the structural core of human cerebral cortex." *PLoS Biol* no. 6 (7):e159. doi: 10.1371/journal.pbio.0060159.

Humphries, M. D., K. Gurney, and T. J. Prescott. 2006. "The brainstem reticular formation is a small-world, not scale-free, network." *Proc Biol Sci* no. 273 (1585):503-11. doi: 10.1098/rspb.2005.3354.

Jones, T. B., P. A. Bandettini, L. Kenworthy, L. K. Case, S. C. Milleville, A. Martin, and R. M. Birn. 2010. "Sources of group differences in functional connectivity: An investigation applied to autism spectrum disorder." *Neuroimage* no. 49 (1):401-414. doi: DOI 10.1016/j.neuroimage.2009.07.051.

Kikuchi, M., S. Ogishima, T. Miyamoto, A. Miyashita, R. Kuwano, J. Nakaya, and H. Tanaka. 2013. "Identification of unstable network modules reveals disease modules associated with the progression of Alzheimer's disease." *PLoS One* no. 8 (11):e76162. doi: 10.1371/journal.pone.0076162.

Li, K. Z., and U. Lindenberger. 2002. "Relations between aging sensory/sensorimotor and cognitive functions." *Neurosci Biobehav Rev* no. 26 (7):777-83.

Meier, T. B., A. S. Desphande, S. Vergun, V. A. Nair, J. Song, B. B. Biswal, M. E. Meyerand, R. M. Birn, and V. Prabhakaran. 2012. "Support vector machine classification and characterization of age-related reorganization of functional brain networks." *Neuroimage* no. 60 (1):601-613. doi: DOI 10.1016/j.neuroimage.2011.12.052.

Meunier, D., S. Achard, A. Morcom, and E. Bullmore. 2009. "Age-related changes in modular organization of human brain functional networks." *Neuroimage* no. 44 (3):715-23. doi: 10.1016/j.neuroimage.2008.09.062.

Meunier, D., R. Lambiotte, A. Fornito, K. D. Ersche, and E. T. Bullmore. 2009. "Hierarchical modularity in human brain functional networks." *Front Neuroinform* no. 3:37. doi: 10.3389/neuro.11.037.2009.

Mevel, K., B. Grassiot, G. Chetelat, G. Defer, B. Desgranges, and F. Eustache. 2010. "[The default mode network: cognitive role and pathological disturbances]." *Rev Neurol (Paris)* no. 166 (11):859-72. doi: 10.1016/j.neurol.2010.01.008.

Morcom, A. M., J. Li, and M. D. Rugg. 2007. "Age effects on the neural correlates of episodic retrieval: increased cortical recruitment with matched performance." *Cereb Cortex* no. 17 (11):2491-506. doi: 10.1093/cercor/bhl155.

Newman, M. E. J. 2004. "Fast algorithm for detecting community structure in networks." *Physical Review E* no. 69 (6). doi: Artn 066133

Doi 10.1103/Physreve.69.066133.

Newman, M. E. J. 2006a. "Finding community structure in networks using the eigenvectors of matrices." *Physical Review E* no. 74 (3). doi: Artn 036104

Doi 10.1103/Physreve.74.036104.

Newman, M. E. J. 2006b. "Modularity and community structure in networks." *Proceedings of the National Academy of Sciences of the United States of America* no. 103 (23):8577-8582. doi: DOI 10.1073/pnas.0601602103.

Newman, M. E. J., and M. Girvan. 2004. "Finding and evaluating community structure in networks." *Physical Review E* no. 69 (2). doi: Artn 026113

Doi 10.1103/Physreve.69.026113.

Pardo, J. V., J. T. Lee, S. A. Sheikh, C. Surerus-Johnson, H. Shah, K. R. Munch, J. V. Carlis, S. M. Lewis, M. A. Kuskowski, and M. W. Dysken. 2007. "Where the brain grows old: decline in anterior cingulate and medial prefrontal function with normal aging." *Neuroimage* no. 35 (3):1231-7. doi: 10.1016/j.neuroimage.2006.12.044.

Peng, D., F. Shi, T. Shen, Z. Peng, C. Zhang, X. Liu, M. Qiu, J. Liu, K. Jiang, Y. Fang, and D. Shen. 2014. "Altered brain network modules induce helplessness in major depressive disorder." *J Affect Disord* no. 168C:21-29. doi: 10.1016/j.jad.2014.05.061.

Power, J. D., A. L. Cohen, S. M. Nelson, G. S. Wig, K. A. Barnes, J. A. Church, A. C. Vogel, T. O. Laumann, F. M. Miezin, B. L. Schlaggar, and S. E. Petersen. 2011. "Functional Network Organization of the Human Brain." *Neuron* no. 72 (4):665-678. doi: DOI 10.1016/j.neuron.2011.09.006.

Raz, N., U. Lindenberger, K. M. Rodrigue, K. M. Kennedy, D. Head, A. Williamson, C. Dahle, D. Gerstorf, and J. D. Acker. 2005. "Regional brain changes in aging healthy adults: general trends, individual differences and modifiers." *Cereb Cortex* no. 15 (11):1676-89. doi: 10.1093/cercor/bhi044.

Rubinov, M., and O. Sporns. 2010. "Complex network measures of brain connectivity: uses and interpretations." *Neuroimage* no. 52 (3):1059-69. doi: 10.1016/j.neuroimage.2009.10.003.

Rubinov, M., and O. Sporns. 2011. "Weight-conserving characterization of complex functional brain networks." *Neuroimage* no. 56 (4):2068-79. doi: 10.1016/j.neuroimage.2011.03.069.

Rypma, B., D. A. Eldreth, and D. Rebbechi. 2007. "Age-related differences in activation-performance relations in delayed-response tasks: a multiple component analysis." *Cortex* no. 43 (1):65-76.

Saad, Z. S., D. R. Glen, G. Chen, M. S. Beauchamp, R. Desai, and R. W. Cox. 2009. "A new method for improving functional-to-structural MRI alignment using local Pearson correlation." *Neuroimage* no. 44 (3):839-848. doi: DOI 10.1016/j.neuroimage.2008.09.037.

Salthouse, T. A. 1991. *Toward a General Theory of Expertise: Prospects and Limits*. New York: Cambridge University Press.

Salthouse, T. A. 1996. "The processing-speed theory of adult age differences in cognition." *Psychol Rev* no. 103 (3):403-28.

Satterthwaite, T. D., D. H. Wolf, J. Loughead, K. Ruparel, M. A. Elliott, H. Hakonarson, R. C. Gur, and R. E. Gur. 2012. "Impact of in-scanner head motion on multiple measures of functional connectivity: Relevance for studies of neurodevelopment in youth." *Neuroimage* no. 60 (1):623-632. doi: DOI 10.1016/j.neuroimage.2011.12.063.

Seghier, M. L. 2013. "The angular gyrus: multiple functions and multiple subdivisions." *Neuroscientist* no. 19 (1):43-61. doi: 10.1177/1073858412440596.

Seidler, R. D., J. A. Bernard, T. B. Burutolu, B. W. Fling, M. T. Gordon, J. T. Gwin, Y. Kwak, and D. B. Lipps. 2010. "Motor control and aging: links to age-related brain structural, functional, and biochemical effects." *Neurosci Biobehav Rev* no. 34 (5):721-33. doi: 10.1016/j.neubiorev.2009.10.005.

Smith, S. M., M. Jenkinson, M. W. Woolrich, C. F. Beckmann, T. E. J. Behrens, H. Johansen-Berg, P. R. Bannister, M. De Luca, I. Drobnjak, D. E. Flitney, R. K. Niazy, J. Saunders, J. Vickers, Y. Y. Zhang, N. De Stefano, J. M. Brady, and P. M. Matthews. 2004. "Advances in functional and structural MR image analysis and implementation as FSL." *Neuroimage* no. 23:S208-S219. doi: DOI 10.1016/j.neuroimage.2004.07.051.

Song, J., A. S. Desphande, T. B. Meier, D. L. Tudorascu, S. Vergun, V. A. Nair, B. B. Biswal, M. E. Meyerand, R. M. Birn, P. Bellec, and V. Prabhakaran. 2012. "Age-related differences in test-retest reliability in resting-state brain functional connectivity." *PLoS One* no. 7 (12):e49847. doi: 10.1371/journal.pone.0049847.

Sorg, C., V. Riedl, M. Muhlau, V. D. Calhoun, T. Eichele, L. Laer, A. Drzezga, H. Forstl, A. Kurz, C. Zimmer, and A. M. Wohlschlager. 2007. "Selective changes of resting-state networks in individuals at risk for Alzheimer's disease." *Proceedings of the National Academy of Sciences of the United States of America* no. 104 (47):18760-18765. doi: DOI 10.1073/pnas.0708803104.

Sun, Y., B. Danila, K. Josic, and K. E. Bassler. 2009. "Improved community structure detection using a modified fine-tuning strategy." *Epl* no. 86 (2). doi: Artn 28004
Doi 10.1209/0295-5075/86/28004.

Szentagothai, J. 1975. "The 'module-concept' in cerebral cortex architecture." *Brain Res* no. 95 (2-3):475-96.

Van Dijk, K. R. A., M. R. Sabuncu, and R. L. Buckner. 2012. "The influence of head motion on intrinsic functional connectivity MRI." *Neuroimage* no. 59 (1):431-438. doi: DOI 10.1016/j.neuroimage.2011.07.044.

Xu, C. P., S. W. Zhang, T. Fang, M. X. Ma, C. C. Qian, H. F. Chen, H. W. Zhu, Y. J. Li, and Z. X. Liu. 2013. "Altered Functional Connectivity within and between Brain Modules in

Absence Epilepsy: A Resting-State Functional Magnetic Resonance Imaging Study." *Biomed Research International*. doi: Artn 734893
Doi 10.1155/2013/734893.

Figure 1 Adjacency Matrices shown at threshold of 8% (Young—upper panel, Older—bottom panel)

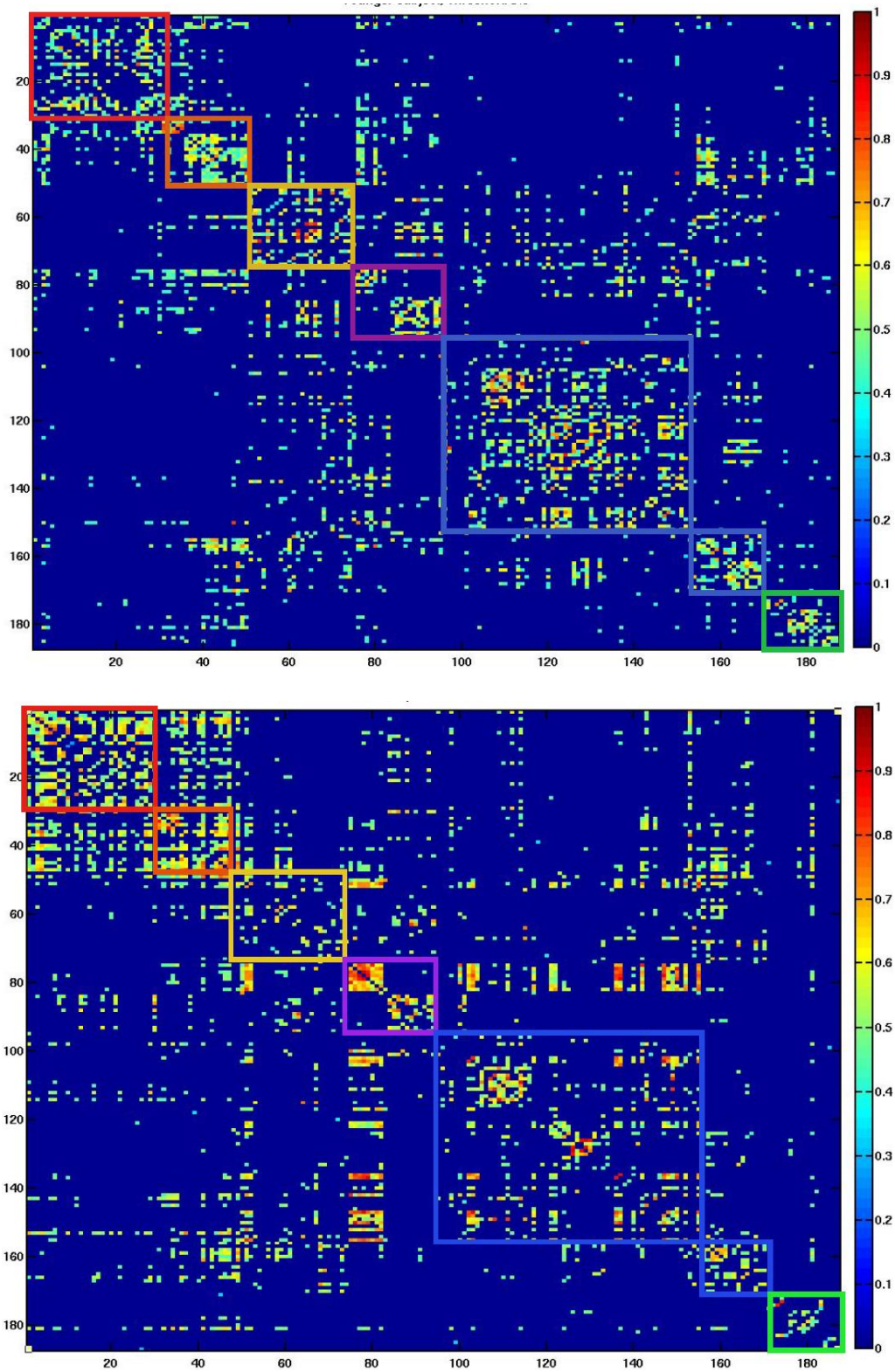

Functional networks are illustrated using adjacency matrices. Rows and columns denote the 187 nodes and each element of the matrix denotes a link between the corresponding nodes. Square blocks from the top left to the bottom right along the main diagonal represent the sensorimotor (red; 35 regions), cingulo-opercular task control (orange; 14 regions), fronto-parietal task control (gold; 25 regions), dorsal/ventral attention (magenta, 20 regions), default mode (medium blue, 58 regions), salience (royal blue; 18 regions) and subcortical/cerebellar (green; 19 regions) networks. Elements within each block represent within-network functional connections and elements outside of blocks represent between-network connections.

Figure 2

a) Modularity (Young—red; Older—blue)

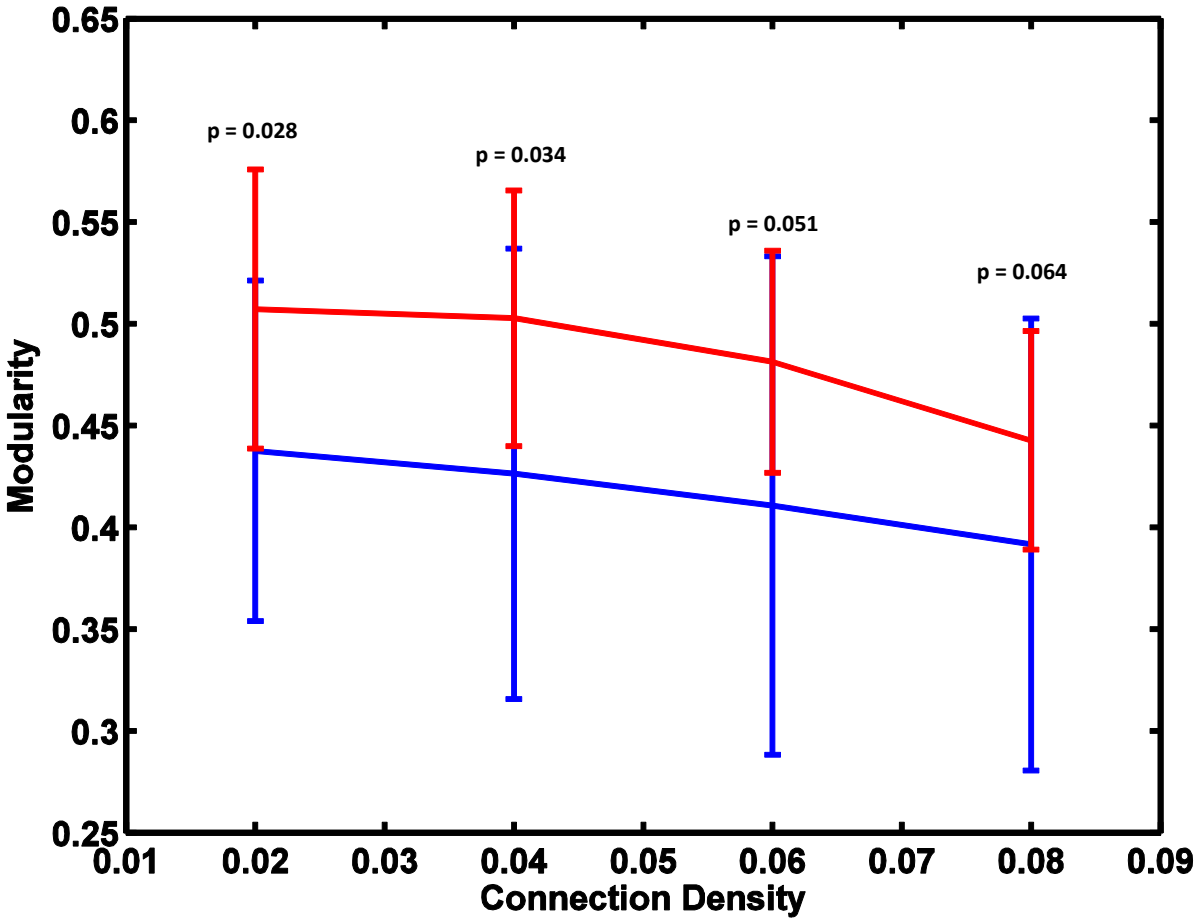

b) Global efficiency (Young—red; Older—blue)

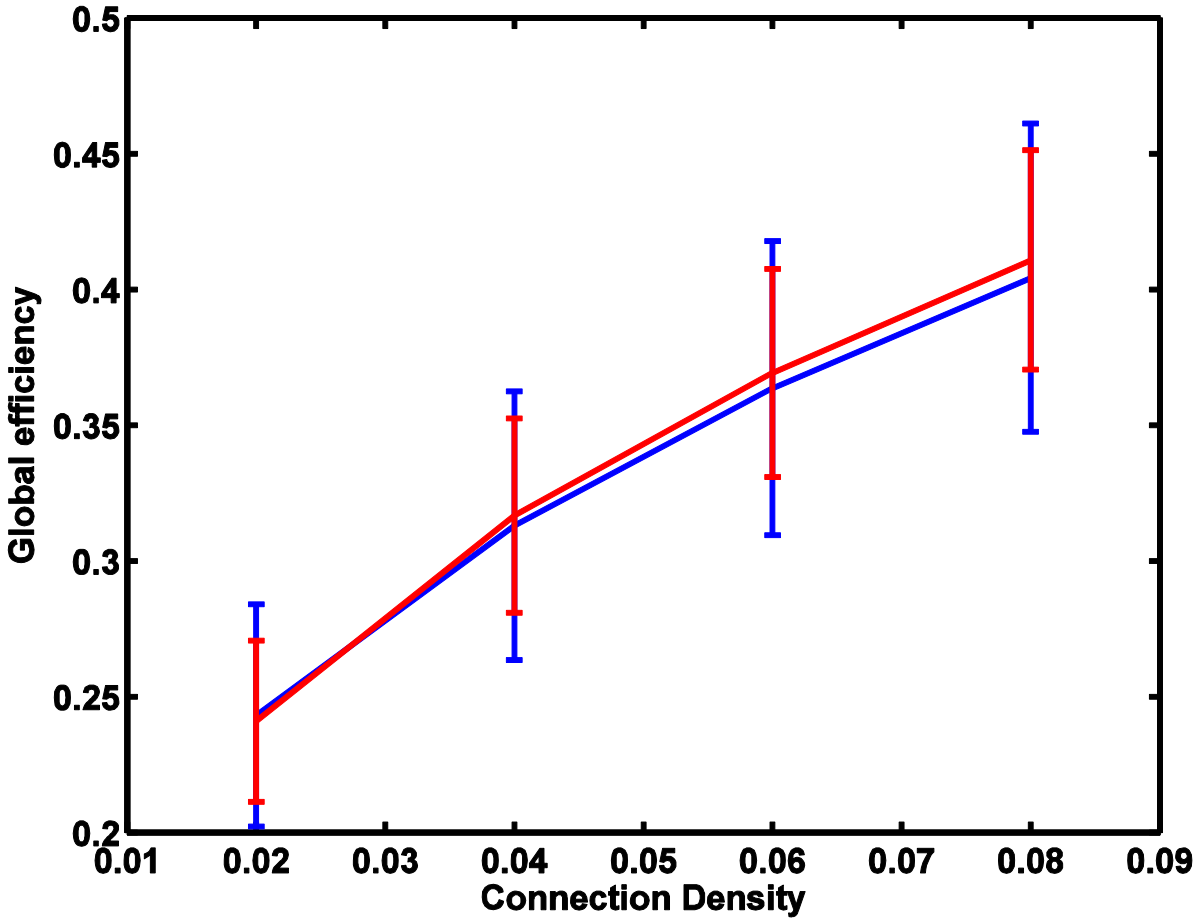

c) Local efficiency (Young—red; Older—blue)

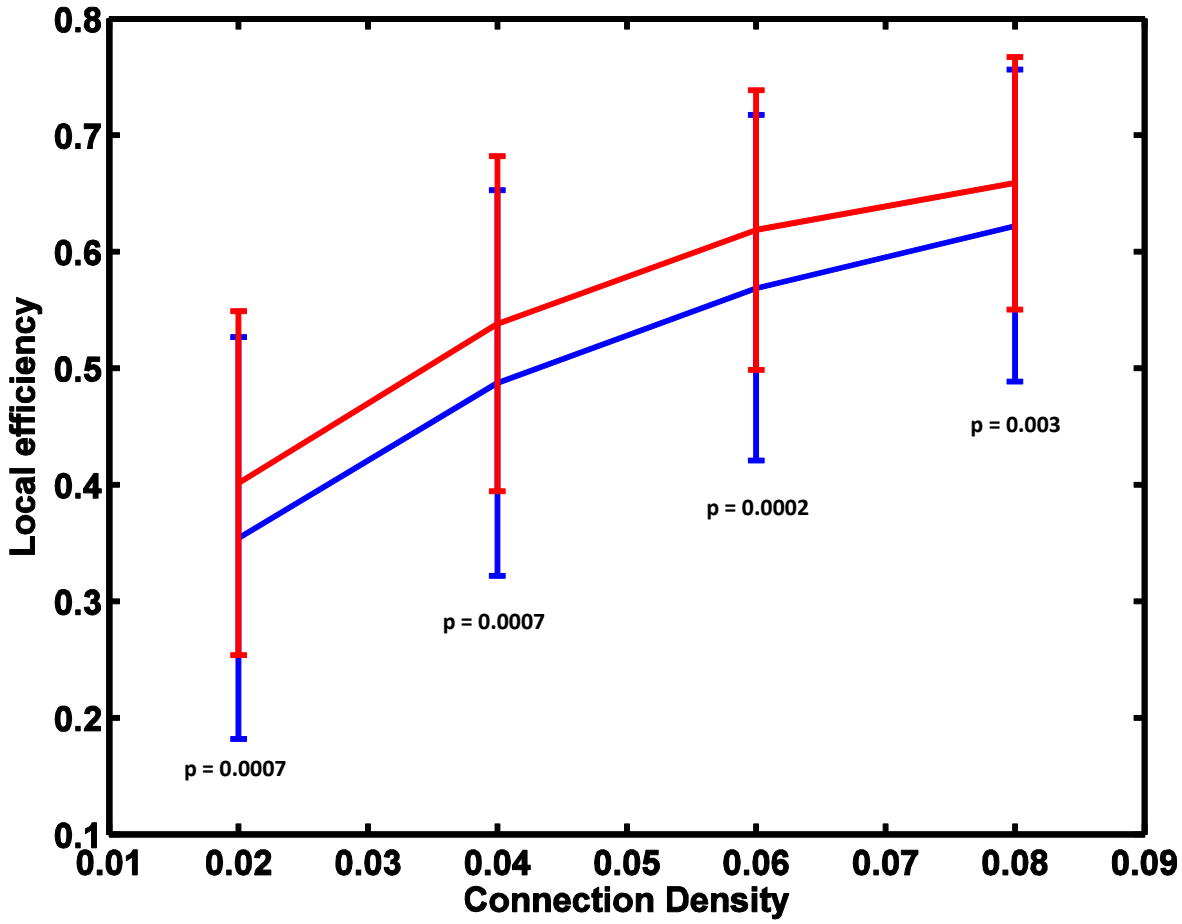

d) Strength (Young—red; Older—blue)

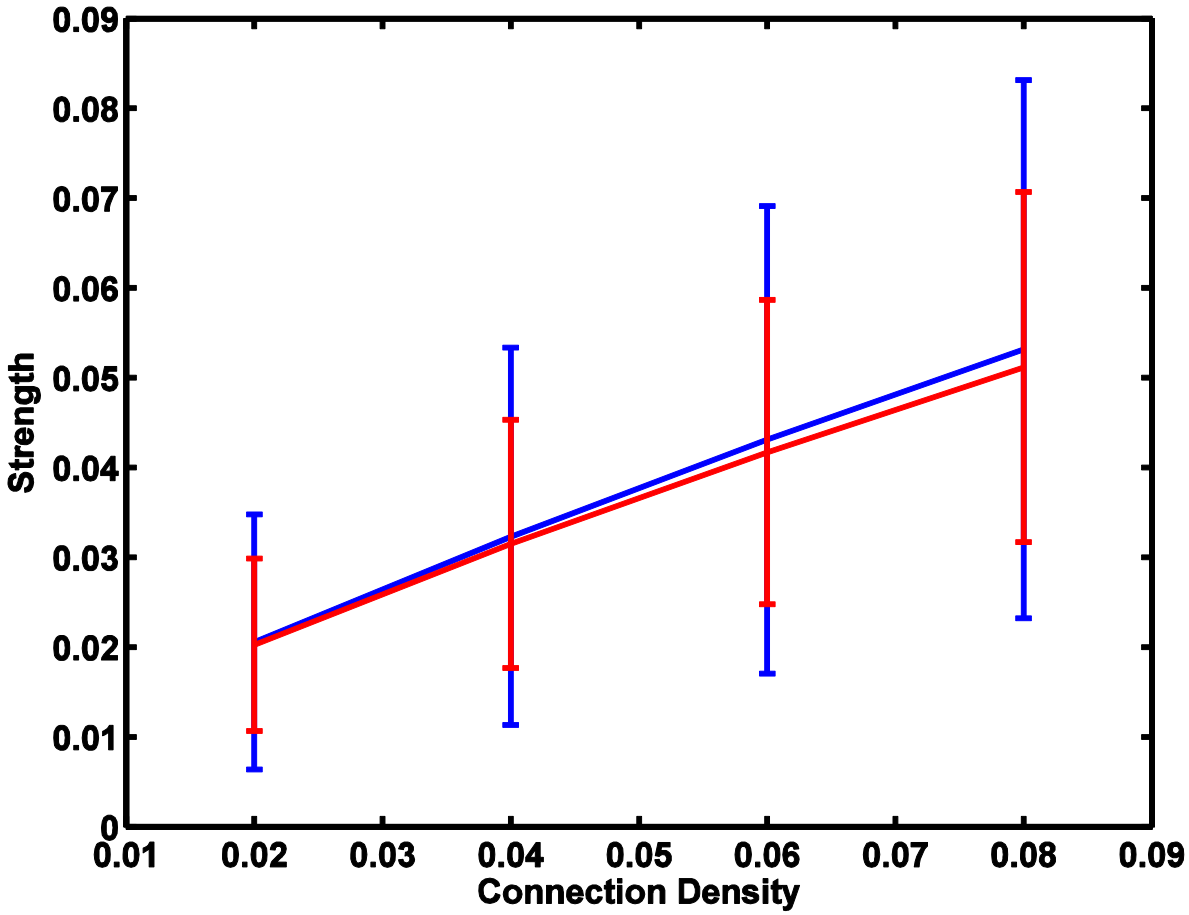

The older group (blue lines) showed decreased modularity and local efficiency compared with the young group (red lines) across a range of thresholds (i.e., connection density). Group comparison was tested using the Wilcoxon rank sum test with p-value of significance shown at each threshold. No significant group difference was observed in the global efficiency and the strength of functional connectivity.

Figure 3 Hub disruption index of within-module functional connectivity

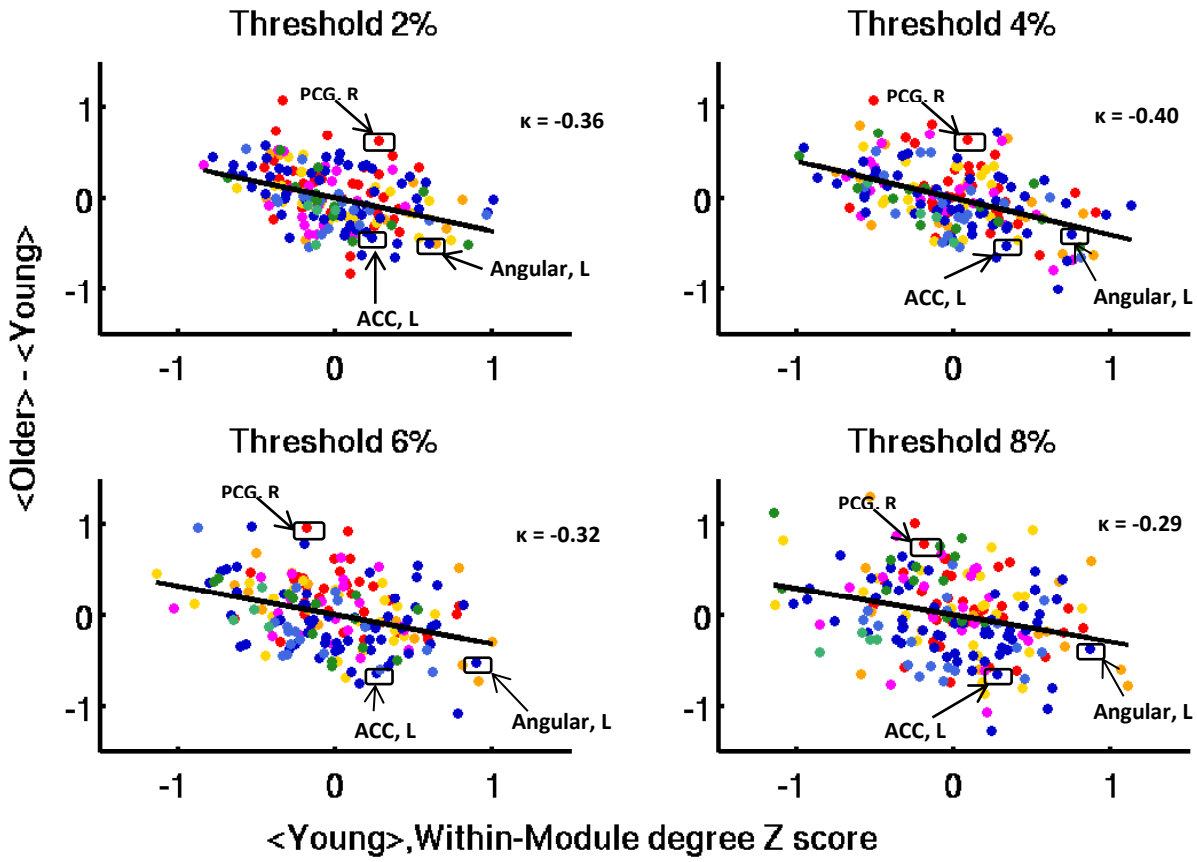

The hub disruption index of within-module functional connectivity is plotted at each threshold of connection density. Each data point is color-coded representing a node belonging to a particular functional network (i.e., red dots represent nodes belonging to the sensorimotor network and blue dots represent nodes belong to the default mode network). The mean value of within-module degree z-score of each node in the younger group <Young> (x-axis) is plotted against the difference between groups in mean value of within-module degree z-score of each node <Older> - <Young> (y-axis). A node with high number of connections within a module (i.e., measured as within-module degree z-score) in the younger group showed an abnormal reduction of connections in the older group, e.g., the left anterior cingulate cortex (ACC) and left anterior cingulate from the default mode network, whereas a node with few number of within-module

connections in the young group showed an abnormal increase of connections in the older group, e.g., the right precentral gyrus from the sensorimotor network. The solid black line represents a linear regression fitting to the data and the slope of the line is defined as the hub disruption index, κ (Achard et al. 2012). The negative hub disruption index across different levels of thresholding suggested an overall disruption of global modularity in the older group.

Reference:

Achard, S., C. Delon-Martin, P. E. Vertes, F. Renard, M. Schenck, F. Schneider, C. Heinrich, S. Kremer, and E. T. Bullmore. 2012. "Hubs of brain functional networks are radically reorganized in comatose patients." *Proc Natl Acad Sci U S A* no. 109 (50):20608-13. doi: 10.1073/pnas.1208933109.

Figure 4 Hub disruption index of global efficiency

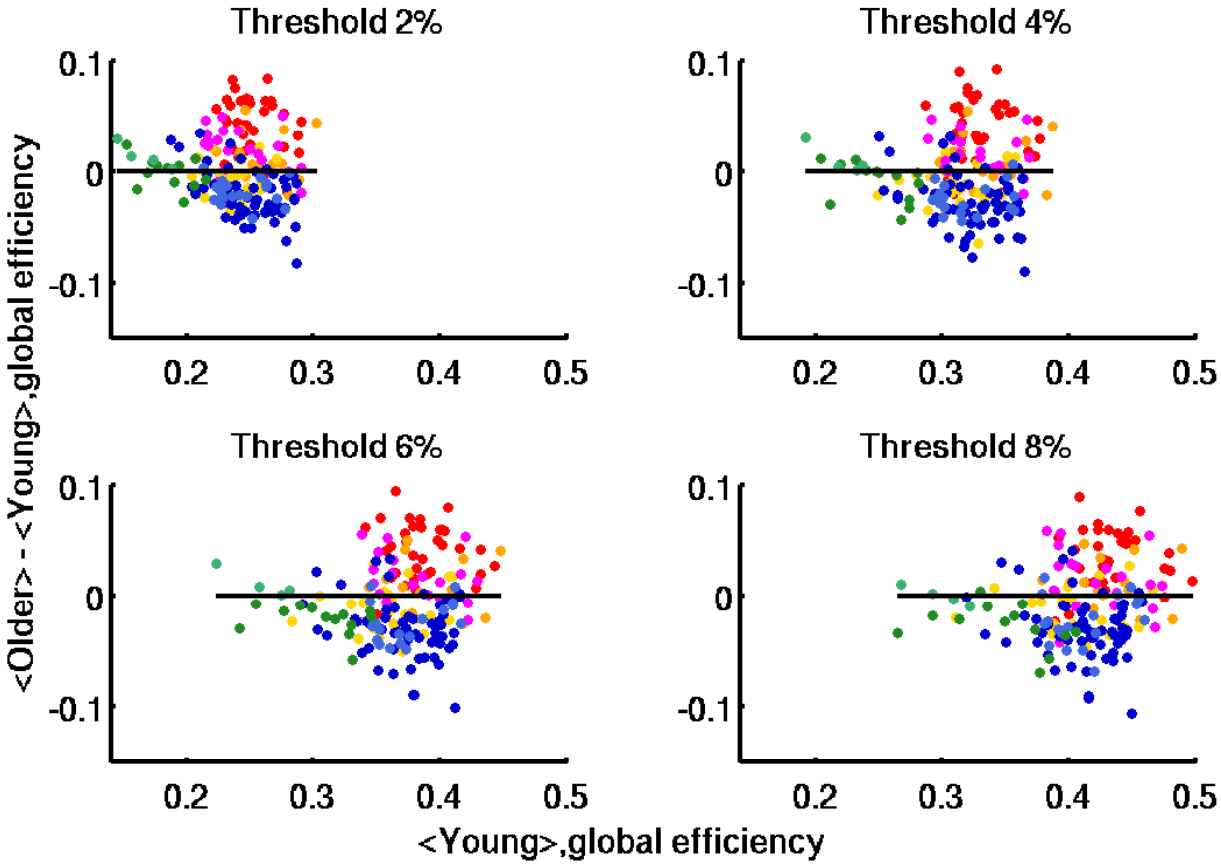

In the figure, each black horizontal line represents equivalent global efficiency for the older group vs. the younger group. The hub disruption index of global efficiency was close to zero. However, nodes belonging to the sensorimotor network (red) showed increased global efficiency consistently while nodes belonging to the default mode network (medium blue) showed decreased global efficiency consistently.

Figure 5 Hub disruption index of local efficiency

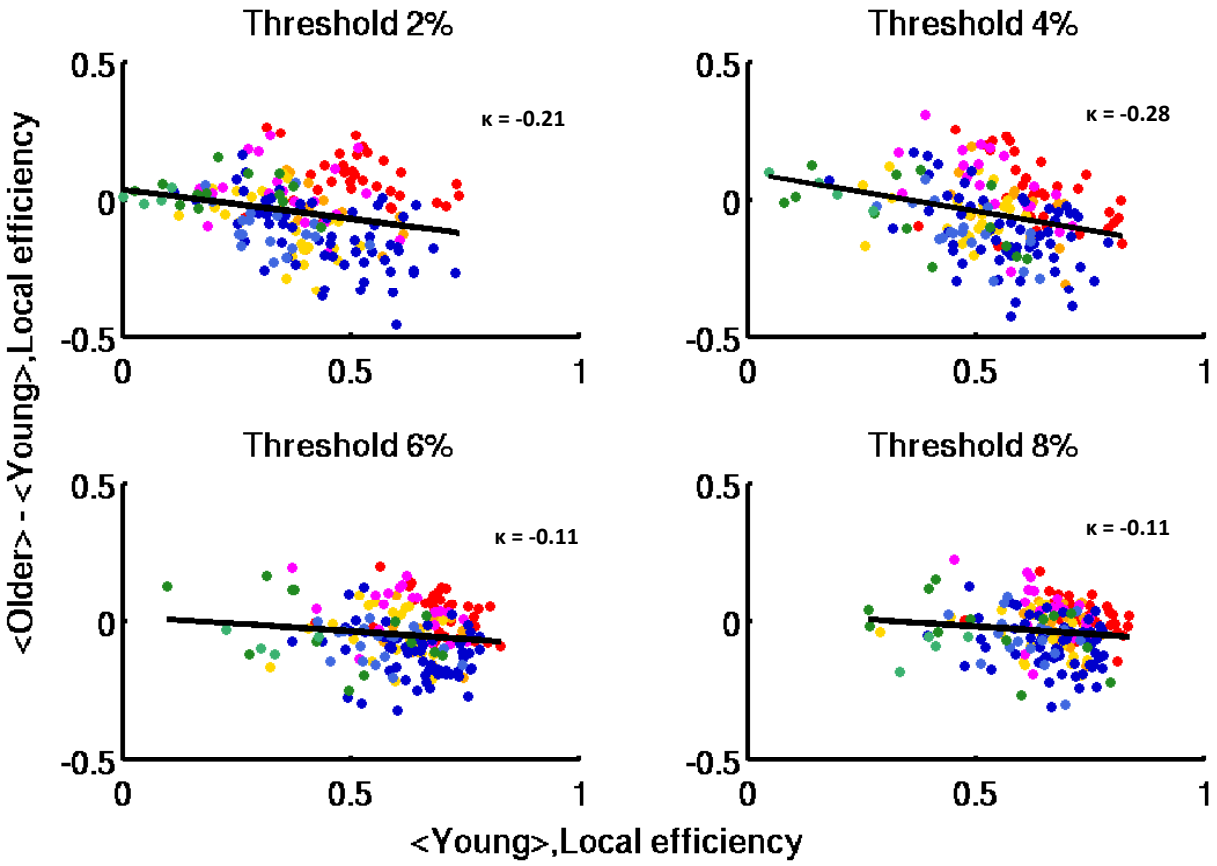

The hub disruption index of local efficiency is plotted at each threshold of connection density. The mean value of local efficiency of each node in the younger group <Young> (x-axis) is plotted against the difference between groups in mean local efficiency of each node <Older> - <Young> (y-axis). The hub disruption index of local efficiency was estimated as the gradient of the solid black line fitted to the scatterplots. Negative hub disruption indices were observed across different thresholds, indicating an overall disruption of local efficiency in the older group. The sensorimotor network (red dots) and the default mode network (blue dots) are the two most distinguishable networks showing consistent disruption.

Figure 6 Distribution of functional connectivity strength (Young—red; Older—blue)

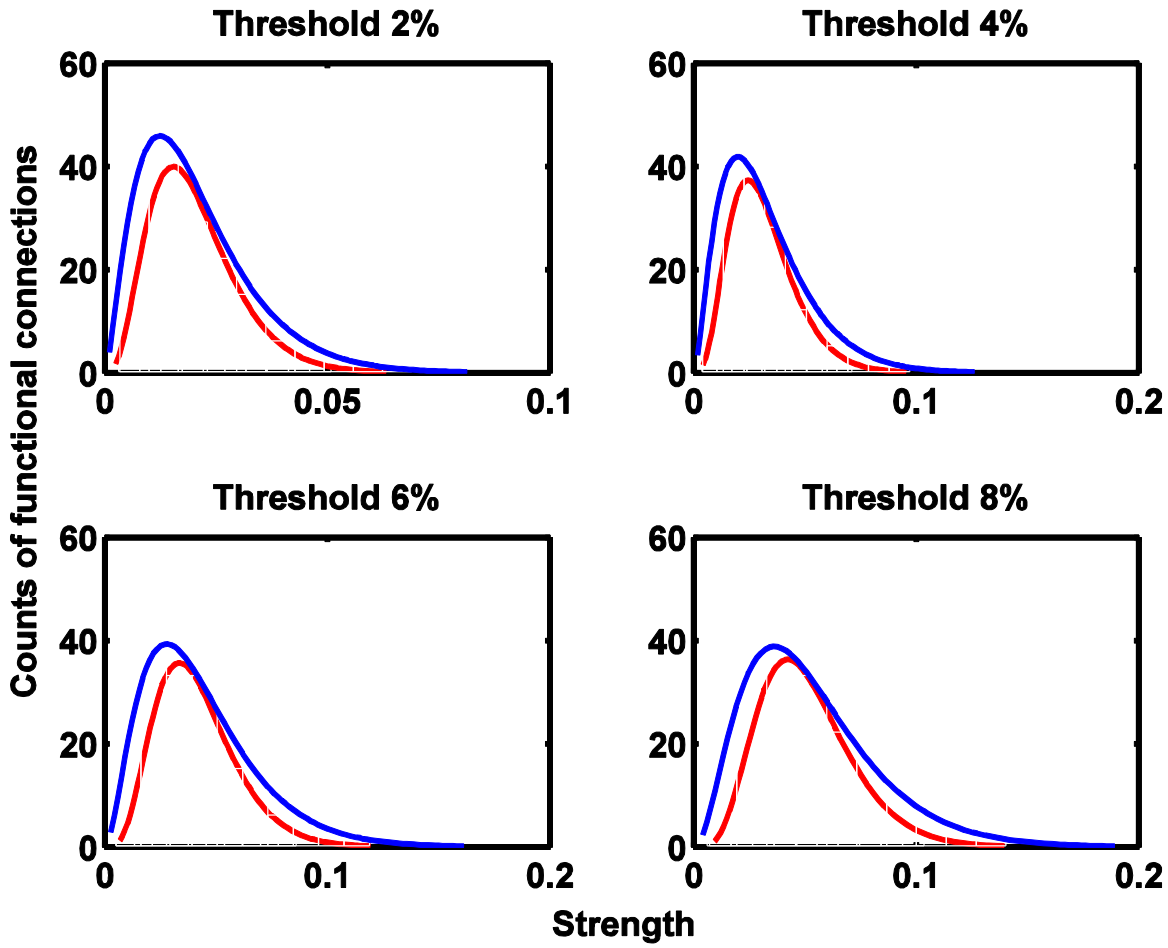

The figure illustrates the distribution of functional connectivity strength compared between the two groups (histogram with a gamma distribution fit; older group—blue lines; young group—red lines).

Figure 7 Hub disruption index of strength

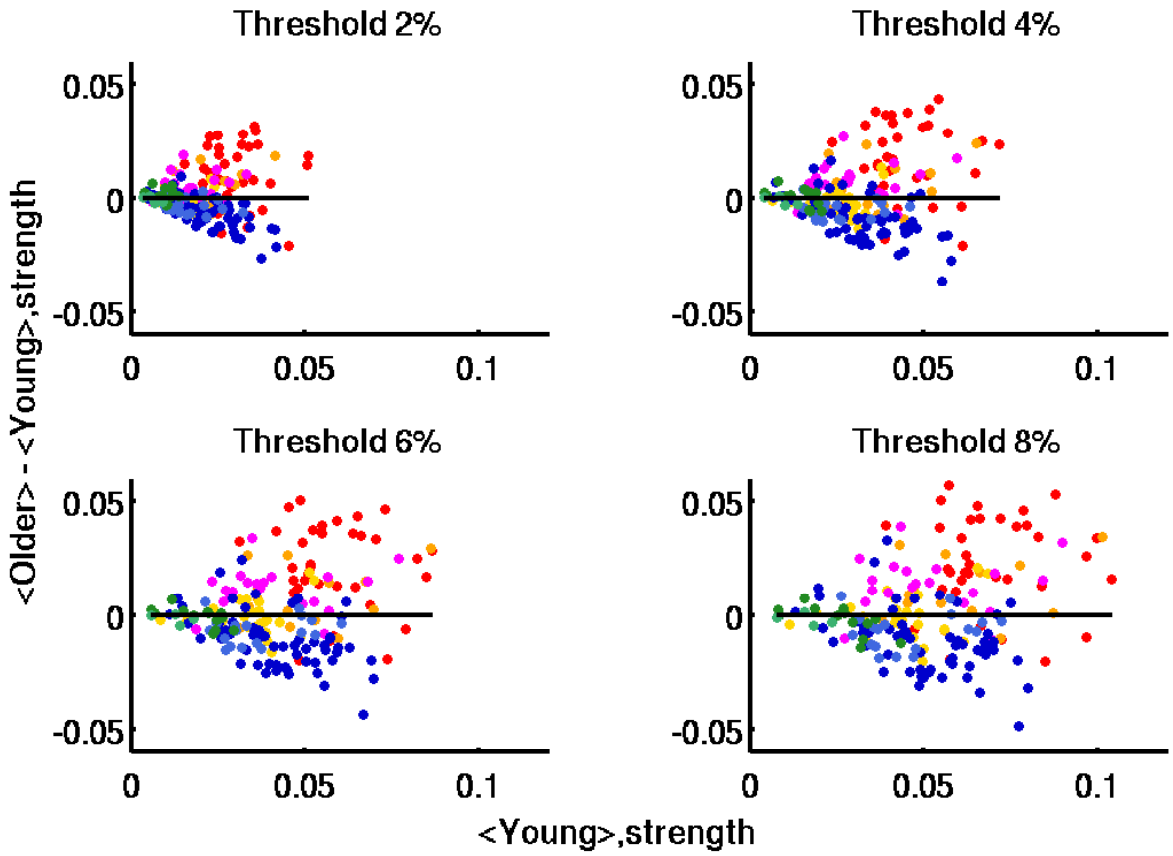

In the figure, each black horizontal line represents equivalent function connectivity strength estimated for the older group vs. the younger group. However, nodes belonging to the sensorimotor network (red) showed increased strength consistently while nodes belonging to the default mode network (medium blue) showed decreased strength.

Figure 8 Age-related changes in functional connectivity strength

a) within the default mode network (DMN) (Young—red; Older—blue)

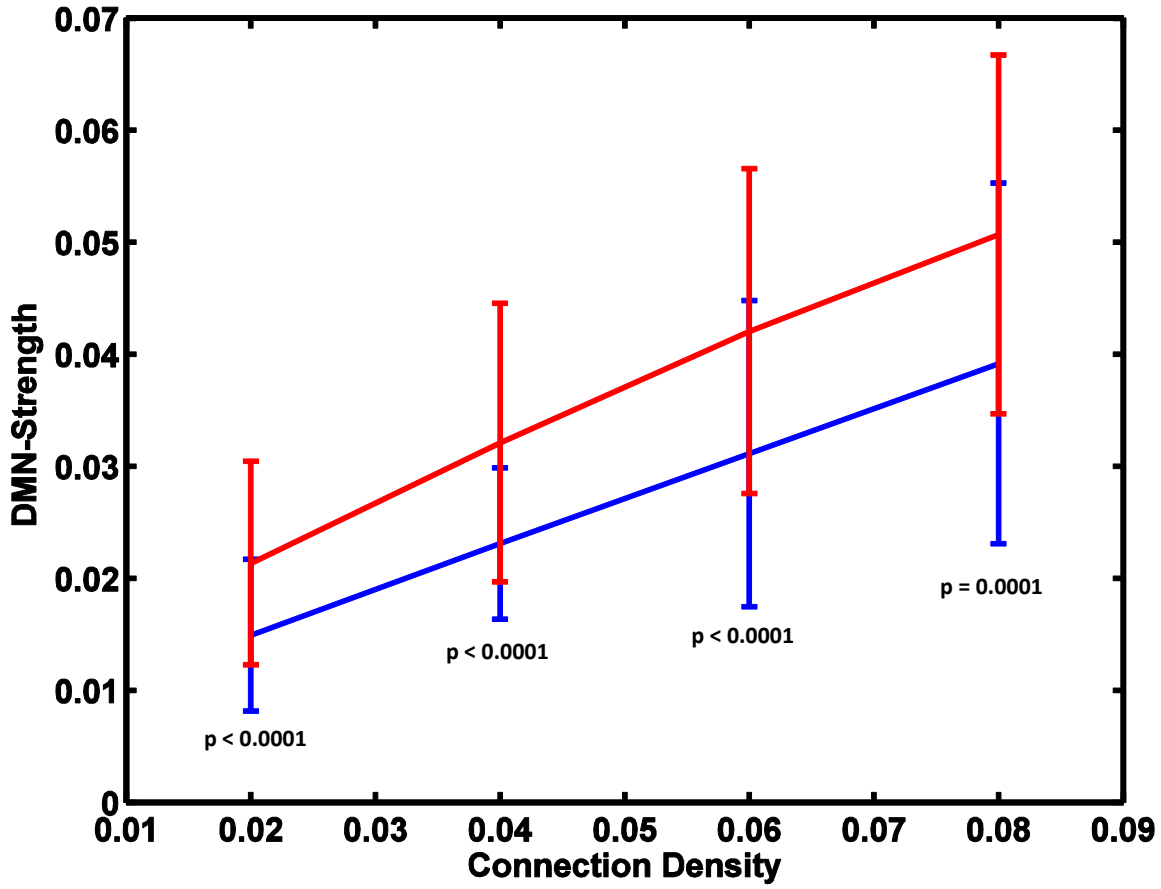

b) within the sensorimotor network (Young—red; Older—blue)

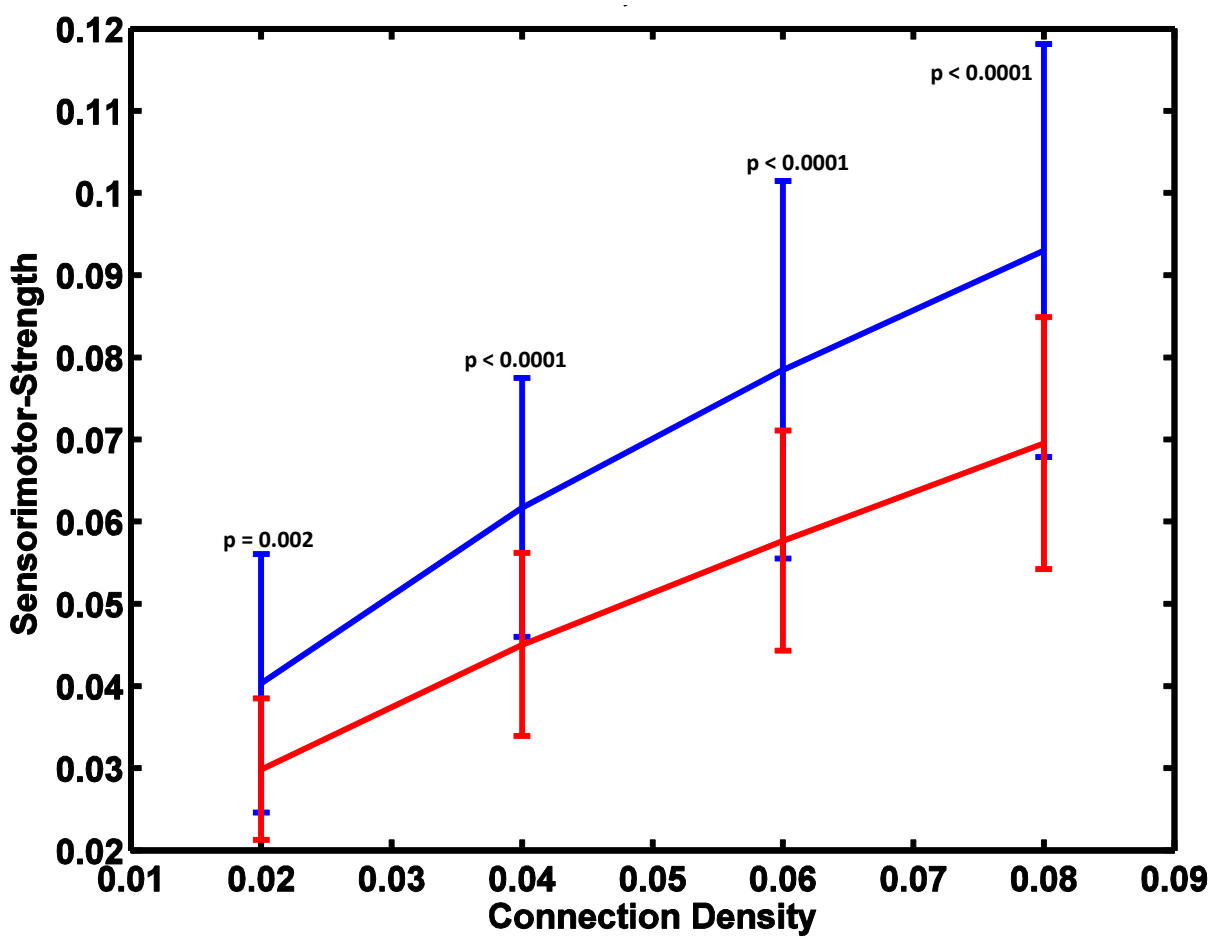

Differences of functional connectivity strength within the default mode network (a) and the sensorimotor network (b) between the older (blue lines) and younger group (red lines) are plotted across different thresholds of connection density. Significantly decreased strength within the DMN (p-value ≤ 0.0001) and increased strength within the sensorimotor network (p-value < 0.01) was observed in the older group (Wilcoxon rank sum test).

Figure 9 Hub disruption index of strength – DMN

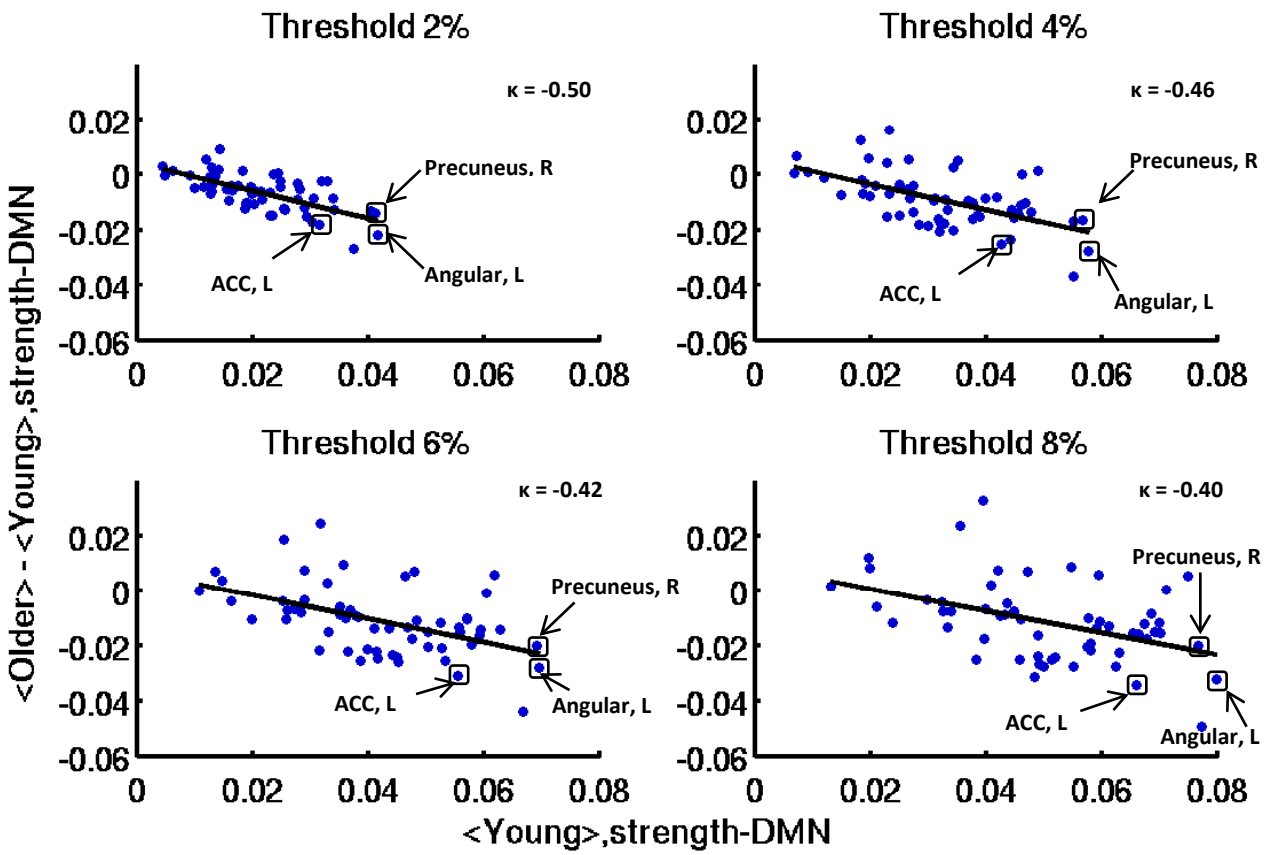

For all nodes belonging to the DMN, the mean value of strength of each of these nodes in the younger group <Young> (x-axis) is plotted against the difference between groups in mean strength of each node <Older> - <Young> (y-axis). The hub disruption index of strength was estimated as the gradient of the solid black line fitted to the scatterplots. The left angular gyrus (AG), left anterior cingulate cortex (ACC) and the right precuneus strongly connected to all other nodes within the DMN in the younger group, showed abnormal reduction of strength in the older group.

Figure 10 Changes in Functional strength in the sensorimotor network

a) within the sensorimotor network

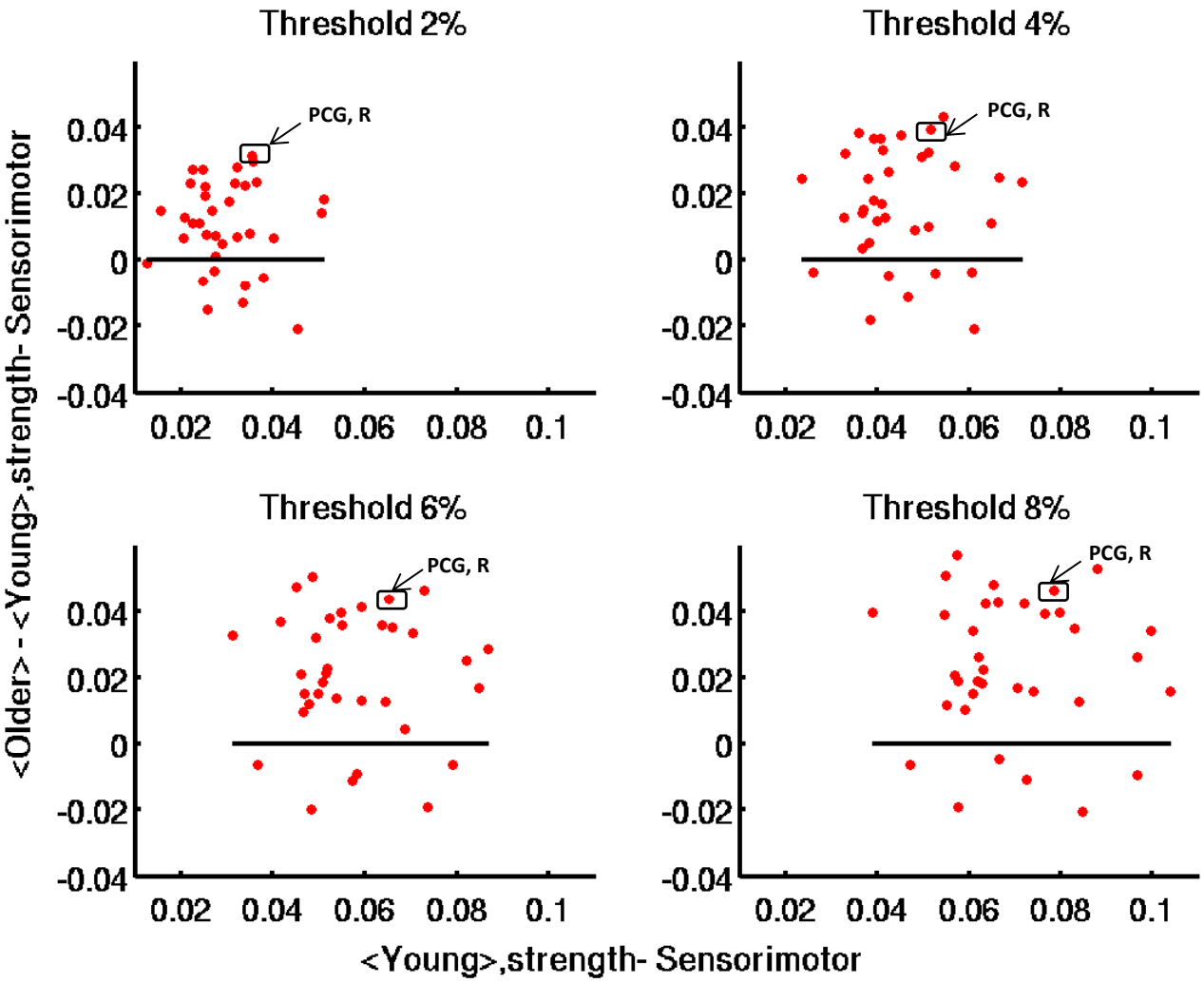

The red horizontal line represents equivalent strength within the sensorimotor network estimated for the older group vs. the younger group. The majority of sensorimotor regions showed increased strength in the older group (i.e., above the horizontal zero line) such as the precentral gyrus (PCG), showing strengthened connections in the older group.

b) Between the sensorimotor network and all other networks

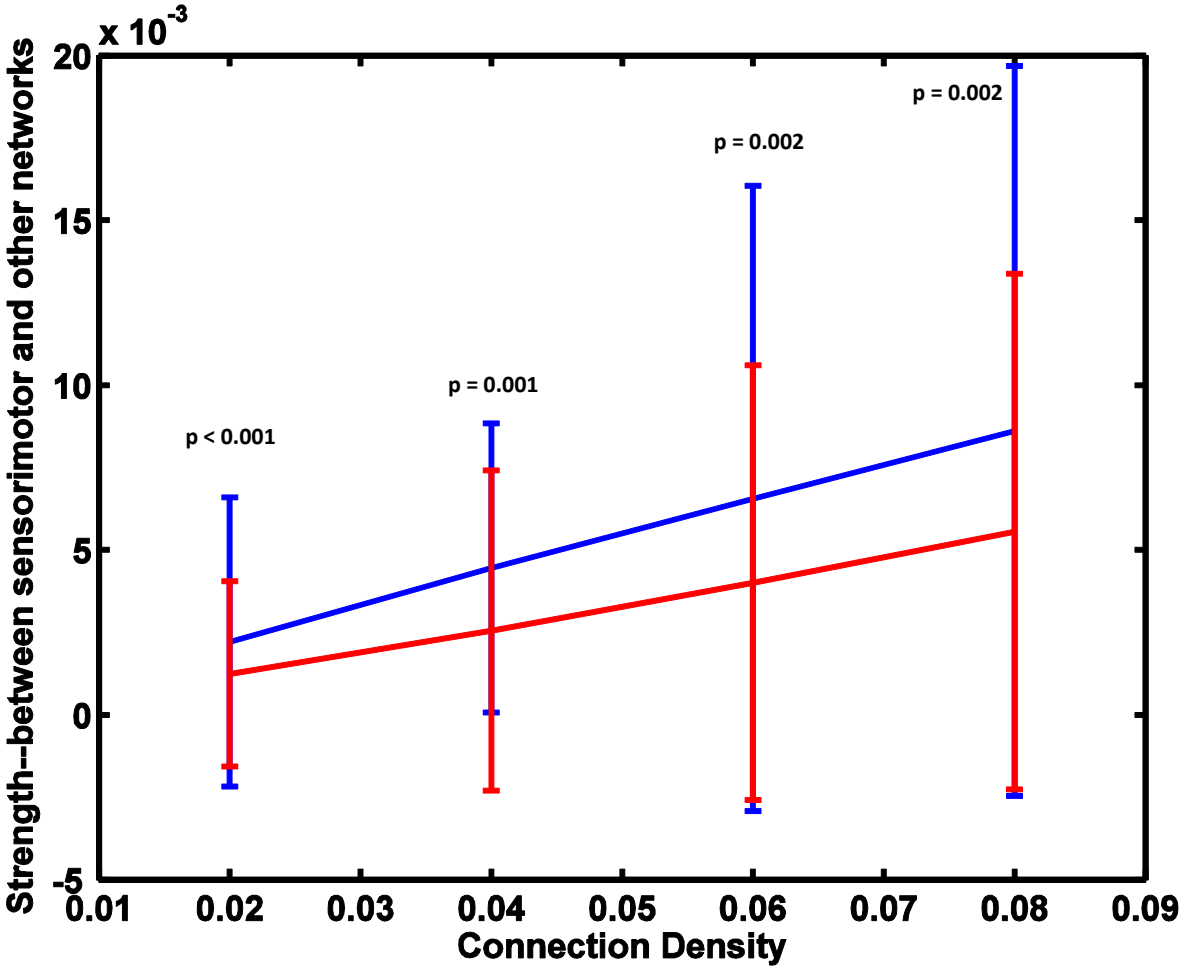

Group differences of functional connectivity strength between the sensorimotor network and all other networks are plotted across different thresholds of connection density (older group-blue line, younger group-red line). Significantly increased strength between the sensorimotor and all other networks (p-value < 0.01) was observed in the older group (Wilcoxon rank sum test).

c) Hub-disruption between the sensorimotor network and all other networks

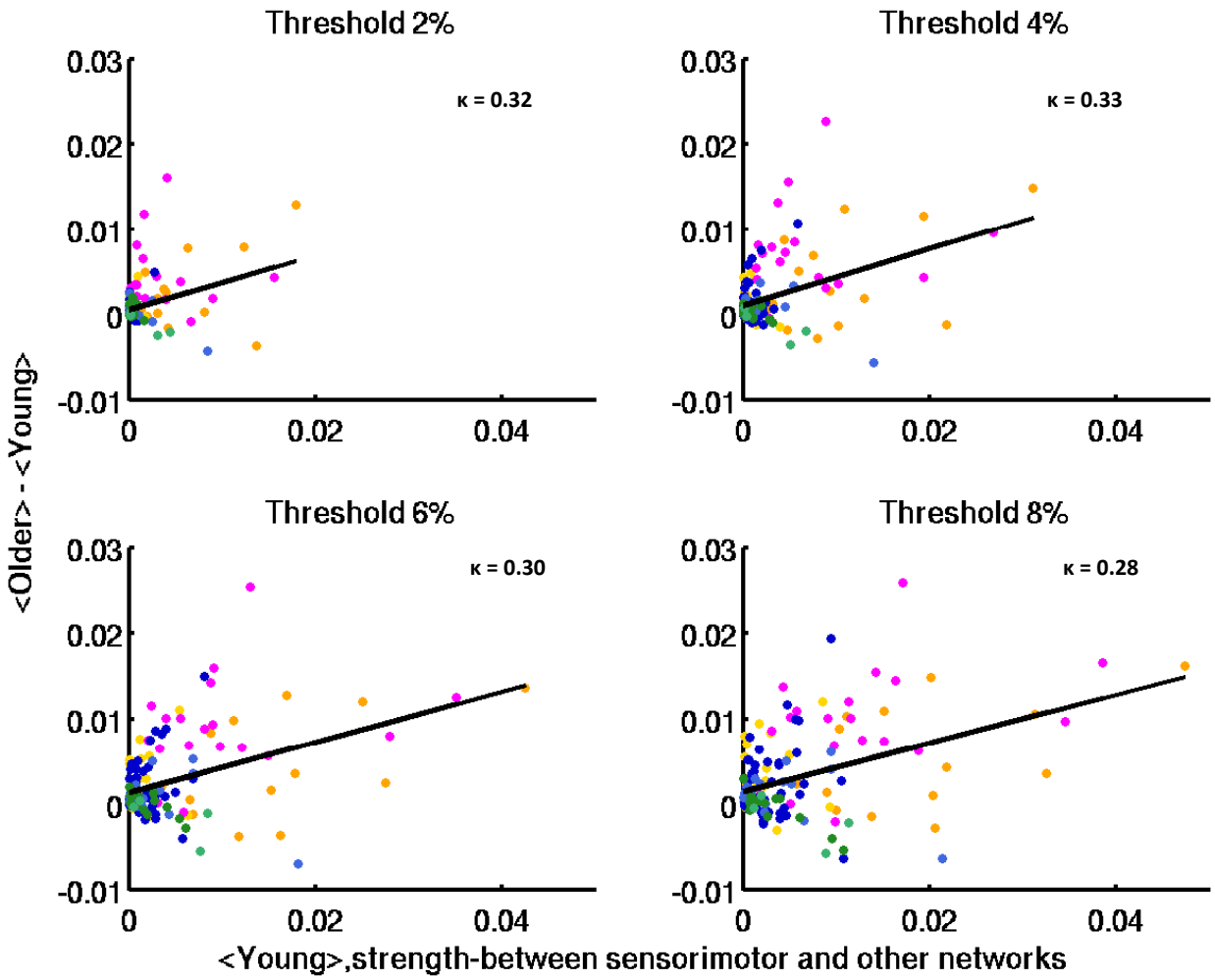

The figure shows age-related regional changes in functional connectivity strength between the sensorimotor and all other networks. Positive hub disruption indices are indicated by the slope of the solid black line fitted to each scatter plot. The dorsal/ventral attention network (magenta) showed strengthened connections to the sensorimotor network.

Supplementary Materials

Figure S1 Effects of aging on strength of functional connections between networks (threshold level of top 2% functional connections).

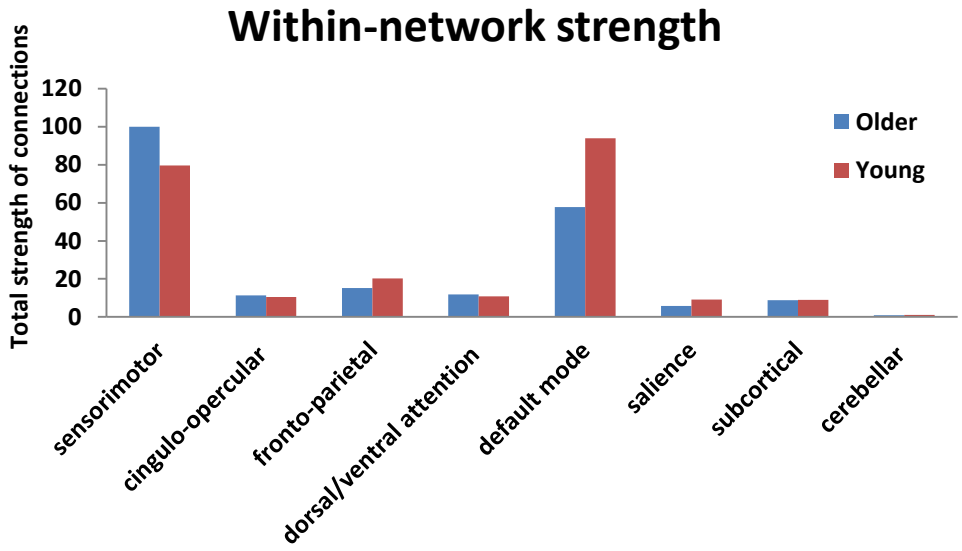

a)

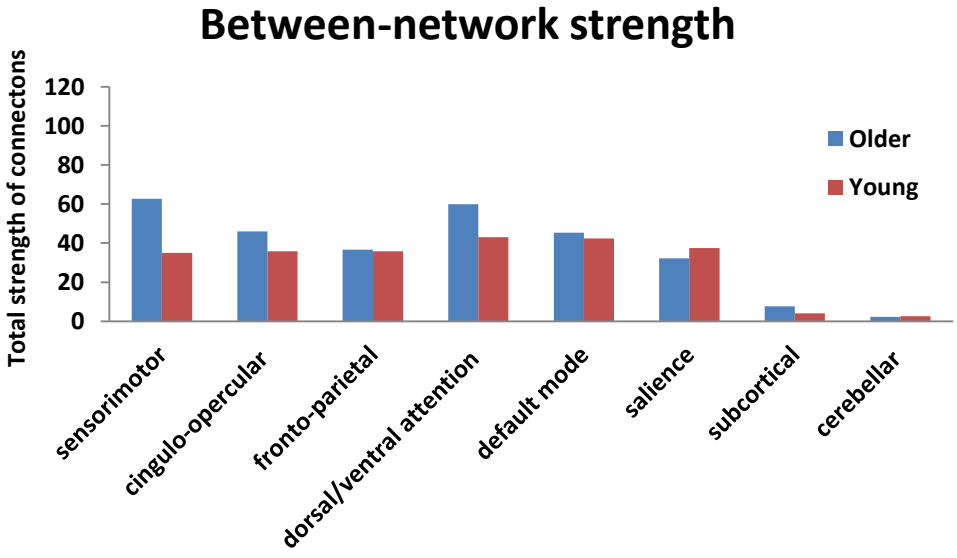

b)

Bar chart provides direct group comparison of functional strength associated with each network.

a) Within-network connections. Binomial proportion tests followed by multiple comparisons

correction showed aging was associated with significant increases within the sensorimotor network (corrected p-value = 0.024) and decreases in the DMN (corrected p-value = 0.024). b) Between-network analyses revealed no significant group differences in functional strength for between-network connections.

Figure S2 Effects of aging on number of functional connections within each functional network (threshold level of top 2% functional connections).

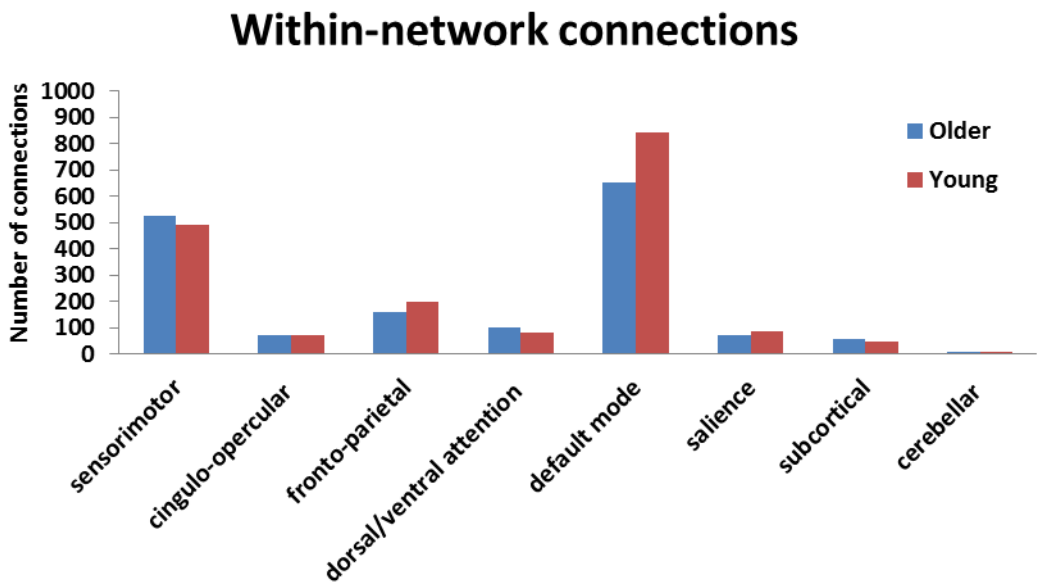

a)

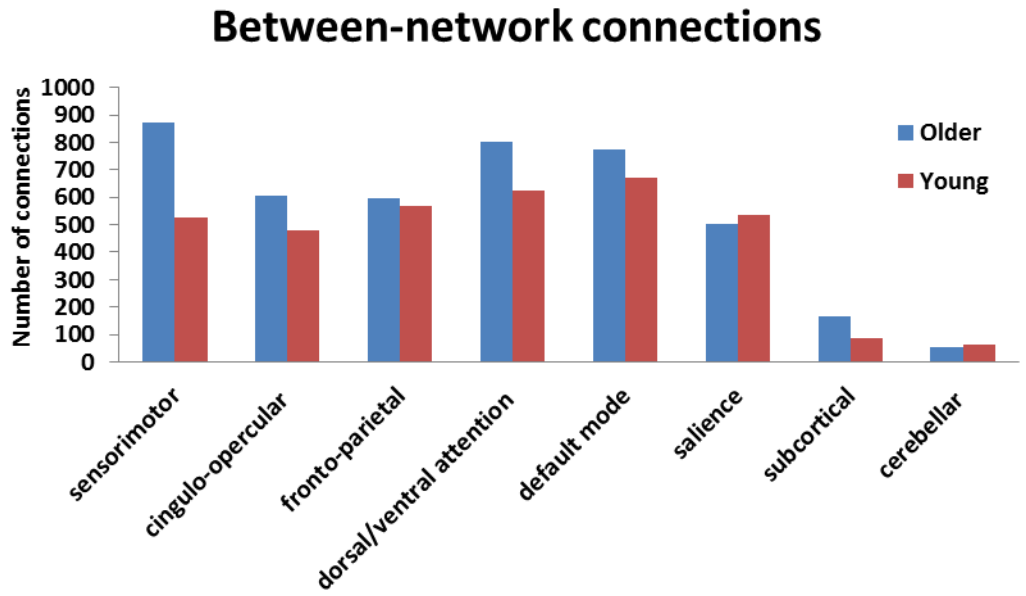

b)

c)

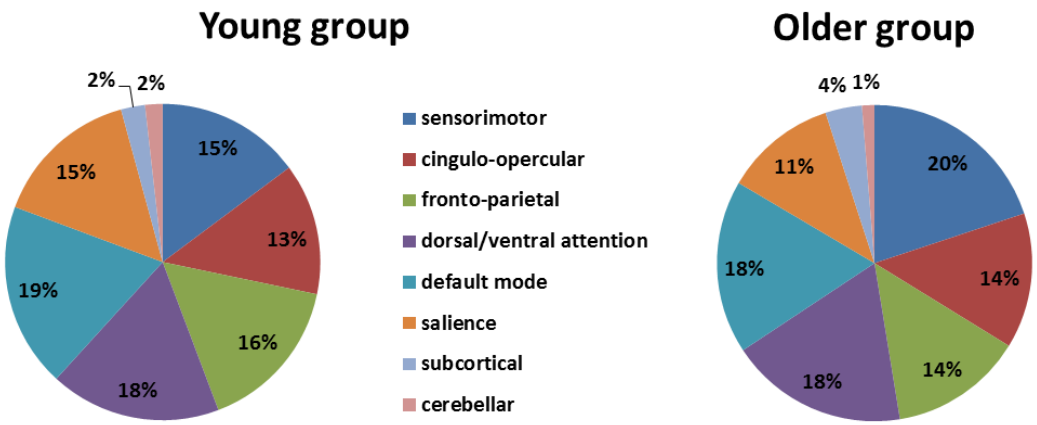

Bar charts (a-b) and a pie chart (c) provided direct group comparisons of number of functional connections belonging to each network at threshold level of top 2% functional connections. a) Within-network connections. Binomial proportion tests followed by multiple comparisons correction showed aging was associated with significant increases within the sensorimotor network (corrected p-value = 0.005) and decreases in the DMN (corrected p-value = 0.0005). b-c) Between-network connections. The older group showed significantly increased between-network functional connections in the sensorimotor (corrected p-value < 0.00001) and subcortical (corrected p-value = 0.005) networks. The older group also showed significantly decreased proportion of between-network connections in the frontal-parietal (corrected p-value = 0.006) and salience (corrected p-value < 0.00001) networks (relative to the total number of between-network connections).

Figure S3 Age-related changes in local efficiency

b) within the default mode network (DMN) (Young—red; Older—blue)

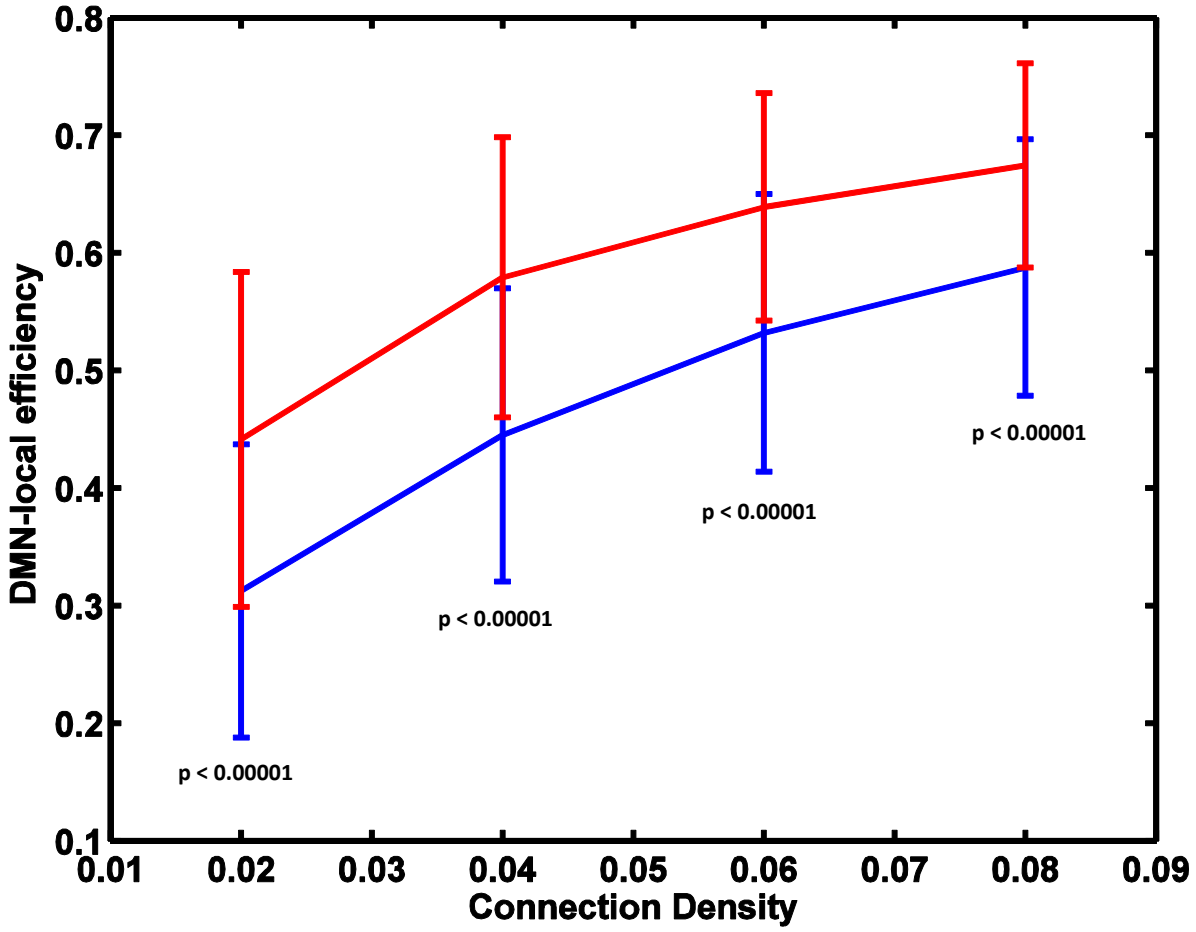

b) within the sensorimotor network (Young—red; Older—blue)

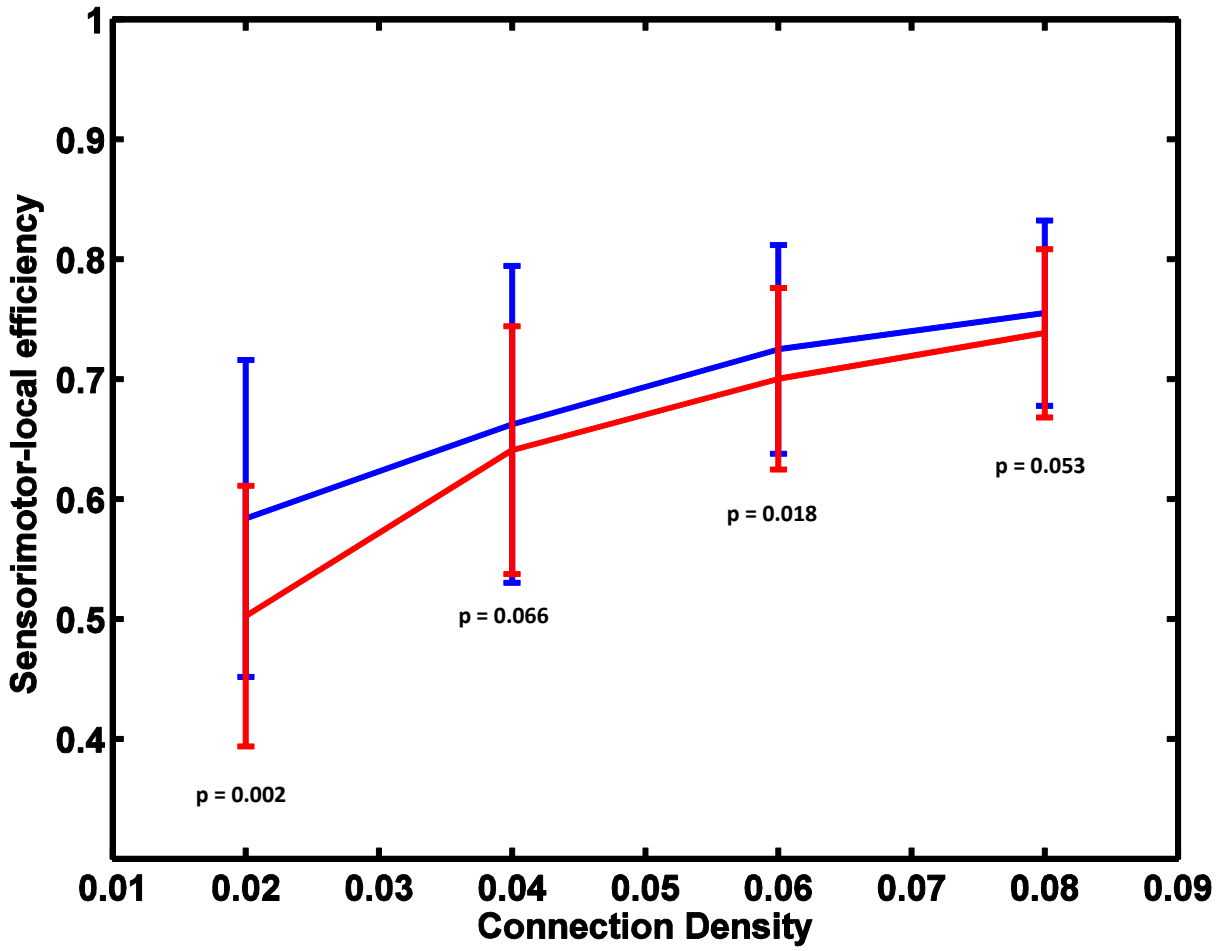

Age-related differences of local efficiency in the default mode network (a) and the sensorimotor network (b) between the older (blue line) and younger group (red line) are plotted across different thresholds of connection density. Significant reduction of local efficiency was observed within the DMN (Wilcoxon rank sum test, p-value < 0.00001). Local efficacy was increased within the sensorimotor network in the older group at threshold of top 2% and 6% connections (Wilcoxon rank sum test, p-values < 0.02).

Figure S4 Age-related changes in global efficiency

a) within the default mode network (DMN) (Young—red; Older—blue)

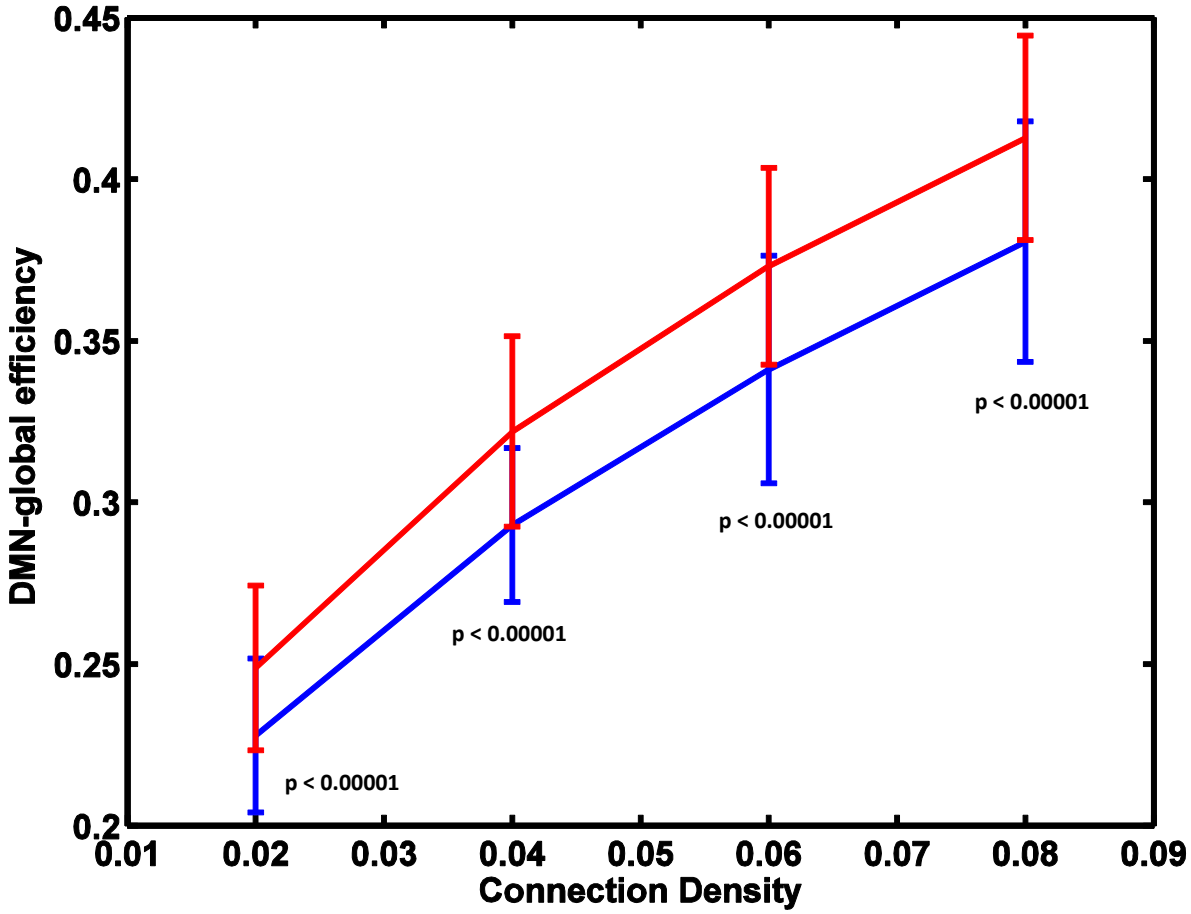

b) within the sensorimotor network (Young—red; Older—blue)

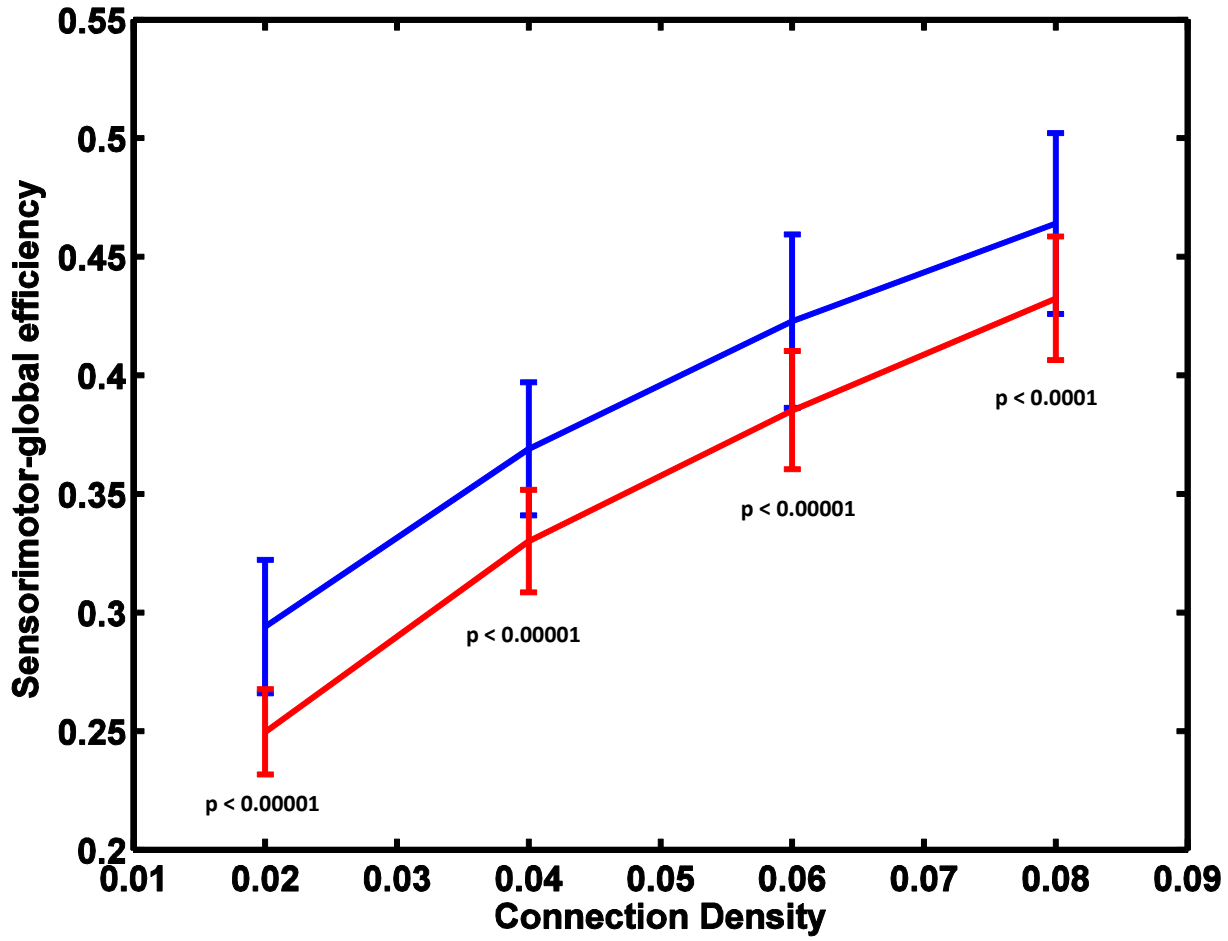

Age-related differences of global efficiency in the default mode network (a) and the sensorimotor network (b) between the older (blue lines) and younger group (red lines) are plotted across different thresholds of connection density. Global efficiency was significantly decreased in the DMN (Wilcoxon rank sum test, p-value < 0.00001) but increased in the sensorimotor network (Wilcoxon rank sum test, p-value < 0.0001).

Table S1 Group comparison of strength and degree between the sensorimotor and attention network (threshold level of top 2% functional connections)

	Strength	***Degree***
Young	10.69	149
Older	24.56↑	297↑

The older group showed significantly increased number of functional connections (Binomial proportion tests, p-value < 0.00001) as well as the strength (Binomial proportion tests, p-value < 0.05) between the sensorimotor and attention networks. Arrows indicate directional changes of network measures with aging.

Appendix: Network measures and findings are made at connection-density threshold of 10%, 20%, 30% and 40%.

Figure S5: Adjacency matrices at threshold of 20%

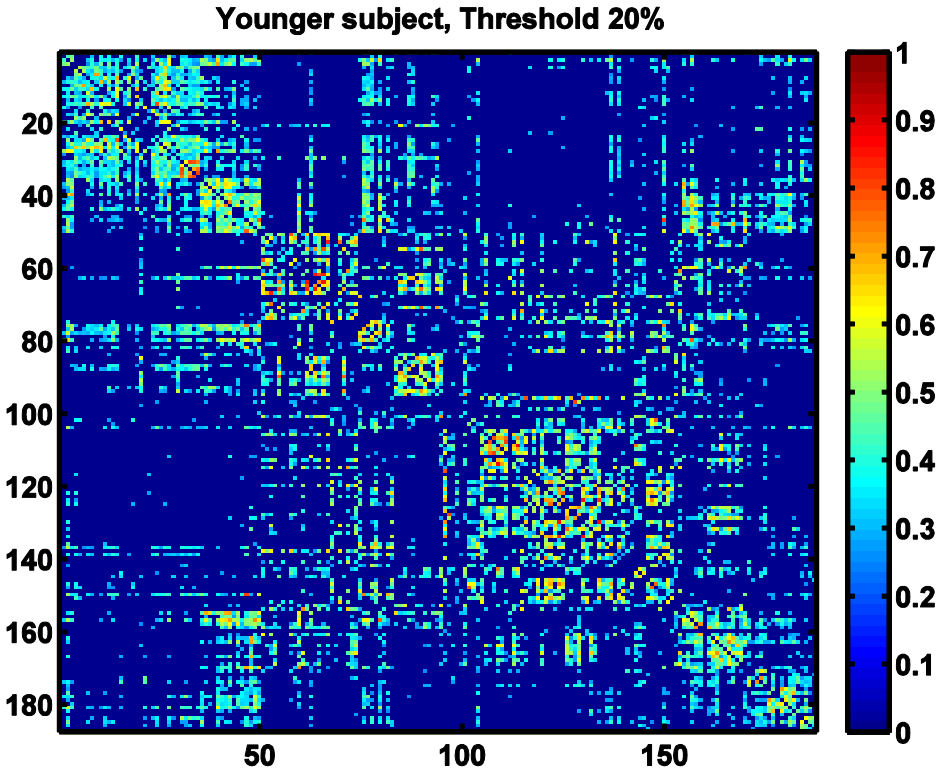

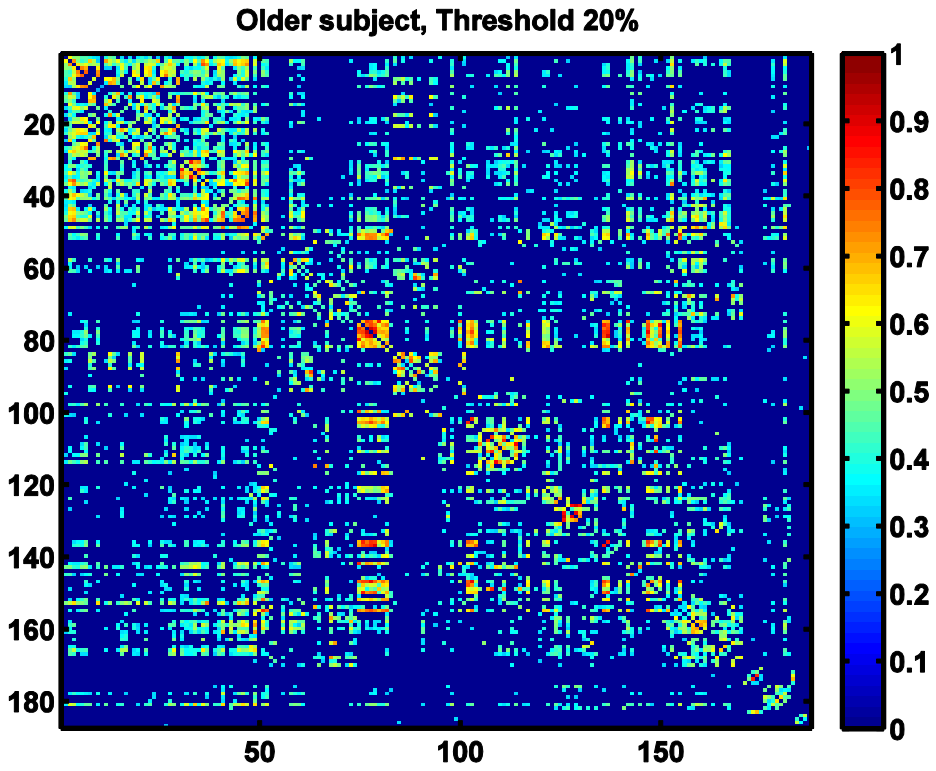

Shown are adjacency matrices of two representative subjects from each group with connection-density threshold of 20%. Rows and columns denote 187 nodes and each element of the matrix denotes a link between the corresponding nodes.

Figure S6: Modularity (Young—red; Older—blue)

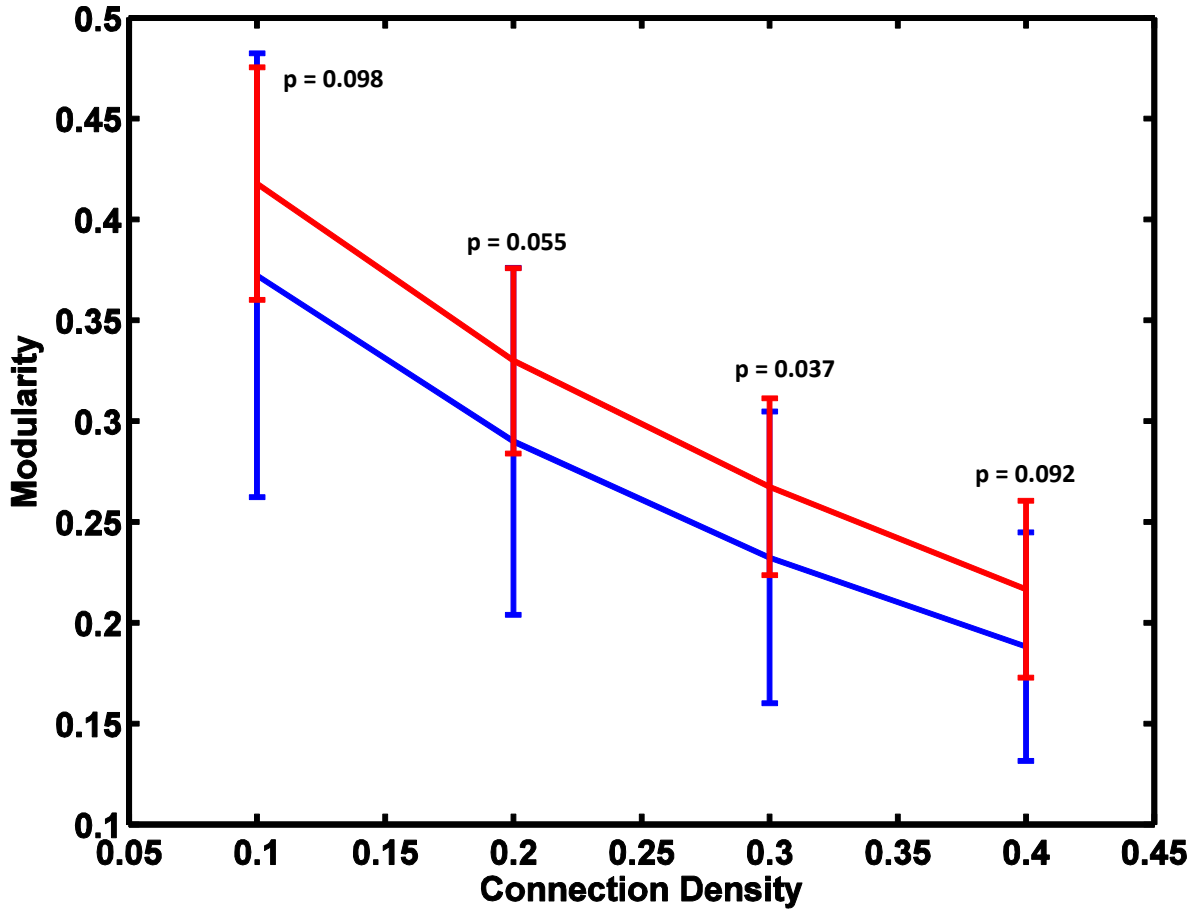

Modularity consistently decreases with increased connection density for both groups (older group—blue line, young group—red line). The measure of modularity is significantly greater in the young group at threshold of 30%. However, group mean values of modularity decreased below 0.3 above the threshold or connection density of 0.1, which were indicative of random community structure (Newman and Girvan 2004).

Figure S7: Hub disruption index of within-module functional connectivity

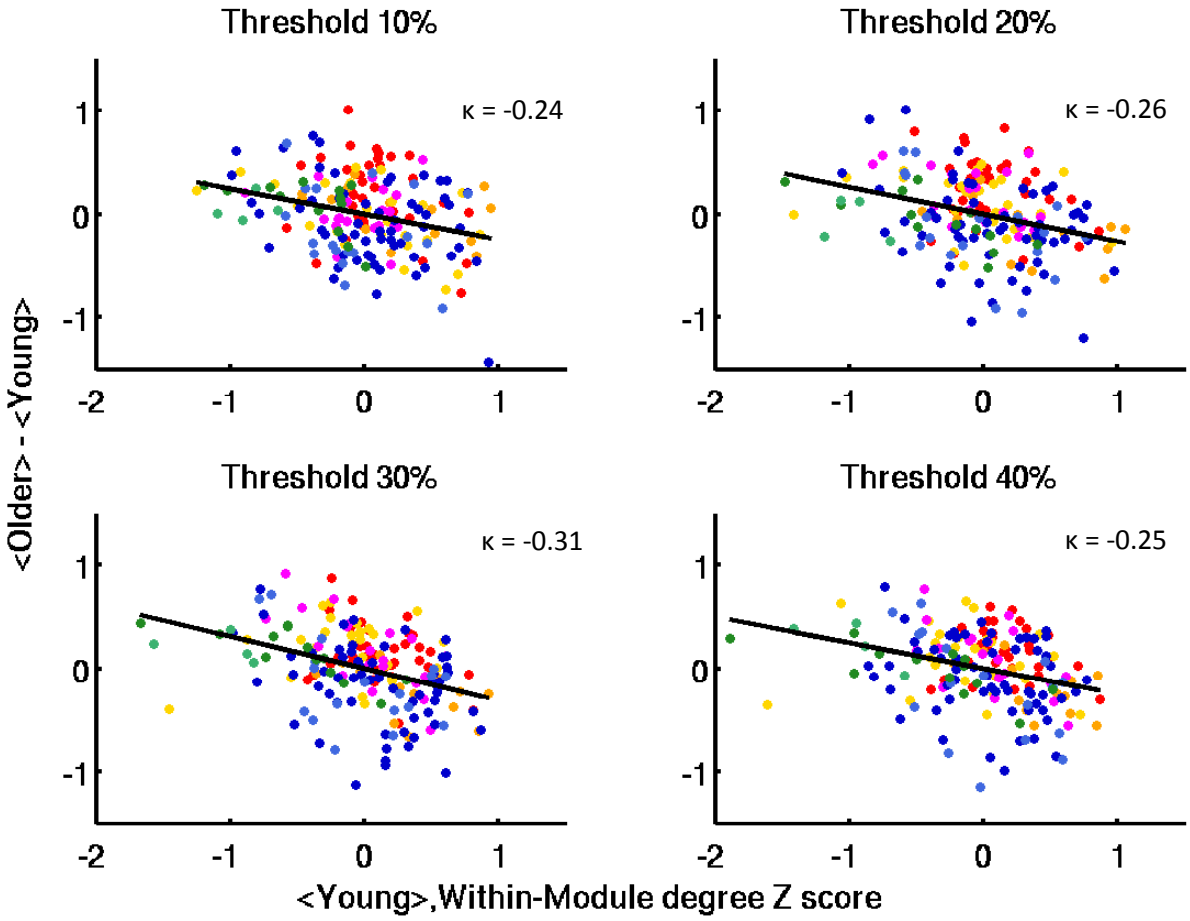

The hub disruption index of within-module degree *z* score is plotted at each threshold of connection density. Each data point is color-coded representing a node belonging to a particular functional network (i.e., red dots represent nodes belonging to the sensorimotor network and blue dots represent nodes belong to the default mode network). The mean value of within-module degree z-score of each node in the younger group <Young> (x-axis) is plotted against the difference between groups in mean value of within-module degree z-score of each node <Older> - <Young> (y-axis).

Figure S8 Global efficiency (Young—red; Older—blue)

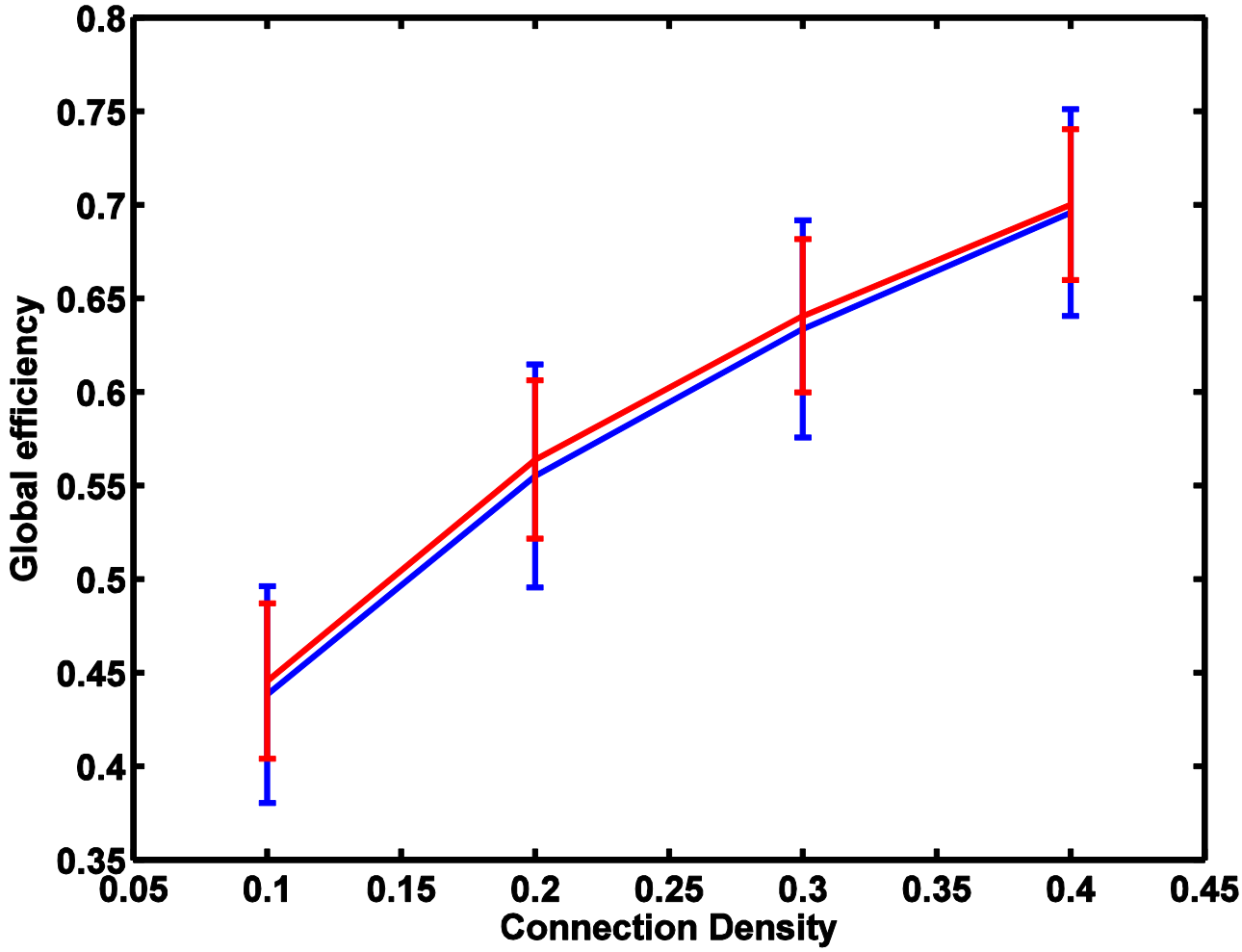

Global efficiency was compared between the two groups (older group—blue line, young group—red line) across different thresholds. No significant group difference was observed.

Figure S9 Hub disruption index of global efficiency

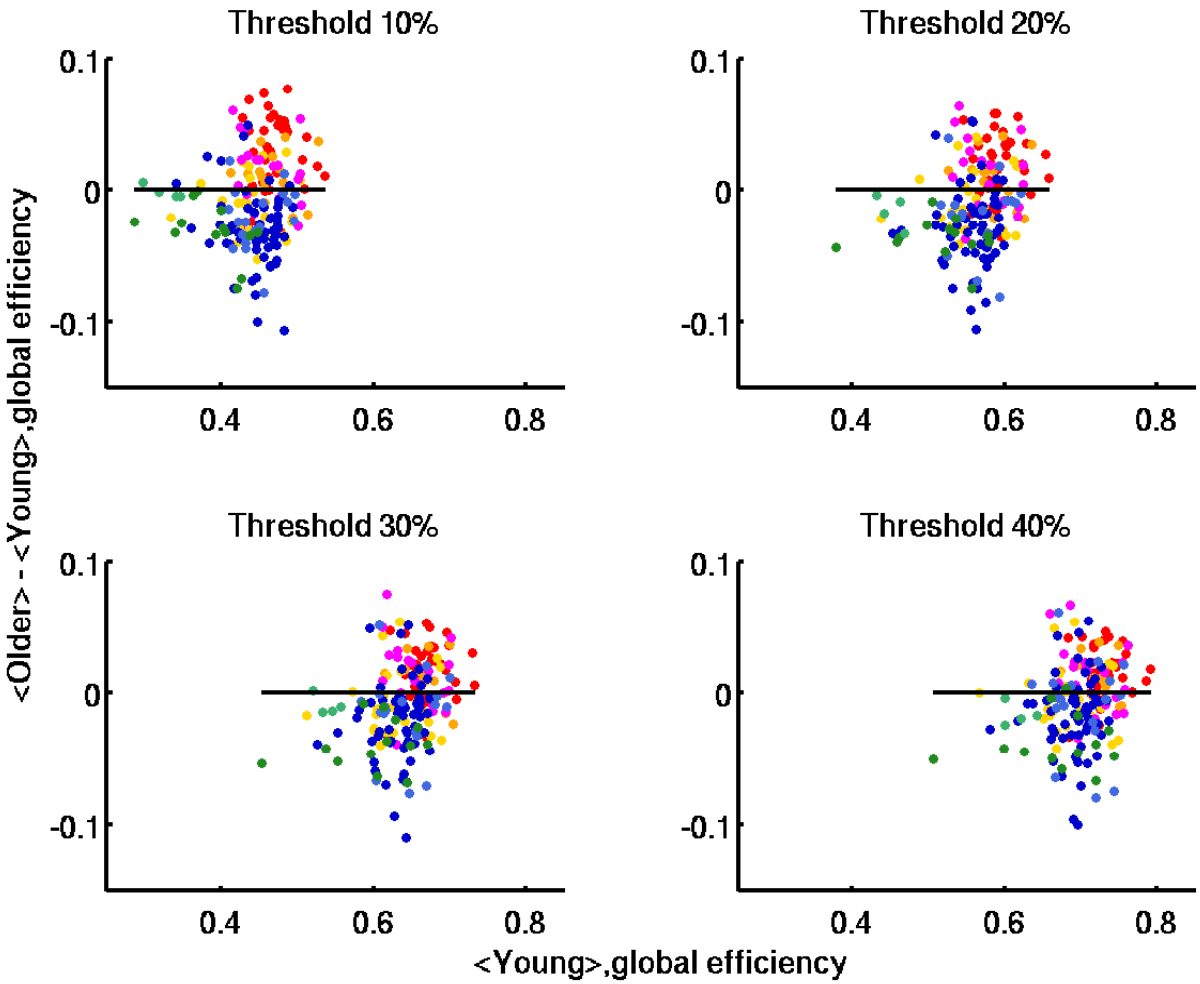

In Figure S9, the black horizontal line represents equivalent global efficiency for the older group vs. the younger group. Nodes belonging to the sensorimotor network (red) showed increased global efficiency while nodes belonging to the default mode network (medium blue), salience network (royal blue) and subcortical/cerebellar network (green) showed decreased global efficiency.

Figure S10 Local efficiency (Young—red; Older—blue)

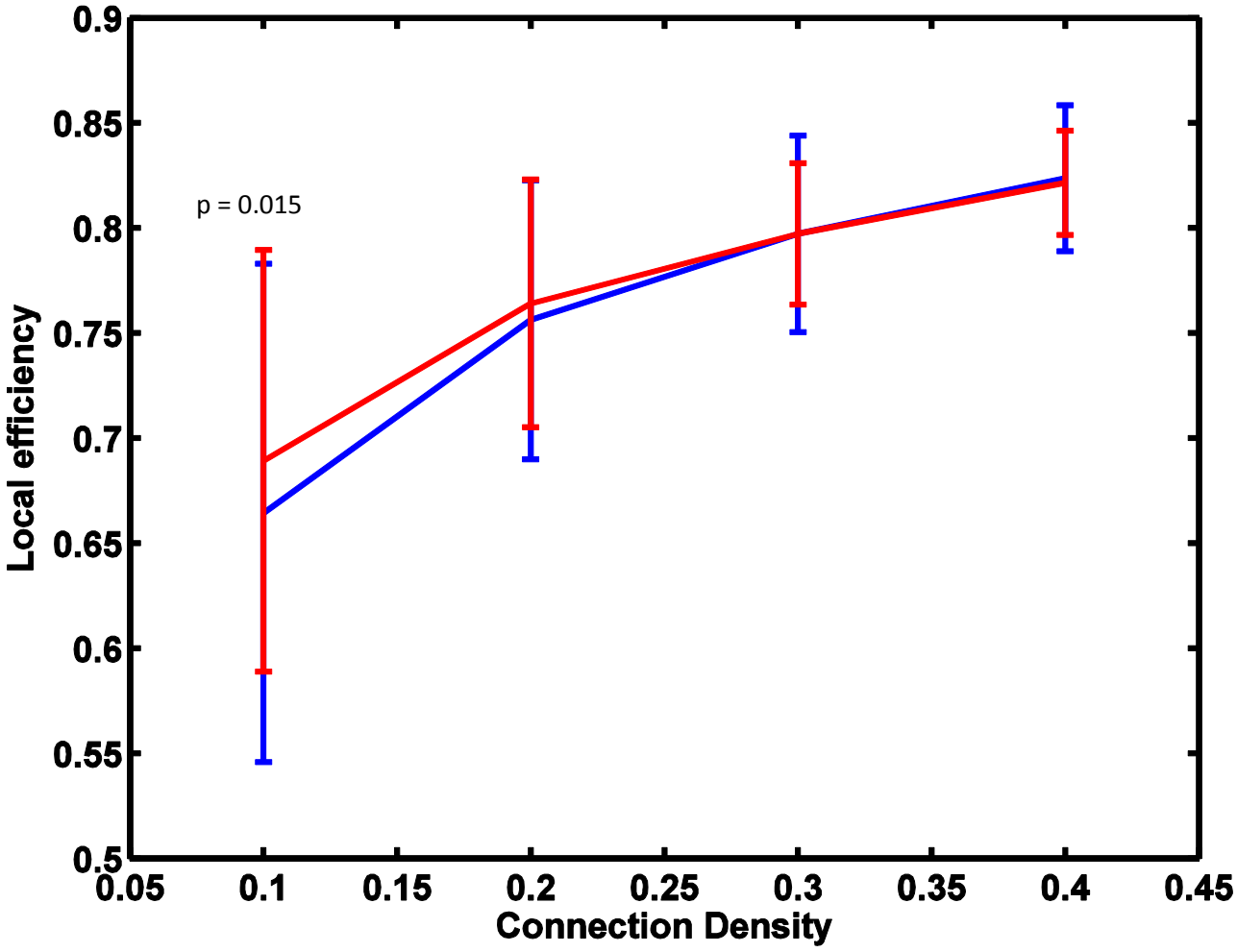

Differences in local efficiency between the older (blue line) and younger group (red line) are plotted across different thresholds of connection density. Significant group differences (i.e., local efficiency, younger > older) were only observed at connection-density threshold of 10% (Wilcoxon rank sum test, p-value = 0.015).

Figure S11 Hub disruption index of local efficiency

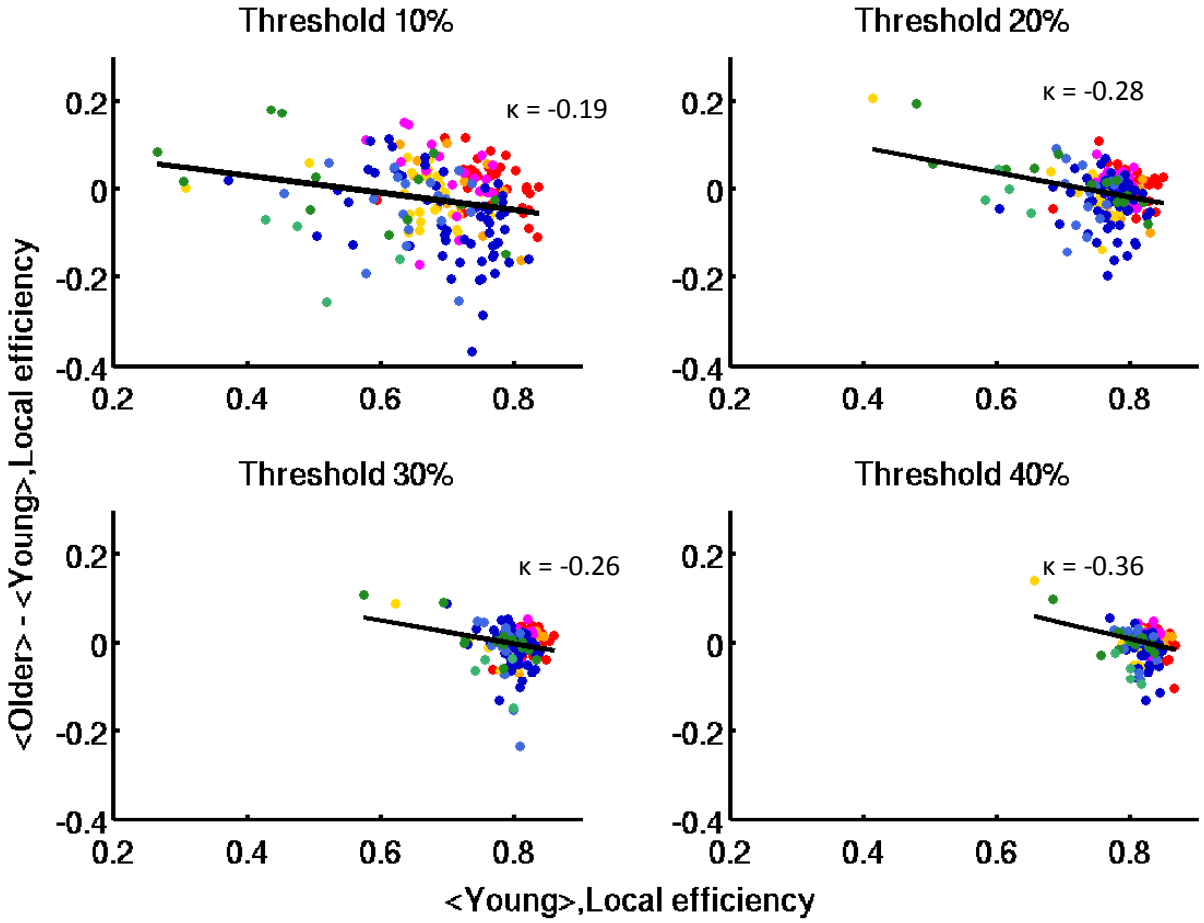

The hub disruption index of local efficiency is plotted at each threshold of connection density. The mean value of local efficiency of each node in the younger group <Young> (x-axis) is plotted against the difference between groups in mean local efficiency of each node <Older> - <Young> (y-axis). The hub disruption index of local efficiency was estimated as the gradient of the solid black lines fitted to the scatterplots. Negative hub disruption indices were observed across different thresholds, indicating regional disruption of local efficiency in the older group.

Figure S12: Strength (Young—red; Older—blue)

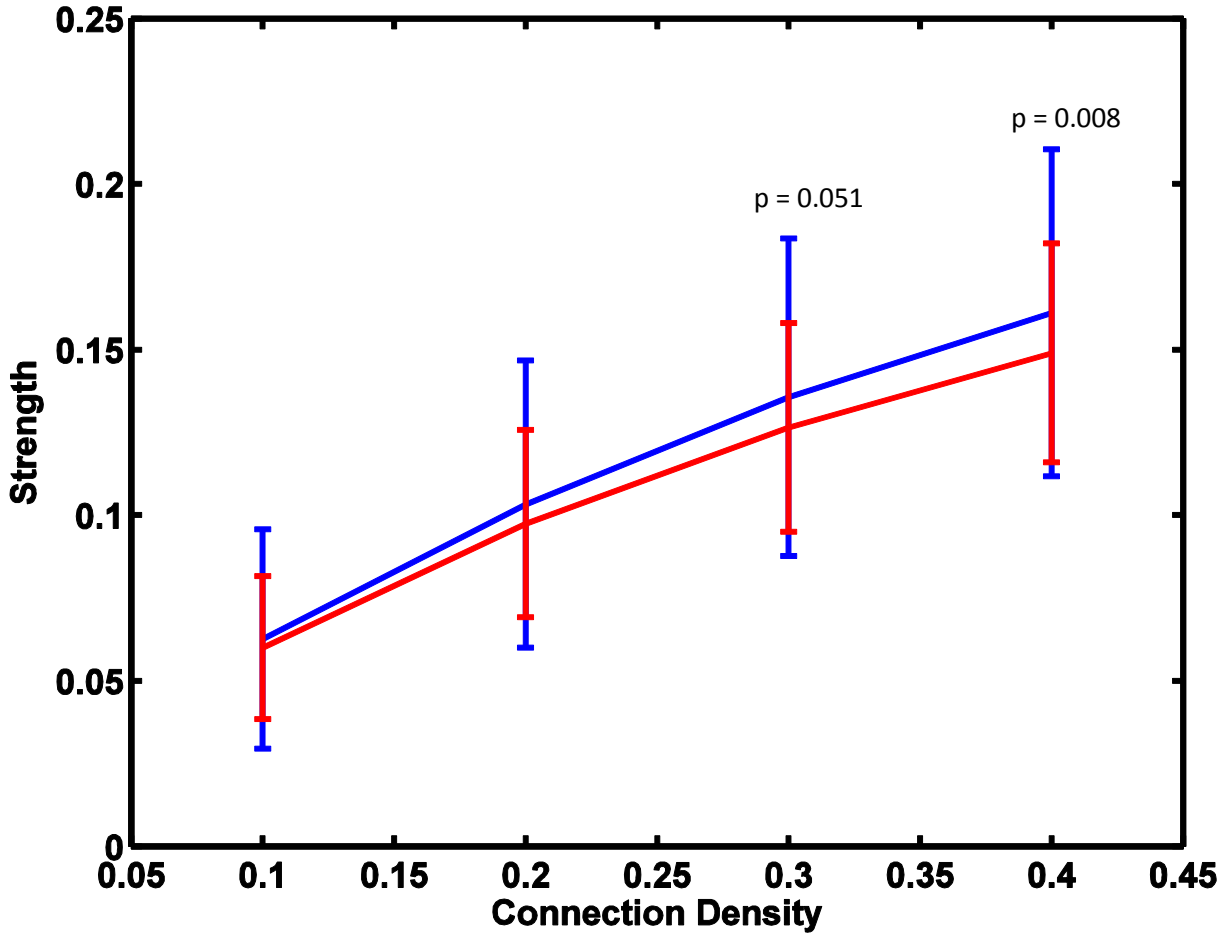

The strength of functional connectivity was compared between the two groups across different thresholds (older group—blue line, young group—red line). Significant group difference was observed at threshold of 40% (Wilcoxon rank sum test, p-value = 0.008).

Figure S13 Distribution of functional connectivity strength (Young—red; Older—blue)

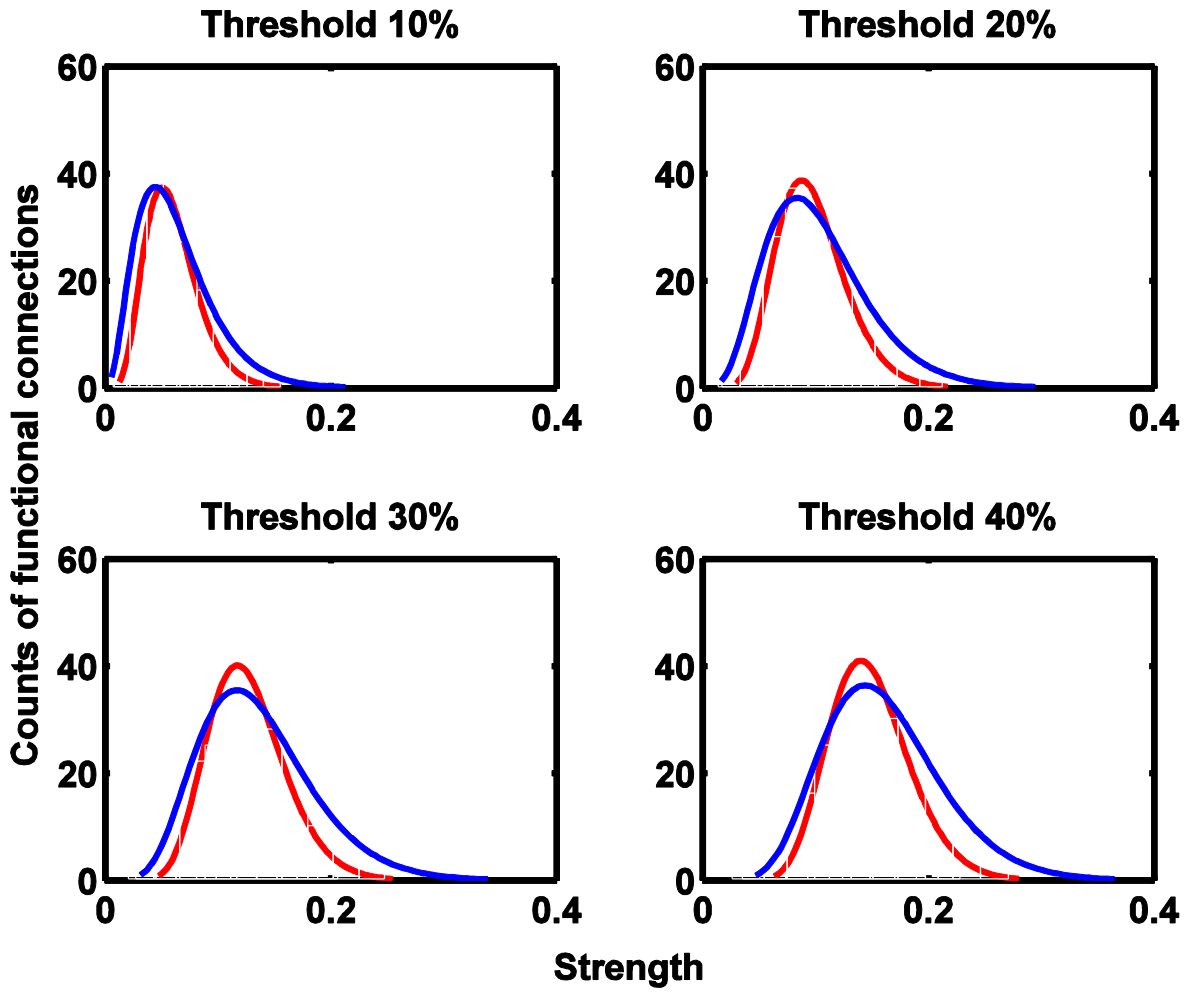

The figure illustrates the distribution of functional connectivity strength compared between the two groups (histogram with a gamma distribution fit; older group—blue lines, young group—red lines).

Figure S14 Hub disruption index of strength

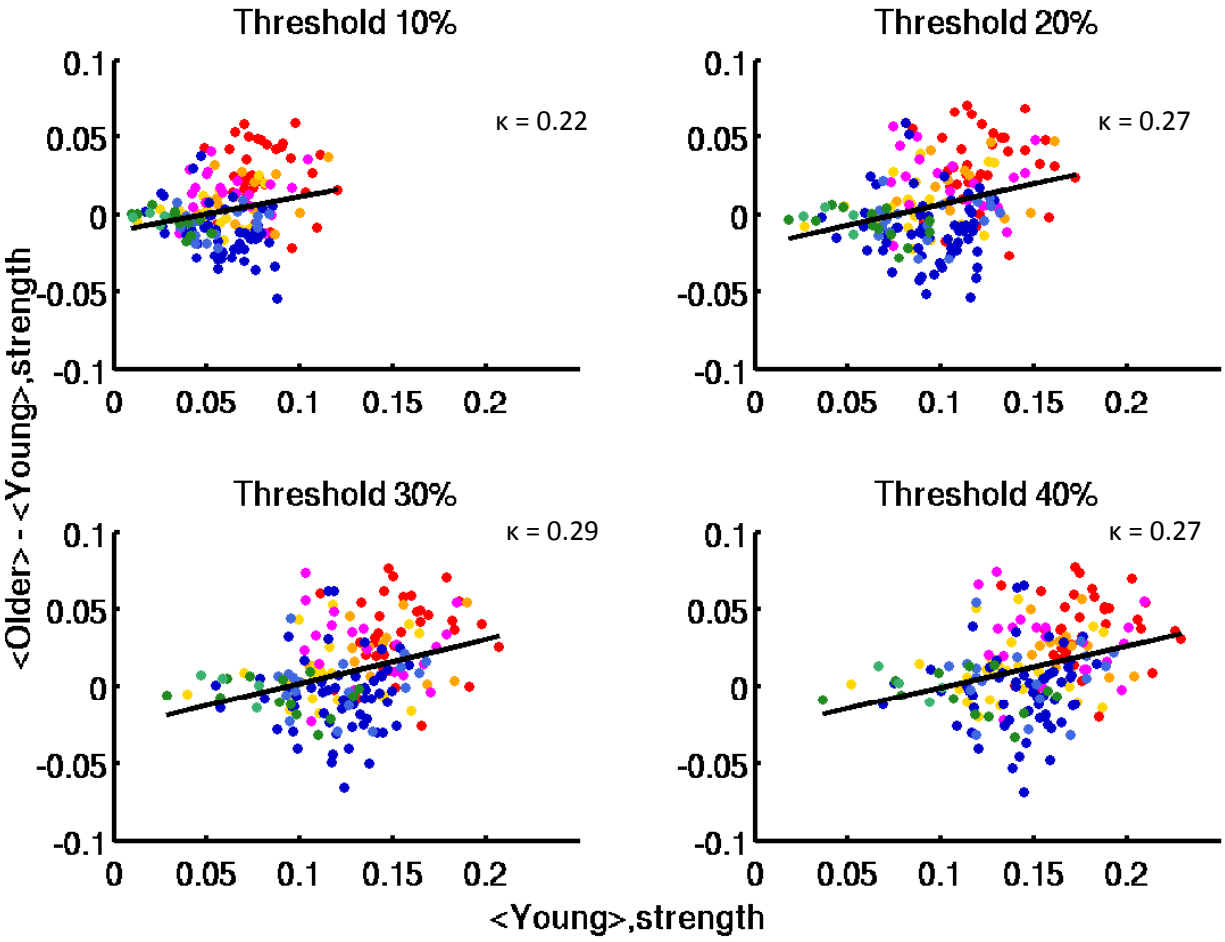

The mean value of strength of each node in the younger group <Young> (x-axis) is plotted against the difference between groups in mean strength of each node <Older> - <Young> (y-axis). The hub disruption index of strength was estimated as the gradient of the solid black lines fitted to the scatterplots. Positive hub disruption indices indicate regional increases in the strength of functional connectivity with aging.

Chapter IV

Disrupted Brain Functional Organization in Epilepsy Revealed by Graph Theory Analysis

Jie Song, Veena A. Nair, Wolfgang Gaggl, Vivek Prabhakaran

In preparation

Abstract

Objective: The human brain is a rather complex and dynamic system that can be modeled as a large-scale brain network in order to better understand the reorganizational changes secondary to epilepsy. In this study, we developed a brain functional network model using graph theory methods applied to the resting-state fMRI data acquired from a group of epilepsy patients and age-matched healthy controls.

Methods: Brain functional network model was constructed based on resting-state functional connectivity. A minimum spanning tree combined with proportional thresholding approach was used to obtain sparse connectivity matrices for each subject, which formed the basis of brain networks. We examined the brain reorganizational changes in epilepsy thoroughly at the level of the whole brain, the functional network and individual brain regions.

Results: At the whole brain level, local efficiency was significantly decreased in epilepsy patients compared with the healthy controls. However, global efficiency was significantly increased in epilepsy due to increased number of functional connections between networks (yet weakly connected). At the functional network level, there were significant proportion of newly-formed connections between the default mode network and other networks, and between subcortical network and other networks, whereas a significant proportion of decreasing connections between the cingulo-opercular task-control network and other networks. Individual brain regions from different functional networks, however, showed distinct pattern of reorganizational changes in epilepsy.

Significance: These findings suggest that epilepsy disrupts brain efficiency in a consistent pattern at the whole brain level yet alters brain functional networks and individual brain regions differently.

Key Words: epilepsy, functional networks, graph theory, network analysis

Introduction

The human brain is a complex structure that can be modeled as a network or a graph represented by a collection of nodes (i.e., cortical and subcortical brain regions) and links (i.e., associations between nodes) (Sporns et al., 2005). This approach is based on graph theory which provides a powerful way of examining the dynamic interactions among multiple brain regions and how these interactions together produce complex behaviors in human beings. This approach has provided insights into many neurological disorders including epilepsy, and has the potential as useful biomarkers for diagnostic and prognostic purposes (Haneef & Chiang, 2014). In the present study, we developed a network model based on resting-state functional connectivity using graph theory in order to examine the epileptic reorganizational changes in brain functional networks. Higher-order graph theoretic measures such as local efficiency and global efficiency along with lower-order measures such as strength and degree are estimated to quantify brain network organization and to compare the epileptic brain with age-matched healthy controls. By definition, an epileptic seizure is a transient occurrence of signs and/or symptoms due to abnormal excessive or synchronous neuronal activity in the brain (Fisher et al., 2005). This regional abnormal neuronal activity could potentially disrupt the connectivity basis of individual brain regions as well as brain networks. Therefore, in the current study, we hypothesize that the local and global efficiency can be affected by epilepsy and that epileptic disruptions may display distinct pattern across brain regions and networks.

Previous studies on epilepsy have shown topological changes of whole brain functional networks in temporal lobe epilepsy (Wang et al., 2014) and in idiopathic generalized epilepsy (Zhang et

al., 2011). Here, we examined brain functional network reorganization at the level of whole brain, individual functional networks and individual brain regions in order to better understand the underlying mechanism of these reorganizational changes.

We observed significantly decreased local efficiency but increased global efficiency in the epilepsy patient group. Although functional strength was similar for both groups, we found that between-network connections were increased, especially in the default mode and subcortical networks. Brain regions such as medial temporal lobe showed consistent disruptions similarly as observed brain-wide, whereas some regions such as the posterior cingulate cortex and postcentral gyrus displayed opposite direction of alterations. These findings suggest that epilepsy disrupts information processing in local network and brain-wide distributed networks by forming weak connections between networks. Epileptic disruptions at individual brain regions can have distinct pattern of alterations, suggesting that individual regions displaying abnormal network properties may be important in understanding the pathogenesis of epilepsy.

Materials and Methods

Subjects

Current findings are based on data acquired from 9 epilepsy patients (33.8 ± 9.4 years, 6 F/3 M) and 9 age-matched healthy control subjects (33 ± 10.4 years, 6 F/3 M) (Table 1). Five patients were identified with temporal lobe epilepsy and 4 patients were idiopathic with unidentifiable seizure origins. No significant age or gender differences were found between the two groups. This study was approved by the University of Wisconsin-Madison's Health Sciences Institutional Review Board. All subjects provided written informed consent. Subject profiles are shown in Table S1.

Neuroimaging data acquisition

Each epilepsy patient received a 5-minute resting-state fMRI scan as part of the clinical examination from a 3.0 Tesla whole-body MRI scanner (DISCOVERY MR750, General Electric Medical Systems, Waukesha, WI, USA) with an 8-channel head coil. MR imaging parameters are: single shot EPI sequence, axial plane, TR = 2000 ms, TE = 30 ms, flip angle = 75°, slice thickness = 5 mm, number of slice = 28, acquisition matrix = 64 × 64, FOV = 240 × 240 mm^2, voxel size = 3.75 × 3.75 × 5 mm^3, NEX = 1. T1-weighted structural images were acquired axially (TR = 8.688 ms, TE = 3.468 ms, TI = 450 ms, flip angle = 12º, FOV = 240 × 240 mm^2, voxel size = 0.47 × 0.47 × 1.2 mm^3, number of slices = 136).

Each age-matched healthy control subject received a 10-minute resting-state fMRI scan from the same scanner. MR imaging parameters are: single shot EPI sequence, sagittal plane, TR = 2600 ms, TE = 22 ms, flip angle = 60°, slice thickness = 3.5 mm, number of slice = 40, acquisition matrix = 64 × 64, FOV = 224 × 224 mm^2, voxel size = 3.5 × 3.5 × 3.5 mm^3, NEX = 1. T1-weighted structural images with 1 mm isotropic voxels were acquired axially (TR = 8.132 ms, TE = 3.18 ms, TI = 450 ms, flip angle = 12º, FOV = 256 × 256 mm^2, number of slices = 156).

Imaging data pre-processing

Resting-state fMRI data was processed in AFNI (Cox, 1996) following the processing pipeline (Jo et al., 2013) for controlling head motion. Head motion has been shown to significantly affect the resting-state functional connectivity measures (Saad et al., 2009; Satterthwaite et al., 2012; Van Dijk et al., 2012). In current study, a secondary motion correction was performed to exclude fMRI volumes (i.e., time frames/points) with motion above a threshold. A score of motion

measurement corresponding to each volume was calculated as the square root of the sum of squares of the derivatives (SSD) of the six time courses of the motion parameters (Birn et al., 2013; Jones et al., 2010; Meier et al., 2012). A stringent threshold of SSD was set at 0.2 mm; in other words, any time frame associated with a score of SSD greater than 0.2 mm was censored and later excluded using the –censor option provided in the AFNI program, 3dDeconvolve. This option essentially performed zero-filling to maintain the same sampling rate for each subject. Besides controlling motion effect, to avoid potential confounding effect due to different time length of rs-fMRI scan (i.e., 5-minute for epilepsy patients while 10-minute for healthy controls), we only used the first 5-minute scan from each age-matched healthy control subject.

Brain network construction

Brain networks were constructed based on resting-state functional connectivity (RSFC). Total 187 brain regions of interest (ROIs) were predefined within the sensorimotor, cingulo-opercular task control, fronto-parietal task control, dorsal/ventral attention, default mode, salience and subcortical/cerebellar networks (Power et al., 2011). An averaged time series signal resulting from the pre-processed rs-fMRI data was extracted from each of these 187 regions with a radius of 4mm. Pearson correlation coefficient (r_{ij}) was calculated for the *i*th and *j*th ROI. This process generated a 187 × 187 connectivity matrix for each subject within each group. We then thresholded each of these connectivity matrix using a minimum spanning tree (MST) approach in order to obtain a sparse connectivity matrix with optimal functional connections for detecting epileptic disruptions on the brain networks. Each MST per subject was a spanning tree of a weighted sub-graph that is fully connected with all nodes containing maximum total weights of all links, which can be considered as the "skeleton structure" of the brain network for each

subject. However, these MSTs do not form clusters or loops among individual brain regions which keeps it from a biologically meaningful sparse representation of brain networks (Alexander-Bloch et al., 2010). In order to obtain a sparse yet biologically meaningful connectivity matrix, extra connections were added to the MST to form clusters or loops among brain regions. To do so, the top 2%, 4%, 6% and 8% of the remaining connections from the MST-extracted connectivity matrix were added to the MST, respectively. This resulted in 4 sparse connectivity matrix with 4-level of highest proportion of functional connections from the original connectivity matrix for each subject. This approach ensured that 1) each sparse connectivity matrix for each epilepsy patient and healthy control subject contained equal number of functional connections, and that 2) a range of different proportional thresholds was examined to examine the effect of thresholding on group comparsions.

Network analysis

Graph theoretic analyses were applied to the sparse connectivity matrices. Graph metrics, including local efficiency, global efficiency and strength, were estimated using the Brain Connectivity Toolbox (Rubinov & Sporns, 2010) with adaptation made for calculating these metrics for individual brain regions.

Local efficiency is a measure of information transmission among locally connected regions, such as in a module or a sub-network, whereas global efficiency is a measure of system-wide (i.e., over the whole brain) information transmission. Local efficiency implies that to what extent connections are being segregated into local clusters or sub-networks (Achard et al., 2012), whereas global efficiency indicates that to what extent connections are being integrated into a system-wide network (Rubinov & Sporns, 2010). Strength and degree are two lower-level graph

metrics that measure how strongly connections are formed over the whole brain or at individual brain regions. Strength is estimated as the mean value of weights (i.e., Pearson's cross-correlation coefficients) of all functional connections linking to a particular brain region or across multiple brain regions. Degree, a binary measure of functional strength, is estimated as the number of functional connections linking to a particular brain region and that survived thresholding.

Estimating brain networks disruptions in epilepsy

Epilepsy may disrupt brain network organization differently across regional locations and functional networks. We adopted a similar approach that was originally used for detecting functional network changes in comatose patients and referred as the hub disruption index, κ (Achard et al., 2012). The hub disruption index for a given graph metric, e.g., strength, was constructed by subtracting the mean regional strength of the healthy control group from the mean strength of the corresponding brain region in the epilepsy group and plotting this group mean difference against the healthy control group mean. The gradient of a straight line fitted to the data was referred as a hub disruption index, κ. This approach essentially provided a form of visualization as well as estimation for examining network and brain regional disruptions all together from a single plot.

Statistical analysis

Group comparison was conducted for each graph metric at each threshold level using the Wilcoxon rank sum test. Binomial proportion tests were later used to compare the proportions of strength and degree of each network to the total strength and degree in whole-brain networks,

respectively between the two groups (Song et al., 2012). FDR correction was applied for multiple comparisons.

Results

Disrupted local efficiency in epilepsy

At the brain-wide level, we found that local efficiency was significantly decreased in epilepsy across a range of thresholds (Figure 1). Group-mean local efficiency increased monotonically as a function of increasing connection density (i.e., proportional thresholds). The measure of local efficiency estimated for individual brain regions on average over all subjects in each group also showed decrease in regions such as the medial temporal lobe of the default mode network (DMN) and postcentral gyrus (PCG) of the sensorimotor network. However, increased local efficiency was observed in some regions such as the posterior cingulate cortex (PCC) and angular gyrus from the DMN, thalamus from the subcortical network, and cerebellar vermis from the cerebellar network. A negative hub disruption index ($\kappa < -0.6$) was observed across all thresholds (Figure 2). In other words, brain regions with high information processing efficiency in healthy control subjects showed great reduction in epilepsy patients (i.e., medial temporal lobe), whereas brain regions with normal information processing efficiency in healthy controls showed abnormal increase in patients (i.e., PCC and PCG).

Disrupted global efficiency in epilepsy

At the brain-wide level, global efficiency was significantly increased in epilepsy across a range of thresholds (Figure 3). Group-mean global efficiency increased monotonically as a function of increasing connection density. A negative hub disruption index of global efficiency ($\kappa < -0.4$)

was observed across all thresholds (Figure S1). Similar to what we have seen in local efficiency, we observed distinct pattern of changes in global efficiency across different brain regions. The medial temporal lobe and PCG continued to show decreased global efficiency, whereas the PCC, angular gyrus, thalamus and cerebellar vermis continued to show increased global efficiency.

Increased between-network functional connections yet weakly connected

At the brain-wide level, both groups had similar functional connection strength that increased monotonically as a function of increasing connection density (Figure 4). A negative hub disruption index of functional strength ($\kappa < -0.4$) was observed across all thresholds (Figure S2). To further examine the reorganizational changes for each functional network, we conducted a second-level analysis based on two basic graph metrics—the strength and degree. We found that within each functional network, the number and strength of connections were statistically similar between the two groups (Binomial proportional tests, p-value > 0.05; Figure S3). However, there was increased number of between-network connections in the epilepsy patients (Figure 5). Three functional networks showed significant group differences (Table 1). Epilepsy patients had significantly decreased proportion of between-network connections in cingulo-opercular task control network (Binomial proportional tests, corrected p-value < 0.001) and significantly increased proportion of between-network connections in the DMN and subcortical network (Binomial proportional tests, corrected p-values < 0.001). However, the corresponding functional strength of these newly-formed between-network connections was not significantly different between the two groups (Table S2), suggesting that these connections were weakly connected.

Discussion

Previous studies have examined brain efficiency in both functional and anatomical white matter networks in epilepsy (Bernhardt et al., 2011; Liu et al., 2014; Vlooswijk et al., 2011; Wang et al., 2014; Zhang et al., 2011). However, the findings have remained conflicting potentially due to the data processing approach. In our study, we matched each epilepsy patient with an age-matched healthy control subject and have taken stringent steps to safeguard againat head motion artifact following the recommended data processing pipeline (Jo et al., 2013). Furthermore, graph-theory metrics were assessed following consideration of different thresholds upon network calculations. Besides these traditional graph metrics, a "hub-disruption" index was calculated for these metrics to better visualize the epileptic disruptions across different networks and brain regions.

Disrupted network efficiency

Consist with a previous study based on 41 epilepsy patients and 23 healthy controls (Vlooswijk et al., 2011), we observed a whole-brain disruption of both local and global efficiency. Local efficiency was significantly decreased in patients with epilepsy (Figure 1), suggesting impaired regional information transmission and a disruption of network segregation (Rubinov & Sporns, 2010). On the contrary, global efficiency was significantly increased in epilepsy (Figure 3), suggesting more efficiency for global information transmission, which may be a marker of abnormal transmission such as seizure propagation (Rubinov & Sporns, 2010). When examined at functional network level, both local and global efficiency tends to decline with a negative hub-disruption index compared with healthy controls (Figures 2 and S1), indicating an exchange of brain hub to non-hub regions. In addition, this regional reorganization reveals an alteration of

functional importance of individual regions within the same functional network due to epilepsy, which may not be easily observed from a brain-wide network analysis.

We observed that the medial temporal lobe from the DMN and postcentral gyrus from the sensorimotor network showed consistently decreased efficiency, whereas the PCC and angular gyrus from the DMN, thalamus from the subcortical network, and cerebellar vermis from the cerebellar network showed increased efficiency. These regions are critical areas in corresponding functional networks. To further examine if these changes are adaptive or maladaptive, we conducted secondary network analyses for each functional network.

Abnormally increased weak connections between networks

A finer-grained network analysis was performed to examine the changes in the number and strength of connections within and between networks. Besides similar whole-brain functional strength for both groups (Figure 4), within each functional network, we observed statistically similar number and strength of connections (Figure S3). However, there was markedly increased number of between-network connections (Figure 5) in epilepsy group. Further statistical analysis demonstrated that the DMN and subcortical networks had significantly increased number of connections to all other networks (Table 1). There was also a small yet significant amount of connections that disappeared between cingulo-opercular network and other networks. Overall there was an increase in between-network connections in epilepsy group. Nevertheless, these newly-formed connections between networks were shown to be weakly connected as the functional strength of between-network connections was statistically similar between the epilepsy and healthy control subjects (Table S2). This finding further supports the observation of

increased global efficiency which is potentially elevated by the increased amount of shortest path length for long-distance information processing (Rubinov & Sporns, 2010).

Conclusion

In the current study, graph theoretic analysis was applied to resting-state functional connectivity to examine the brain functional network reorganization at the presence of epilepsy. It provided direct evidence of large-scale network disruption in epilepsy patients. Compared with age-matched healthy control subjects, these patients demonstrated impaired local efficiency and increased global efficiency at brain-wide level. When examined at functional network level, these patients showed increased number of connections between networks that are weakly connected, supporting the observations of abnormally high global efficiency. At individual brain regional level, however, epileptic effect led to distinct pattern of alterations. Our findings suggest that brain-wide network efficiency is affected at the presence of epilepsy. With a finer-grained network analysis at network and individual brain regional level, epileptic disruption on functional properties can be better understood.

Limitations

This study does have limitations. The small sample size (n = 9) and the heterogeneity of seizure location were the primary limitations of this study. Five of nine patients were identified with medial temporal epilepsy while the other four patients had no specific seizure location identified from their clinical reports. Next step of this study is to examine brain functional reorganization in temporal lobe epilepsy and evaluate the potential relationship between graph theoretic and clinical measures.

Acknowledgements:

The authors thank all patients and healthy volunteers for their participation. This work was supported by NIH grants RC1MH090912-01, K23NS086852, T32GM008692, UL1TR000427, and T32EB011434, by a Coulter Translational Research Award, an American Heart Association Postdoctoral Fellow Research Award, UW Milwaukee-Madison Intercampus Grants, by funding from the UW Graduate School, and by Grants from the Shapiro Foundation and Foundation of ASNR award.

Disclosure of Conflict of Interest

The authors have no conflicts of interest to report, as this research was conducted in the absence of commercial and financial relationships that might compromise the integrity of the results reported herein.

References:

Achard S, Delon-Martin C, Vertes PE, Renard F, Schenck M, Schneider F, Heinrich C, Kremer S, Bullmore ET. (2012) Hubs of brain functional networks are radically reorganized in comatose patients. *Proc Natl Acad Sci U S A* 109:20608-20613.

Alexander-Bloch AF, Gogtay N, Meunier D, Birn R, Clasen L, Lalonde F, Lenroot R, Giedd J, Bullmore ET. (2010) Disrupted modularity and local connectivity of brain functional networks in childhood-onset schizophrenia. *Front Syst Neurosci* 4:147.

Bernhardt BC, Chen Z, He Y, Evans AC, Bernasconi N. (2011) Graph-theoretical analysis reveals disrupted small-world organization of cortical thickness correlation networks in temporal lobe epilepsy. *Cereb Cortex* 21:2147-2157.

Birn RM, Molloy EK, Patriat R, Parker T, Meier TB, Kirk GR, Nair VA, Meyerand ME, Prabhakaran V. (2013) The effect of scan length on the reliability of resting-state fMRI connectivity estimates. *NeuroImage* 83:550-558.

Cox RW. (1996) AFNI: software for analysis and visualization of functional magnetic resonance neuroimages. *Comput Biomed Res* 29:162-173.

Fisher RS, van Emde Boas W, Blume W, Elger C, Genton P, Lee P, Engel J, Jr. (2005) Epileptic seizures and epilepsy: definitions proposed by the International League Against Epilepsy (ILAE) and the International Bureau for Epilepsy (IBE). *Epilepsia* 46:470-472.

Haneef Z, Chiang S. (2014) Clinical correlates of graph theory findings in temporal lobe epilepsy. *Seizure*.

Jo HJ, Gotts SJ, Reynolds RC, Bandettini PA, Martin A, Cox RW, Saad ZS. (2013) Effective Preprocessing Procedures Virtually Eliminate Distance-Dependent Motion Artifacts in Resting State FMRI. *J Appl Math* 2013.

Jones TB, Bandettini PA, Kenworthy L, Case LK, Milleville SC, Martin A, Birn RM. (2010) Sources of group differences in functional connectivity: An investigation applied to autism spectrum disorder. *NeuroImage* 49:401-414.

Liu M, Chen Z, Beaulieu C, Gross DW. (2014) Disrupted anatomic white matter network in left mesial temporal lobe epilepsy. *Epilepsia* 55:674-682.

Meier TB, Desphande AS, Vergun S, Nair VA, Song J, Biswal BB, Meyerand ME, Birn RM, Prabhakaran V. (2012) Support vector machine classification and characterization of age-related reorganization of functional brain networks. *NeuroImage* 60:601-613.

Power JD, Cohen AL, Nelson SM, Wig GS, Barnes KA, Church JA, Vogel AC, Laumann TO, Miezin FM, Schlaggar BL, Petersen SE. (2011) Functional Network Organization of the Human Brain. *Neuron* 72:665-678.

Rubinov M, Sporns O. (2010) Complex network measures of brain connectivity: uses and interpretations. *NeuroImage* 52:1059-1069.

Saad ZS, Glen DR, Chen G, Beauchamp MS, Desai R, Cox RW. (2009) A new method for improving functional-to-structural MRI alignment using local Pearson correlation. *NeuroImage* 44:839-848.

Satterthwaite TD, Wolf DH, Loughead J, Ruparel K, Elliott MA, Hakonarson H, Gur RC, Gur RE. (2012) Impact of in-scanner head motion on multiple measures of functional connectivity: Relevance for studies of neurodevelopment in youth. *NeuroImage* 60:623-632.

Song J, Desphande AS, Meier TB, Tudorascu DL, Vergun S, Nair VA, Biswal BB, Meyerand ME, Birn RM, Bellec P, Prabhakaran V. (2012) Age-related differences in test-retest reliability in resting-state brain functional connectivity. *PLoS One* 7:e49847.

Sporns O, Tononi G, Kotter R. (2005) The human connectome: A structural description of the human brain. *PLoS Comput Biol* 1:245-251.

Van Dijk KRA, Sabuncu MR, Buckner RL. (2012) The influence of head motion on intrinsic functional connectivity MRI. *NeuroImage* 59:431-438.

Vlooswijk MC, Vaessen MJ, Jansen JF, de Krom MC, Majoie HJ, Hofman PA, Aldenkamp AP, Backes WH. (2011) Loss of network efficiency associated with cognitive decline in chronic epilepsy. *Neurology* 77:938-944.

Wang J, Qiu S, Xu Y, Liu Z, Wen X, Hu X, Zhang R, Li M, Wang W, Huang R. (2014) Graph theoretical analysis reveals disrupted topological properties of whole brain functional networks in temporal lobe epilepsy. *Clin Neurophysiol* 125:1744-1756.

Zhang Z, Liao W, Chen H, Mantini D, Ding JR, Xu Q, Wang Z, Yuan C, Chen G, Jiao Q, Lu G. (2011) Altered functional-structural coupling of large-scale brain networks in idiopathic generalized epilepsy. *Brain* 134:2912-2928.

Figure/Table Legends

Supporting Information:

Figure 1 Decreased local efficiency in epilepsy

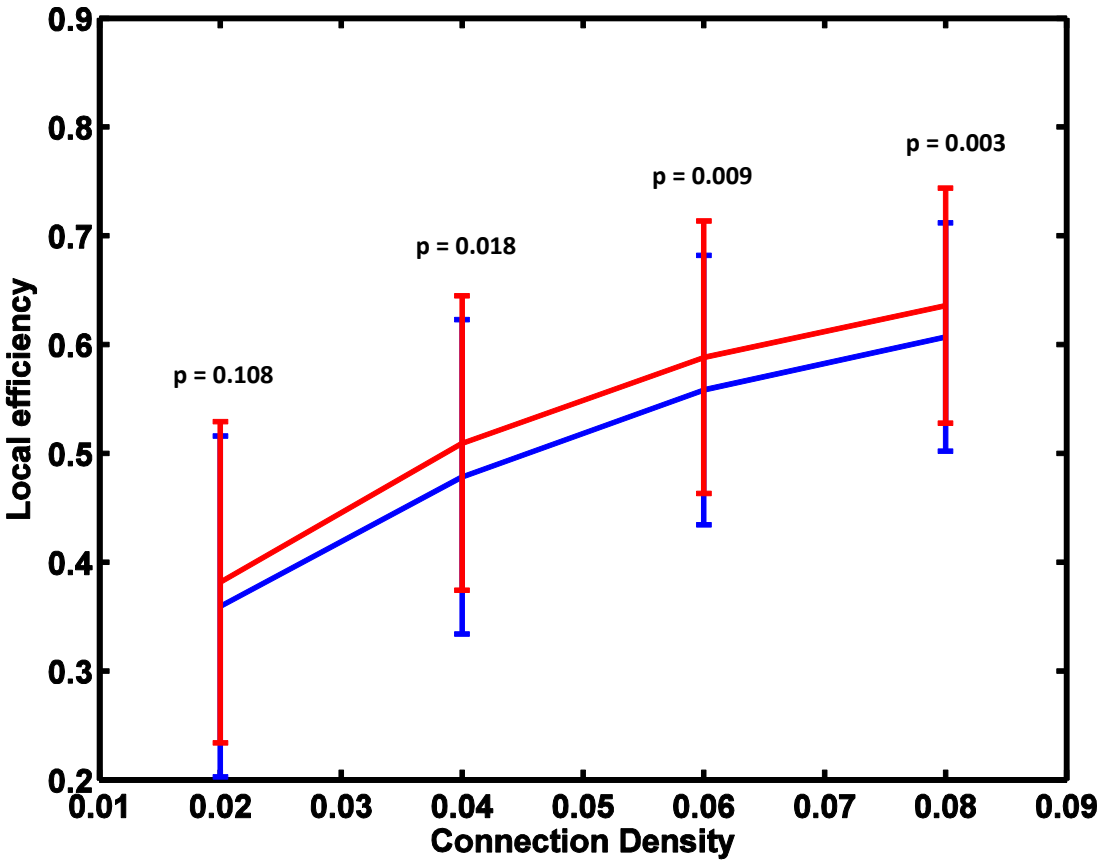

Shown are group comparison based on the Wilcoxon rank sum tests. Epilepsy patients show significantly decreased local efficiency across a range of thresholds/connection density (Epilepsy-blue line, Healthy control-red line).

Figure 2 Hub disruption index of local efficiency

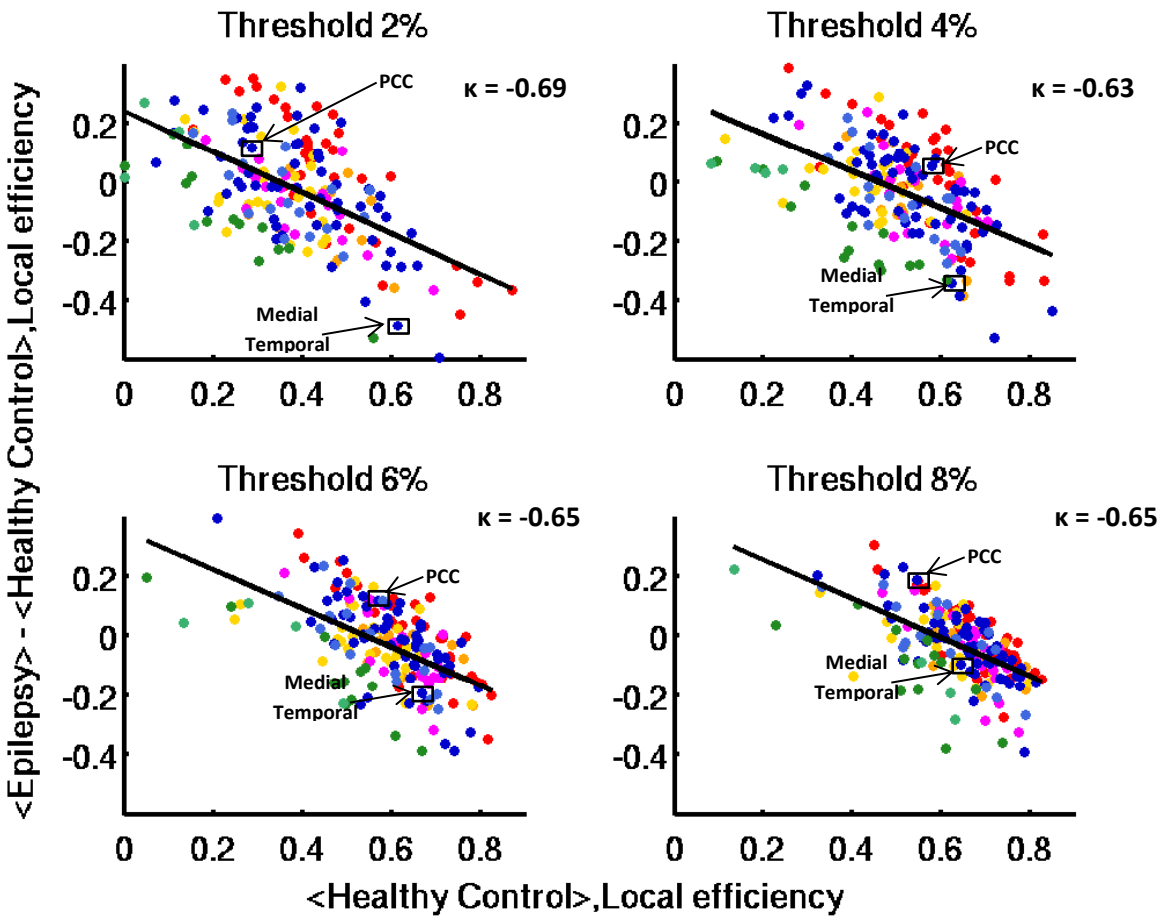

The hub disruption index of local efficiency is plotted at each threshold of connection density. The mean value of local efficiency of each node in the healthy control group <Healthy Control> (x-axis) is plotted against the difference between groups in mean local efficiency of each node <Epilepsy> - <Healthy Control> (y-axis). The hub disruption index of local efficiency is then estimated as the gradient of the solid black line fitted to the scatterplots. Negative hub disruption indices are observed across different thresholds, indicating an overall disruption of local efficiency in the epilepsy group. Compared to the healthy control group, epilepsy patients show distinct pattern of regional changes in local efficiency. The posterior cingulate cortex (PCC) has increased local efficiency, whereas the medial temporal lobe shows decreased local efficiency.

Figure 3 Increased global efficiency in epilepsy

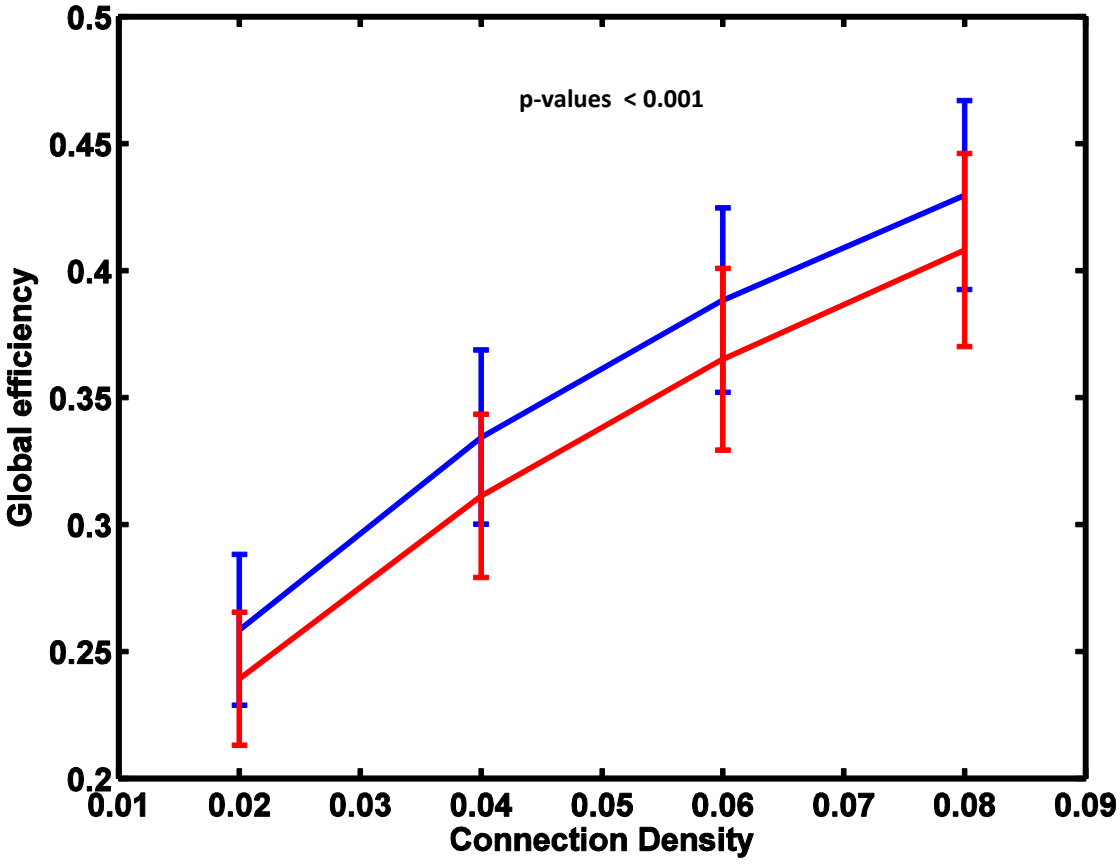

Global efficiency is significantly increased in the epilepsy group (Wilcoxon rank sum tests, p-value < 0.001 with multiple comparison correction) (Epilepsy-blue line, Healthy control-red line).

Figure 4 Similar functional strength for both groups

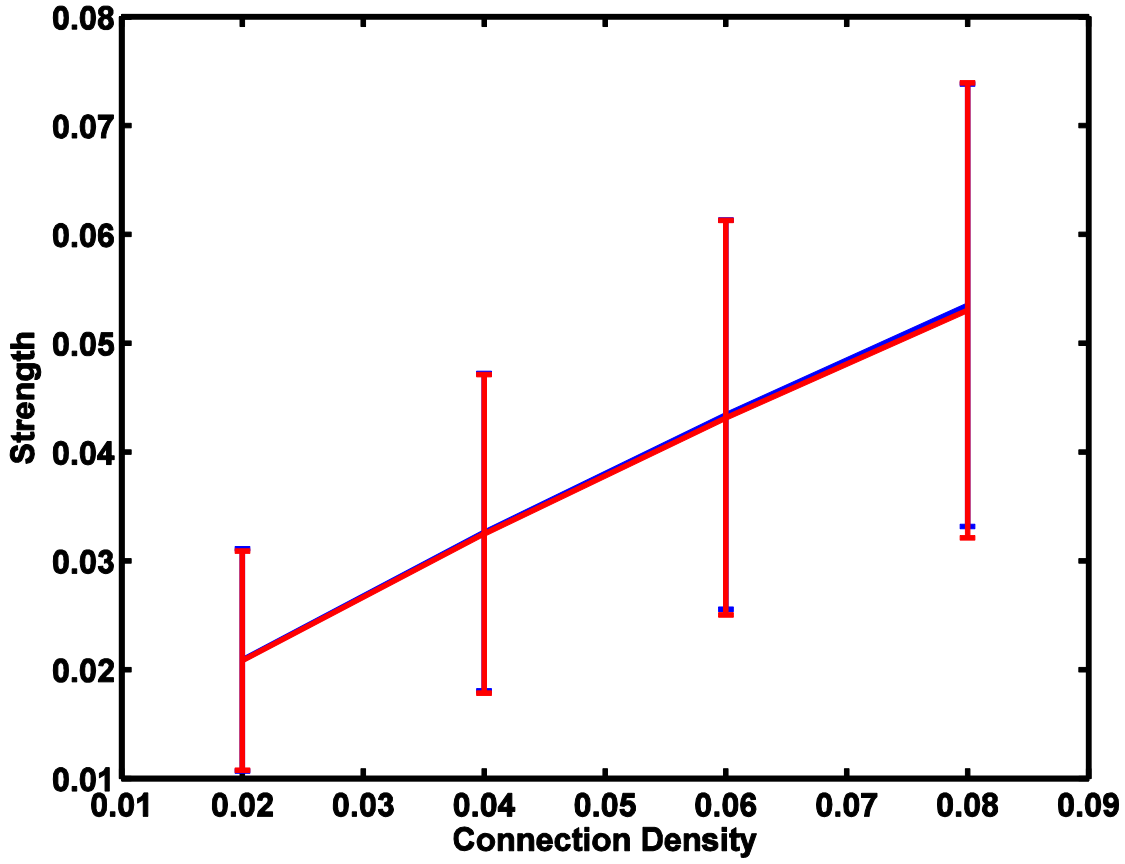

Functional strength is similar for both groups (Wilcoxon rank sum tests, p-values > 0.05) (Epilepsy-blue line, Healthy control-red line).

Figure 5 Increased number of between-network functional connections in epilepsy

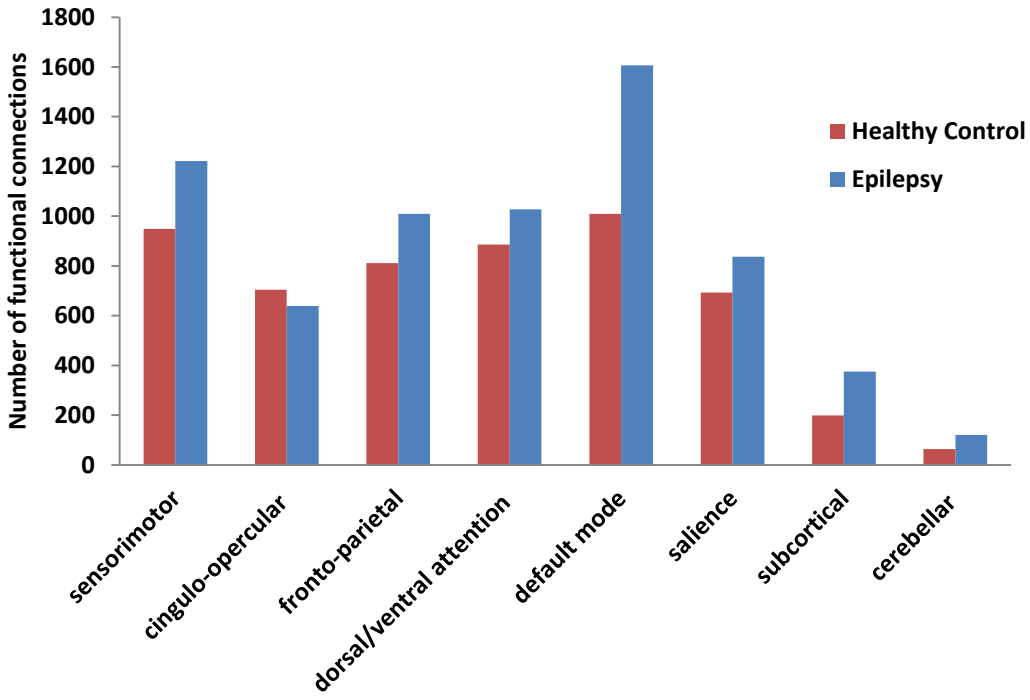

There is increased number of functional connections between networks in epilepsy patients.

Table 1 Degree of functional connections between networks

Functional Network	Healthy Control	Epilepsy	corrected p-value	Directional change
sensorimotor	0.179	0.179		
cingulo-opercular	**0.132**	**0.093**	<0.001	⬇
fronto-parietal	0.153	0.148		
dorsal/ventral attention	0.167	0.150	0.06	
default mode	**0.190**	**0.235**	<0.001	⬆
salience	0.130	0.122		
subcortical	**0.037**	**0.055**	<0.001	⬆
cerebellar	0.012	0.018	0.07	

Binomial proportional test was used to compare the proportion of between-network for each functional network followed by multiple comparison correction. The cingulo-opercular network showed significantly decreased between-network connections (p-value < 0.001), whereas the default mode and subcortical network showed significantly increased between-network connections (p-value < 0.001).

Supplementary Materials

Figure S1 Hub disruption index of global efficiency

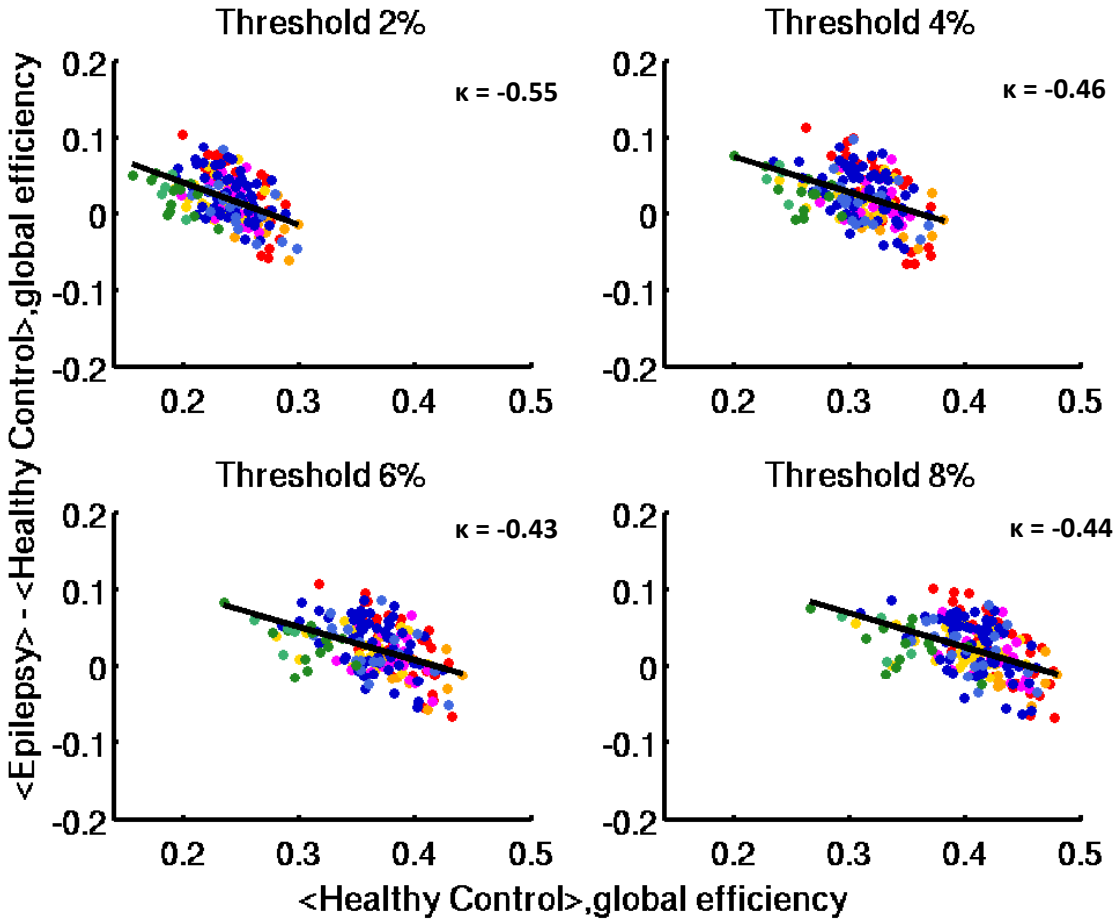

The hub disruption index of global efficiency is plotted at each threshold of connection density. The mean value of global efficiency of each node in the healthy control group <Healthy Control> (x-axis) is plotted against the difference between groups in mean global efficiency of each node <Epilepsy> - <Healthy Control> (y-axis). The hub disruption index of global efficiency is estimated as the gradient of the solid black line fitted to the scatterplots. Negative hub disruption indices are observed across different thresholds, indicating an overall disruption of global efficiency in the epilepsy group.

Figure S2 Hub disruption index of strength

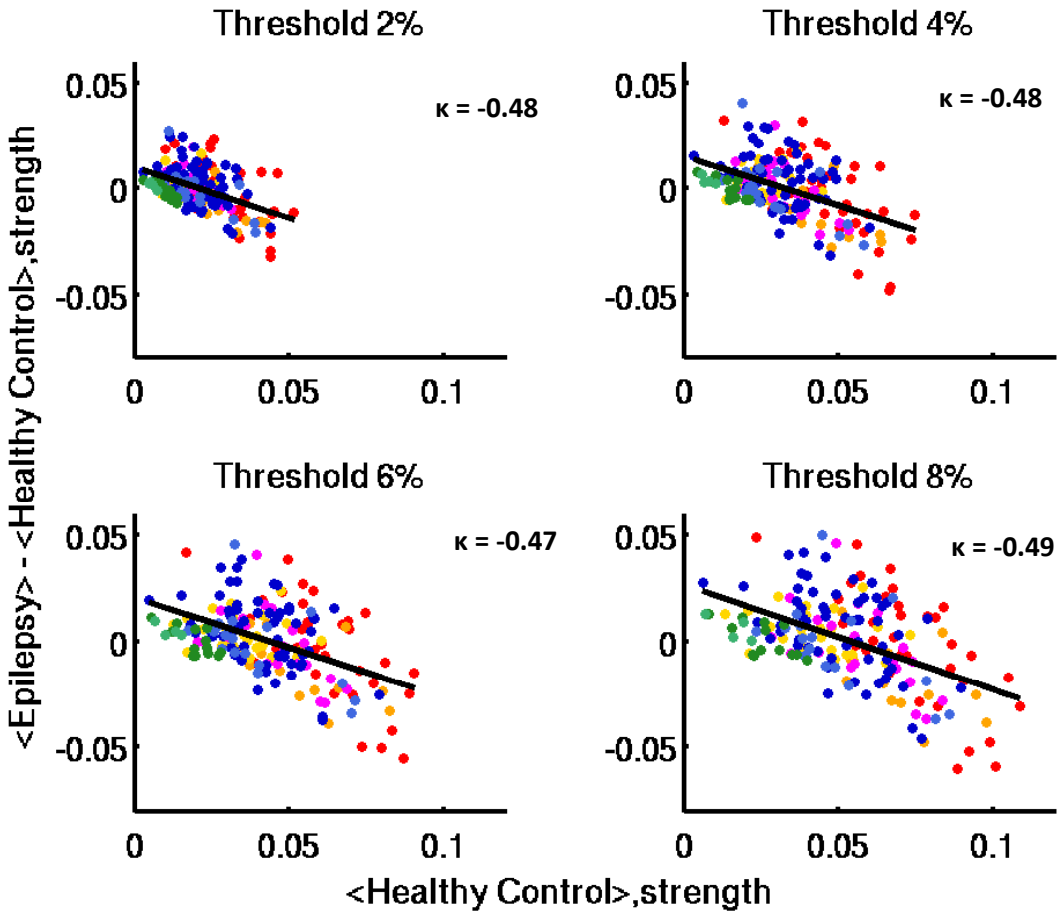

The hub disruption index of strength is plotted at each threshold of connection density. The mean value of nodal strength in the healthy control group <healthy Control> (x-axis) is plotted against the difference between groups in the mean nodal strength <Epilepsy> - <Healthy Control> (y-axis). The hub disruption index of strength is estimated as the gradient of the solid black line fitted to the scatterplots. Negative hub disruption indices are observed across different thresholds, indicating an overall disruption of strength in the epilepsy group.

Figure S3 Strength and degree of within-network functional connections

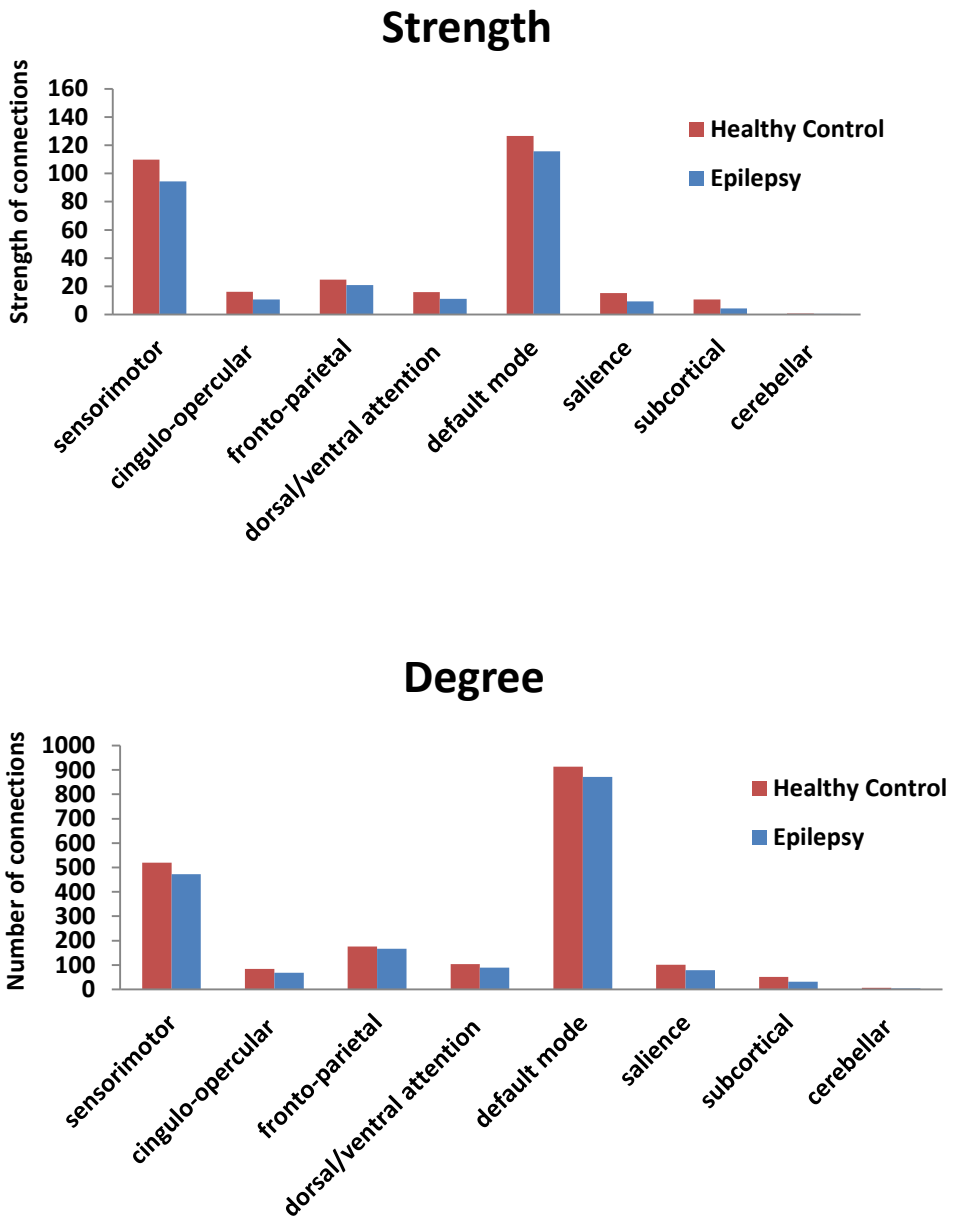

Within each functional network, both groups had statistically similar strength and degree of connections (Binomial proportion test, p-values > 0.05 after multiple comparison correction).

Table S1: Characteristics of epilepsy patients and healthy control subjects

Epilepsy Patient ID	Age (years)	Gender	Epilepsy origin location	Healthy Control ID	Age (years)	Gender
638AF	25	F	Not specified	026	25	M
593LW	26	F	Not specified	005	25	F
500HM	27	F	Not specified	009	27	F
522EC	28	F	mesial temporal sclerosis	023	28	M
595AM	31	F	Not specified	019	29	F
551SK	33	M	Not specified	014	29	F
518AF	37	F	right mesial temporal lobe	028	32	M
539RS	44	M	post left temporal cavernoma resection; partial temporal lobectomy	030	50	F
484KF	53	M	mesial temporal sclerosis	054	52	F
	33.8 ± 9.4	**6F/3M**	**5 known temporal lobe**		**33 ± 10.4**	**6F/3M**

Table S2 Strength of functional connections between networks

Functional Network	**Proportion of strength in each network**	
	Healthy Control	**Epilepsy**
sensorimotor	0.185	0.176
cingulo-opercular	0.150	0.102
fronto-parietal	0.142	0.149
dorsal/ventral attention	0.181	0.159
default mode	0.168	0.230
salience	0.138	0.128
subcortical	0.029	0.043
cerebellar	0.008	0.013

Shown here are the proportions of between-network connection strength in each individual network relative to the total between-network connection strength across all networks in each group. Both groups had similar between-network connection strength (Binomial proportion test, corrected p-values > 0.05).

Chapter V

Conclusion

Conclusion of the thesis

The human brain undergoes changes which reshape its own structure and function through thoughts and activities in the course of individual lives. This type of changes is known as neuroplasticity and is explained with clarity and thoroughness in the book of 'the brain that changes itself'(Doidge 2007). The work presented in this thesis is intended to probe one small piece of neuroplasticity accompanied by normal healthy aging. It describes the application of statistical and mathematical approaches combined with functional magnetic resonance imaging (fMRI) data to understanding brain functional reorganization with aging and under the presence of epilepsy.

Previous studies had shown aging plays a significant role in brain reorganization in the form of age-related neural decline, such as cerebral atrophy and synaptic loss, but it remained unclear how these structural changes ultimately affect the brain functions. In addition, numerous studies had used resting-state fMRI (rs-fMRI) to study brain functions. However, questions remained unclear whether these measures were reliable across different individuals and across time. Furthermore, how aging might affect this reliability was largely unknown. This work was able to advance the understanding of how normal healthy aging interfaces with the brain functional reorganization measured via rs-fMRI. First, this work verifies that rs-fMRI is a stable measurement that can be used to assess the brain functional connectivity across different scan sessions. Second, the effect of aging on the reliability of rs-fMRI measures is investigated *the first time* with findings suggesting that these measures are stable yet their reliability is affected by aging. Furthermore, the brain functional reorganization is elucidated by examining the brain as a network model using graph theory, and identifies how brain reorganizes itself globally and regionally with aging. Finally, it identifies two important brain functional networks showing

distinct patterns of reorganizational changes. Based on the work investigating brain changes with aging, this brain network model is further applied to a group of epilepsy patients and measures how brain networks are modified under the influences of seizures. By comparing these brain connectivity measures to those from age-matched healthy controls, this thesis shows how epilepsy induced brain changes may produce abnormally increased functional connections among brain networks and these newly-formed weak connections may ultimately lead to a decreased efficiency for brain processing information effectively within each functional division. Many studies have utilized brain imaging to understand the brain functional changes with aging and with other neurological and neurodegenerative diseases, including stroke (Di Carlo 2009), Alzheimer's disease (AD), Parkinson's disease (PD) ,amyotrophic lateral sclerosis (ALS), and fontotemporal dementia (Risacher and Saykin 2013). In chapter II we used resting-state fMRI (rs-fMRI) to measure brain functional connectivity in two groups of healthy individuals classified by age. First we showed rs-fMRI is a stable way to measure connections between brain regions which are functionally connected. *This is the first study to examine the reliability of rs-fMRI measures in older adults and compare these measures to those in younger adults*. We showed moderate to high reliability of resting-state functional connectivity (RSFC) in both younger and older adults and a high consistency of large-scale patterns of connections observed across subjects. However, comparing to reliable functional connections in the older group to the younger group, we then confirmed that the number of reliable connections is significantly decreased in the older group, suggesting an underlying changes in RSFC associated with aging. Global signal regression (GSR) is another factor that could potentially modulate RSFC during the process of rs-fMRI signal processing (Saad et al. 2012). There are no other rs-fMRI issues more controversial than GSR. GSR used to be a common practice in rs-fMRI preprocessing but

was brought into attention after the report of tendency of GSR to zero-center the distribution of correlation values (Fox et al. 2009, Murphy et al. 2009). Therefore, we also investigated how GSR potentially affects RSFC and the test-retest reliability alongside of the aging effect. We found GSR tends to reduce the reliability of RSFC in the two age-groups by reducing the number of reliable connections. Given the fact that GSR approach remains in wide use in many rs-fMRI studies, we suggested its application should be interpreted with caution especially when examining group differences. Our finding was later confirmed in a recent case study of Autism spectrum disorders which reported that GSR systematically alters functional connections and influences group comparisons (Gotts et al. 2013).

RSFC results from chapter II implicated that aging modulates brain functional organization. It is important to understand the aspects of brain reorganization that are critical in normal aging. In chapter III, we developed a brain network model using graph theory methods applied to the rs-fMRI data acquired from two groups of normal healthy adults classified by age. This mathematic approach allows a systematic examination of brain reorganizational changes at brain-wide level and at local regional level.

We found that brain functional networks demonstrated modular organization in both groups with modularity decreased with aging, suggesting less distinct functional divisions across whole brain networks. Local efficiency was also decreased with aging but not global efficiency. In addition, we also observed consistent disruptions of network properties at regional level in the older group, particularly, in two major functional networks--the default mode network (DMN) and the sensorimotor network. Local efficiency, global efficiency and regional strength were decreased in DMN and increased in the sensorimotor network in the older group. These results indicate that besides brain-wide reorganizational changes observed in the elderly, aging likely disrupts

individual brain networks differently depending on the functional properties. *This work is the first study to demonstrate age- related brain functional reorganization globally and locally using a network analysis approach*.

In chapter III, We demonstrated that the network model is a reasonably effective way to quantify brain functional reorganization with aging and proved this network is reliably reproducible in different subjects and using different rs-fMRI datasets. In order to utilize this network approach for a better understating of disease-related brain reorganization, application in patient population is necessary. In chapter IV we applied network analysis to the rs-fMRI data acquired from a group of epilepsy patients and compared network measures to age-matched healthy control subjects. We were able to show that the epilepsy patients lost optimal modular organization in functional networks. Moreover, the patients showed significant decreases in efficiency for processing information in local functional divisions. These results suggest impaired and less efficient functional networks in epilepsy.

To conclude, what are the benefits of using network analysis in neuroimaging research? First, with the increasing interests in the concept of "Big data", there are few limitations in acquiring large and complex datasets, instead, the challenge rests in deriving information from analysis of a single large dataset. Graph theory-based network analysis is one of powerful approaches that can provide an abstract representation that eventually reduce the complexity when dealing with a large, complex datasets such as the neural networks. Second, network analysis not only allows to quantify the hierarchy and modular structures, and examine information traffic flow at different scales of a global graph, it also provides the flexibility to identify critical areas at regional level and determine information processing at local neighborhood. Third, human brains vary in size and shape across individuals. Network analysis can hid these features and help to identify

similarities and differences in the topological organization of the brain networks. Finally, using the same frame of references, brain networks can be constructed based on structural, functional or effective connectivity and comparisons can be made across different types of networks.

Future directions

Age-related brain functional reorganization related to cognitive performance

There has been increasing interests in the neuroscience community in relating individual or group differences in brain functional connectivity with behavioral or cognitive measures. Although a recent study reported correlations between network measures and subject cognitive performance, none of these correlations survive multiple comparison correction (Geerligs et al. 2014). Given the observed changes in the two important functional networks—the DMN and the sensorimotor network, we tested how these changes was related to the actual cognitive performance. In the younger group, we found that the within-modular degree z-score of the DMN is significantly and negatively correlated with the response time in the spatial working memory after multiple comparison correction. This suggests greater functional connectivity within the DMN is correlated with faster response times in spatial working memory task in younger adults. For future studies, more extensive behavioral tasks and multiple scan sessions would be helpful for evaluating the correlations between network measures and behavioral performances.

Age-related structural reorganization in relation to functional reorganization

The brain structural changes with aging have documented in previous studies with evidence from postmodern findings and neuroimaging analyses. Brain functioning is increasingly seen as a

complex interplay of dynamic neural systems that rely on the integrity of structural and functional networks. We have used diffusion tensor imaging (DTI) data combined with task-fMRI data to examine the brain structural and functional changes while recovering from stroke (Song 2014). Results from this preliminary work showed a significant relationship between structural integrity (i.e., measured as fractional anisotropy (FA) values) of white matter tracts and the corticomotor activity in stroke patients. For future studies, structural connectivity constructed from DTI data would reveal more details in terms of underlying structural changes alongside the observed functional changes in the elderly, especially in brain regions belonging to the DMN and the sensorimotor network.

Homogeneous epilepsy patients

The application of brain network analysis in epilepsy reveals brain-wide alteration of functional networks with consistent observation of deceased efficiency of local information processing. However, this group of epilepsy had seizures originated from various brain regions which could affect individual brain networks differently. The confounding effects of anti-epileptic drugs, which can affect normal neuronal function, were not controlled for due to lack of sufficient information. In this thesis, we showed the proof-of-concept application of brain-wide network analysis in epilepsy patients to identify brain reorganizational changes. An intriguing direction for future research would be to collect data from many more epilepsy patients and segregate them based on the type of seizures, or the location of seizure origins with a control for confounding effect of anti-epileptic drugs.

Brain network analysis in stroke patients

The ability for brain network modeling to examine whole brain-wide network changes suggests that it may prove efficacious in other disease processes. Indeed, a recent study is already applied graph-theory based network analysis to a group of stroke patients (Wang et al. 2010). However, this study only examined the functional reorganization of the motor execution network constructed from 21 brain regions. Although this study was able to show low efficiency of local information processing in stroke affected motor executive network, it remains largely unknown about the dynamic changes of whole brain functional network after stroke. Preliminary work has been done using DTI to examining brain structural and functional changes while recovery from stroke, which suggests that corticomotor functional activity measured by task-fMRI is significantly correlated with underlying structural changes in white matter tracts (Song 2014). A combined structural and functional network analysis would provide a better understanding of stroke recovery and allow for examining brain changes at global brain-wide level and at local regional level such as critical areas in motor and language networks or regions that are affected by stroke.

Brain network analysis utilized for guiding clinical decision-making

Brain network analysis not only holds promise as potential biomarkers for identifying the epileptogenic zone as shown in Chapter IV, it also has potential to provide clinicians with clinically useful biomarkers for assisting clinical decision-making in brain tumor patients. One application I have tried on is to identify functionally important brain regions near the tumor region based on their nodal degree. This information provides the neurosurgeon with information of critical regions they may want to avoid cutting while taking into account the presence of tumor. To further validate this approach, transcranial magnetic stimulation (TMS) can be used

for determining the functional importance of particular regions. One limitation of this approach is the time-length for data processing and network constructing. It is semi-automated and needs to be validated and fully automated in order to provide important and effective information for pre-surgical planning.

References

Di Carlo, A. 2009. "Human and economic burden of stroke." *Age and Ageing* no. 38 (1):4-5. doi: DOI 10.1093/ageing/afn282.

Doidge, N. 2007. *The Brain That Changes Itself: Stories of Personal Triumph from the Frontiers of Brain Science*: Penguin Books.

Fox, M. D., D. Y. Zhang, A. Z. Snyder, and M. E. Raichle. 2009. "The Global Signal and Observed Anticorrelated Resting State Brain Networks." *Journal of Neurophysiology* no. 101 (6):3270-3283. doi: DOI 10.1152/jn.90777.2008.

Geerligs, L., R. J. Renken, E. Saliasi, N. M. Maurits, and M. M. Lorist. 2014. "A Brain-Wide Study of Age-Related Changes in Functional Connectivity." *Cereb Cortex*. doi: 10.1093/cercor/bhu012.

Gotts, S. J., Z. S. Saad, H. J. Jo, G. L. Wallace, R. W. Cox, and A. Martin. 2013. "The perils of global signal regression for group comparisons: a case study of Autism Spectrum Disorders." *Front Hum Neurosci* no. 7:356. doi: 10.3389/fnhum.2013.00356.

Murphy, K., R. M. Birn, D. A. Handwerker, T. B. Jones, and P. A. Bandettini. 2009. "The impact of global signal regression on resting state correlations: Are anti-correlated networks introduced?" *Neuroimage* no. 44 (3):893-905. doi: DOI 10.1016/j.neuroimage.2008.09.036.

Risacher, S. L., and A. J. Saykin. 2013. "Neuroimaging Biomarkers of Neurodegenerative Diseases and Dementia." *Seminars in Neurology* no. 33 (4):386-416. doi: DOI 10.1055/s-0033-1359312.

Saad, Z. S., S. J. Gotts, K. Murphy, G. Chen, H. J. Jo, A. Martin, and R. W. Cox. 2012. "Trouble at rest: how correlation patterns and group differences become distorted after global signal regression." *Brain Connect* no. 2 (1):25-32. doi: 10.1089/brain.2012.0080.

Song, J; Young, B.M.; Nigogosyan, Z.; Walton, L.M.; Nair, V.A.; Grogan, S.W.; Tyler, M.E.; Farrar-Edwards, D.; Caldera, K.E.; Sattin, J.A.; Williams, J.C.; Prabhakaran V. 2014. "Characterizing Relationships of DTI, fMRI, and Motor Recovery in Stroke Rehabilitation Utilizing Brain-Computer Interface Technology " *Frontiers in Neuroengineering* no. 7: 31.2014

Wang, L., C. S. Yu, H. Chen, W. Qin, Y. He, F. M. Fan, Y. J. Zhang, M. L. Wang, K. C. Li, Y. F. Zang, T. S. Woodward, and C. Z. Zhu. 2010. "Dynamic functional reorganization of the motor execution network after stroke." *Brain* no. 133:1224-1238. doi: Doi 10.1093/Brain/Awq043.

Appendix:

A Tutorial in Human Brain Functional Network Analysis using Graph Theory

Jie Song[1,2] MS jsong46@wisc.edu

[1] Department of Biomedical Engineering, University of Wisconsin-Madison, Madison, WI, USA.
[2] Department of Radiology, University of Wisconsin-Madison, Madison, WI, USA.

Abstract

The human brain is a rather complex and dynamic system that can be modeled as a large-scale brain network in order to better understand the organizational properties as well as the reorganizational mechanism under disease conditions. This tutorial describes an approach for developing a brain functional network model that has been applied in normal healthy population as well as in epilepsy patients to examine the aging and epileptic effect on brain network reorganization. To note, this tutorial intends to provide one way to construct brain functional network model based on resting-state functional connectivity. Based on the sparse connectivity matrices, graph theory is applied to extract several topological features including higher-order measures such as modularity, local and global efficiency and lower-order measures including strength and degree. These metrics are assessed following consideration of different thresholds upon network calculations. As an introduction for new researchers in the field of network analysis, the challenges of graph theory analysis facing are discussed as well.

Key Words: graph theory, network analysis, functional networks, resting-state function connectivity

Introduction

The human brain is a complex structure that can be model as a network or a graph represented by a collection of nodes (i.e., cortical and subcortical brain regions) and links (i.e., associations between nodes)(Sporns et al., 2005). This approach is based on graph theory which provides a powerful way of examining the dynamic neuronal interactions from the macro scale of whole-brain to micro scale of voxels, and examining how these interactions together produce complex behaviors in human beings. Within the neuronal network, white matter tracts (i.e., structural connectivity) form anatomical networks, individual brain regions (i.e., volume of grey matter) exhibit underlying, nonlinear statistical dependencies (i.e., functional connectivity) which form brain functional networks and with a priori knowledge of directional or causal interactions among brain regions (i.e., effective connectivity), functional networks can also be formed via effective connectivity. Graph theory analysis has been applied into these three major modalities of complex neural networks (Park & Friston, 2013). This tutorial, however, is focused on the analysis on functional networks based on resting-state fMRI data. General reviews on graph theoretical applications can be found from (Bullmore & Sporns, 2009).

Methods

Workflow for network connectivity analysis

Network connectivity is the input for graph theory analysis and is also the output of general connectivity analysis. Here network connectivity is estimated from resting-state fMRI data. The

workflow for yielding functional connectivity starts with high-resolution anatomical MRI scans (Figure 1). These scans are later used to register the location of brain regions. Next step is to obtain time series of resting-state fMRI data from different brain regions. Deriving time series of fMRI data from each brain region is part of data preprocessing. A detailed description of preprocessing steps can be found from Chapter III of the thesis or Song et al. (2014, Brain Connectivity). Pearson's correlation coefficients between the fMRI time series can be calculated and represented as a correlation matrix or resting-state functional connectivity (RSFC) matrix for each subject and each scan. Elements of the RSFC matrix have values ranging from -1 to 1. To note, time series and the correlation matrices can be generated using the @ROI_Corr_Mat option in the AFNI program (Cox, 1996). The RSFC matrix can be interpreted as a weighted matrix with correlation coefficients as weights of the links/edges, or it can be binarized in that only correlation coefficients above a threshold represent a "true" network connection and are assigned with values of 1s.

Thresholding brain networks

Thresholding a RSFC matrix is critical for obtaining a sparse adjacency matrix in that it should be optimal and contain not too little functional connections for detecting group differences but not too many functional connections that it may dilute group differences. The most commonly used approach for thresholding is to globally threshold the RSFC matrix at a fixed threshold, ρ, for any rij between -1 to 1. One potential problem with this global thresholding method is that once thresholded, the sparse RSFC matrices are not fully connected from node to node (Alexander-Bloch et al., 2010). This disconnectedness of the resulting graphs may ultimately change the properties of the original global and local functional connectivity, which may bias the

comparisons of graph-theoretic metrics between different groups of subjects. This tutorial introduces a minimum spanning tree (MST) approach that has been explored and used in building network model in normal healthy population as well as epilepsy patients (seen from Chapter III and IV). Each MST per subject is a spanning tree of a weighted sub-graph that is fully connected with all nodes having maximum total weight of all links. Although the MST sparsely represents a "skeleton structure" of the brain graph, it does not form clusters or loops among individual brain regions, which keeps it from a biologically meaningful sparse representation (Alexander-Bloch et al. 2010). To obtain a sparse, fully connected and biologically meaningful graph, extra links need to be added to the MST from the remaining RSFC matrix. To do so, a proportional thresholding method is recommended as in this way thresholding less likely rely on a concrete value of certain threshold. By proportionally thresholding the RSFC matrix, it preserves a proportion of the strongest weights. All other weights are set to 0s. The top 2% to 40% of thresholds have been examined in Chapter III. One main reason is that graphs become more random above a threshold level of 50% (Humphries et al., 2006).

Deriving graph theoretical measures

Graph theoretical measures are calculated using the Brain Connectivity Toolbox (https://sites.google.com/site/bctnet/). It is an open-source toolbox which contains a large selection of complex network measures in Matlab (Rubinov & Sporns, 2010). The sparse RSFC matrices can be put into the functions directly for calculating network measures. For example, to threshold the RSFC proportionally, one would choose the function of 'threshold_proportional'. This function requires two inputs—the RSFC matrix and the value of proportion. Once decided

the proportion of weights to preserve, one would put the two inputs to the function of 'threshold_proportional', which will automatically calculating a sparse RSFC. Similarly, clicking open any functions within this toolbox in Matlab, determining the inputs and setting up the required parameters described in the script, there should be output generated without problems.

Discussions

Controlling head-motion artifact

Head motion has been shown to significantly affect the RSFC measures (Saad et al., 2009; Van Dijk et al., 2012), which could potentially alter the graph theoretical metrics as RSFC is the basis for graph theory analysis. Therefore, motion correction is critical in the preprocessing steps. Using the –censor option provided in the AFNI program, 3dDeconvolve is recommended. This option essentially includes the fMRI volumes (i.e., time frames/points) with corresponding motion below a stringent threshold and excludes the volumes with corresponding motion above the predefined threshold. Each corresponding motion is quantified as the square root of the sum of squares of the derivatives (SSD) of the six time courses of the motion parameters (Jones et al., 2010). Besides censoring out motion-confounded volumes, a motion-match procedure was introduced in Chapter III. This method has provided reliable measures for different scan sessions with different subject group. Results were reported in Chapter III.

Network thresholding

As mentioned in Chapter III, one way to control the thresholding effect is by evaluating the modularity measure. The human brain, at least the healthy brain, demonstrates modular organization (Alexander-Bloch et al., 2010). A modularity value greater than 0.3 is indicative of

non-random community structure (Newman & Girvan, 2004). Therefore, a threshold that produces modularity less than 0.3 is not recommended.

Graph theory pitfalls

Although graph theory based network analysis has shown great promise for studying the brain (Chapter V), it is still facing challenges. Individual brain regions of interest (ROIs) are generally treated as uniform and homogeneous in terms of neuronal activities. However, at the neuronal level, neural responses could produce different functional patterns due to the dynamic interactions of axons and dendrites. This could also be expected at the global level in terms of the size and layer architecture of cortical and subcortical brain regions. Future studies examining the effect of properties and behavior of individual nodes on graph theory analysis will provide insights into this question. Another challenge is that with increasingly amount of imaging data, network analysis is facing a computational problem. Research raw data can be easier to collect than analyzed. For instance, correlation analysis between brain voxels from MRI data can take a considerable amount of time. It might need even more time when detecting the modular structures using optimization and/or iteration approach. High-performance computing will be in great need for large-scale voxel network analysis.

Figure 1 Workflow for functional connectivity analysis.

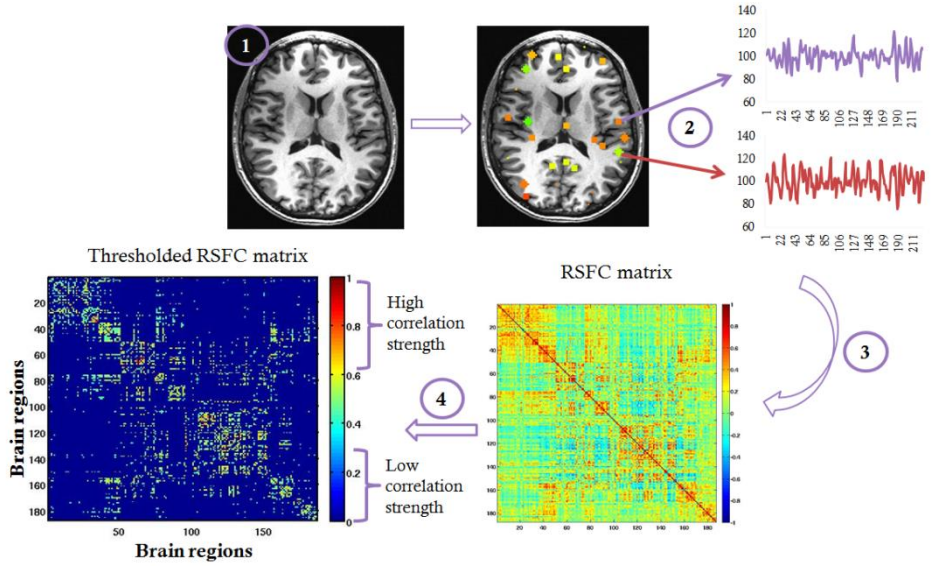

References:

Alexander-Bloch AF, Gogtay N, Meunier D, Birn R, Clasen L, Lalonde F, Lenroot R, Giedd J, Bullmore ET. (2010) Disrupted modularity and local connectivity of brain functional networks in childhood-onset schizophrenia. *Front Syst Neurosci* 4:147.

Bullmore E, Sporns O. (2009) Complex brain networks: graph theoretical analysis of structural and functional systems. *Nature Reviews Neuroscience* 10:186-198.

Cox RW. (1996) AFNI: software for analysis and visualization of functional magnetic resonance neuroimages. *Comput Biomed Res* 29:162-173.

Humphries MD, Gurney K, Prescott TJ. (2006) The brainstem reticular formation is a small-world, not scale-free, network. *Proc Biol Sci* 273:503-511.

Jones TB, Bandettini PA, Kenworthy L, Case LK, Milleville SC, Martin A, Birn RM. (2010) Sources of group differences in functional connectivity: An investigation applied to autism spectrum disorder. *NeuroImage* 49:401-414.

Newman MEJ, Girvan M. (2004) Finding and evaluating community structure in networks. *Physical Review E* 69.

Park HJ, Friston K. (2013) Structural and functional brain networks: from connections to cognition. *Science* 342:1238411.

Rubinov M, Sporns O. (2010) Complex network measures of brain connectivity: uses and interpretations. *NeuroImage* 52:1059-1069.

Saad ZS, Glen DR, Chen G, Beauchamp MS, Desai R, Cox RW. (2009) A new method for improving functional-to-structural MRI alignment using local Pearson correlation. *NeuroImage* 44:839-848.

Sporns O, Tononi G, Kotter R. (2005) The human connectome: A structural description of the human brain. *PLoS Comput Biol* 1:245-251.

Van Dijk KRA, Sabuncu MR, Buckner RL. (2012) The influence of head motion on intrinsic functional connectivity MRI. *NeuroImage* 59:431-438.